Velocity Field and Transverse Dispersion in Vegetated Flows

Suraya Sharil

Thesis Submitted in Partial Fulfilment of the Requirement for the
Degree of Doctor of Philosophy

Division of Civil and Structural Engineering
School of Engineering
Cardiff University
October 2012

Abstract

In recent years aquatic vegetation has become more accepted and important in the river restoration schemes and preserving river ecology. The purpose of this thesis is to investigate the influence of emergent vegetation on velocity and turbulence fields in order to have a better understanding of the effect of vegetation on the transverse mixing processes. To achieve this objective, a series of experiments was conducted in an open channel flume with emergent rigid rods in both staggered and aligned arrangements. Detailed velocity, turbulence and dye tracer measurement were carried out for six vegetation densities relating to solid volume fractions (SVF) in the range 0.51 % to 7.79 %. In sparse vegetation (SVF < 10 %) as expected the normalised spatially-averaged longitudinal velocity reduces as the vegetation density increases with approximately 30 % to 50 % reduction when the solid volume fraction is doubled. Results indicated that in sparse vegetation, the normalised turbulence intensities increased with increasing solid volume fraction. The bulk drag coefficient increased with increasing vegetation density whilst decreased with increasing stem Reynolds number. The transverse mixing coefficient increases with both increasing vegetation density and stem Reynolds number. The current study showed that for sparse vegetation (SVF < 10%), the transverse mixing coefficient has a stronger correlation with turbulence intensity compared to transverse shear. Therefore indicating that within sparse vegetated flows, turbulence dominates over transverse shear in transverse mixing. In addition to that, transverse mixing also correlate better with double-averaged turbulence intensity compared to turbulent kinetic energy. This reflects that the turbulence in the longitudinal direction plays a greater contribution to the overall transverse dispersion than the contribution of the total turbulence in all three directions. Finally two vegetation transverse dispersions models proposed by other researcher for randomly distributed vegetation were tested against data from the current study. Both models were found to predict reasonably well.

Acknowledgement

I wish to thank all those who have made this work possible and in particular the following;

Both my first and second supervisor Dr Catherine A.M.E. Wilson and Dr Steve W Rees for their help and advice,

Division of Civil and Structural Engineering, School of Engineering, Cardiff University that provide good research environment especially with the assistance from the staff of Research Office and the technicians from the Engineering Laboratories,

Universiti Kebangsaan Malaysia and Malaysian Higher Education Ministry for funding the PhD scholarship,

Dr James Shucksmith and Dr Patricia Xavier for their invaluable data,

My fellow PhD friends especially to the Trevithick Group for we share so much tears and joy,

Not forgotten my IKRAM mates for which is very dear to my soul,

And especially to my dear family for their endless love and support, for I love them so much,

Last but not least, Abdul Azim Ismail for his endless love, encouragements and support.

Contents

List of Figures

List of Tables

Notations

A = cross-sectional area
c = tracer concentration
c_t = average tracer concentration within the parcel at time t
C = cross-sectional averaged concentration
$\bar{c}$ = depth averaged tracer concentration
C_d = vegetation drag coefficient
d = stems diameter
e_m = molecular diffusion coefficient
e_t = turbulent diffusion coefficient
e_x = turbulent diffusion coefficient in longitudinal directions
e_y = turbulent diffusion coefficient in transverse directions
e_z = turbulent diffusion coefficient in vertical directions
F_D = Drag force
h = flow depth
H = mean flow depth
I_x = advective flux in x direction;
J_x = diffusive fluxes entering the parcel through the moving boundaries located at x
J_y = diffusive fluxes entering the parcel through the moving boundaries located at y
J_z = diffusive fluxes entering the parcel through the moving boundaries located at x, y, z
$J_{x+\Delta x}$ = diffusive fluxes leaving the parcel through the moving boundaries located at $x + \Delta x$
$J_{y+\Delta y}$ = diffusive fluxes leaving the parcel through the moving boundaries located at $y + \Delta y$
$J_{z+\Delta z}$ = diffusive fluxes leaving the parcel through the moving boundaries located at $z + \Delta z$
K_d = mechanical dispersion
K_h = depth shear dispersion
K_x = longitudinal dispersion coefficient
K_y = longitudinal dispersion coefficient
L = Length scale
M = mass of tracer injected
M_t, = tracer mass in the moving control volume at times t
$M_{t+\Delta t}$ = tracer mass in the moving control volume at times $t + \Delta t$
Δt = time interval
u_x = velocity in x direction
u_y = velocity in y direction
u_z = velocity in z direction
U = cross-sectional mean velocity

U^* = averaged shear velocity
u^* = shear velocity
Re_d = stems Reynolds number
Re_s = pore Reynolds number
v_x = longitudinal depth averaged velocities
v_y = transverse depth averaged velocities
$\mu_p(t)$ = pth spatial moment after time t
σ_x^2 = spatial variance
σ_t^2 = temporal variance
$v_q(x)$ = qth temporal moment at the fixed location x
u', = instantaneous component of velocity u
v' = instantaneous component of velocity v
w' = instantaneous component of velocity w
S = distance between vegetations
w_w = wake width
W = channel width
τ = shear stress
ε = eddy viscosity
ρ = fluid density
SVF = solid volume fraction
Φ = solid volume fraction
δ_x = longitudinal distance of the control volume
δ_y = transverse distance of the control volume
m = number of cylinders per unit area
n = manning's coefficient
R = hydraulics radius
S_o = bed slope
f = Darcy coefficient
C = Chezy coefficient
C_d' = vegetal drag coefficient
λ = vegetal area coefficient
a = frontal area
k = turbulent kinetic energy
α = scale factor
β = scale factor
G = geometry factor
s_{nc} = centre to centre distance to the nearest neighbour cylinder
k = turbulent kinetic energy per unit mass
$P_{snc\rangle r^*}$ = fraction of cylinders with a nearest neighbour farther than r^*
$P_{snc\langle 5d}$ = fraction of cylinders with a nearest neighbour less than $5d$
r^* = $2d$
γ = scaling constant
WF = wake fraction
$\bar{u}_z$ = longitudinal time-averaged velocity averaged in the vertical (z) direction

$\overline{u_x}$ = longitudinal time-averaged velocity averaged in the longitudinal (x) direction

$\overline{v}_x$ = transverse time-averaged velocity averaged in the longitudinal (x) direction

$\overline{u}_{xz}$ = longitudinal time-averaged velocity averaged in the longitudinal (x) and vertical (z) directions

$\overline{u}_{xy}$ = longitudinal time-averaged velocity averaged in the longitudinal (x) and transverse (y) directions

$\sqrt{\overline{u_x'^2}}$ = longitudinal time-averaged turbulence intensity averaged in the longitudinal (x) direction

$\sqrt{\overline{u'}^2_{xyz}}\Big/U$ = longitudinal time-averaged turbulence intensity averaged in the longitudinal (x), transverse (y) and vertical (z) directions

Chapter 1 – Introduction

1.0 Introduction

Water is an essential resource required for sustaining life and livelihoods: safe water is required for drinking, hygiene and providing food; and adequate water to produce energy and support economic activities such as industry and transportation. Water in the natural environment ensures the provision of a multitude of ecosystem services to meet basic human needs and support economic and cultural activities. The challenge for twenty-first century governance is to place water at the heart of decision-making at all levels – horizontally across departments and sectors, and vertically at local, national, regional and global scales (WWAP, 2012).

Although water is the most widely occurring substances on earth, only 2.53 % freshwater while the remainder is salt water. Some two thirds of this freshwater is locked up in glaciers and permanent snow cover. Precipitation is the main source of water for all human uses and for ecosystems. This precipitation is taken up by plants and soils, evaporates into the atmosphere via evapotranspiration, and runs off to the sea via rivers, and to lakes and wetlands. Humankind's control of runoff is now global and plays a significant role in the hydrological cycle. Per capita use is increasing (with better lifestyles) and population is growing. Thus the percentage of the water demand is increasing. Together with spatial and temporal variations in available water, the consequence is that water for all our uses is becoming scarce and leading to a water crisis (WWAP, 2003).

Freshwater resources are further reduced by pollution. Some 2 million tons of waste per day are disposed of within receiving waters, including industrial wastes and chemicals, human waste and agricultural wastes (fertilizers, pesticides and pesticide residues). Estimate of global wastewater production is about 1,500 km^3. Assuming that 1 litre of wastewater pollutes 8 litres of freshwater, the present burden of pollution may be up to 12,000 km^3 worldwide. As ever, the poor are the worst affected, with 50 % of the population of developing countries exposed to polluted water sources (WWAP, 2003).

It is urgent for the world community to restore and conserve the water source and recent research show that aquatic plants in rivers and streams may play a major role in the health of large areas of ocean coastal waters (Brehm, 2008).

Aquatic vegetation plays a vital role in maintaining the overall integrity of aquatic eco-systems. Vegetation stabilizes aquatic ecosystems by reducing nutrient concentrations and shoreline erosion, providing food and habitat for aquatic fauna, and increasing water clarity, producing oxygen, reducing shore erosion (Liffen, 2011).

Traditionally, people have removed vegetation growing along rivers to speed the passage of waters and prevent flooding, but that practice has changed in recent years. Ecologists now advocate replanting, because vegetation provides important habitat. In addition, aquatic plants and the microbial populations they support remove excess nutrients from the water. The removal of too many plants contributes to nutrient overload in rivers, which can subsequently lead to coastal dead zones oxygen deprived areas of coastal water where nothing can survive. Therefore it is important to understand more precisely how water moves through and around aquatic canopies, and know that the vortices control the water renewal and momentum exchange and transport. This knowledge will provide a better understanding on how the size and shape of the aquatic plant will impact the stream restoration (Brehm, 2008).

1.1 Vegetation and Flow

The status of vegetation within river systems has changed in recent years. Both aquatic and riparian vegetation have become central to river restoration schemes and the importance of their preservation to river ecology has now been recognized. The reduction in mean flow and production of turbulence induced by a vegetated region relative to a non-vegetated region means that this is of fundamental significance to flood conveyance estimation, as well as to contaminant and sediment transport (Wilson et al., 2003).

1.2 Vegetation and Solute Mixing

Solute is generally defined as any dissolved substance or entity that is transported downstream by the flowing water. Under this definition, solutes may be pollutants, such as pesticides and hydrocarbons or naturally occurring substances such as dissolved gases, nutrient and trace elements (Runkel and Bencala, 1995). The additional drag exerted by plants reduces the mean flow within vegetation regions relative to the non-vegetated ones. Besides affecting the mean velocity, vegetation also affects turbulence intensity and the turbulent diffusion (Nepf, 1999). Rutherford (1994) categorised the solute mixing processes into three types depending upon the distance between the solutes source and the plumes downstream; i.e. longitudinal mixing (far-field), transverse mixing (mid-field) and vertical mixing (near-field). This thesis focuses attention on the transverse mixing process because it is very important in water quality management for example in managing the point source pollution from the side of a river or a contaminant spill from the river bank, and there is limited published research on both the process of transverse mixing and observed values of the transverse dispersion coefficient (Rutherford, 1994). Indeed in one-dimensional solute transport numerical modelling studies this is a key input parameter and at present there are few empirical models available which help a user decide on the appropriate value to use.

1.3 Thesis Objectives

The purpose of the research presented in this thesis is to investigate the influence of the emergent vegetation canopies on velocity and turbulence fields in order to have a better understanding of the effect vegetation on the transverse mixing processes. The objectives of this thesis can be listed as follows:

(i) To study the impact of stem density on the velocity and turbulence structure in emergent vegetated flows;

(ii) To understand which hydrodynamic processes are most influential in driving transverse dispersion in emergent vegetated flows at high stem Reynolds numbers (1000 to 3000);

(iii) To examine which pertinent vegetation canopy parameters can be used to scale the transverse dispersion coefficient for sparse vegetation densities (solid volume fractions ranging from 0.51 % to 7.79 % and solid volume less than 10 % is considered as sparse density) which are arranged in both staggered and aligned arrangements; and

(iv) To test the applicability and performance of proposed transverse mixing models in the literature with the results from this study.

1.4 Thesis Structure

This thesis is organised according to the following structure:

- Chapter 2 – Introduction to the concepts of open channel including the impact of vegetation on flow parameters. A review of the theory of longitudinal and transverse solute mixing processes and the effect of vegetation on these mixing processes.

- Chapter 3 – Description of the facility, instrumentation and measurement techniques used to fulfil the research objectives.

- Chapter 4 – Presentation and discussion of the velocities and turbulence results from the experimental work.

- Chapter 5 – Presentation and discussion of the dye tracer results from the experimental work.

- Chapter 6 – Conclusion from the thesis.

Chapter 2 – Background Theory

2.0 Introduction

This chapter is comprised of four parts. The first part describes the fundamental theories of hydraulics in open channel flow and the second part presents the impact of the vegetation on the flow parameters. The third part review on the solute mixing processes in open channel flow and the last part explain the impact of vegetation in mixing processes.

2.1 Types of Flow in Open Channels

Flow in an open channel may be uniform or non-uniform. It is said to be uniform if the velocity of the fluid does not change in magnitude or direction from one section to another in the part of the channel under consideration. This is achieved when the water surface is parallel to the base of the channel (Massey and Smith, 1998).

The flow in which the water surface is not parallel to the base of the channel is said to be non-uniform or varied since the flow depth and hence the velocity varies from one cross-section to another. The change in flow depth may be rapid or gradual and it is common to refer these as rapidly varied flow and gradually varied flow. Flow is termed steady or unsteady according to whether the velocity or flow depth at a particular point the channel varies with time (Massey and Smith, 1998).

The two sets of classifications (uniform versus non-uniform; steady versus unsteady) are not mutually exclusive. Some flows exhibit changes with respect to both time and distance while others change with respect to time or distance only. However, the majority of flows will fall into one of the classifications and these are summarised in in Table 2.1 (Chadwick and Morfett, 1998).

Table 2.1 Typical flow classifications (reproduced from Chadwick and Morfett (1998))

Type of flow	**Descriptions**
Steady uniform flow	The discharge is constant with time, and the cross-section through which the flow passes is of constant area
Steady non-uniform flow	The discharge is constant with time, but cross-sectional area varies with distance
Unsteady uniform flow	The cross-section through the flow is constant but the discharge varies with time
Unsteady non-uniform flow	The cross-section and discharge vary with both time and distance.

2.1.1 Laminar and Turbulence Flow

At lower velocities particles of fluid may be observed to be moving entirely in a straight line and this flow is called as laminar flow. The flow is turbulent when the path of individual particles of fluid are sinuous, intertwining and crossing one another in a disorderly manner (Massey, 1989). The existence of these distinct flow regimes was first investigated by Osborne Reynolds in 1883.

The criterion for determining whether the flow is laminar or turbulent is the Reynolds Number (*Re*).

$$\mathrm{Re} = \frac{\rho UL}{\mu} = \frac{UL}{\upsilon} \qquad (2.1)$$

where ρ = fluid density, μ = dynamic viscosity, υ = kinematic viscosity, U = cross-sectional average velocity and L = length scale for open channel flow which is commonly taken as hydraulic radius, flow depth or channel width depending on the context of the study . For a Reynolds number less than 500 the flow is considered as laminar flow and for turbulence flow the Reynolds number is usually 2000 and above (Chadwick and Morfett, 1998).

2.1.2 Shearing Action in Turbulence Flow

Turbulence flow can be decomposed into temporal average component $\left(\overline{u}, \overline{v}, \overline{w}\right)$ and instantaneous component of velocity $\left(u', v', w'\right)$ at any time and can be expressed as in equation 2.2 (a) to (c). Where *u* is the longitudinal velocity aligned with the *x* axis direction (main flow direction), *v* is the transverse velocity in aligned with the *y* axis direction (perpendicular to the main flow direction) and *w* is the vertical velocity aligned with the z axis.

$$u = \overline{u} + u' \tag{2.2a}$$

$$v = \overline{v} + v' \tag{2.2b}$$

$$w = \overline{w} + w' \tag{2.2c}$$

In turbulence flow the streamline might be broken down into eddy formation. The size or scale of individual eddy will be related to the local shearing rate and to the corresponding instability. The passage of a succession of eddies lead to a measurable fluctuation in the velocity. The magnitude of the fluctuation is measured by the root mean square of *u'*. This measure is usually known as the *intensity of turbulence* and is the ratio of $\sqrt{\overline{u'^2}}/u$, where *u'* is the fluctuating component in *x* direction from the time-averaged velocity *u* at a point in space (*v'* refers to the *y* direction and *w'* refers to the *z* direction). There are two elementary models of turbulence, which are *Reynolds stress* model and *Prandtl eddy* model.

2.1.3 The Reynolds Stress Model

If two dimensional flow of horizontal plane is considered, *u'* and *v'* are the fluctuating components of velocity in the *x* and *y* directions. Hence, during a time interval *dt*, the mass of fluid in the *y* direction through a small horizontal element of area *δA* is

$$\rho v'\,\delta A\,\delta t \tag{2.3}$$

This mass has an instantaneous horizontal velocity of *u + u'*. Its momentum, *δM,* is therefore

$$\delta M = \rho v'\,\delta A\,\delta t(u + u') \tag{2.4}$$

Hence the transport rate of momentum during the particular instant is

$$\frac{\delta M}{\delta t} = \rho v'\,\delta A\left(u + u'\right) = \rho \overline{v'}\delta A u + \rho \overline{v'u'}\delta A \tag{2.5}$$

The average transport rate of momentum will be a function of the time-averaged velocities of the fluid particles. The magnitude of *u* remains constant and the averaged values of *u'* and *v'* must be zero (i.e. $\overline{u'} = \overline{v'} = 0$) but the product of $\overline{u'v'}$ may not be zero.

$$average\frac{\delta M}{\delta t} = \rho \overline{u'v'}\delta A \tag{2.6}$$

The existence of momentum implies the existence of a corresponding force within the fluid

$$\delta F = \rho \overline{u'v'}\delta A \tag{2.7}$$

Since stress (*τ)* is a ratio of force to area

$$\tau_{xy} = \frac{\delta F}{\delta A} = -\rho \overline{u'v'} \tag{2.8a}$$

This termed is known as Reynolds stress and conventionally expressed with a negative sign. By the same process deriving Reynolds stress in the vertical plane gives

$$\tau_{xz} = \frac{\delta F}{\delta A} = -\rho \overline{u'w'} \tag{2.8b}$$

Boussinesq (1877) suggested that Reynolds stress can be related to the gradient in mean velocity and in the case of turbulent flow the viscous stresses are often ignored as shown in equation (2.9) where ε is the eddy viscosity which depends on the size and intensity of the turbulent eddies.

$$\tau = \rho \varepsilon \frac{du}{dz} \tag{2.9}$$

2.1.4 Prandtl Eddy Model

As shown in Figure 2.1, consider a flow moving in a straight line, at a point (x, y) in the flow, the velocity of flow is u with cross-sectional area δA and the eddy is rotating rather like a wheel. The tangential velocity of eddy is u', and thus the mass flow transferred at any cross-section will be $\rho \delta A u'$. The rate of interchange of mass is therefore $2\rho \delta A u'$.

Between the plane at y and the plane at plane at $y + \delta y$, the velocity increases from u to $u + \delta u$, so it is reasonable to assume that

$$\delta u = u' = \delta y \frac{du}{dy} \tag{2.10}$$

So

$$\text{rate of interchange} = 2\rho \delta A \delta y \, du/dy \tag{2.11}$$

The rate of interchange of momentum is the product of the rate of mass interchange and the change in velocity in the *y* direction. Therefore, the rate of change of momentum across eddy is

$$\frac{dM}{dt} = 2\rho\delta A\left(\delta y\frac{\delta u}{dy}\right)\left(2\delta y\frac{du}{dy}\right) \tag{2.12}$$

Since shear stress (*τ)* is the ratio of the force to the area in the shear plane, and force =*dM/dt*, therefore

$$\tau = \rho\left(\delta y\frac{du}{dy}\right)^2 = \mu_T\frac{du}{dy} \tag{2.13}$$

Where μ_T is the eddy viscosity and is given by

$$\begin{aligned} \mu_T &= \rho\delta y^2\left(\frac{du}{dy}\right) \\ &= \rho l^2\left(\frac{du}{dy}\right) \end{aligned} \tag{2.14}$$

Equation (2.13) was introduced by Prandtl (1925) to quantify the eddy viscosity (ε) in turbulent flow and *l* was termed as the mixing length and the relation between the eddy viscosity and mixing length was determined as

$$\varepsilon = \rho l^2\frac{du}{dz} \tag{2.15}$$

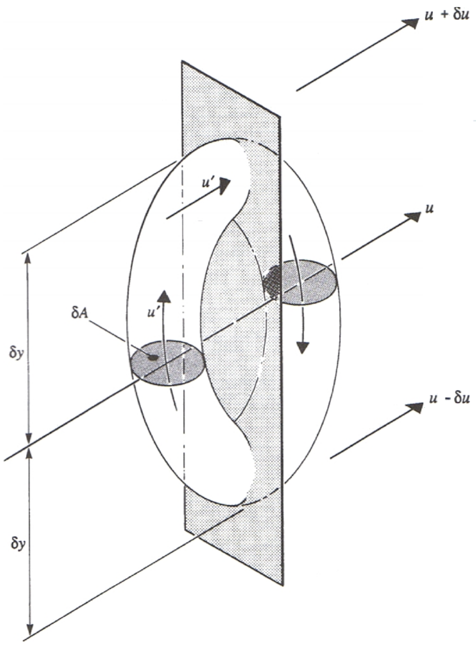

Figure 2.1 Prandtl eddy model (reproduced from Chadwick and Morfett, 1999)

2.1.5 The Boundary Layer

In 1904 Prandtl developed the concept of the boundary layer which provides an important link between ideal fluid flow and the real fluid flow. The fluid at the boundaries has zero velocity relative to the open flow and there is a steep velocity gradient from the boundary into the flow as display in Figure 2.2. Boundary layer is the layer which the fluid had its velocity affected by the boundary shear forces that reduces the flow relative to the boundary (Streeter and Wylie, 1979).

As shown in Figure 2.3 for smooth upstream boundaries the boundaries layer starts out as a laminar boundary layer in which the fluid particles move in smooth layers. As the laminar boundary layer increases in thickness, it becomes unstable and finally transform into a turbulent boundary layer in which the fluid particles move in random paths, although their velocity has been reduced by the action of viscosity at the boundary. When the boundary layer has become turbulent, there is still a very thin layer near to the boundary that has laminar motion called the laminar sublayer (Streeter and Wylie, 1979).

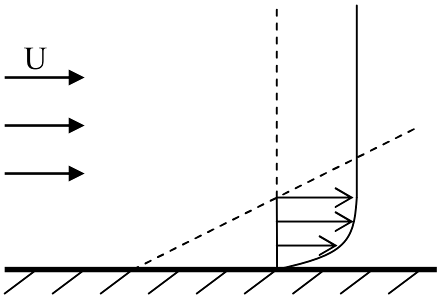

Figure 2.2 Development of a boundary layer (adapted from Chadwick and Morfett (1999))

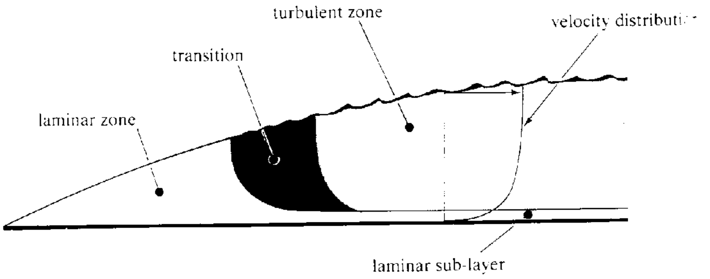

Figure 2.3 Structure of a boundary layer (reproduced from Chadwick and Morfett (1999))7

2.1.6 Flow Separation

As shown in Figure 2.4 around the upstream half of the bluff shape body the fluid is deflected outwards the streamlines converge as the flow accelerates and a boundary layer grows progressively. After the fluid passes the Y-Y axis the flow is decelerating. The fluid in the boundary layer is travelling at a lower speed than the fluid in the free stream and a point is reached at which negative velocities arise at the inner part of the boundary layer. The line traced by the points zero velocity downstream of the body divides the zones of the positive and negative velocity, indicates that the flow separation has occurred. The development of the negative velocity zone further implies that the pressures within the zone are low compared with those in the free stream. Fluid from further out in the boundary layer is therefore drawn inwards to the low pressure zone. The effect of all this powerful eddies is generated, which are then drawn downstream by the flow thus forming the wake zone (Chadwick and Morfett, 1999).

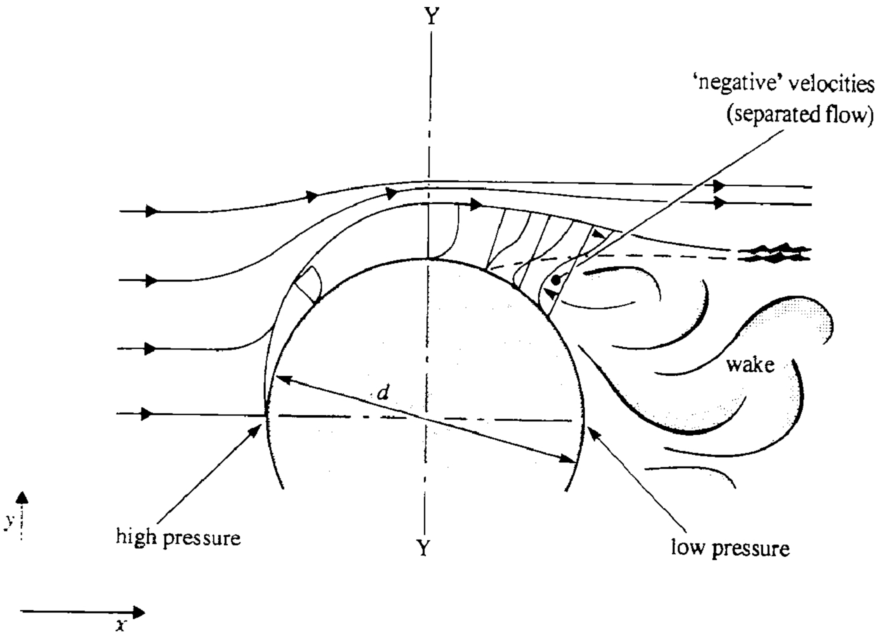

Figure 2.4 Flow separation (reproduced from Chadwick and Morfett, 1999)

2.1.7 Drag Forces on a Body

Total drag on an immersed body is made up of two contributions namely the pressure (or form) drag and the skin friction drag. The form drag is defined as the component of resultant force acting on the body which is in the direction of the relative motion. The frictional drag is the force acting in the direction of relative motion due to fluid shear stress at the surface. The relative contribution of pressure and friction drag to the profile drag depends upon the shape and its orientation with respect to the flow. It is usually laborious to theoretically calculate the total drag therefore, it is usually simpler to measure the profile drag experimentally as a force component in a wind tunnel and it is accepted to express the measure forces as drag coefficient as equation (2.16) and Figure 2.5 display the variation of drag coefficient in relation stem Reynolds number for a single cylindrical rod.

$$C_d = \frac{\text{drag force}}{\frac{1}{2}\rho A_p U^2} \tag{2.16}$$

where C_d is the drag coefficient and A_p is the cross-sectional area of body perpendicular to the direction of the incident flow. Since drag force is the total force due to both friction and form components, therefore C_d is therefore is a function of the body shape and the Reynolds number (Douglas et al., 1979).

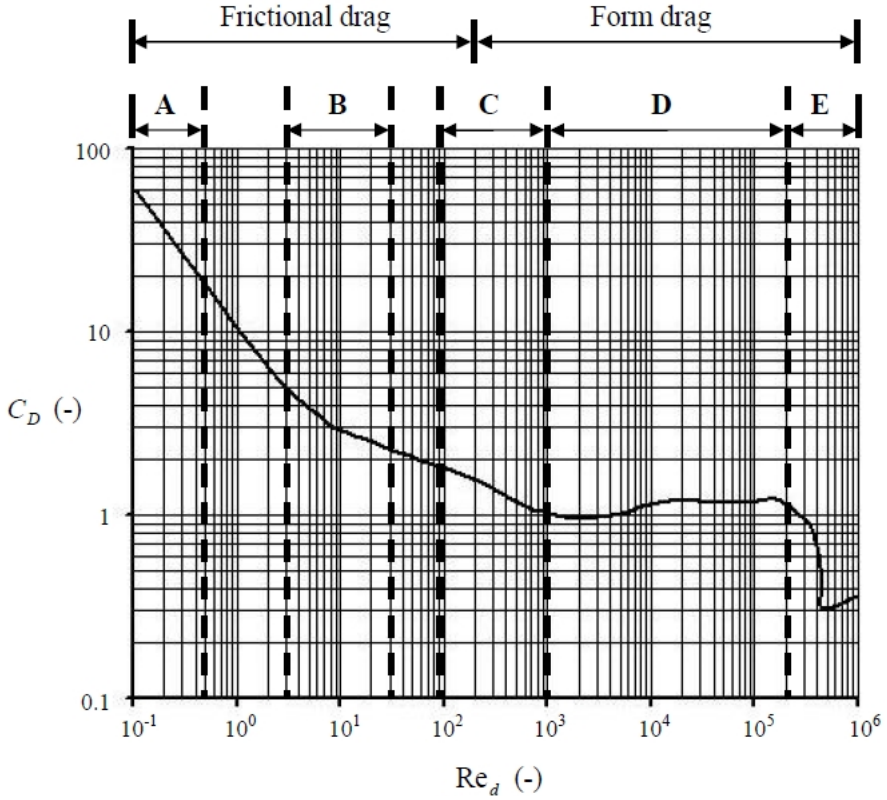

Figure 2.5 Variations in drag coefficient, C_d with the stem Reynolds number for a single cylinder (reproduced from Schlichting, 1955)

For infinite length of a circular cylinder placed in a flow, at very low value of Reynolds number (i.e. Re < 0.5) the inertia forces are negligible and the flow pattern is very similar to ideal flow, and the streamlines come together behind cylinder as indicated in Figure 2.6a. The form drag is negligible and the total drag profile is nearly all due to skin friction (Douglas et al., 1979).

If the Reynolds number increased to a range 2 to 30 the boundary layer separates symmetrically from the two sides at the positions S (refer to Figure 2.6b) and two symmetrical eddies are formed which rotate in opposite directions. At these Reynolds numbers eddies remain unchanged in position, their energy being maintained by the flow from the separated boundary layer. Behind eddies, the main streamlines come together, and the length of the wake is limited (Douglas et al., 1979).

Further increase in Reynolds number eddies elongate as shown in Figure 2.6c. For a circular cylinder, eddies are unstable at a Reynolds number of approximately 40 to 70 and a periodic oscillation of the wake is observed (refer to Figure 2.6d). Then at a certain limiting value of Reynolds number (usually about 90 for a circular cylinder in unconfined flow), eddies break off from each side of the cylinder alternately and are washed downstream (Douglas et al., 1979).

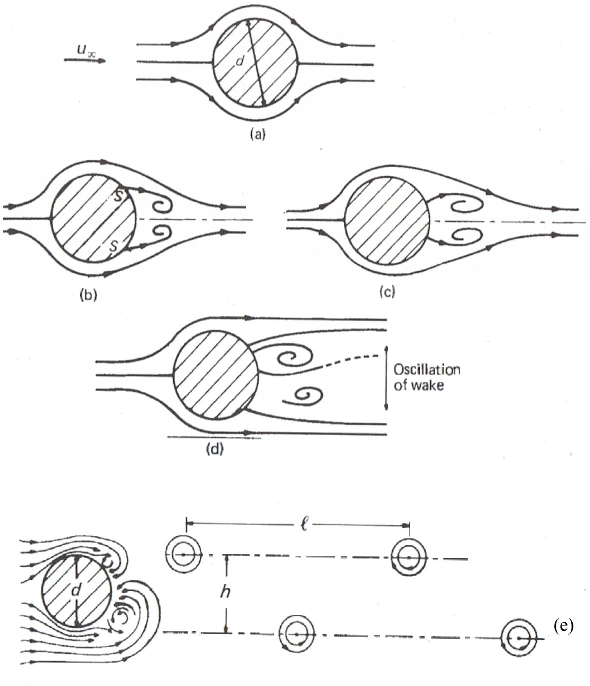

Figure 2.6 Development of a wake behind a cylinder and vortex street (reproduced from Massey and Smith, 1998)

For a certain range of Reynolds number above the limiting value, eddies are continuously shed alternately from the two sides of the cylinder and as a result form two rows of vortices in its wakes known as a vortex street or vortex trail (refer to Figure 2.6e). Each time a vortex is shed from the cylinder, the lateral symmetry of the flow pattern and the pressure distribution round the cylinder are distributed. The shedding of vortices alternately from the two sides of cylinder therefore producing alternating lateral forces and these may cause a forced vibration of the cylinder at the same frequency. The frequency, f which vortices are shed from an infinitely long circular cylinder, is given by the empirical formula of equation (2.17) and this is for Reynolds number in the range of 250 to 2 x 10^5 (Douglas et al., 1979).

$$\frac{fd}{U} = 0.198\left(1 - \frac{19.7}{\mathrm{Re}}\right) \qquad (2.17)$$

2.2 The Impact of Vegetation on Flow Parameters

2.2.1 Definitions Solid Volume Fraction

Before further discussion in the impact of vegetation on flow parameters, it is important to define solid volume fraction (SVF). This thesis defines solid volume fraction as solid volume of vegetation per unit volume of fluid as shown in equation (2.18a) and (2.18b). Equation (2.18a) is for aligned vegetation arrangement and equation (2.18b) is used to calculate SVF for staggered arrangement.

$$\text{SVF (aligned)} = \phi = \frac{\pi d^2}{4\delta_x \delta_y} \times 100\% \qquad (2.18a)$$

$$\text{SVF (staggered)} = \phi = \frac{\pi d^2}{8\delta_x \delta_y} \times 100\% \qquad (2.18b)$$

where d is the cylinder diameter, δ_x is the longitudinal distance of the control volume and δ_y is the transverse distance of the control volume. In Nepf et al. (1997), Nepf (1999) and Tanino and Nepf (2008) because these research work dealt with random arrangement, therefore equation (2.19) was used to calculate the solid volume fraction, where m is the number of cylinders per unit area and d is the cylinders diameter. This non-dimensional SVF then multiply by 100 % to be comparable with present work SVF.

$$\phi = \frac{m\pi d^2}{4} \tag{2.19}$$

2.2.2 Flow Resistance of Vegetated Channel

Flow resistance due to vegetation may greatly affect the conveyance of a channel, and thus evaluating the resistance is a critical task in river engineering and restoration (Jarvela, 2002). The most widely used resistance measure, particularly with respect to vegetated channels is the Manning's equation (see equation (2.20), which was named after the Irish engineer Robert Manning (Green, 2005).

$$n = \frac{R^{2/3} S_{\circ}^{1/2}}{U} \tag{2.20}$$

where n is the Manning's coefficient, R is the hydraulic radius, S_o is the bed slope and U is the mean area velocity. Other established flow resistance formulas such as Darcy-Weisbach and Chezy equation have long been used to analyse river flow (Stone and Shen, 2002).

$$f = \frac{8gRS_{\circ}}{U^2} \tag{2.21}$$

$$C = \frac{U}{\sqrt{RS_{\circ}}} \tag{2.22}$$

where f is the Darcy coefficient, C is the Chezy coefficient and g is the acceleration due to gravity. These equations (2.20, 2.21 and 2.22) were developed based on the uniform flow such that the longitudinal weight component of the flow is equal to the force resistance (Malki, 2009).

Petryk and Bosmajian (1975) developed a theoretical model for vegetation based on drag forces exerted by plants and is mainly applicable to floodplain vegetation;

$$n_{tot} = n_b \sqrt{1 + \frac{C_d \sum A_i}{2gAL} n_b^{-2} R^{4/3}} \tag{2.23}$$

where n_b is the flow resistance from the bed, R is the hydraulic radius, C_d is the drag coefficient, A_i is the projected area of the ith plant in the upstream direction, g is the acceleration due to gravity, A is the cross-sectional area of flow and L is the length of channel reach being considered.

Stone and Shen (2002) proposed a flow resistance equation based on momentum balance as shown in equation (2.24). The study shows that the flow resistance is a function of the flow depth, number of stems per unit area, stem length and stem diameter.

$$F = 1.385\left(l^{*-1} - \sqrt{md^2}\right)\sqrt{\frac{gd}{md^2 h}} = 1.385\left(l^{*-1} - \sqrt{4A_{bs}b/\pi}\right)\sqrt{\frac{\pi dg}{4A_{bs}h}} \tag{2.24}$$

where l^* is the submergence ratio; m is the number of stems per unit area; h is the flow depth and A_{bs} is the fraction of the bed area occupied by the stems = $m\pi d^2/4$.

To estimate the drag force on the emergent willow, (Jarvela, 2002) defined vegetal drag coefficient as;

$$C_d' = \lambda C_d \tag{2.25a}$$

$$\lambda = A_p/(AL) \tag{2.25b}$$

where λ is the vegetal area coefficient; A_p is the projected area; A is the cross-sectional area and L is length of the channel reach. Jarvela (2002) further suggest solving of C_d' yield equation (2.26) and by combining equation (2.26) with Darcy-Weisbach equation gives equation (2.27).

$$C_d^{'} = \frac{2gS}{U^2} \qquad (2.26)$$

$$C_d^{'} = f/4R \qquad (2.27)$$

Jarvela (2004) presented a practical tool for estimating the relationship between plant characteristics and wetlands growing natural woody vegetation. This proposed model has the ability to estimate flow resistance for vegetation with leaf (equation 2.28) or without leaf (2.29).

$$f = \frac{4d_r h}{a_x a_y} C_d \qquad (2.28)$$

$$f = 4C_{d\chi} LAI \left(\frac{U}{U_\chi} \right)^\chi \frac{h}{H} \qquad (2.29)$$

where d_r is the characteristic diameter = A_p/h; a_x and a_y are the mean longitudinal and lateral distances respectively between the plants; $C_{d\chi}$ is a species specific drag coefficient; LAI is the leaf area of the upper side of the leaves in a canopy projected onto a flat surface area of the surface under the canopy; U_χ is the unique velocity for a particular species and H is the plant height.

2.2.3 Velocity in Emergent Vegetation

One of the studies in Stone and Shen (2002) whereby a stem layer velocity equation was derived based on steady and uniform flow. This is shown in equation (2.30) and it is applicable to emergent and submerged vegetation. Experimental results present close agreement between the calculated and measured values of stems layer velocity shows that equation (2.30) can accurately predict for both emergent and submerged cases.

$$u = \left(1 - \sqrt{\frac{4A_{bs}}{\pi}} \right) \sqrt{\frac{g\left(1 - A_{bs} l^*\right)\pi d}{2A_{bs} l^* C_d}} \sqrt{S_v} \qquad (2.30)$$

where A_{bs} is the area concentration = $m\pi d^2/4$; m is the number of stems per unit area; l^* = wetted length stems/flow depth ratio; S_v is the friction slope due to stem resistance and C_d is the drag coefficient whereby this research used C_d = 1.05 in the calculation.

Lightbody and Nepf (2006) present a method to estimate the velocity profile in a salt marsh canopies and shown equation (2.31a) and (2.31b). Both equations were based on steady, uniform and fully developed flow whereby the hydrostatic pressure and momentum equation reduces to a simple balance between the vegetation drag and pressure forcing terms. Furthermore equation (2.31b) was derived with the assumption that the drag coefficient is constant over depth.

$$\frac{u(z)}{\tilde{u}} = \sqrt{\frac{\tilde{C}_d \tilde{a}}{C_d(z)a(z)}} \tag{2.31a}$$

$$\frac{u(z)}{\tilde{u}} = \sqrt{\frac{\tilde{a}}{a(z)}} \tag{2.31b}$$

where $\tilde{u}$ is the velocity at a reference height above the bed where vegetation drag dominates; $\tilde{a}$ is the frontal area at the reference height and $\tilde{C}_d$ is the drag coefficient at the reference height. Results show that predicted velocity profiles provides a reasonably good fit to the observations. However the predicted velocity is most deviate from the observations within 10 cm and 70 cm of the bed. At 10 cm from the bed where micro-topography may contribute additional drag and at 70 cm of the bed it is likely that wind shear and other surface processes may be important.

2.2.4 Turbulence in Emergent Vegetation

The presence of vegetation affects the turbulence whereby the conversion of mean kinetic energy to turbulent kinetic energy within stems wakes augments the turbulence intensity (Nepf, 1999). Nepf (1999) developed and tests a model that predicts the turbulence intensity within emergent vegetation. Assuming that the turbulence characteristic length scale is set by stem diameter, therefore Nepf (1999) proposed the turbulence intensity as

$$\frac{\sqrt{k}}{U} = \alpha\left(\overline{C_d}ad\right)^{1/3} \qquad (2.32)$$

where k is the turbulent kinetic energy; α is the non-dimensional constant and $\overline{C_d}$ is the bulk drag coefficient. Experimental results show that turbulence intensity is dependence on the vegetative drag even for sparse vegetation densities (less than 10 %) and the bed drag and the bed shear productions are negligible. In addition the model predicts that turbulence intensity increases with the introduction of sparse vegetation due to the addition of the wake production but the decreases with increasing vegetation density as mean flow is reduced.

Liu (2008) used discrete measurements at multiple locations within the vegetation arrays to observe the velocity and turbulence intensity profiles as water travels through a vegetation array simulated by rigid dowels. Experimental results show that longitudinal and vertical turbulence intensities are highest immediately behind a dowel and weakest in the free stream region. Attaching roughness to the bed contributes to lowering the turbulence intensity and on the other hand by roughening the dowels increases the flow resistance therefore increases the turbulence intensity.

Lui (2008) concluded that these finding shows the flow characteristic changes significantly depending on the measurement location with respect to the dowels. As a result, factors such as plant density and arrangement have significant impacts on the flow behaviour. While many of the flow characteristic are similar within arrays of cylinders and can be averaged to obtain a general picture, the flow behaviour immediately behind a cylinder is very dissimilar to the other areas and should not be ignored. The flow exchanges occurring behind the dowel near the bed and top of the dowel array may have major benefits for stream ecosystem health.

2.3 Solutes Mixing Process

This section will describe the major processes affecting solutes in open channels. Solute is generally defined as any substance or entity that is transported downstream by the flowing water (Runkel and Bencala, 1995).

2.3.1 Advection

Advection is the bodily transport of solutes resulting from an imposed current in river or coastal waters (Fischer et al., 1979). When soluble material is introduced into a flow advection carries it away from the source (Guymer et al., 2005). The amount of tracer transported per unit time per unit area perpendicular to the current is termed advective flux and is the product of velocity and tracer concentration as

$$I_x = uc \tag{2.33}$$

where I_x = advective flux in x direction; u = velocity in x direction and c = tracer concentration (Rutherford, 1994).

2.3.2 Molecular Diffusion

In a stagnant fluid, buoyant tracer will spread slowly at the same rate in all three directions (x, y and z). This spreading results from random molecular motion within the fluid and is termed molecular diffusion. Fick made a hypothesis that the net rate of tracer transfer from a region of high concentration to a region of low concentration is related to the rate proportional to the concentration gradient between these two regions. This is known as Fick's first law which is given as

$$J_x = -e_m \frac{\partial c}{\partial x} \tag{2.34}$$

where J_x = molecular diffusive flux in *x* direction; c = tracer concentration; $\partial c/\partial x$ = tracer concentration gradient in *x* direction; e_m = molecular diffusion coefficient.

In laminar flow the transport and behaviour of a solute is governed by the combined effect of advection and molecular diffusion. According to the conservation of mass, the change rate of mass within the control volume is balanced by the transfer rate of mass across the boundaries of the control volume (see Figure 2.7).

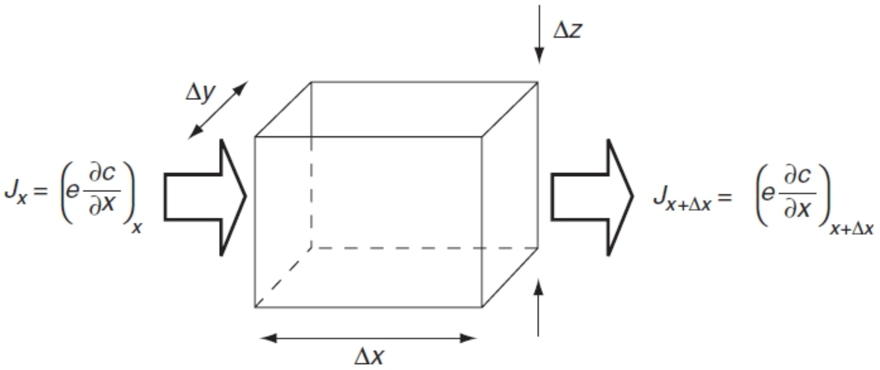

Figure 2.7 Diffusive fluxes into and out of a small fluid (reproduced from Guymer et al. (2005))

Figure 2.7 can be elaborated as equation (2.35);

$$\frac{M_{t+\Delta t} - M_t}{\Delta t} = (J_x - J_{x+\Delta x})\Delta y \Delta z + (J_y - J_{y+\Delta y})\Delta x \Delta z + (J_z - J_{z+\Delta z})\Delta x \Delta y \qquad (2.35)$$

where M_t and $M_{t+\Delta t}$ = tracer masses in the moving control volume at times t and $t+\Delta t$ respectively; J_x, J_y and J_z = diffusive fluxes entering the parcel through the moving boundaries located at *x*, *y*, *z*; $J_{x+\Delta x}$, $J_{y+\Delta y}$, $J_{z+\Delta z}$ = diffusive fluxes leaving the parcel through the moving boundaries located at $x+\Delta x$, $y+\Delta y$, $z+\Delta z$; Δx, Δy and Δz = dimensions of the fluid parcel; and Δt = time interval. Using Taylor's series with assumption that Δt is very small equation (2.35) can be rewritten as

$$M_{t+\Delta t} = M_t + \left(\frac{DM}{Dt} \right)_t \Delta t \qquad (2.36)$$

where D/Dt denote the rate of change with time in a Lagrangian coordinate system travelling at the mean velocity and the mass of tracer at time *t* is

$$M_t = c_t \Delta x \Delta y \Delta z \Delta t \qquad (2.37)$$

where c_t = average tracer concentration within the parcel at time *t* and consequently equation (2.36) can be written as

$$\frac{M_{t+\Delta t}}{\Delta t} - M_t = \left(\frac{Dc}{Dt} \right) \Delta x \Delta y \Delta z \qquad (2.38)$$

The concentration gradient across the boundaries can then be determined using Eulerian operators as shown in equations (2.39a) to (2.39c)

$$J_{x+\Delta x} = J_x + \left(\frac{\partial J_x}{\partial x} \right)_x \Delta x \qquad (2.39a)$$

$$J_{y+\Delta y} = J_y + \left(\frac{\partial J_y}{\partial y} \right)_y \Delta y \qquad (2.39b)$$

$$J_{z+\Delta z} = J_z + \left(\frac{\partial J_z}{\partial z} \right)_z \Delta z \qquad (2.39c)$$

Using equation (2.34) into equation (2.39) and rearranging these to equation (2.40a) to (2.40c)

$$(J_x - J_{x+\Delta x}) \Delta y \Delta z = \frac{\partial}{\partial x} \left(e_m \frac{\partial c}{\partial x} \right) \Delta x \Delta y \Delta z \qquad (2.40a)$$

$$(J_y - J_{y+\Delta y}) \Delta x \Delta z = \frac{\partial}{\partial y} \left(e_m \frac{\partial c}{\partial y} \right) \Delta x \Delta y \Delta z \qquad (2.40b)$$

$$(J_z - J_{z+\Delta z}) \Delta x \Delta y = \frac{\partial}{\partial z} \left(e_m \frac{\partial c}{\partial z} \right) \Delta x \Delta y \Delta z \qquad (2.40c)$$

Then combining equations (2.35), (2.38), (2.40) and noting that the molecular diffusion coefficient, e_m is independent of x, y and z and simplifying gives

$$\frac{Dc}{Dt} = e_m\left(\frac{\partial^2 c}{\partial x^2} + \frac{\partial^2 c}{\partial y^2} + \frac{\partial^2 c}{\partial z^2}\right) \tag{2.41}$$

Equation (2.41) can now be rewritten to the well known three dimensional Fickian diffusion equations in Cartesian coordinates as shown in equation (2.42) which is also known as advection diffusion equation. In laminar flow the molecular diffusion coefficient e_m is assumed constant in all directions (Fischer et al., 1979).

$$\frac{\partial c}{\partial t} + u\frac{\partial c}{\partial x} + v\frac{\partial c}{\partial y} + w\frac{\partial c}{\partial z} = e_m\left(\frac{\partial^2 c}{\partial x^2} + \frac{\partial^2 c}{\partial y^2} + \frac{\partial^2 c}{\partial z^2}\right) \tag{2.42}$$

where u, v and w are the velocities in the respective x, y and z directions.

2.3.3 Turbulent Diffusion

Most river and open channel flows are characterised by a high Reynolds number and are turbulent except in a very thin, viscous sub-layer near the bed. One important feature of turbulent flow is that tracer spreads far more rapidly than in laminar flow. In turbulent flow viscous forces are weak relative to inertial forces. Turbulence is termed stationary if characteristic such as mean velocity, velocity variance and the correlations between velocities remain constant with time. Turbulence is considered homogeneous when the velocity fluctuations and correlation do not vary with location and isotropic if they are the same magnitude in all coordinate directions (Rutherford, 1994).

In turbulent flow tracer mixes more rapidly than can be accounted for just by molecular diffusion. The reason is that of the small eddies continually erode the edges of the tracer cloud increases local concentration gradients and hence allow molecular diffusion to proceed more rapidly. The combined effect of molecular diffusion and turbulent velocity fluctuations is termed turbulent diffusion (Rutherford, 1994).

2.3.4 Taylor's Analysis of Turbulent diffusion

In 1921 Taylor published a theoretical analysis of the spreading of a cloud of tracer particles released into stationary, homogeneous turbulence. If a tracer particles is released at the origin then after a time t it will be located at a longitudinal distance x from the origin where

$$x(t) = \int_{\tau}^{t} u'(\tau) d\tau \qquad (2.43)$$

where $u'(x)$ is the turbulent velocity fluctuation about the mean velocity. If N particles are released then because of the random nature of the turbulent velocity fluctuations they will be at different location x_i (where i = 1, 2, 3 …N) after time t. From the conservation of mass, the ensemble mean variance of the resulting tracer cloud is identically equal to the ensemble mean square displacement of the tracer particles

$$\sigma_x^2 = \left\langle \left(x - \bar{x}\right)^2 \right\rangle \qquad (2.44a)$$

Because a Lagrangian coordinate system is being used, therefore

$$\langle \bar{x} \rangle = 0 \qquad (2.44b)$$

and

$$\sigma_x^2 = \left\langle x^2 \right\rangle \qquad (2.44c)$$

We can rewrite equation (2.43) to

$$x^2(t)=\left[\int_{t_1=0}^{t}u'(t_1)dt_1\right]\left[\int_{t_2=0}^{t}u'(t_2)dt_2\right]=\int_{t_1=0}^{t}\int_{t_2=0}^{t}u'(t_1)u'(t_2)dt_1dt_2 \tag{2.45}$$

In equation (2.45) the product

$$u'(t_1)u'(t_2) \tag{2.46}$$

is the auto-covariance between the velocity of a particle at time t_1 and the velocity of the same particle at a later time t_2. Taking the ensemble average of equation (2.45)

$$\langle x^2\rangle=\int_{t_1}^{t}\int_{t_2}^{t}\langle u'(t_1)u'(t_2)\rangle dt_1dt_2 \tag{2.47}$$

The Lagrangian autocorrelation function is defined

$$R_x(t_2-t_1)=\frac{\langle u'(t_1)u'(t_2)\rangle}{\sqrt{\langle u'^2\rangle}} \tag{2.48}$$

where $\sqrt{\langle u'^2\rangle}$ = intensity of turbulence.

Combining equations (2.47) and (2.48)

$$\langle x^2\rangle=\sqrt{\langle u'^2\rangle}\int_{t_1=0}^{t}\int_{t_2=0}^{t}R_x(t_2-t_1)dt_2dt_1 \tag{2.49}$$

which can be rewritten as equation (2.50) where s is a measure of the time taken for a particle to forget its original velocity

$$\langle x^2\rangle=2\langle u'^2\rangle\int_{s=0}^{t}(t-s)R_x(s)ds \tag{2.50}$$

By definition

$$R_x(0) = 1$$

$$R_x(\infty) = 0$$

At very small values of t, $R_x = 1$ and equation (2.50) becomes

$$\langle x^2 \rangle = \langle u'^2 \rangle t^2 \qquad (2.51)$$

Thus at small times, the variance increases at a rate proportional t^2. At very large t, $R_x = 0$ and equation (2.50) becomes

$$\langle x^2 \rangle \to 2\langle u'^2 \rangle T_x t + \text{constant} \qquad (2.52)$$

where

$$T_x = \int_{s=0}^{\infty} R_x(s) ds \qquad (2.53)$$

T_x is known as the integral Lagrangian time-scale and is a measure of the time taken for a particle to forget its original velocity. The relationship in equation (2.52) implies that some time after the tracer has been released into the turbulent flow the variance of the tracer cloud increases linearly with time. Equation (2.52) also states that the rate at which the variance of the tracer cloud grows increases with the square of the turbulent intensity (i.e. spreading occurs more rapidly in highly turbulent flows).

2.3.5 Fickian Model of Turbulent Diffusion

Taylor's analysis demonstrates that in stationary homogeneous turbulence the variance of a tracer cloud increases linearly with time. This suggests that turbulent diffusion can also be modelled using Fick's law provided sufficient time has elapsed since tracer injection. The following equation can be derived which can be compared to equation (2.42) and is known as Fickian model of turbulent diffusion as

$$\frac{\partial c}{\partial t}+u\frac{\partial c}{\partial x}+v\frac{\partial c}{\partial y}+w\frac{\partial c}{\partial z}=(e_m+e_t)\left(\frac{\partial^2 c}{\partial x^2}+\frac{\partial^2 c}{\partial y^2}+\frac{\partial^2 c}{\partial z^2}\right) \qquad (2.54)$$

where e_t = turbulent diffusion coefficient and e_m = molecular diffusion coefficient. The turbulent diffusion coefficient is much larger than the molecular turbulent diffusion. The molecular diffusion coefficient e_m is a property of the fluid and so is homogeneous throughout the fluid and is isotropic. The turbulent diffusion coefficient e_t (also known as the turbulent eddy viscosity or eddy viscosity) is a property of velocity field and as such may vary spatially. If the flow is assumed stationary and the turbulent diffusion coefficient is non-isotropic and non-uniform, equation (2.54) can be rewritten and the diffusion coefficients are constant

$$\frac{\partial c}{\partial t}+u\frac{\partial c}{\partial x}+v\frac{\partial c}{\partial y}+w\frac{\partial c}{\partial z}=e_x\frac{\partial^2 c}{\partial x^2}+e_y\frac{\partial^2 c}{\partial y^2}+e_z\frac{\partial^2 c}{\partial z^2} \qquad (2.55)$$

where e_x = turbulent diffusion coefficient in longitudinal (x) direction, e_y = turbulent diffusion coefficient in transverse (y) direction and e_z = turbulent diffusion coefficient in vertical (z) direction.

2.3.6 Simplifying The Mixing Equations

If the mixing process from a point source is considered in an open channel Rutherford (1994) has defined the mixing zones as near-field, mid-field and far-field.

Open channels typically have a length much greater than their width and a width that is much greater than their depth. Therefore the solute will first achieve well mixed conditions (i.e. constant concentration across the plane) across the vertical (*z*) plane or known as the near-field zone, followed by the transverse plane (*y*) in the mid-field zone, before spreading over the longitudinal plane (*x*) in the far-field zone (Shucksmith, 2008). Rutherford (1994) described the general characteristic of tracer plumes from three different types of tracer as Figure 2.8. Below a point source both vertical and transverse gradient are significant in the near field, transverse concentration gradients are significant in the mid field and tracer is well mixed across channel in the far-field. If the tracer is released uniformly from vertical line source than the plumes will vertically well mixed immediately after injection. Similar if the tracer is released uniformly from a transverse line source then the plumes will well mix in the transverse direction immediately after injection (Rutherford, 1994).

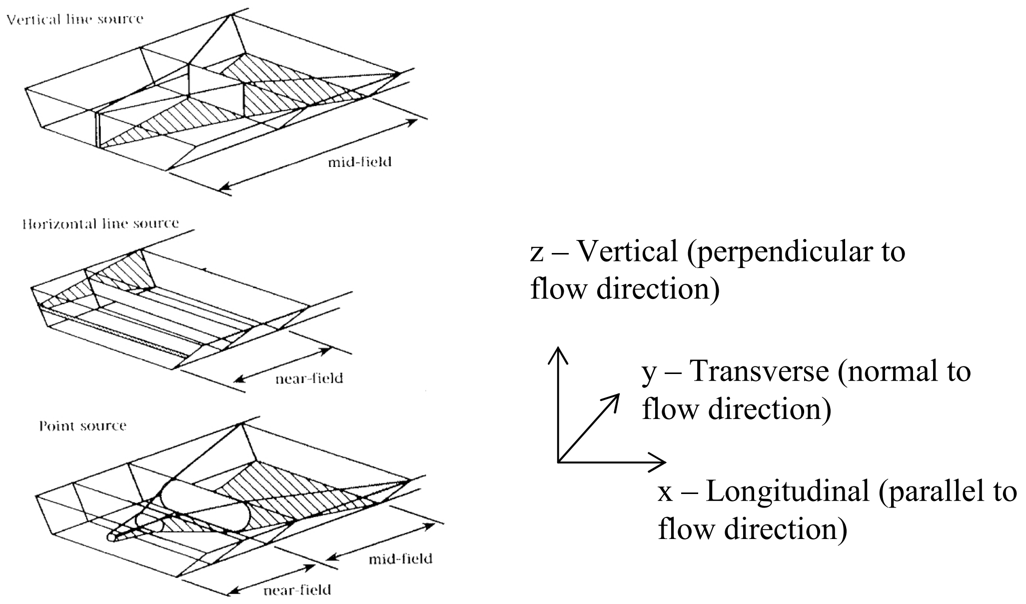

Figure 2.8 General characteristic of tracer plumes downstream from different types of tracer source (reproduced from Rutherford, 1994)

Equation (2.55) describes mixing in three dimensions (*x*, *y* and *z*) which require detailed knowledge of water depth, velocities and diffusion coefficients. First if we consider near-field zone and it is possible that the x axis is aligned with the flow direction (i.e. in a straight channel) and it is assumed that the transverse and vertical velocities are equal to zero $\left(u_y = u_z = 0\right)$. In this situation equation (2.55) becomes

$$\frac{\partial c}{\partial t} + u\frac{\partial c}{\partial x} = \frac{\partial}{\partial x}\left(e_x \frac{\partial c}{\partial x}\right) + \frac{\partial}{\partial x}\left(e_y \frac{\partial c}{\partial y}\right) + \frac{\partial}{\partial z}\left(e_z \frac{\partial c}{\partial z}\right) \qquad (2.56)$$

If the tracer source is steady then the first term in equation (2.56) vanishes and the longitudinal concentration gradients become negligibly small and so the equation reduces to

$$u\frac{\partial c}{\partial x} = \frac{\partial}{\partial x}\left(e_y \frac{\partial c}{\partial y}\right) + \frac{\partial}{\partial z}\left(e_z \frac{\partial c}{\partial z}\right) \qquad (2.57)$$

If the tracer originates from a steady transverse line source then the transverse concentration gradient is small and so the equation becomes

$$u\frac{\partial c}{\partial x} = \frac{\partial}{\partial z}\left(e_z \frac{\partial c}{\partial z}\right) \qquad (2.58)$$

In the mid-field mixing region the vertical concentration gradients are small and the three-dimensional advection-diffusion equation can be averaged over the depth to yield the following two-dimensional equation

$$\frac{\partial \bar{c}}{\partial t} + \frac{\partial}{\partial x}\left(hu_z\bar{c}\right) + \frac{\partial}{\partial y}\left(hv_z\bar{c}\right) = \frac{\partial}{\partial x}\left[h\left(e_x + k_x\right)\frac{\partial \bar{c}}{\partial x}\right] + \frac{\partial}{\partial y}\left[h\left(e_y + k_y\right)\frac{\partial \bar{c}}{\partial y}\right] \qquad (2.59)$$

where k_x and k_y = longitudinal and transverse dispersion coefficient which accounts for the effects on the depth averaged tracer concentration of depth variations in the longitudinal and transverse velocity; $\bar{c}$ = depth-averaged tracer concentration; u_z and v_z = longitudinal and transverse depth averaged velocities; h = local depth. In rivers, longitudinal and transverse dispersion coefficients is much larger than longitudinal and transverse turbulent diffusion coefficients, equation (2.59) can be rewritten as

$$\frac{\partial \bar{c}}{\partial t}+u_h\frac{\partial \bar{c}}{\partial x}+v_h\frac{\partial \bar{c}}{\partial y}=\frac{1}{h}\frac{\partial}{\partial x}\left(hk_x\frac{\partial \bar{c}}{\partial x}\right)+\frac{1}{h}\frac{\partial}{\partial y}\left(hk_y\frac{\partial \bar{c}}{\partial y}\right) \tag{2.60}$$

In the far-field the tracer eventually mixes across the channel where the vertical and transverse concentration gradients are small. The three-dimensional advection diffusion equation can be averaged over both the depth and the width to yield the one-dimensional equation

$$\frac{\partial C}{\partial t}+U\frac{\partial C}{\partial x}=\frac{1}{A}\frac{\partial}{\partial x}\left(AK_x\frac{\partial C}{\partial x}\right) \tag{2.61}$$

where C = cross-sectional averaged concentration; U = cross-sectional averaged velocity; A = cross-sectional area; and K_x = longitudinal dispersion coefficient (Rutherford, 1994).

2.3.7 The Mechanisms Causing Longitudinal Dispersion

Longitudinal dispersion arises because the vertical and transverse velocity shear carry the tracer downstream more slowly near the bed and the banks than in the mid-channel (Rutherford, 1994). Fischer (1967) showed that in river channels transverse velocity shear makes a greater contribution to longitudinal dispersion than vertical velocity shear.

According to Taylor (1953; 1954) at some point downstream from the source an equilibrium becomes established between velocity shear (which acts to spread tracer along the channel) and transverse mixing (which promotes uniform concentrations and hence counteracts the effects of velocity shear). Beyond this point the longitudinal variance of the cross-sectional averaged tracer concentration increases linearly with time. Skewness introduced by velocity shear in the advective zone begins to decay slowly and eventually the spatial tracer distribution becomes Gaussian (Rutherford, 1994).

This suggests that the cross-sectional averaged concentration can be modelled using Fick's Law. For a uniform channel

$$\frac{\partial C}{\partial t}+U\frac{\partial C}{\partial x}=K_x\frac{\partial^2 C}{\partial x^2} \tag{2.62}$$

If U and K_x are assumed to be constant then the solution to equation (2.62) for an instantaneous point source is

$$C(x,t)=\frac{M}{A\sqrt{4\pi K_x t}}\exp\left[-\frac{(x-Ut)^2}{4K_x t}\right] \tag{2.63}$$

where M = mass of tracer injected at x = 0 and t = 0; and A = cross-sectional area of the channel.

The longitudinal (spatial) moments of the cross-sectional averaged tracer concentration are estimated from

$$\mu_p(t)=\int_{x=-\infty}^{\infty} x^p C(x,t)dx \tag{2.64}$$

where $\mu_p(t)$ = pth spatial moment after time t; x = longitudinal displacement; and p = 0, 1, 2, … etc. The spatial variance is

$$\sigma_x^2(t)=\frac{\int_{x=-\infty}^{\infty}\left(x-\bar{x}\right)^2 C(x,t)dx}{\int_{x=-\infty}^{\infty} C(x,t)dx}=\frac{\mu_2(t)}{\mu_0(t)} \tag{2.65}$$

and the location of the centroid is

$$\bar{x} = \frac{\int_{x=-\infty}^{\infty} xC(x,t)dx}{\int_{x=-\infty}^{\infty} C(x,t)dx} = \frac{\mu_1(t)}{\mu_0(t)} \tag{2.66}$$

This requires data measurement of spatial tracer profiles at a fixed time. Commonly in field data, tracer is measured over time at a fixed site (temporal profiles). The temporal moment can be estimated from

$$\nu_q(x) = \int_{t=-\infty}^{\infty} t^q C(x,t)dt \tag{2.67}$$

where $\nu_q(x)$ = qth temporal moment at the fixed location x; t is time and q = 0, 1, 2, … ect. The temporal variance is

$$\sigma_t^2(t) = \frac{\int_{t=-\infty}^{\infty} \left(t-\bar{t}\right)^2 C(x,t)dt}{\int_{t=-\infty}^{\infty} C(x,t)dt} = \frac{\nu_2(t)}{\nu_0(t)} \tag{2.68}$$

where the time of passage of the centroid is

$$\bar{t} = \frac{\int_{t=-\infty}^{\infty} tC(x,t)dt}{\int_{t=-\infty}^{\infty} C(x,t)dx} = \frac{\nu_1(t)}{\nu_0(t)} \tag{2.69}$$

Once the tracer cloud enters the equilibrium zone longitudinal dispersion can be determined either from

$$K_x = \frac{1}{2}\frac{d\sigma_x^2(t)}{dt} = \frac{1}{2}\frac{\sigma_x^2(t_2)-\sigma_x^2(t_1)}{t_2-t_1} \tag{2.70}$$

where t_1 and t_2 = times at which the spatial variances are determined, or

$$\begin{aligned} K_x &= \frac{1}{2}\frac{d}{dt}\left[U^2\sigma_t^2(x)\right] = \frac{1}{2}U^2\frac{\sigma_t^2(x_2)-\sigma_t^2(x_1)}{\overline{t_2}-\overline{t_1}} \\ &= \frac{1}{2}U^3\frac{\sigma_t^2(x_2)-\sigma_t^2(x_1)}{x_2-x_1} \end{aligned} \quad (2.71)$$

where $\overline{t_1}$ and $\overline{t_2}$ = times of passage of the centroid at sites 1 and 2; and x_1 and x_2 = locations of sites 1 and 2.

2.3.8 Mechanism of Transverse Mixing

Transverse mixing arises from both turbulence and vertical variations in transverse velocity (Boxall and Guymer, 2003). Transverse mixing dominates the mid-field zone and equation (2.59) is the depth-averaged mixing equation which is restated here

$$\frac{\partial \bar{c}}{\partial t}+\frac{\partial}{\partial x}\left(hu_z\bar{c}\right)+\frac{\partial}{\partial y}\left(hv_z\bar{c}\right)=\frac{\partial}{\partial x}\left[h\left(e_x+k_x\right)\frac{\partial \bar{c}}{\partial x}\right]+\frac{\partial}{\partial y}\left[h\left(e_y+k_y\right)\frac{\partial \bar{c}}{\partial y}\right] \quad (2.59)$$

where $\bar{c}$ = depth-averaged tracer concentration; h = local depth; u_z and v_z = depth averaged velocities in the x and y directions; e_x and e_y = turbulent diffusion coefficients in x and y directions; k_x = longitudinal dispersion coefficient (which accounts for the effects of vertical variations of longitudinal velocity); and k_y = transverse dispersion coefficient (which accounts for the effects of vertical variations of transverse velocity).

The depth averaged mixing equation (2.59) highlights that the transverse mixing is determined by two processes; turbulent diffusion or the turbulent eddy viscosity (quantified by the diffusivity e_y) and vertical variations in the transverse velocity (quantified by the dispersion coefficient k_y). These two coefficients arise from distinct processes but turbulent diffusion e_y is usually dropped considering that transverse dispersion coefficient k_y is much larger than diffusion (Rutherford, 1994).

Rutherford (1994) reported from a number of sources on transverse dispersion in natural channels that the transverse diffusion normalised by the product of the flow depth and shear velocity is in the following range for straight natural channels

$$0.15 \langle \frac{e_y + k_y}{Hu*} \langle 0.30 \tag{2.72}$$

and for gently meandering natural channels

$$0.3 \langle \frac{k_y}{Hu^*} \langle 0.9 \tag{2.73a}$$

$$u^* = \sqrt{gRS} \approx \sqrt{gHS} \tag{2.73b}$$

where H = mean depth; u^* = average shear velocity; R = hydraulic radius and S = bed slope. Shear velocity is commonly used to scale transverse mixing coefficient and this is suitable for wide open channel because the turbulence which drives transverse mixing is generated by vertical velocity shear due to bed friction.

Chau (2000) conducted experiments to investigate the transverse mixing coefficients in an open channel under different flow and bottom roughness conditions. In a straight rectangular channel, the parameters affecting the transverse mixing coefficients are cross-sectional averaged velocity (U), mean flow depth (H), width (W), shear velocity (u^*), fluid density (ρ) and viscosity (μ). This is shown in Fischer et al. (1979) as

$$\frac{k_y}{u^* H} = \Phi\left(\frac{u^*}{U}, \frac{W}{H}, \frac{\rho u H}{\mu}\right) \tag{2.74}$$

where k_y = transverse mixing coefficient. For high turbulent flows with rough boundaries, the effect of viscosity can be neglected. Hence, the relationship can be written as

$$\frac{k_y}{u^* H} = \Phi\left(f, \frac{W}{H}\right) \tag{2.75}$$

where f = Darcy-Weisbach friction factor. The calculation for complete mixing from a centreline (refer to equation 2.76a) and side discharge (refer to equation 2.76b) are given as

$$k_y = \frac{0.1UW_d^2}{L_m} \tag{2.76a}$$

and

$$k_y = \frac{0.4UW_d^2}{L_m} \tag{2.76b}$$

where W_d = dispersion width; L_m = length of the complete mixing. Dispersion width is defined as the width within which concentration values are higher than 5% of the mean concentration. Using linear regression for all data, an average value of the experimental results was found and given as

$$k_y = 0.18Hu^* \tag{2.77}$$

Chau (2000) commented that if this equation is used for practical purposes, the result is correct within an error band of approximately 30%.

According to Jeon et al. (2007) major factors which influence dispersion of pollutant in natural stream can be categorized into three groups: fluid properties, hydraulic characteristics of the stream and geometric configurations. The fluid properties include the fluid density (ρ) and fluid viscosity (μ). The cross-sectional mean velocity (U), shear velocity (u^*), channel width (W) and depth of flow (H) can be included in the category of bulk hydraulic characteristics. The bed forms (S_f) and sinuosity (S_n) can be regarded as the geometric configurations. The transverse dispersion coefficient can be related to these parameters as

$$k_y = \Phi\left(\rho, \mu, U, u^*, H, W, S_f, S_n\right) \tag{2.78}$$

By using Buckingham's Pi-theorem, a new functional relationship between normalized terms is derived as

$$\frac{k_y}{Hu^*} = \Phi\left(\frac{UH\rho}{\mu}, S_f, S_n, \frac{U}{u^*}, \frac{W}{H}\right) \tag{2.79}$$

where $UH\rho/\mu$ = Reynolds number; W/H = width to depth ratio and U/u^* = friction term. Bed shape factor S_f and sinuosity S_n indicates vertical and transverse irregularities in natural streams, respectively.

The effects of the bed shape (vertical irregularities of the natural stream) can be negligible and are included in the friction term. For fully turbulent flow in rough open channels, such as natural streams, the effect of the Reynolds number is also negligible thus equation (2.79) reduces to

$$\frac{k_y}{Hu^*} = \Phi\left(S_n, \frac{U}{u^*}, \frac{W}{H}\right) \tag{2.80}$$

Jeon et al. (2007) derived the new equation (2.81) by the least square method using a total of 32 data sets from 16 streams. Among those sets, 16 sets were used for deriving new equation, and the other 16 sets were used for verifying the equation.

$$\frac{k_y}{Hu^*} = 0.0291\left(\frac{U}{u^*}\right)^{0.463}\left(\frac{W}{H}\right)^{0.299}\left(S_n\right)^{0.733} \tag{2.81}$$

2.3.9 Mechanism of Vertical Mixing

In turbulent flow vertical mixing is caused by turbulence generated by the bed friction. As was described earlier in section 2.1.3 turbulent shear stress present in turbulent flow known as Reynolds stress and can be defined as

$$\tau_t = \rho \nu_t \frac{\partial \langle \bar{u} \rangle}{\partial z} \tag{2.82}$$

where τ_t = turbulent shear stress; ν_t = turbulent eddy viscosity and $\langle \bar{u} \rangle$ = time averaged mean velocity. It can be further defined in terms of the velocity fluctuations

$$\tau_t = -\rho \langle u'v' \rangle \tag{2.83}$$

where u' and v' = turbulent velocity fluctuations in the x and y direction. In plane turbulent shear flow (turbulent generated at the river bed) the shear stress varies linearly with depth and vanishes at surface so that a vertical profile of turbulent shear stress can be described by

$$\tau_t = \tau_\circ \left(1 - \frac{z}{h}\right) \tag{2.84}$$

where $\tau_\circ$ = the bed shear stress; z = distance from bed; h = water depth. Reynolds analogy states that the vertical eddy diffusivity similar to eddy viscosity

$$e_z \approx \nu_t \tag{2.85}$$

where e_z = vertical eddy diffusivity. Rearranging equation (2.84), (2.85) into (2.83) gives

$$e_z = \left[\tau_\circ \left(1 - \frac{z}{h}\right)\right] \Big/ \left(\rho \frac{\partial \langle u_x \rangle}{\partial z}\right) \tag{2.86}$$

Assuming that velocity varies logarithmically with depth and the vertical eddy diffusivity is given by

$$e_z = \kappa u^* z\left(1 - \frac{z}{h}\right) \tag{2.87}$$

where κ = von Karman's constant. The vertical diffusivity varies parabolically with depth, vanishing at both the bed and the water surface.

The three-dimensional advection-diffusion equation is given by

$$\frac{\partial c}{\partial t} + u\frac{\partial c}{\partial x} + v\frac{\partial c}{\partial y} + w\frac{\partial c}{\partial z} = e_x\frac{\partial^2 c}{\partial x^2} + e_y\frac{\partial^2 c}{\partial y^2} + e_z\frac{\partial^2 c}{\partial z^2} \tag{2.88}$$

If a tracer is injected from a steady transverse line source, equation (2.88) can be simplified to

$$u\frac{\partial c}{\partial x} = \frac{\partial}{\partial z}\left(e_z\frac{\partial c}{\partial z}\right) \tag{2.89}$$

where u and e_z are both constant. In uniform plane flow u and e_z do not vary transversely or with distance downstream, but both vary with depth.

2.4 Effect of Vegetation on Mixing

This section will review the effect of vegetation on longitudinal, transverse and vertical mixing based on selected related studies.

2.4.1 Effect of Vegetation on Longitudinal Mixing

Nepf et al. (1997) studied the influence of emergent vegetation on longitudinal dispersion in a laboratory flume for three cross-sectional averaged flow velocities (i.e. 2.9, 5.5 and 7.4 cm s^{-1}) and three plant population densities (SVF was equal to 1 %, 1.5 % and 5.5 %) with stem Reynolds numbers (Re_d) ranged from 170 to 440. SVF (ϕ) is the ratio of solid volume of blockage per unit volume of flow as been defined in section 2.2.1. Vegetation was emulated using rigid rods in random arrangements. In the case of no rods, the longitudinal dispersion coefficient agrees with previously reported values of dispersion coefficient and is within the range 1.0 cm^2s^{-1} uncertainty. In contrast for all cases with rods, the predicted dispersion coefficient from the proposed equation (2.89) is less than the observed. It was suggested that the reduction in dispersion is caused by the recirculation zone behind each stem trapped and delayed a fraction of mass enhancing the longitudinal dispersion and for high plant population density, mechanical dispersion (see equation (2.90)) which is defined as the dispersive process caused by dense obstructions may also be important factor. In mechanical dispersion the fluid elements, may start at the same longitudinal position but ends up separate by a distance due to differences in the path lines through the array. Nepf et al. (1997) also commented that within sparse arrays of cylinders (SVF < 10%) vortex shedding is thought to be delayed until the stem Reynolds number is greater than 200.

$$K_x = -\frac{1}{hK_z}\int_0^h u'\int_0^z\int_0^z u'dzdzdz = \frac{I}{K_z} \tag{2.89}$$

$$K_d = \frac{\sigma^2}{2T_m} \tag{2.90a}$$

$$T_m = \frac{L_x}{u} + N_s Ddt \tag{2.90b}$$

where K_x is the longitudinal dispersion coefficient; K_z is the vertical dispersion coefficient; I reflects the mean shear in the velocity profile; K_d is the mechanical dispersion coefficient; σ is spatial variance of the particles released within an array; T_m is the mean time for the particle to traverse the array; L_x is the total length of the dowel array; N_s is the step size chosen by dowel to traverse the array and D is the probability the particle encounter a stem.

Lightbody and Nepf (2006) studied the dispersion processes arising from stem scale and depth scale velocity heterogeneity, which are important within regions of vegetation characterized by a single morphology for emergent conditions. Within such regions, depth scale and stem scale dispersion processes contribute additively and dominate the total longitudinal dispersion K_x

$$K_x = K_d + K_h \tag{2.91}$$

where K_d is the mechanical dispersion resulting from velocity heterogeneity on the scale of the stem diameter. When every particle has sampled a sufficient number of wakes, this process reaches a Fickian limit and K_d achieves a constant value. K_h is the depth shear dispersion produces by depth scale heterogeneity. Once a cloud of material has spread over depth, so that the vertical heterogeneity in velocity has been fully sampled, the Fickian limit is reached and K_h will be constant. Lightbody and Nepf (2006) proposed

$$K_d = \frac{1}{2} C_d^{3/2} ud \tag{2.92}$$

where C_d = vegetation drag coefficient; u = longitudinal flow velocity spatially averaged over a horizontal scale; d = stem diameter. K_h is given by Taylor's analysis (Fischer et al., 1979) and is defined as

$$K_h = -\frac{1}{h}\int_0^h u' \int_0^z \frac{1}{e_z} \int_0^z u' dzdzdz \tag{2.93}$$

where $u'(z) = u(z) - u_z$ is the deviation from depth-averaged velocity u_z; e_z = vertical diffusion.

Near the tracer source, depth shear dispersion K_h is much larger than stem shear dispersion K_d. Lightbody and Nepf (2006) laboratory results indicated that stem shear dispersion K_d can be neglected at the distance of 80 cm from the point released (non Fickian distance). From calculation it was estimated that $K_x/u_h h \approx K_h/u_h h$, but an order magnitude smaller if compared with what would be observed if the Fickian limit is reached.

Shucksmith et al. (2010) planted natural vegetation (i.e. reed and carex) within laboratory channel and series of experiments quantifying velocity, turbulence and longitudinal mixing were conducted over a series period of time to allow vegetation growth to measure the impact of the vegetation growth to longitudinal mixing. Even though is not the main focus of the present study to go into details on real vegetation behaviour, but nevertheless data from Shucksmith (2008), reflects the complexity nature of the real vegetation on mixing process. Shucksmith (2008) study how the vegetation age affect the mixing processes, for that carex and reeds were grew in a flume. The vegetation was arranged in a staggered formation of two to three plants in a row with the initial planting of 2.5 plants per metre length. Shucksmith (2008) measured the width of the plant at the base as the stem diameter in which carex was about 0.05 m to 0.056 m diameter meanwhile 0.002 m to 0.003 m diameter for reeds depending on the age of the vegetation.

According to Shucksmith et al. (2010) distributing emergent vegetation evenly over the entire width of a natural channel will reduce the spatial variation of velocity over the channel width and depth and the magnitude of Reynolds stress. In such conditions a reduced longitudinal mixing coefficient would be expected relative a non-vegetated channel due to the reduced velocity shear. Theoretically the dominant factor influencing mixing in emergent conditions will be the degree of reduction in spatial variation of velocity over the channel cross-section. In artificially vegetated systems where much of the previous research has been conducted using cylindrical rods set in regular arrangements and hence the distribution of plant blockage over the width and depth is relatively uniform, mixing has been shown to be dominated by stem scale processes, characterized by stem generated Reynolds stresses.

Shucksmith et al. (2010) also suggested for emergent vegetation which mixing is dominated by stem scale processes it may be suitable to scale mixing against a parameter which includes spatially-averaged horizontal Reynolds stress such as $\sqrt{\langle \overline{u'v'} \rangle}$. For comparison purposes longitudinal mixing coefficients were plotted against flow depth and velocity shear $\left(hu^*\right)$, cross-sectional averaged velocity and flow depth (Uh) and Reynolds stress and flow depth $\left(\sqrt{\left(\overline{u'v'}\right)}h\right)$. Values obtained from a linear best fit relationship suggested that no definite relationships between the longitudinal mixing and the aforementioned parameters were found but in general, mixing appears to decrease as the scaling parameters increase.

2.4.2 The Effect Vegetation on Transverse Mixing

Transverse mixing is dominated by turbulence and secondary currents. In vegetated channels it may be expected that secondary currents will be damped somewhat by the presence of vegetation and increased flow resistance (Shucksmith, 2008). Vegetation arrangements are thought to convert mean kinetic energy into turbulent kinetic energy within the stem's wake and this is illustrated by the increase in turbulence intensity in the wake region. Since the turbulence is produced by the stem the characteristic length scale of turbulence is determined by the stem's diameter within the array or plant arrangement. Nepf (1999) defined turbulent diffusivity as

$$K_t = \alpha_1 \sqrt{k} d \tag{2.94a}$$

and

$$\frac{\sqrt{k}}{U} = \alpha_2 \left(\overline{C_D} a d\right)^{1/3} \tag{2.94b}$$

where d = stem diameter; k = turbulent kinetic energy and α_1, α_2 = scale factor related to array drag and turbulent kinetic energy and since these is not isotropic, therefore the scale factor will differ for vertical and horizontal diffusion. Nepf (1999) results from experiments conducted with rigid rods in a random arrangement show that the turbulence intensity ($\sqrt{k}/U$) could be predicted reasonably well using the above drag model (equation (2.94b)), however observed diffusion rates were greater than those predicted by the turbulent diffusion model alone (equation (2.94a)). To explain the difference, Nepf (1999) introduced the process of mechanical diffusion for vegetated flows, which was defined earlier in section 2.4.1. Nepf's model of mechanical diffusion may be described with the aid of Figure 2.09. Particles are released at (x,y) = ($0,0$) and advected through the array at a mean velocity, U. At each time interval, Δt the particles move downstream a distance of $\Delta x = U\Delta t$. At the same time each particle has probability $[a\Delta x]$ of encountering a stem, and if a stem is encountered the particle is forced to move right or left along the y axis with $\Delta y = \beta d$ where β is a scale factor.

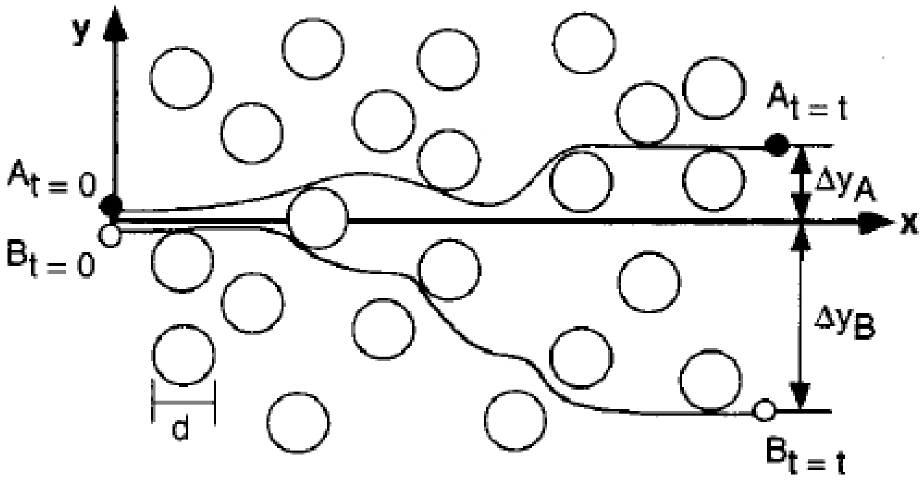

Figure 2.09 Mechanical diffusion arises from the physical obstruction of the flow by the stems (reproduced from Nepf (1999)).

After N_s steps where N_s is large, the lateral (y) position of individual particles is given by Gaussian probability distribution with variance where

$$\sigma^2 = \left[\frac{a\Delta x(\beta d)^2 t}{\Delta t}\right] = \beta^2 [ad] Udt \qquad (2.95a)$$

$$a = md = \frac{dh}{\Delta S^2 h} = \frac{d}{\Delta S^2} \qquad (2.95b)$$

where a = frontal vegetation area (per metre); ΔS = mean spacing between cylinders; m = number of cylinders per unit area.

For a large number of particles this model describes the Fickian diffusion process for which the variance of the particles increases linearly with time, such that the mechanical diffusion may be taken to be

$$K_d = \frac{\beta^2}{2}\left[ad\right]Ud \tag{2.96}$$

Process of mechanical and turbulent diffusion are independent, and thus their contribution to the total lateral diffusion are additive

$$K_y = K_t + K_d \tag{2.97}$$

And rearranging equation (2.94) and (2.96) gives

$$\frac{K_y}{Ud} = \alpha\left(C_D ad\right)^{1/3} + \left(\frac{\beta^2}{2}\right)ad \tag{2.98}$$

Serra et al. (2004) described wake area generated by a distributed plant array of stem diameter, *d* and width of the wake, w_w as shown in Figure 2.10. The number of stems per unit area, *m* can be related to characteristic distance between the stems, *S* as

$$m = \frac{G}{S^2} \tag{2.99}$$

where G = geometry factor of the plant distribution.

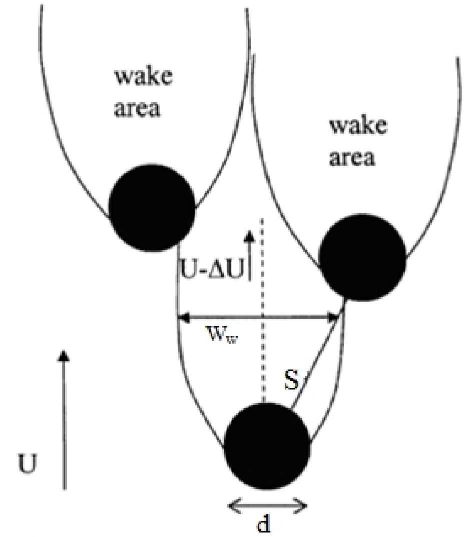

Figure 2.10 Schematic diagrams of wakes generated by cylinders (reproduced from Serra et al., 2004)

It is known that flow behaviour is controlled by the stem Reynolds number and according to Serra et al. (2004) the velocity field is also influenced by the ratio of the stem diameter to the characteristic distance between the stems (d/S). The vegetation provides an additional source of drag to the flow which the drag force per unit length F_D can be related to the deficit velocity in the wake and the width of the wake as

$$F_D \propto \rho\left(\left(U-\Delta U\right)w_w\right)^2 \qquad (2.100)$$

where ρ is the fluid density; w_w = width of the wake and drag coefficient as

$$C_D = F_D \frac{1}{2}\rho U^2 d \qquad (2.101)$$

The wake of a given element can interact with a downstream element located at a distance of stem diameter, *d* and the transverse velocity, *V* induced by the stem can be estimated as

$$V \propto \frac{\Delta U w_w}{S} \propto \frac{C_d U d}{S} \qquad (2.102)$$

The transverse diffusion coefficient K_y can be related to the transverse velocity (*V)* and to the transverse scale of the flow. There are two possible transverse length scales, the stem diameter d and the characteristic distance between stems (*S).* Serra et al. (2004) propose that near the stem, the wake width is related to the stem diameter and it grows in laminar flow according to

$$\delta \cong \sqrt{v\xi / U} \tag{2.103}$$

where δ is the incremental growth beyond stem diameter (*d)* at a downstream distance, ζ. In cases of wetlands where plant stems are densely distributed, the incremental growth δ is small compared to the stem diameter *d*. Hence since Serra et al. (2004) focused their investigation on stem Reynolds numbers in the range of 10 to 100 they considered the stem diameter *d* to be the most appropriate parameter to scale the diffusivity and therefore proposed

$$K_y = \beta C_d U \frac{d^2}{S} \text{ or } \frac{K_y}{Ud}\frac{S}{d} = \beta C_d \tag{2.104}$$

where β is a dimensionless constant which experimentally shown approximately 1. Normalized transverse diffusion (K_y/Ud) data from Serra et al. (2004) and result from the low Reynolds number of Nepf et al. (1997) are plotted as a function of $(d/S)^2$ and result shows that mechanical diffusion model by Nepf (1999) slightly underestimate the experimental data, however the general trend show a reasonable agreement with Nepf's prediction.

The experimental set up for this study was designed to mimic the Tres Rios constructed wetland located in Pheonix, Arizona. The vegetation densities examined, in terms of SVF were 10 %, 20 % and 35 % with low stem Reynolds number (10 to 100). Compared to the data sets from Nepf's study (1999) where vegetation densities varied from SVFs of 0.6 % to 6 % and higher stem Reynolds number (i.e Re_d >≈200).

Tanino and Nepf (2008) conducted an experimental study to measure the transverse dispersion in random arrays of emergent cylinders with SVF ranging from 1 % to 35 %. Experiments were conducted at stem Reynolds numbers between 30 and 700. This research also introduced pore Reynolds number as given by equation (2.105) which is based on the pore velocity, U_p and mean pore scale, s or surface to surface distance between the neighbours of cylinders. The pore velocity is the average of velocity, u over all fluid volume within the array and is determined as $U_p=Q/(HW(1-\phi)$ where Q is the volumetric flow rate, H is the mean water depth and W is the width of the laboratory flume in which the array was contained (Tanino and Nepf, 2008).

$$\mathrm{Re}_s = \frac{U_p s}{\nu} \tag{2.105}$$

Experimental results showed that transverse dispersion is independent of pore Reynolds number for pore scale Reynolds numbers greater than 250. The transverse dispersion coefficient was normalised by the product of the pore velocity, U_p and the stem diameter i.e. $K_y / U_p d$. It was reported that the normalised transverse dispersion coefficient increased rapidly for SVFs in the range of 0 % to 3.1 %, decreases in the range of SVFs from 3.1 % to 20 % and then increased again more gradually for SVF 20 % to 35 %.

Tanino and Nepf (2008) associate solute transport in random arrays with temporal and spatial fluctuation and is expected to be linear sum of three coefficients, which includes spatial fluctuation, the temporal fluctuation and the mechanical diffusion. Therefore Tanino and Nepf (2008) proposed a net transverse dispersion model which is the linear superposition of the turbulent diffusion model and dispersion model due to the spatially heterogeneous velocity field. Mechanical diffusion is not considered because it is negligible in the turbulent flow.

Tanino and Nepf (2008) commented that this model can accurately describe the normalized transverse dispersion calculated from observation experimental results, and proposed that the net transverse dispersion is based on two assumptions: only turbulent eddies with characteristic length greater than stem diameter $(l_e \geq d)$

contribute significantly to net lateral dispersion and neighbouring cylinder centres must be farther than *2d* from each other for the pore space to contain such eddies. The net transverse dispersion model proposed is given by equation (2.106)

$$\frac{K_y}{\langle\bar{u}\rangle d} = \gamma_1 \frac{4}{\pi} \phi \left\langle \frac{\sqrt{k}}{\langle\bar{u}\rangle} \right\rangle P_{snc\rangle r^*} \frac{\langle s_n^2 \rangle_{snc\rangle r^*}}{d^2} + \gamma_2 P_{snc\langle 5d} \frac{\pi}{4096} \left(\frac{d^2}{k_\perp} \right)^{3/2} \frac{1-\phi}{\phi^2} \qquad (2.106)$$

where ϕ = cylinder volume fraction; m = number of cylinders per unit area; s_{nc} = centre to centre distance to the nearest neighbour cylinder; k = turbulent kinetic energy per unit mass; $P_{snc\rangle r^*}$ = fraction of cylinders with a nearest neighbour farther than r^*; $P_{snc\langle 5d}$ = fraction of cylinders with a nearest neighbour less than $5d$; $r^* = 2d$ and γ = scaling constant. Good agreement with this model and experimental observation was found and this supports the two assumptions of the net transverse dispersion model which are given above.

Table 2.2 List of parameters used in the net transverse dispersion model by Tanino and Nepf (2008) in equation (2.106)

Parameters	Definition
$\left\langle \frac{\sqrt{k_t}}{\langle\bar{u}\rangle} \right\rangle \approx \left\langle \frac{\sqrt{k_t}}{U_p} \right\rangle = \begin{Bmatrix} 1.1\left[C_D^{form} \frac{l_t}{d} \frac{\phi}{(1-\phi)\pi/2} \right]^{1/3} \\ 0.88\left[C_D^{form} \frac{\langle S_n \rangle_A}{d} \frac{\phi}{(1-\phi)\pi/2} \right]^{1/3} \end{Bmatrix}$	Turbulence intensity
$C_D^{form} = 2\left[(0.46 \pm 0.11) + (3.8 \pm 0.5)\phi\right]$	Inertial contribution to the mean drag (in the direction of the mean flow).
$P_{s_{nc}>r*} \equiv P\left(\pi r^{*2} < a < \infty\right) = \int_{\pi r^{*2}}^{\infty} \left(f(a;\lambda)da\right) = \frac{e^{-\lambda\pi r^{*2}}}{e^{-\lambda A_L}}$	The probability that a cylinder in the random array has its nearest neighbour farther than $r = r^*$.

$P_{sn_c<5d} \equiv P\left(0 < a < \pi(sd)^2\right) = 1 - \frac{e^{-25\lambda\pi d^2}}{e^{-\lambda A_L}}$	The probability that a cylinder has its neighbour within $r = 5d$.
$\left\langle s_n^2 \right\rangle_{s_{nc}>r^*}$	S_n is the distance surface to surface of the nearest neighbour farther than r^*.
$U_p = \frac{Q}{\left[\left\langle \overline{H} \right\rangle W(1-\phi)\right]}$	Pore velocity
$A_L = \pi r_e^2 = \pi d^2 \left\{\frac{2}{\pi}\left[\sqrt{2} + \ln\left(1+\sqrt{2}\right)\right]\right\}^{2/3}$	A circular invalid area for a cylinder.
$\lambda = \frac{N_c}{A}$	Number of random coordinates generated per unit area.
$k_\perp \approx \left\langle s_n \right\rangle_A$; this is valid for sparse vegetation	Permeability

In predicting the contribution of transverse dispersion from turbulent diffusion, fully turbulent flow is referred to flow that has achieved the maximum mean turbulence intensity and is therefore independent of the stem Reynolds number (Tanino and Nepf, 2008). This model predicts that for SVF greater than 19 %, turbulent diffusion makes a negligible contribution to the normalised dispersion coefficient ($K_y/U_p d$) and consequently the contribution from the time-averaged, spatially heterogeneous velocity field dominates. In a dense array, physical reasoning suggests that the time-averaged velocity field are determined primarily by the local cylinder configuration which is independent of the stem Reynolds number.

Conversely for solid volume fractions of less than 19 % in fully turbulent flow, Tanino and Nepf's model (2008) predicts that the turbulent diffusion makes a contribution to the normalised dispersion coefficient ($K_y/U_p d$). Since turbulent diffusion must decrease as Re_d decreases, the theory suggests that the normalised dispersion coefficient will also decrease with decreasing Re_d while the flow remains turbulent (Tanino and Nepf, 2008).

2.4.3 Effect of Vegetation on Vertical Mixing

Nepf et al. (1997) examined the vertical and horizontal diffusivity within an array of emergent cylindrical rods using a continuous injection technique. Continuous dye was injected into the flume channel through a 1.6 mm stainless steel tube at mid-depth and mid-width channel using a syringe pump. 6 mm and 12 mm rod diameter were used to construct five sets vegetation densities including SVF of 0.6 %, 1.4 %, 1.7 %, 3.5 % and 5.3 %. Only one size rod was used at a time and in a random configuration. Series experiment was conducted within stem Reynolds numbers of 66 to 1800.

Analysis shows that vertical diffusivity, e_z have a significant (with regression coefficient, $R^2 = 0.93$ for 12 points) linear correlation with stem Reynolds number (Re_d) and wake fraction (WF). Therefore equation of vertical diffusivity, e_z based on the transverse diffusivity, e_y was proposed

$$e_y = AU_f dWF \tag{2.107}$$

where A = scale factor and was assumed as equal to 1; U_f = free stream velocity and WF = wake fraction and is a function of turbulent wake area to stem area ratio, M and stem area density. However, differences may exist in the characteristic of wake diffusivity, in particular the scale for vertical wake diffusivity (A_z) compared to A in equation (2.107). Experiments result showed that the ratio of scale factors ($A/A_z = 4$) suggested that the turbulent transport within the wake was anisotropic, with transverse transport four times greater than its vertical counterpart. This is likely to arise from the anisotropy in cylinder shape and possibly due to the ratio of the cylinder diameter to flow depth ratio (d/h values of at least 0.06 were examined).

Nepf et al. (1997) also commented that eddy scale is set by stems size, which in turn larger cylinder produce larger eddy scale that create greater turbulent transport. For sparse vegetation there is a possibility that the contribution of bed turbulence generated turbulence is not negligible as was assumed.

Lightbody and Nepf (2006) conducted a field study in a wetland of emergent salt marsh. The vertical diffusion was predicted using the Nepf model (1999) given by

$$e_z = \alpha\sqrt[3]{C_d a d} U d \qquad (2.108a)$$

$$a = \frac{d}{\Delta S^2} \qquad (2.108b)$$

where α = proportionality constant and from laboratory data suggest that α is about 0.1 to 0.2; C_d = drag coefficient; a = frontal vegetation area; ΔS = distance between stems; d = stem diameter and U = spatial average velocity over a horizontal scale large enough to eliminate stem-scale heterogeneity.

The field measurements (K_z/Ud = 0.17 ± 0.08 for ad = 0.005 – 0.010) agreed with Nepf's model (1999) within exceptable experimental uncertainty. This study also indicates that the vertical diffusion is strongly linked to stem density as shown in equation (2.108) which relates the spatial average velocity, U and stem morphology (i.e. frontal vegetation area, a and stem diameter, d).

Higher vertical diffusion was measured in the field study (Lightbody and Nepf, 2006) compared to the laboratory study reported in Nepf et al. (1997) and it was suggested that this was likely as result from the stems and branches of the real vegetation compared to the idealised vertical orientation of the cylindrical rods in the laboratory study.

2.5 Summary

This chapter begins with presentation some of the main theoretical understanding for open channel flow and solute mixing processes. Then review on selected previous work was also presented including the impact of vegetation on the flow parameter and the impact of vegetation on the longitudinal, transverse and vertical mixing processes, which more emphasise will be on the transverse mixing process in emergent vegetated channel.

Current research aims to fill the gap between the previous studies for example present experiment used dowel size of 25 mm and 18 mm with either aligned or staggered arrangement. While Nepf et al. (1997); Nepf (1999); Serra et al. (2004) and Tanino and Nepf (2008) implement random vegetation for the dye tracer test with cylinders diameter 6.4 mm (Nepf, 1999; Tanino and Nepf, 2008) and 10 mm (Serra et al., 2004).

Previous researcher used various range of vegetation density, including solid volume fraction of 1 %, 1.5 % and 5.5 % for Nepf et al. (1997), 0.8 % to 7 % for Nepf (1999), 10 %, 20 % and 35 % for Serra et al. (2004) and 1 % to 35 % for Tanino and Nepf (2008), whereas current experiment applied vegetation density from 0.51 % to 7.8 %.

There were many flow regimes that have been studied, for example Serra et al. (2004) concentrate on the low flow with stem Reynolds number ranging from 10 to 100. Others like Nepf et al. (1997) used both high and low Reynolds number flow (i.e. 66 to 1800). Similar to Tanino (2008) which cover both in the experimental work high and low stem Reynolds number between 60 and 770. While this thesis will look into flow regime between Reynolds number 1000 to 3000.

To summarize, present experimental study used cylinders which were arranged in staggered and aligned configuration creating six vegetation densities from 0.51 % to 7.8 %. Experiment also used considerably high flow with stem Reynolds number from 1000 to 3000. This experiment was designed to fulfil the research objectives describe in Chapter 1 and to fill the gaps between the research areas of transverse mixing study.

Chapter 3 – Laboratory Set-up and Data Collection

3.0 Introduction

This chapter describes the facility, instrumentation and measurement techniques used in the experimental work required to fulfil the aims described in Chapter 1. In this chapter the facility and programme of experiments will be first presented. Sections describing the measurement methods and techniques in order to quantify the following parameters: flow depth, flow rate, velocity and turbulence statistics, and the transverse dispersion coefficient will then follow. The final section described the method used for the transverse mixing analysis.

3.1. Flume Facility

Experimental work was carried out in the Hydraulics Laboratory of Cardiff University using a flume of 10 m length, 1.2 m width and 0.30 m depth (see Figure 3.1). The flume is attached to a re-circulating reservoir and pipe system and to a centrifugal pump operates to continuously supply water from a reservoir tank to the flume. The reservoir tank is located underneath the flume and has a capacity of 8 m^3.

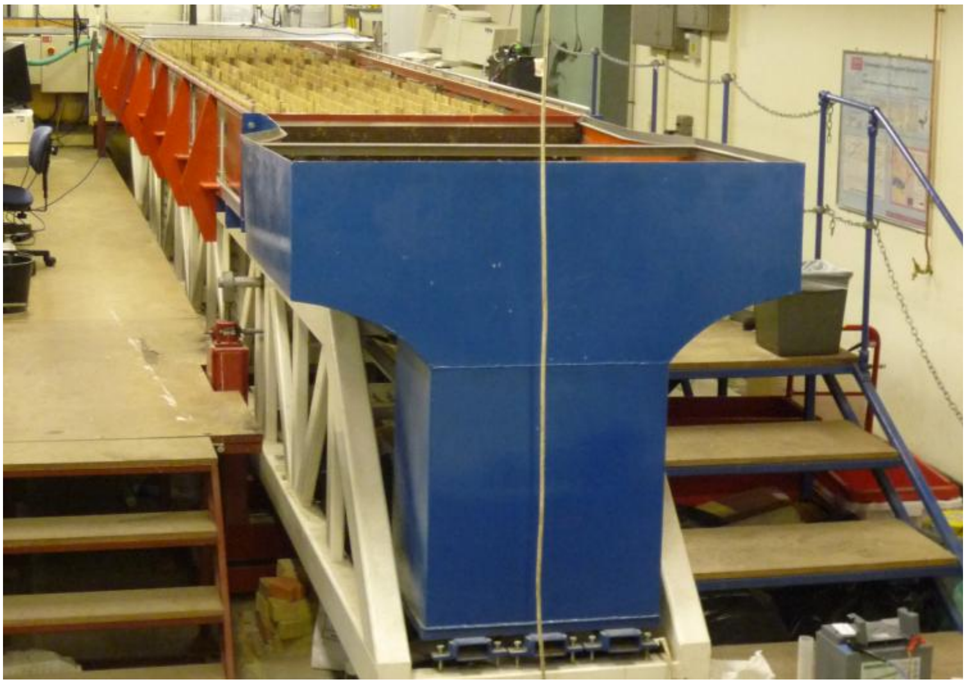

Figure 3.1 View of the flume system from the upstream end of the flume

The flow delivered to the flume is controlled by two valves. One valve is connected to a 50 mm diameter pipe and the second valve is connected to a 200 mm diameter pipe. These valves are controlled electronically through a control panel (see Figure 3.2) and their opening can be adjusted.

The flow conveyed to the flume was measured using a propeller type flow meter which was installed in the delivery pipe and the number of revolutions per minute are measured using a logging system manufactured by inflow, INC and known as a Flow Automation 4000 Series (see Figure 3.3). As the flow enters the flume at the upstream end it is delivered to a stilling area before it enters a honeycomb straightening section which is 50 mm long. At the downstream end the water surface profile is controlled by a vertical tailgate weir. The flow then enters the reservoir and is re-circulated to the upstream end of the flume.

Figure 3.2 Valve control panel

Figure 3.3 Flow Automation 4000 Series

The longitudinal bed slope and measurement rails of the flume were adjusted to a gradient of 0.001. This was set by adjusting two supports located at the two pivoting section of the flume. The bed and side wall are constructed from glass with steel frames. A sheet of PVC material with series of holes was attached to the glass bed allowing the simulated vegetation to be slotted in to place. Flume holes were located laterally every 60 mm (hole centreline to hole centreline) and a total of 20 holes were constructed in each row across the 1.2 m flume width. The longitudinal distance between each row of holes was 105 mm (centre to centre) and in total there were 88 rows of holes along the full length of the flume. Six vegetation densities were examined in the experimental programme and details of each experiment are presented in Table 3.1.

Canopies of emergent vegetation elements were simulated using arrays of rigid rods of uniform diameter configured in a number of arrangements. Rods were constructed from wooden dowels of diameters (d) 25 mm and 18 mm. The rods were 300 mm and 180 mm in length respectively for 25 mm diameter rods and 18 mm diameter rods. The parameters δx and δy present the distance between rods centre to centre in the longitudinal and lateral flow directions respectively. The dowels were arranged in both aligned and staggered arrangement and in some experiments two different of rods were used in the same arrangement (see Figure 3.4 (a) to (d) and Table 3.1).

Table 3.1 Experimental details where the rod configuration covers the complete length of flume. In the test name, *S* denotes staggered, *A* represent aligned and *M* indicates mixed rods diameter used in the vegetation arrangement; δ_x and δ_y are the longitudinal and transverse distance of the control volume; *S* is the spacing surface to surface between two nearest cylinders; *d* is the stems diameter; *m* is the numbers of cylinders per metre square; *Q* is flow discharge; *h* is the flow depth; U_p is the pore velocity; *U* is the mean area velocity; Re_d is the stem Reynolds number; Re_s is the pore Reynolds number.

Test Name	SVF Φ (%)	Rod alignment	d (mm)	δ_x (m)	δ_y (m)	S (m)	$\frac{d}{S}$	m (m^{-2})	N_r	Q (m^3/s)	h (m)	h/d	U_p (m/s)	U (m/s)	Re_d	Re_s
0.51S	0.505	Staggered	18	0.210	0.12	0.224	0.080	19.8	5	0.017	0.090	5	0.158	0.157	2,826	35,392
0.97S	0.974	Staggered	25	0.210	0.12	0.217	0.115	19.8	5	0.016	0.135	5.4	0.100	0.099	2,475	21,700
2.96AM	2.958	Aligned (mixed d)	18,25	0.105	0.12	0.084	0.256	81.5	10	0.006	0.064	2.98	0.081	0.078	1,677	6,804
3.90A	3.896	Aligned	25	0.105	0.12	0.080	0.313	81.5	10	0.015	0.145	5.8	0.090	0.086	2,150	7,200
5.92AM	5.915	Aligned (mixed d)	18,25	0.105	0.06	0.039	0.551	163.0	20	0.006	0.121	5.63	0.044	0.041	881.5	1,716
7.79A	7.792	Aligned	25	0.105	0.06	0.035	0.714	163.0	20	0.015	0.257	10.28	0.053	0.049	1,225	1,855

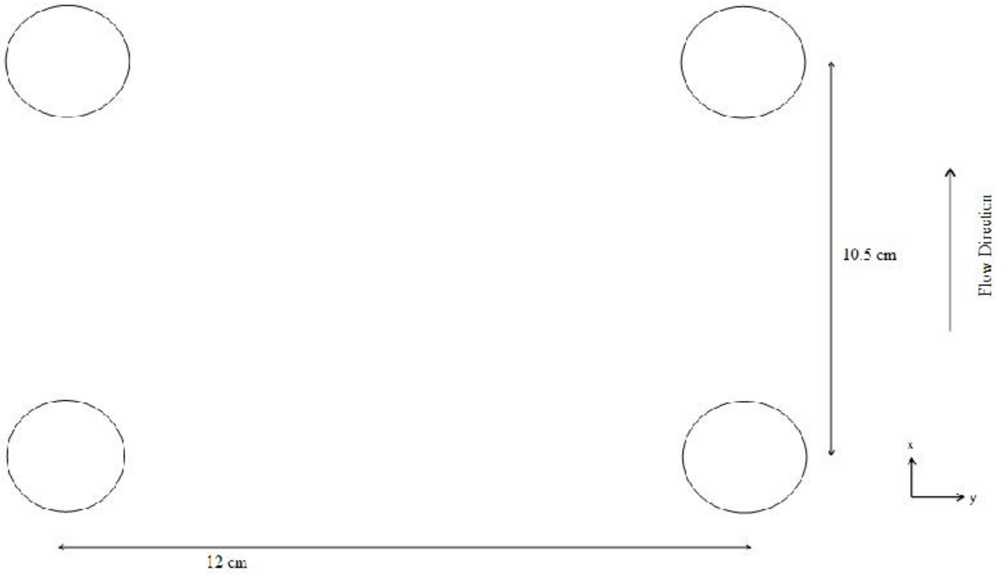

Figure 3.4 (a) Aligned arrangement control volume for test 3.90A (SVF = 3.896 %)

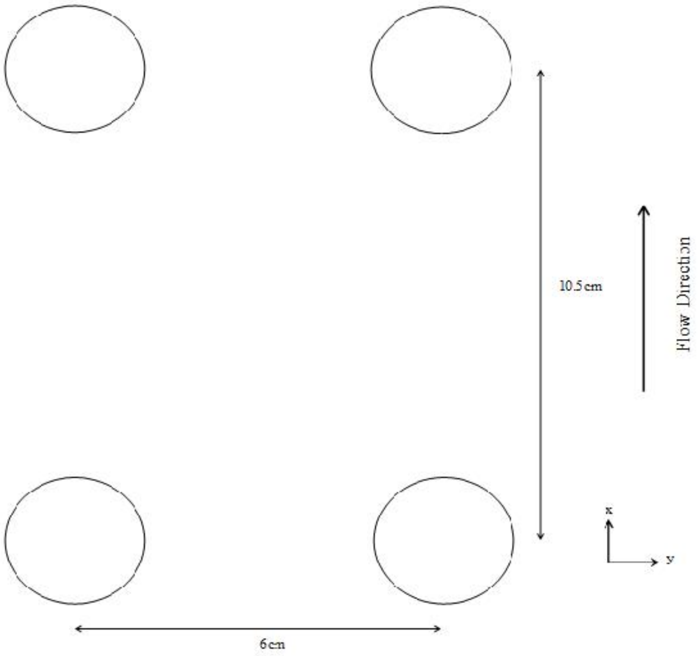

Figure 3.4 (b) Aligned arrangement control volume for test 7.79A (SVF = 7.792 %)

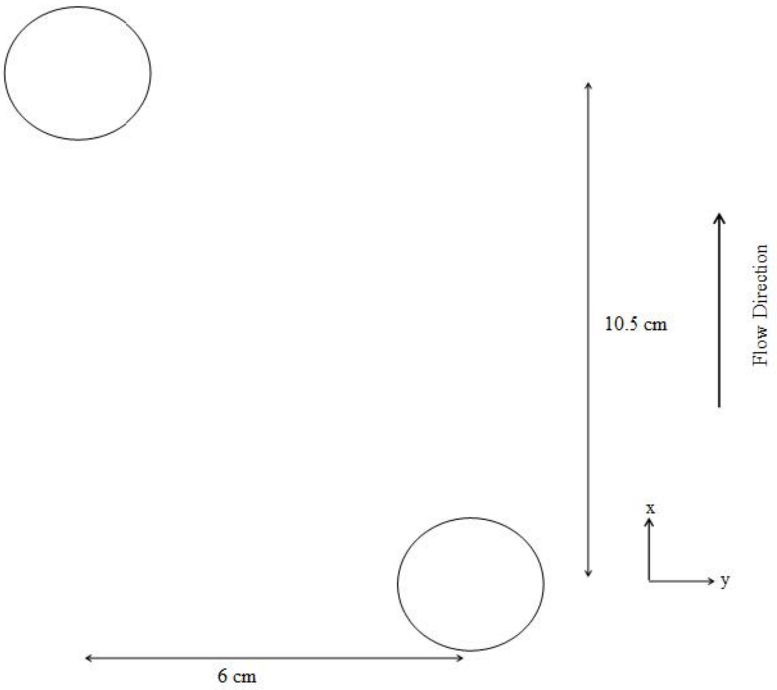

Figure 3.4 (c) Staggered arrangement control volume for test 3.90S (SVF = 3.896 %)

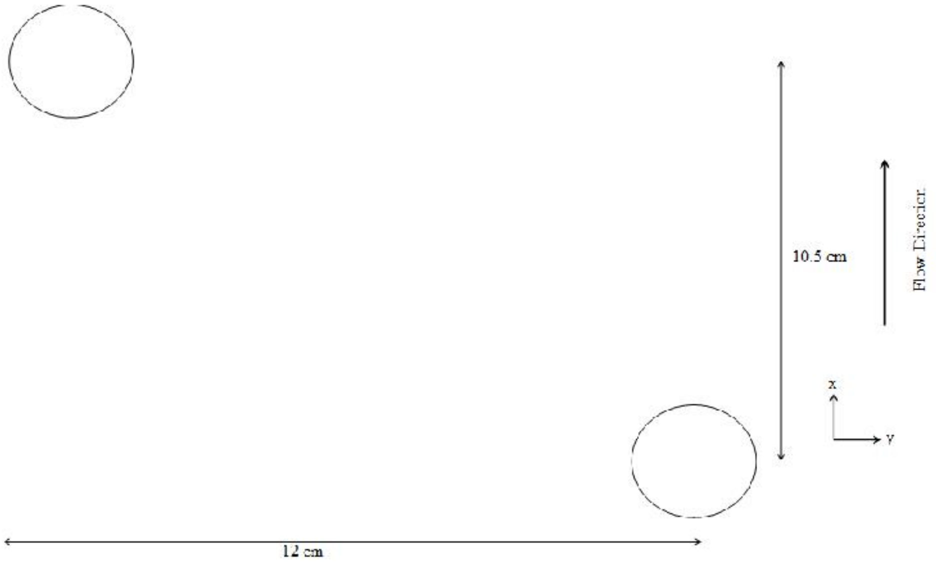

Figure 3.4 (d) Staggered arrangement control volume for test 0.97S (SVF = 0.974 %)

The density of the rods can be defined by the parameter Solid Volume Fraction (*SVF* or ¤), number of rods per square metre (*N*) and number of plants in a row (N_r) whereby *SVF* (¤) as previously mention in section 2.2.1 is the ratio of solid volume of blockage per unit volume of flow as shown in equations (3.1a) and (3.1b) where *d* is the rod diameter.

$$\mathrm{SVF\,(linear)} = \text{¤} = \frac{\text{®}d^2}{4\delta_x \delta_y} \times 100\% \tag{3.1a}$$

$$\mathrm{SVF\,(staggered)} = \text{¤} = \frac{\text{®}d^2}{8\delta_x \delta_y} \times 100\% \tag{3.1b}$$

Figure 3.5 (a) shows the aligned arrangement of rods in the laboratory flume for test 3.90A and Figure 3.5 (b) displays the staggered vegetation for test 0.97S.

Figure 3.5 (a) Rods in aligned arrangement for test 3.90A

Figure 3.5 (b) Rods in staggered arrangement for test 0.97S

3.2. Experimental Programme

As described earlier in Chapter 1 in order to fulfil the main objective of the thesis dye tracer experiments were conducted in order to investigate the impact of the vegetation density at high stem Reynolds numbers (1000+) on the transverse mixing characteristics in open channel flow. Furthermore in order to understand the flow mechanics in greater detail concurrent velocity and turbulence statistics within the control volume were measured for selected set-ups. As discussed in Chapter 2 the transverse dispersion is usually quantified by the transverse mixing coefficient (Ky).

A tracer was injected continuously at a point located at mid-flow depth between two cylinders along the flume centreline at injection point (see Figures 3.6 and 3.7). Figures 3.6 (a) to (f) present the position of the injection point and the location of cross-section 1 (C1), cross-section 2 (C2) and cross-section 3 (C3) where the dye were sampled transversely across the flume. Prior to the tracer experiment, a tank of 75 litres of 1000 ppb dye tracer concentration was prepared and this tank was located next to the injection cross-section (see Figure 3.7).

The delivery tube conveying the injection concentration was 5 mm in diameter and the injection rate was controlled by a centrifugal pump (see Figure 3.7). The pumping rate was manually controlled using a valve and this was set at a flow rate which corresponded to a similar area mean velocity to the test flow condition. This was important to minimise the additional mixing due to injection momentum (Shucksmith, 2008).

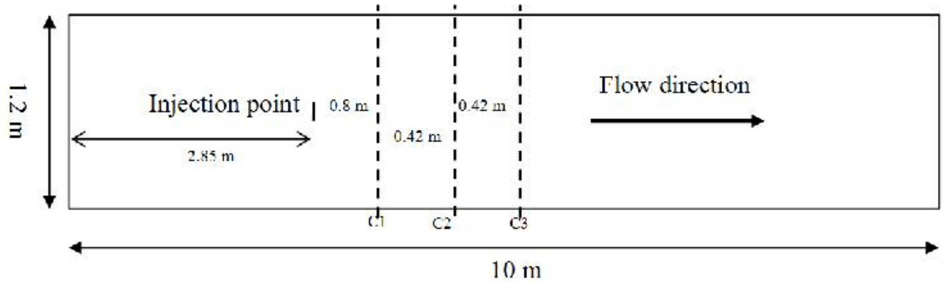

Figure 3.6 (a) Flume dimensions and concentration measurement cross-sections and injection point location for test 0.51S (SVF 0.505 % in a staggered configuration).

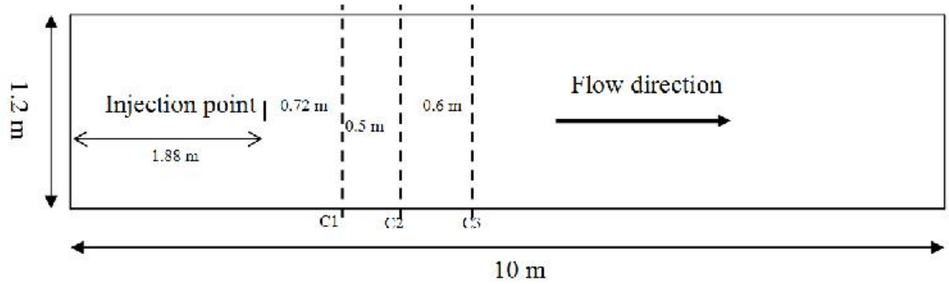

Figure 3.6 (b) Flume dimensions and concentration measurement cross-sections and injection point location for test 0.97S (SVF 0.974 % in a staggered configuration).

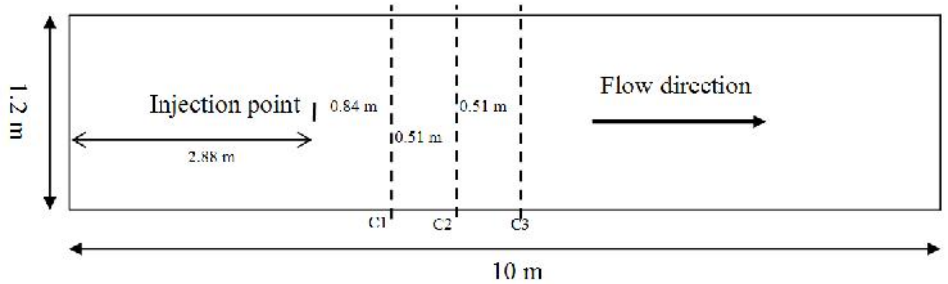

Figure 3.6 (c) Flume dimensions and concentration measurement cross-sections and injection point location for test 2.96AM (SVF 2.958 % in an aligned configuration).

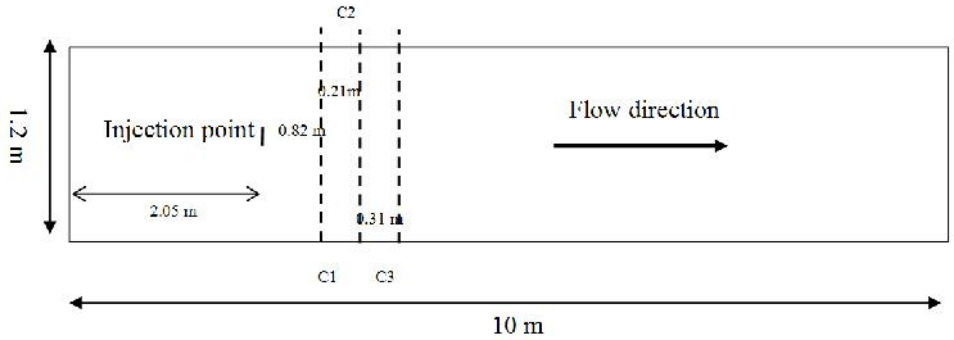

Figure 3.6 (d) Flume dimensions and concentration measurement cross-sections and injection point location for test 3.90A (SVF 3.896 % in an aligned configuration).

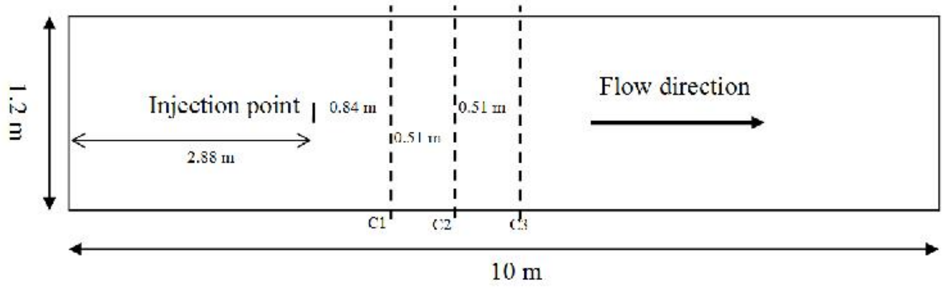

Figure 3.6 (e) Flume dimensions and concentration measurement cross-sections and injection point location for test 5.92AM (SVF 5.915 % in an aligned configuration).

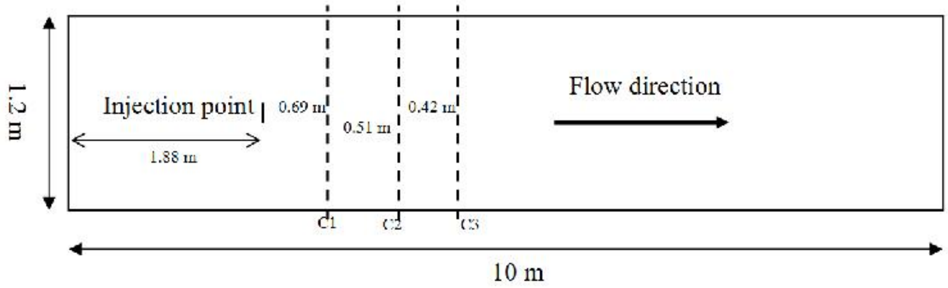

Figure 3.6 (f) Flume dimensions and concentration measurement cross-sections and injection point location for test 7.79A (SVF 7.792 % in an aligned configuration).

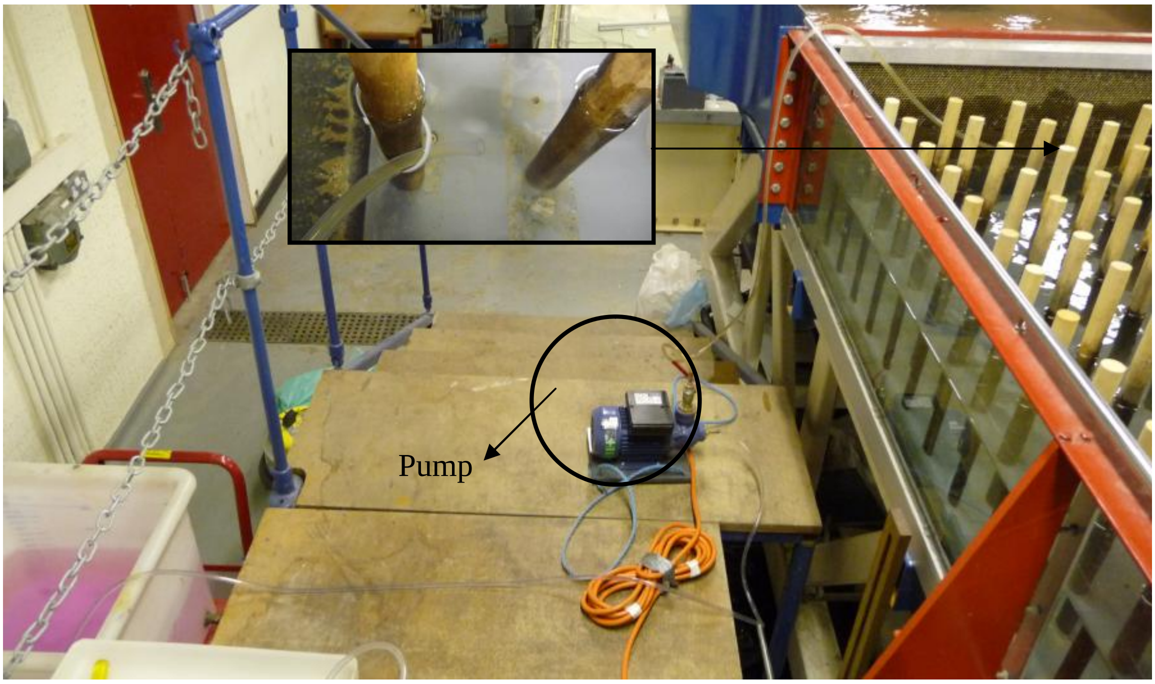

Figure 3.7: Dye tracer injection method used in the tests. The reservoir containing the injection concentration is located on the left and is pumped through a delivery tube to the cross-section in the flume.

To ensure that a dye tracer was injected at a steady and continuous rate, a dye tracer was injected continuously for 10 minutes before conducting the test. At this stage the injected dye increased with constant concentration gradient as shown in Figure 3.8. For each cross-section (C1, C2 and C3), there were 37 sampling points spaced at increments of 25 mm. The sampling period for each point was two minutes at mid depth of the flow depth. Two minutes was chosen to be reasonable between accuracy and time consuming and the limitation of the dye source from the tank.

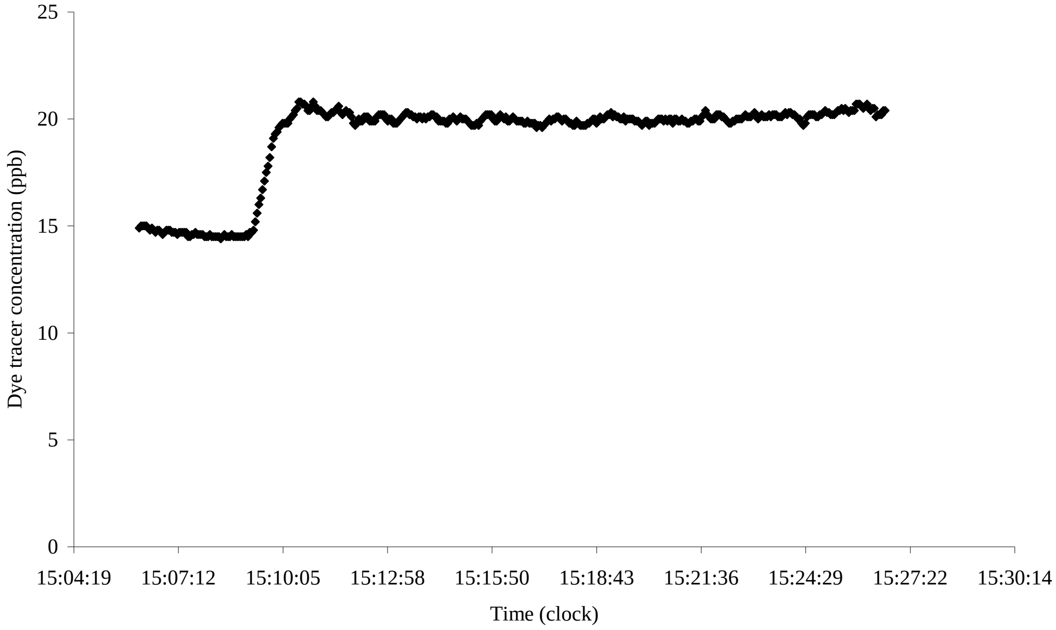

Figure 3.8 20 minutes time series of dye concentration (ppb) measured at the centreline of the flume

3.3 Fluorometer Measurements

3.3.1 Fluorometer Calibration

A Fluorometer 10-AU manufactured by Turner Design was used to measure tracer concentration in the experiments presented in this thesis (see Figure 3.9). A Fluorometer measures a fluid’s concentration via fluorescence. Fluorescence has the ability to absorb light at one wavelength and almost instantly emit light at a new and longer wavelength (Turner Design, 1993). A source of light from the lamp transmits light to pass through a filter to measure the concentration. This will radiate wavelengths proportional to the amount of fluorescent substance present (Wilson, 1986).

Figure 3.9 Fluorometer 10-AU from Turner Design

The concentration value displayed by the Fluorometer is based on two known concentration solutions through a calibration procedure. It is very important to calibrate the instrument before any experiment and it is a good practice to re-calibrate it at least once a week (Boxall, 2000).

Calibration consists of introducing a blank solution of zero concentration, and a standard solution that is about 80% of the highest concentration to be investigated. The concentration varies linearly with fluorescence between the blank and standard concentration however beyond the maximum concentration to be examined it is not accurate to assume a linear relationship. Furthermore fluorescence is sensitive to temperature, and it is important to maintain the same temperature throughout the experiment and the calibration procedure.

For all experiments Rhodamine WT supplied by Cole-Parmer with 2.5 % active ingredient was used as the tracer. Rhodamine WT was selected as is highly detectable and has a slow rate of decay (Shucksmith, 2008).

3.3.2 Dye Injection System

Figure 3.10 shows the dye injection system used to study the transverse dispersion in vegetated flume. A tank of 1000 ppb of dye was prepared prior to experiment (Figure 3.10 a) and was injected continuously using a pump (Figure 3.10 b). As mentioned above the pump was manually adjusted to control the volume of the point injection to be similar the water flow (Figure 3.10 c). The second pump then drew the dye plume from the desired sampling point to the Fluorometer to be measured (Figure 3.10 d and 3.10 e).

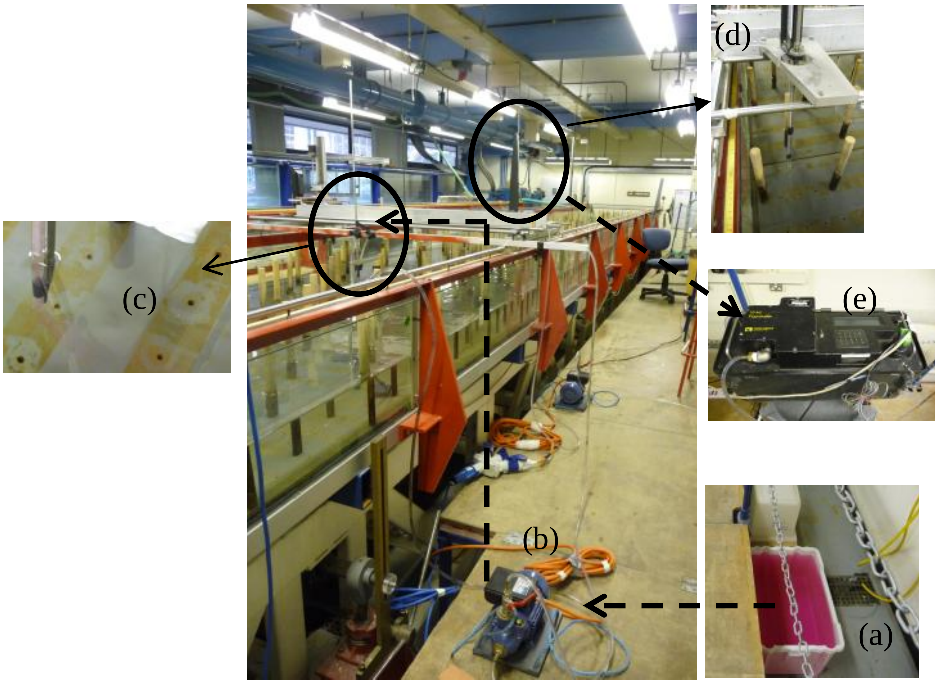

Figure 3.10 Layout of dye injection system used in the study

3.3.3 Concentration Sampling Procedure

Figure 3.6 (a) to (f) show the injection point and the position of cross-section 1 (C1), cross-section 2 (C2) and cross-section 3 (C3). The measurement of the dye tracer along each cross-section started at 150 mm from the left hand side of the flume, looking in the downstream direction, and was measured every 25 mm across the flume. The last sample was taken at a distance of 1050 mm from the left hand side of the flume (150 mm from the right hand side wall). In total 37 sampling points were measured in each cross-section and as discussed earlier, dye tracer was sampled at three cross-sections downstream of the injection point.

3.4 Velocity and Turbulence Measurements

Velocity was measured using a downward looking 3-D Acoustic Doppler Velocimeter (ADV) device known as a Vectrino which was manufactured by Nortek AS. The measurement technique is based from the Doppler Effect whereby a short pulse of sound is transmitted by the probe head, and the change in its frequency of the reflected sound pulse is measured by the probe receivers (Nortek, 2004). The frequency of the Vectrino used in the experiment was 200 Hz and the Nortek Vectrino is shown in Figure 3.11.

The acoustic signal is emitted by a central transducer towards a sampling volume, the centre of which is approximately 50 mm away (see Figure 3.12). The acoustic signal is reflected by ambient particles in the flow field and measured by four receiver arms (Nortek, 2004) see Figure 3.12.

The ADV was mounted vertically on a carriage and was adjusted to move either in the longitudinal or in the lateral direction across flume width. The velocity was measured in 10 mm and 20 mm vertical increments from the bed to 100 mm and 300 mm above bed depending on the test and flow condition. Further details of the velocity measurement will be explained in Chapter 4.

Figure 3.11: Acoustic Doppler Velocimeter (ADV) Vectrino (200 Hz) from Nortek

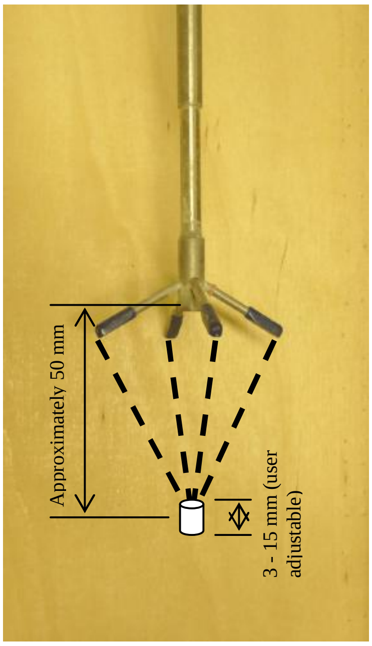

Figure 3.12: The position of the sampling volume below the transducer and four receivers.

It is important to obtain a good estimation of sampling time for each velocity measurement in order to capture accurate time-averaged statistics of the velocity and turbulence fields. To determine the necessary sampling period needed, tests were performed for sampling times of one, two, three and four minutes. Results show that the optimum sampling time was one minute for measurement using Vectrino with sampling rate 200 Hz sampling rate. Figure 3.13 (a) to (d) present the cumulative time-averaged velocity for one, two, three and four minutes test.

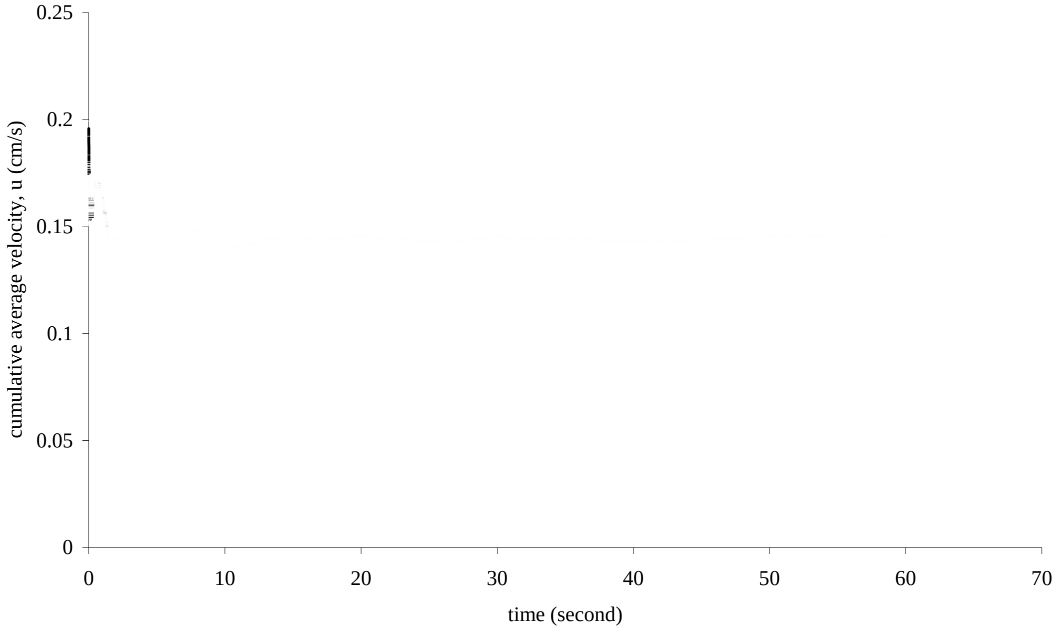

Figure 3.13 (a) One minute time series of the cumulative time-averaged velocity for Vectrino with a 200 Hz sampling rate.

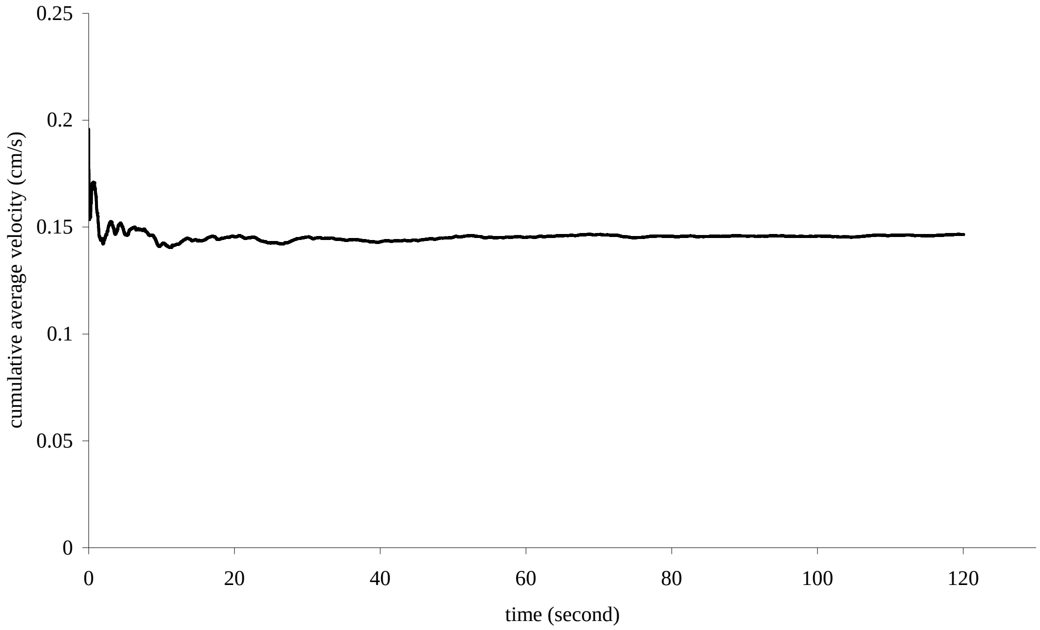

Figure 3.13 (b) Two minutes time series of the cumulative time-averaged velocity for Vectrino with a 200 Hz sampling rate.

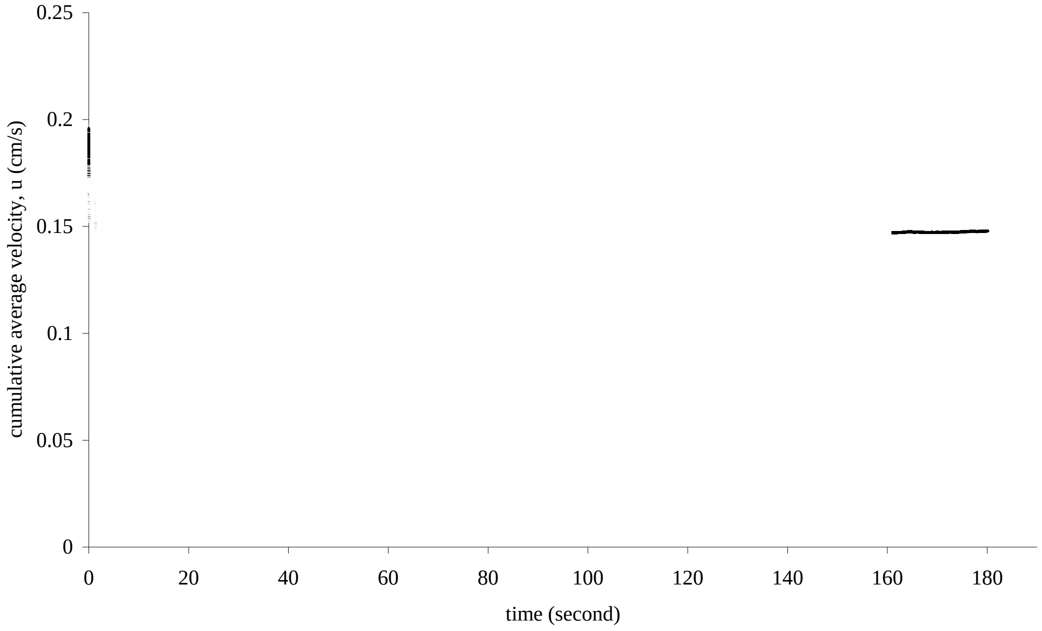

Figure 3.13 (c) Three minutes time series of the cumulative time-averaged velocity for Vectrino with a 200 Hz sampling rate.

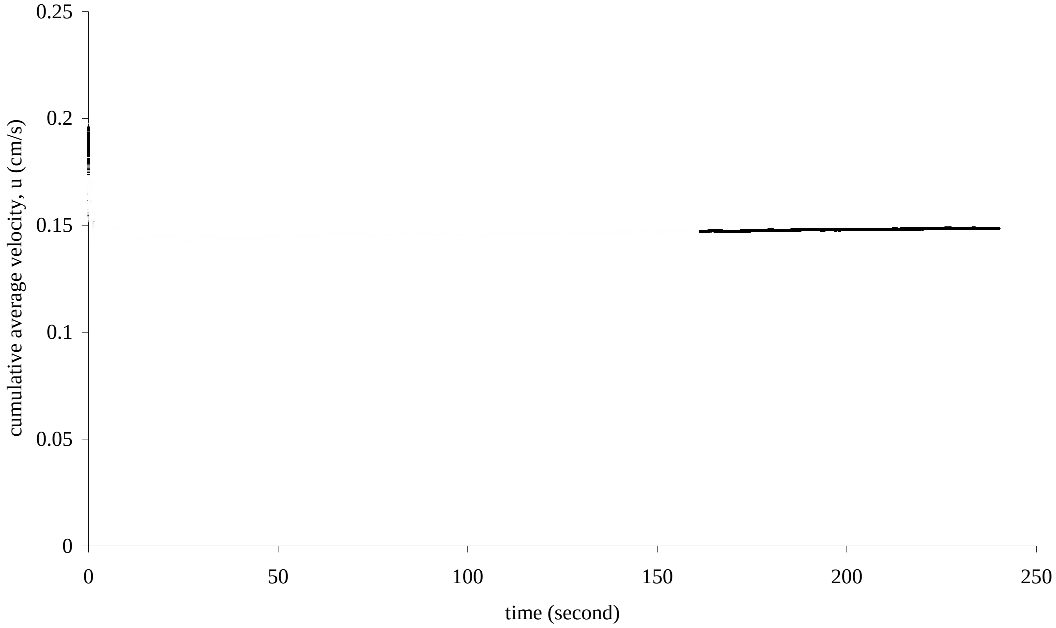

Figure 3.13 (d) Four minutes time series of the cumulative time-averaged velocity for Vectrino with a 200 Hz sampling rate.

3.4.1 Probe Data Processing

The quality of the velocity output is quantified by two parameters: the signal to noise ratio (SNR) and the correlation (COR) (Wahl, 2000).

The SNR parameter strength of the signal received compared to the noise level of the instrument. The manufacturers recommend a SNR value of at least 5 when measuring time-averaged flow velocities, and 15 or higher when measuring instantaneous velocities and turbulence (Wahl, 2000).

The correlation parameter, COR, is an indicator of the relative consistency of the behaviour of the particles in the sampling volume during the sampling period. The value varies from 0 to 100, and the manufacturers have typically recommend filtering to remove any samples with correlation scores below 70 (Wahl, 2000).

Another important filter known as the spike detection filter was developed by Nikora and Goring (Nikora and Goring, 2002). It is based on the concept that there should be a physical upper limit to the change in flow velocity that can occur in a flow, and any measurements that indicate higher accelerations should be excluded from the analysis (Wahl, 2000).

To filter the velocity and turbulence data, in terms of the values of SNR, COR and spike detection, a program called WinADV written by Wahl (2000) for Bureau of Reclamations Water Resources Research Laboratory, and made available to the public via the Internet in 1996 (Wahl, 2000). Originally WinADV was developed to filter the velocity data from the ADV with 25 Hz frequency however this program is also compatible with Vectrino of 200 Hz. The only different is that, using Vectrino data with WinADV usually takes longer processing time relative to ADV data of 25 Hz. In this thesis, WinADV was used to filter all the velocity data from the Vectrino before further analysis is continued.

3.4.2 Vectrino Rotational Error

Velocity measurement is subject to error including the inaccurate of the instrument alignment. Shucksmith (2008) shows that for miss-alignment of the probe less than 10 degree the error in primary velocity, *u* is small (less than 2 %) and miss-alignment for transverse velocity, *v* is larger up to 50 % error at six degrees rotation. If the rotational error is constant over the entire vertical profile, than the data can be analysed and corrected.

3.4.3 Velocity Measurement Procedure using the Vectrino

Figure 3.14 (a) to (d) present the plan view measurement of sampling point locations for four different vegetation densities. Velocity measurements for tests 3.90A and 7.79A (aligned arrangement) was completed by the author and the velocity measurements for tests 0.97S and 3.90S (staggered arrangement) was conducted by Xavier (2009) however author assisted Xavier through each experiment. For tests 3.90A and 7.79A the vertical distance between measurements was 10 mm for 8 to 19 points depending upon the water depth and with the first measurement was taken at 10 mm from the bed. While Xavier (2009) used a vertical distance of 20 mm between measurements and the first measurement was taken 7.5 mm from the bed. Velocity measurement for aligned arrangements of vegetation was measured half section of the control volume (see Figure 3.14 (c) and (d)). This was considered reasonable because the flow was uniform and therefore symmetrical along the centreline of each control volume.

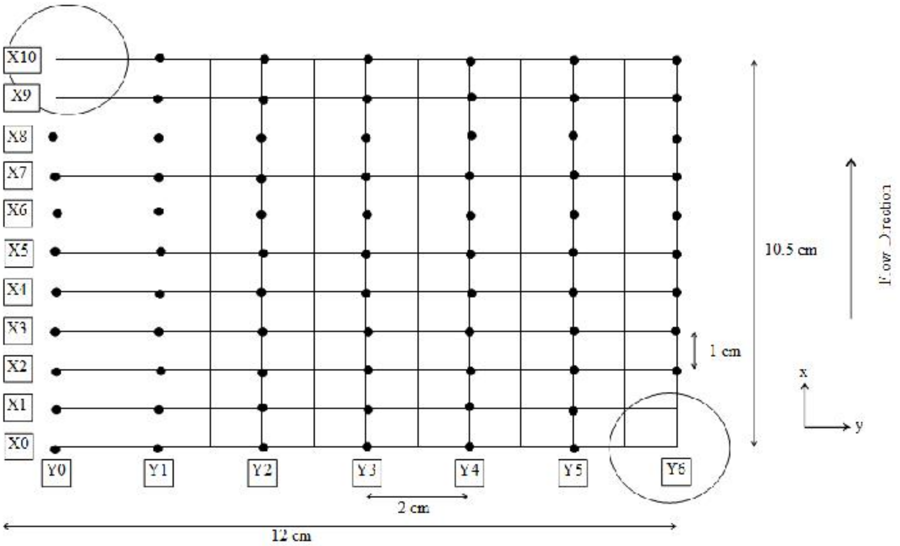

Figure 3.14 (a) Staggered arrangement control volume for test 0.97S (SVF = 0.97 %)

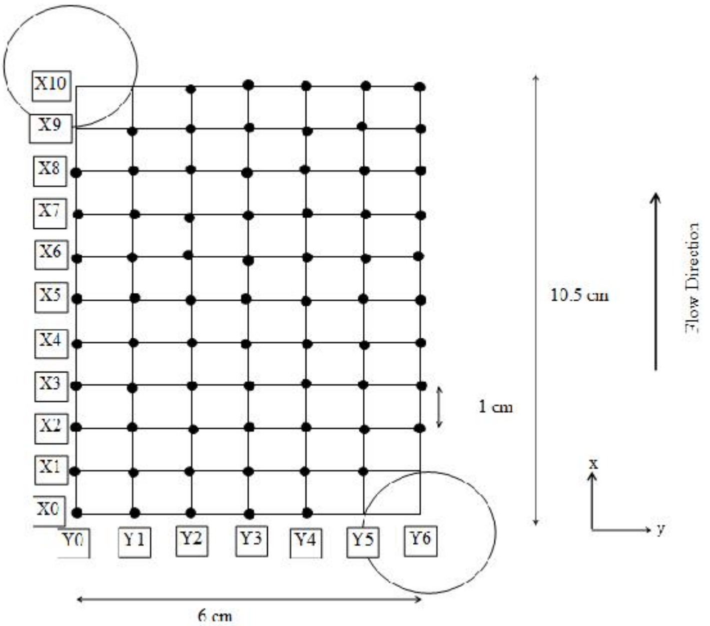

Figure 3.14 (b) Staggered arrangement control volume for test 3.90S (SVF = 3.90 %)

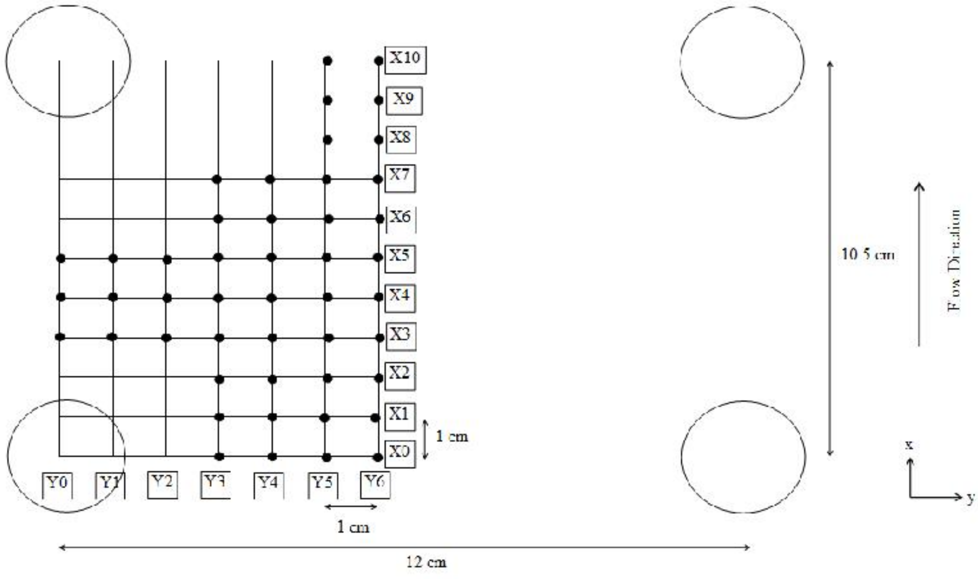

Figure 3.14 (c) Aligned arrangement control volume for test 3.90A (SVF = 3.90 %)

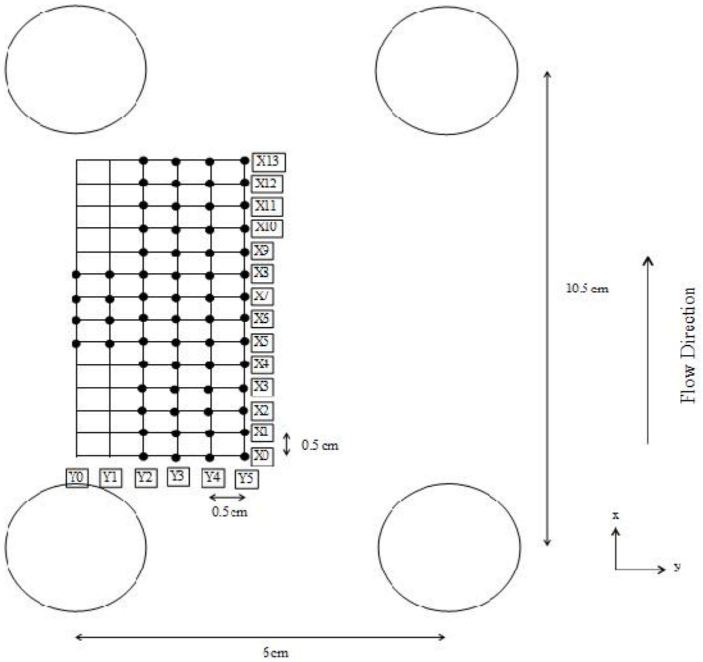

Figure 3.14 (d) Aligned arrangement control volume for test 7.79A (SVF = 7.79 %)

3.5 Establishing Uniform Flow Conditions

Uniform flow is a condition defined when the velocity of the flow does not change, either in magnitude or direction from one cross-section to another in the channel under consideration. This condition can be achieved when the water surface profile is parallel to the channel bed and the energy line is parallel to both (Massey, 1989).

Uniform flow condition was established for two set of vegetation density which includes tests 3.90A and 7.79A. After all the dowels were fully attached through out the flume, the weir is engaged to certain height. After five to 10 minutes when the flow was stable, eight water depths were measured from upstream to downstream within 1 metre gap from one measurement to the other. The flow depth was measured from the bottom of the flume to water surface using measurement ruler within ± 0.01 m accuracy. These processes were repeated for five to six times using different weir height. Figure 3.15 is an example of the water depth measurement for test 7.79A with the weir height of 170 mm and the water surface gradient is approximately 0.0041.

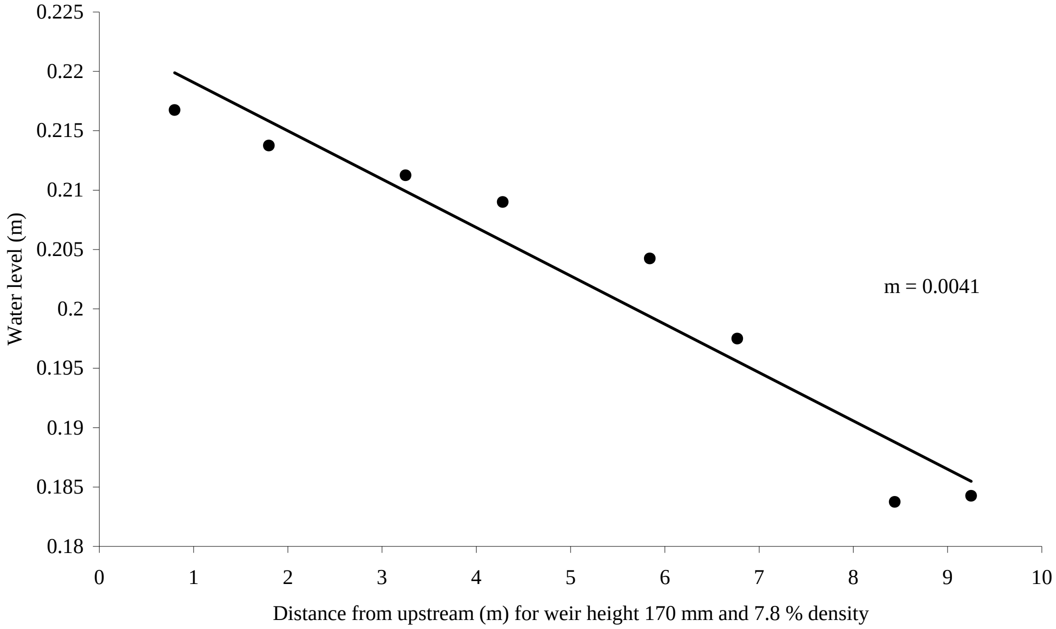

Figure 3.15 Water surface profiles for test 7.79A with 170 mm weir height

The water surface gradients from six weir heights were then used to produce a plot of the energy line slope against weir height (see Figure 3.16). A best fit line was used to determine using the Excel function of Trendline. The best fit line equation was used to calculate the weir height for the water surface gradient of 0.001 that can emulate uniform flow condition. The same procedure was used for each vegetation density.

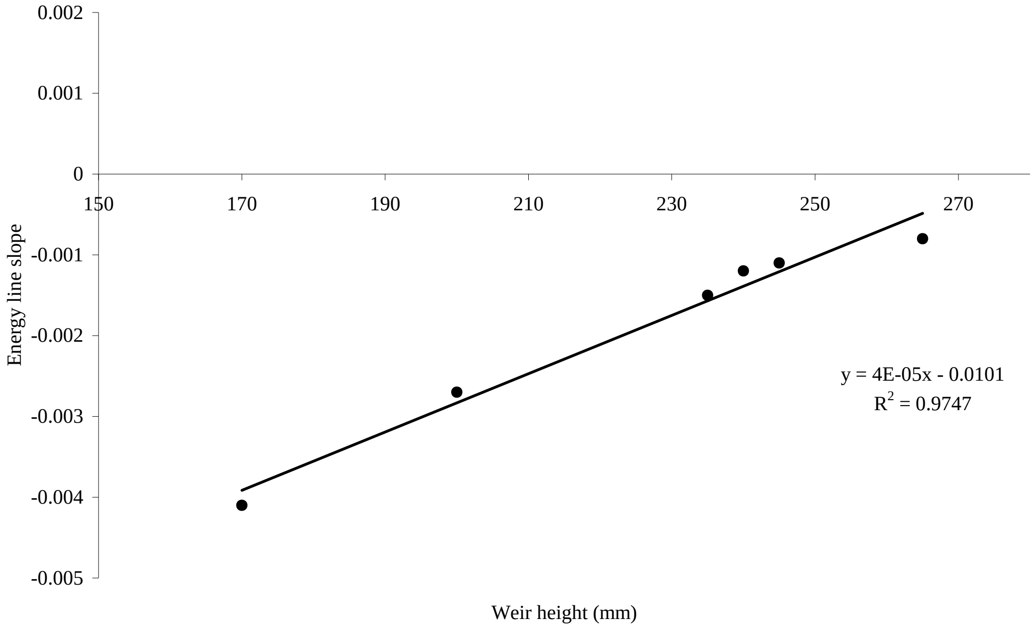

Figure 3.16 Energy line slope and weir height for test 7.79A

3.6 Transverse Mixing Data Analysis

3.6.1 Background Concentration Removal

As mentioned previously (in section 3.1) the flume is connected to a re-circulating flow system, and thus it is expected that there will be an increase in background concentration over time. Therefore a correction technique was developed to eliminate the temporal changes in the background concentration from each data set.

An example of the approach used to eliminate the cumulative build up in background concentration is shown in Figure 3.17 (a) to (e). Figure 3.17 (a) shows the time-averaged raw concentration data measured by the Fluorometer across the sampling cross-section. The sample point 1 is located on the left hand side (LHS) of the cross-section looking in the downstream direction and point 37 is located on the RHS of the cross-section.

As mentioned above the sampling time for each point was two minutes. For each sampling point the cumulative build up of the background concentration is calculated from the gradient (i.e. m = 5.909 for test 0.505S) of the time-averaged concentration profile shown in Figure 3.17 (a). This value is then subtracted from the raw time-averaged value multiplied by the concentration gradient (m) and the resulting concentration profile as shown in Figure 3.17 (b). Finally the concentration profile is obtained once all the data in concentration profile in Figure 3.17 (c) and (d) is reduced by the cut off concentration value.

The cut off concentration value was evaluated systematically. The cut off concentration was based on assumption that the dye concentration profile follows a Gaussian distribution (please refer to Figure 3.17 (c) and (d)). Another important assumption is the conservation of mass, for that the ratio area below each dye concentration profile (i.e. C1 and C2) in each set of experiments should be within 95 % to 105 % (please refer to Figure 3.17 (e)).

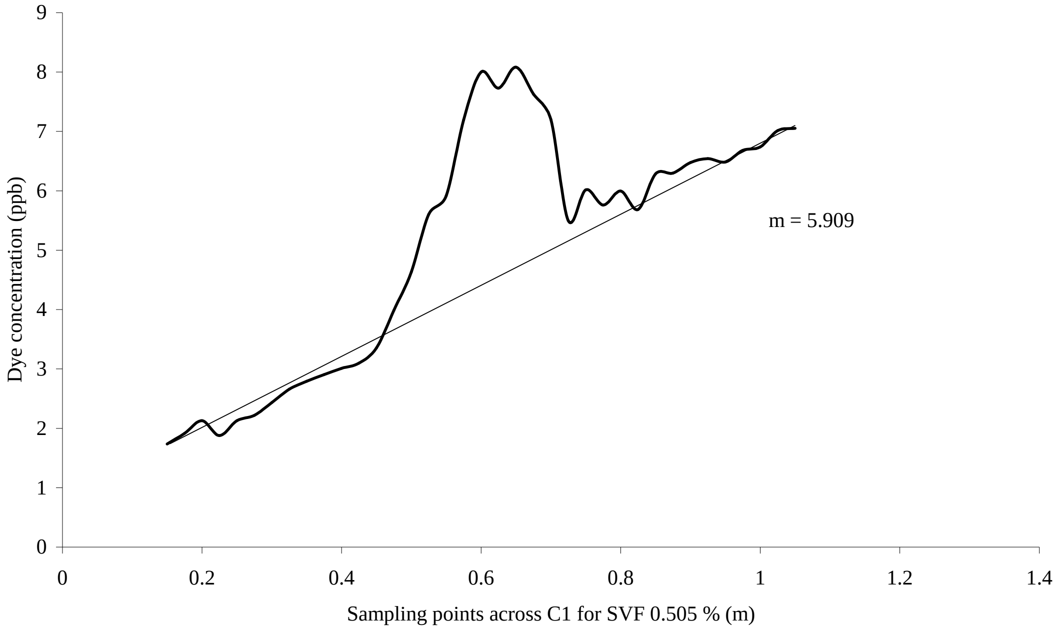

Figure 3.17 (a) The profile of raw dye concentration measured by Fluorometer across section C1

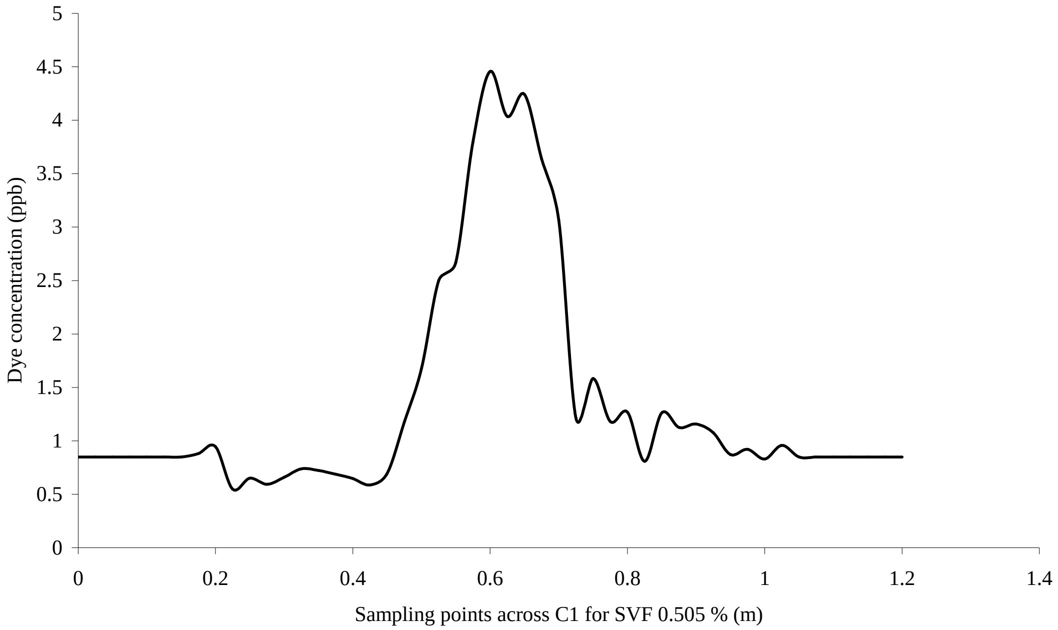

Figure 3.17 (b) The dye concentration profile minus the concentration gradient

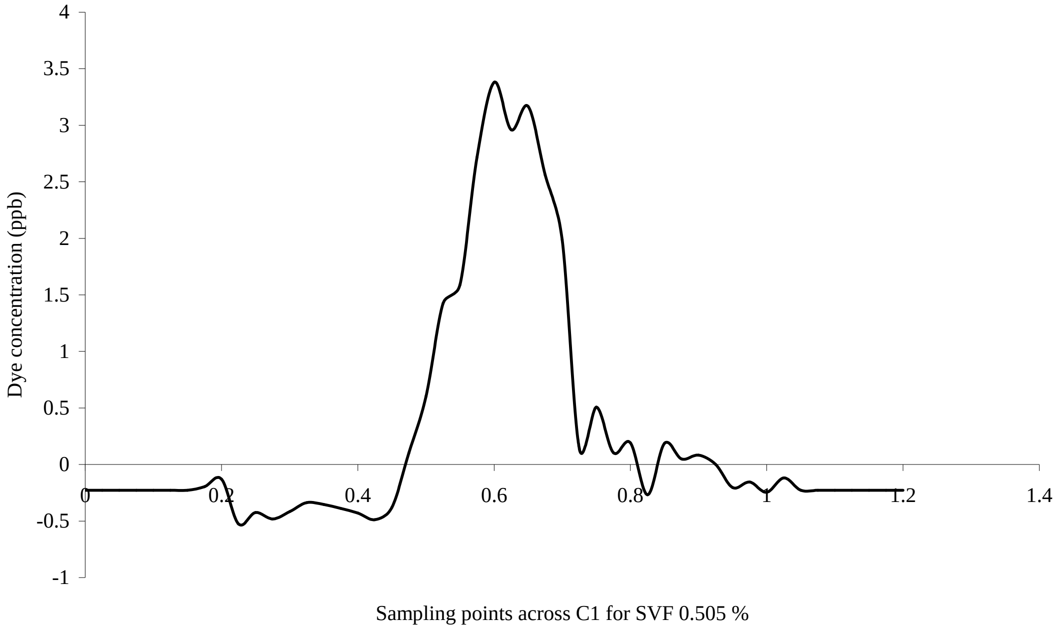

Figure 3.17 (c) The dye concentration profile before the cut off concentration process

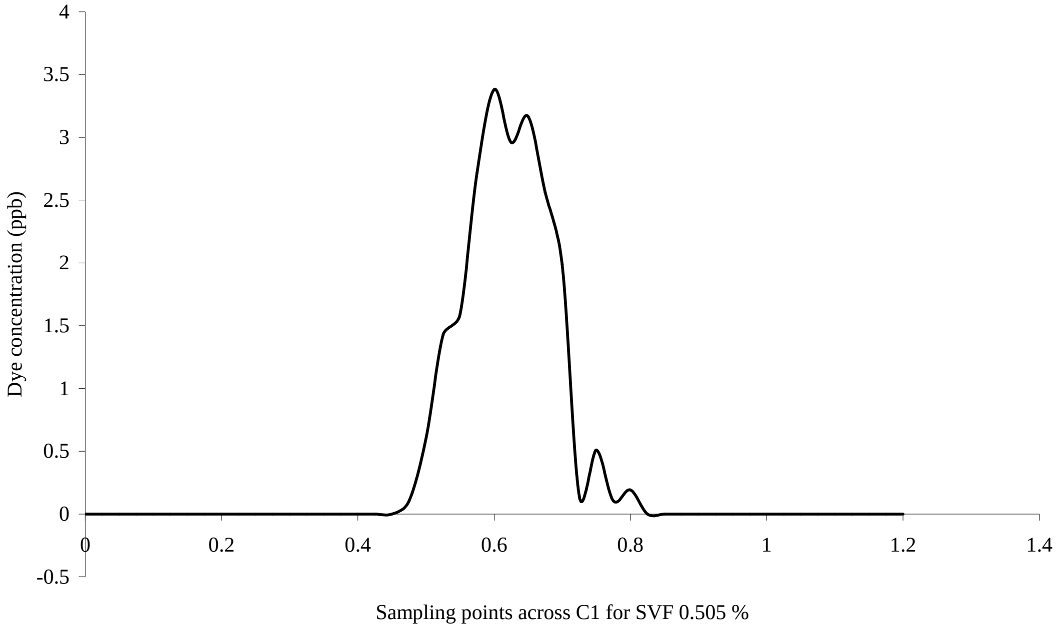

Figure 3.17 (d) The dye concentration profile after the cut off concentration process

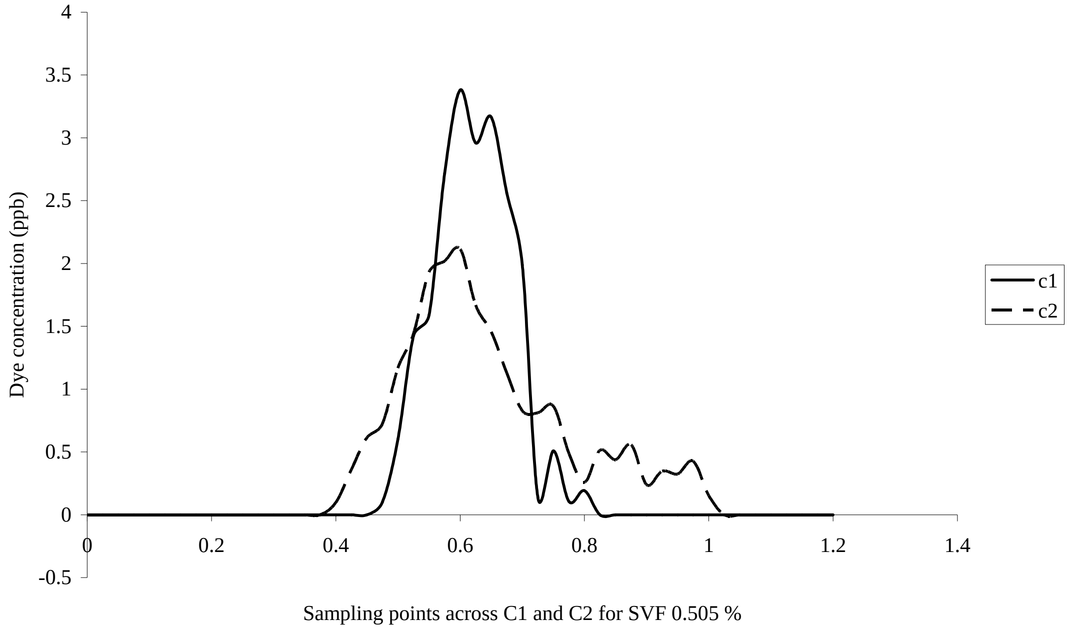

Figure 3.17 (e) The dye concentration profile for sections C1 and C2 which the ratio area below C1 and C2 profiles are within of 95 % to 105 % of the total mass balance. Theoretically mass balance between C1 and C2 should be 100 %, but practically it is very hard if not impossible to achieve, therefore plus minus 5 % is considered an acceptable range.

3.6.2 Trace Start and End Identification

According to Shucksmith (2008) it is important to identify the start and end of each tracer profile. The method of moments is sensitive and inaccurate cut off will cause error. Therefore Shucksmith (2008) developed a computer programming to identify the start and the end of the tracer. The start of the tracer is when the signal rises above 1% of the peak value for 10 consecutive data points. The end of the trace is defined as when the signal falls below 1% of the peak value for 10 consecutive data points. However for the current research work, the start and end of the tracer profiles is evaluated manually based on the mass balance between tracer profiles for each tracer test. For example as shown in Figure 3.17, according to conservation of mass the ratio area between tracer profile of C1 and C2 should be about 95 % to 105 % of the acceptable range. If in the case of ratio C1 and C2 is beyond the acceptable range, therefore adjustment of the cut-off of the start and end for each tracer profiles would be made manually until it fits to the acceptable ratio range.

3.6.3 Mass Balance

According to the conservation of mass for conservative tracer measured at cross-section upstream should be the same with tracer mass measured at the cross-section down-stream. However, based on practical point of view this is very difficult to achieve and the mass balance ratios of the two concentration profiles in the region of 95 % to 105 % is generally good and acceptable (Shucksmith, 2008; Boxall and Guymer, 2001).

3.6.4 Identification of Parameters

The advection diffusion equation parameter identified using the method of moments by measuring the development of the 0th, 1st and the 2nd moment as presented in equation (3.2), (3.3) and (3.4). The calculated moments from of each distribution are referred to determine the area, centroid and variance as shown in equation (3.5), (3.6) and (3.7). However according to Shucksmith (2008), when these parameters are put back into models they usually provide a poor description of mixing and this is largely due to errors of the uncertain level of trace cut off.

$$M_0 = \int_1^\infty c_i dx \tag{3.2}$$

$$M_1 = \int_1^\infty (c_i dx) x_i \tag{3.3}$$

$$M_2 = \int_1^\infty (c_i dx) x_1^2 \tag{3.4}$$

$$Area = M_0 \tag{3.5}$$

$$Centroid = \text{¨} = \frac{M_1}{M_2} \qquad (3.6)$$

$$variance = \pm^{2} = \frac{M_2}{M_0} - \text{¨}^{2} \qquad (3.7)$$

Optimisation procedures aim to improve the accuracy of the final parameters by eliminating errors in the calculation of variance, first arrival times and centroid. This optimisation procedure works by using the routing procedure together with a series refined searches to identify the pair of mixing parameters that give the optimum fit to the measured downstream profile. According to Boxall (2000) and Dennis (2000), optimisation parameters are relatively insensitive to data collection techniques such as the uncertain choice of trace cut off levels. For further details please refer to Shucksmith (2008).

3.6.5 Transverse Mixing Coefficient

The method for calculating transverse mixing coefficient used in this thesis was originally conceived by Boxall and Guymer (2001) and is based on the minimum concentration (C_{min}) and maximum concentration (C_{max}) at each cross-section (see Figure 3.18). The ratio of minimum and maximum concentration (i.e. C_{min}/C_{max}) for each cross-section should be above 0.02 or below 0.75 (see equation 3.9)) or otherwise discarded (Boxall and Guymer, 2001). Then transverse mixing coefficient can be quantified using equation (3.8) and (3.9) where L_1 referred as distance from the injection point to the initial crossing and L_2 is the distance of injection point to well mixed profile (see Figure 3.18).

$$K_y = \sim \frac{Ub^2}{x} \text{ where } L_1 \langle x \langle L_2 \qquad (3.8)$$

$$\sim = 0.0688\left(\frac{C_{\min}}{C_{\max}}\right) + 0.0128 \qquad (3.9)$$

$$\text{For } 0.02\langle\left(\frac{C_{\min}}{C_{\max}}\right)\langle 0.75$$

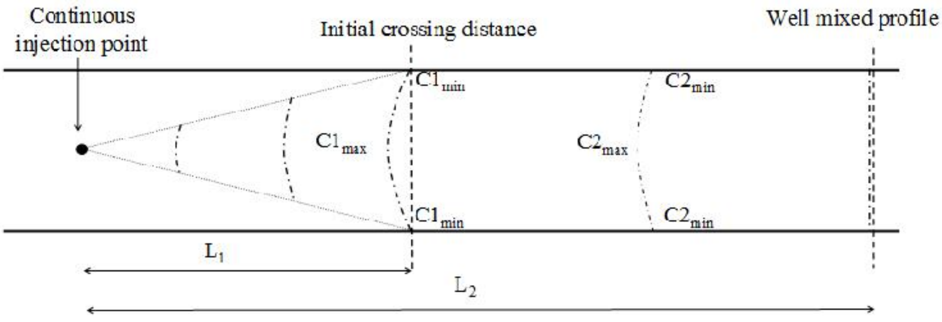

Figure 3.18 Transverse concentration profile using Boxall and Guymer (2001) method (adapted from Shucksmith, 2008)

Shucksmith (2008) also referred to Transverse Method of Moments to calculate the transverse mixing coefficient. In this method if the tracer obeys Fick's law where the variance of a tracer clouds sometime after released increases linearly with time, therefore the transverse mixing coefficient can be estimated as equation (3.10), where U is the mean area velocity, $\pm_y$ is the variance for tracer profile and $x_2 - x_1$ is the longitudinal distance between the first and second cross-sectional considered.

$$K_y = \frac{U}{2}\frac{\pm_y^2(x_2) - \pm_y^2(x_1)}{x_2 - x_1} \qquad (3.10)$$

After each dye tracer test, raw concentration data was downloaded from the Turner Design Fluorometer to a personal computer using DOS version software named IDL_1b1.exe. This software converts the original data files to ASCII files which can be read by Microsoft Office Excel. Then the background concentration removal process to eliminate the cumulative build up of dye concentration as been discussed thoroughly in section 3.6.1. These steps were repeated for every cross-section for six difference vegetation density (see Table 3.1). 'Clean' data were then compiled before further processing. Then each concentration profile for each run was mass balanced as previously been explained in section 3.6.3. Then a parameter identification process based on the method of moments was used to establish the initial value of transverse mixing coefficient before the optimisation process based on routing procedures to improve the accuracy of the results was used as described above in section 3.6.4.

3.7 Summary

In this chapter the experimental facility and programme, flow conditions, measurement methods and techniques have been described. The following two chapters will present the velocity and turbulence fields for selected rod configurations (chapter 4) and the results from the tracer experiments will be presented and discussed in chapter 5.

Chapter 4 – Velocity and Turbulence Characteristics

4.0 Introduction

This chapter presents the velocities and turbulence statistics for a selection of rod densities and configurations. A summary of the experiments conducted for the dye tracing tests and the tests chosen for velocity measurements are given in Table 4.1. Detailed velocity measurements were taken for four different solid volume fractions and rod arrangements namely tests: 0.97S (SVF = 0.97%, staggered), 3.90S (SVF = 3.90%, staggered), 3.90A (SVF = 3.90%, linear) and 7.79A (SVF = 7.79%, linear) using the procedure outlined in Chapter 3. The depth-averaged values of the time-averaged longitudinal velocity component and turbulent kinetic energy for the tests 0.97SL and 0.97SH (SVF = 0.97%, staggered) and tests 3.90SL (SVF = 3.90%, staggered, low water) and 3.90SH (SVF = 3.90%, staggered, high water) have been presented previously (Xavier, 2009). However in this thesis the velocity data sets from these two solid volume fraction arrangements have been reanalysed to fulfil the objective of this thesis and are presented with new data collected by the author.

As outlined in Chapter 3 for each rod density and rod configuration the velocity measurement grid comprised between 47 and 71 sampling positions in the x-y plane (x is the longitudinal direction, y is the transverse direction). For each position in the x-z plane between 5 and 19 measurements were made depending on the flow depth; vertical increments varied from 10 mm to 20 mm. The distance for first velocity measurement for tests 0.97SL, 0.97SH, 3.90SL and 3.90SH was 7.5 mm above the flume bed, and the distance for the first velocity for tests 3.90A and 7.79A was 10 mm above the flume bed. See Table 4.2 for the number of measurement grid points for each test.

Table 4.1 Experimental details for dye tracer tests and velocity measurements. The velocity data from tests 3.90SL, 3.90SH, 0.97SL and 0.97SH was collected by Xavier and Sharil and was presented in Xavier (2009)

	SVF Φ (%)	Rod alignment	d (mm)	δ_x (m)	δ_y (m)	Q (m^3/s)	h (m)	U (m/s)	Re_d	Vel	Dye
0.51S	0.505	Staggered	18	0.210	0.12	0.017	0.090	0.157	2,826		√
0.97S	0.974	Staggered	25	0.210	0.12	0.016	0.135	0.099	2,475		√
2.96M	2.958	Linear (mixed d)	18,25	0.105	0.12	0.006	0.064	0.078	1,677		√
3.90A	3.896	Linear	25	0.105	0.12	0.015	0.145	0.086	2,150	√	√
5.92M	5.915	Linear (mixed d)	18,25	0.105	0.06	0.006	0.121	0.041	881.5		√
7.79A	7.792	Linear	25	0.105	0.06	0.015	0.257	0.049	1,677	√	√
3.90SL	3.896	Staggered	25	0.1	0.06	0.015	0.175	0.071	1,775	√	
3.90SH						0.014	0.22	0.053	1,325	√	
0.97SL	0.974	Staggered	25	0.2	0.12	0.020	0.14	0.119	2,975	√	
0.97SH						0.033	0.24	0.115	2,875	√	

Table 4.2 Detail information of velocity measurement for each vegetation density

	SVF Φ (%)	No of measurement points in x-y plane	No of vertical levels	Vertical increment (mm)
0.97SL	0.974	71	5	20
0.97SH	0.974	71	10	20
3.90SL	3.896	71	7	20
3.90A	3.896	47	8	10
3.90SH	3.896	71	9	20
7.79A	7.792	64	19	10

Text here to explain the notation used for the velocity and turbulence statistics namely

$\overline{u}_z$ means the longitudinal time-averaged velocity averaged in the vertical (z) direction.

$\overline{u_x}$ means the longitudinal time-averaged velocity averaged in the longitudinal (x) direction.

$\overline{v}_x$ means the transverse time-averaged velocity averaged in the longitudinal (x) direction.

$\overline{u}_{xz}$ means the longitudinal time-averaged velocity averaged in the longitudinal (x) and vertical (z) directions.

$\overline{u}_{xy}$ means the longitudinal time-averaged velocity averaged in the longitudinal (x) and transverse (y) directions.

$\sqrt{\overline{u_x'^2}}$ means the longitudinal time-averaged turbulence intensity averaged in the longitudinal (x) direction.

$\sqrt{\overline{u'}^2_{xyz}}/U$ means the longitudinal time-averaged turbulence intensity averaged in the longitudinal (x), transverse (y) and vertical (z) directions divided by cross-sectional area velocity.

4.1 Velocity Structure

4.1.1 Transverse Profiles of Longitudinal Velocities

For each vertical profile in the *x-y* plane, the depth-averaged value of the longitudinal velocity was computed. The transverse variation of the depth-averaged longitudinal velocity is plotted for each cross-section in the control volume (see Figure 4.1 (a) to 4.1 (f)) whereby X0 relates to the most upstream cross-section and X10 (i.e. 3.90A, 3.90S and 0.97S) and X13 (i.e. 7.79A) relate to the most downstream cross-section in the control volume. Each of the following plots is looking in the downstream direction and relates to the control volume of located in the middle of the cross-section of the flume so side wall effects are limited. The measurement grids for each test and vegetation arrangement were presented in Section 3.4.3.

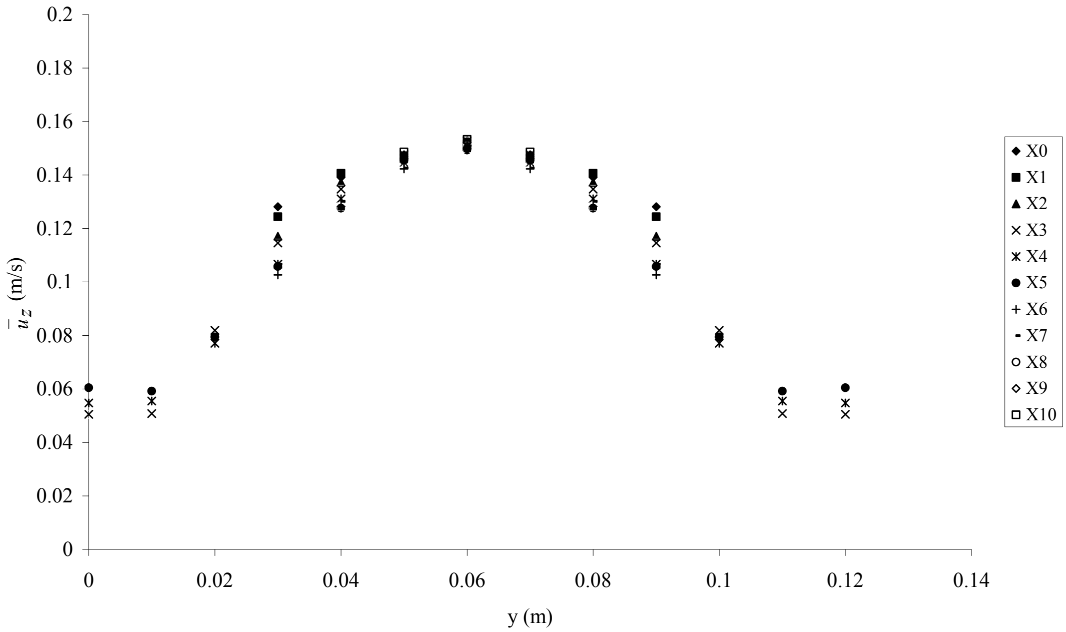

Figure 4.1 (a) Transverse variation of the depth-averaged longitudinal velocity, $\bar{u}_z$ for test 3.90A. X0 relates to the most upstream cross-section and X10 relates to the most downstream cross-section.

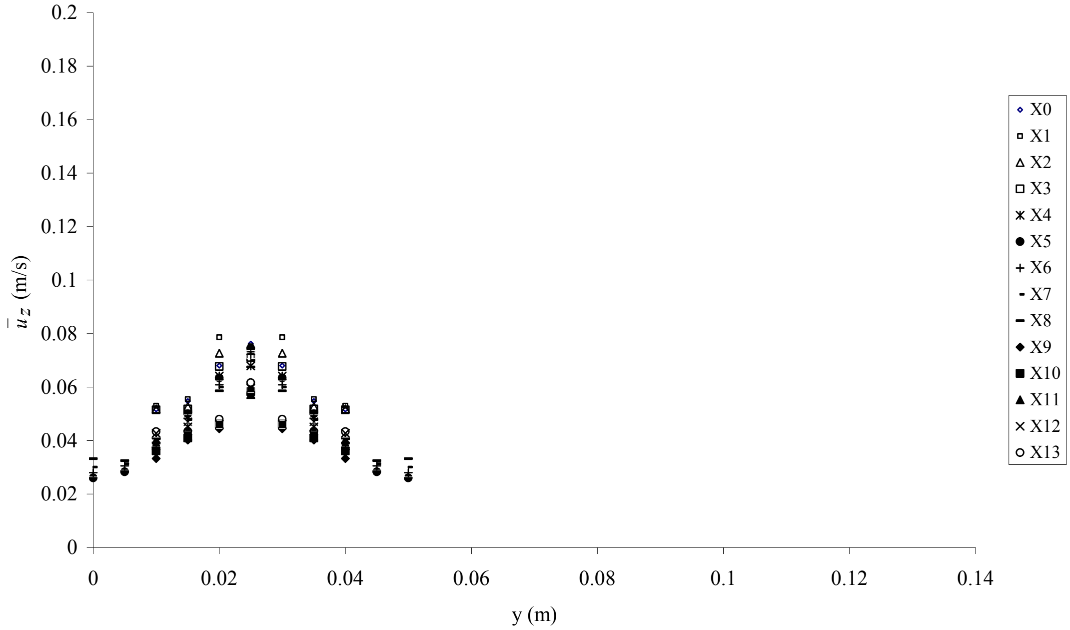

Figure 4.1 (b) Transverse variation of the depth averaged longitudinal velocity, $\bar{u}_z$ for test 7.79A. X0 relates to the most upstream cross-section and X13 relates to the most downstream cross-section.

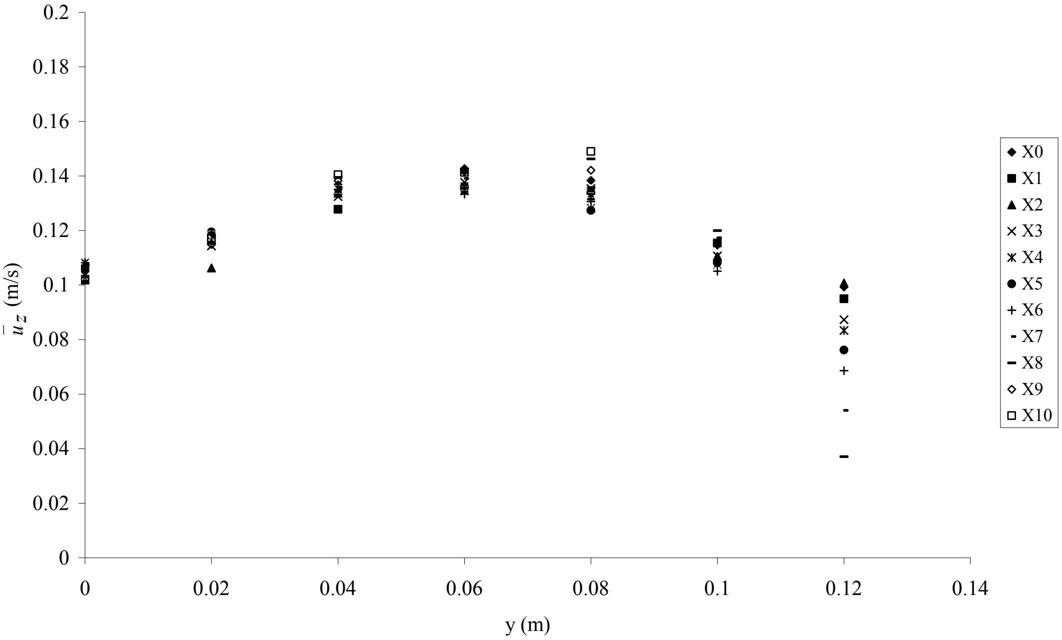

Figure 4.1 (c) Transverse variation of the depth averaged longitudinal velocity, $\bar{u}_z$ for test 0.97SL. X0 relates to the most upstream cross-section and X10 relates to the most downstream cross-section.

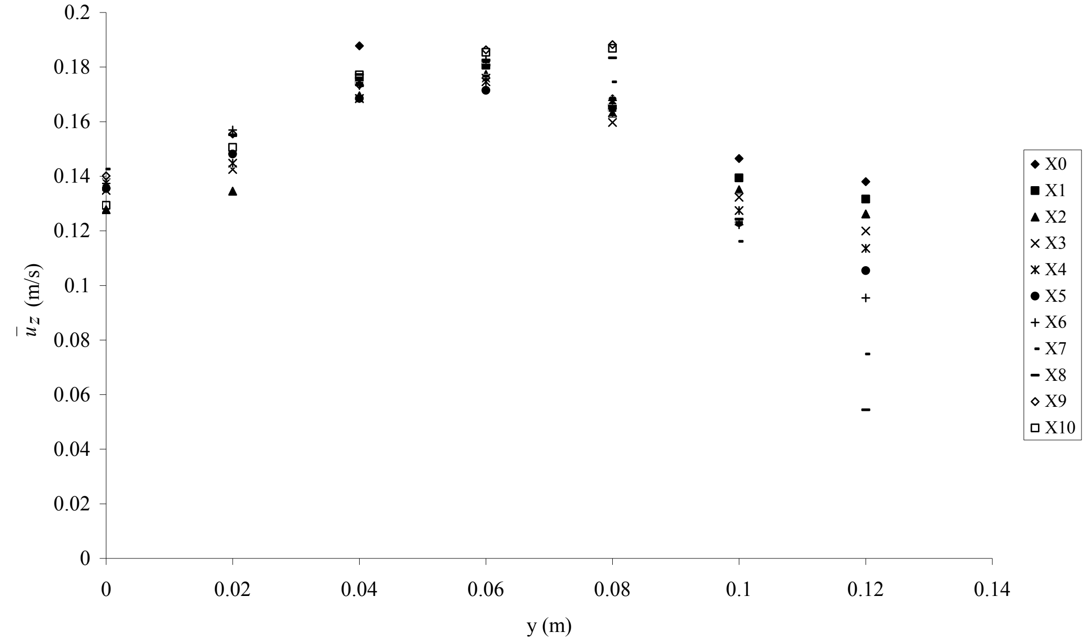

Figure 4.1 (d) Transverse variation of the depth averaged longitudinal velocity, $\bar{u}_z$ for test 0.97SH. X0 relates to the most upstream cross-section and X10 relates to the most downstream cross-section.

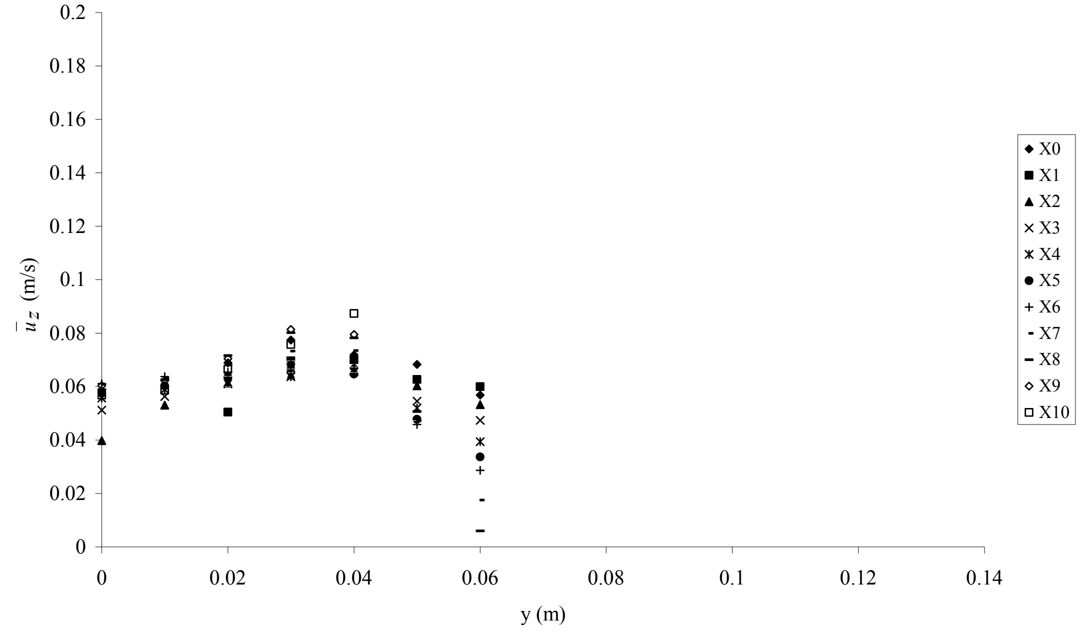

Figure 4.1 (e) Transverse variation of the depth averaged longitudinal velocity, $\bar{u}_z$ for 3.90SH. X0 relates to the most upstream cross-section and X10 relates to the most downstream cross-section.

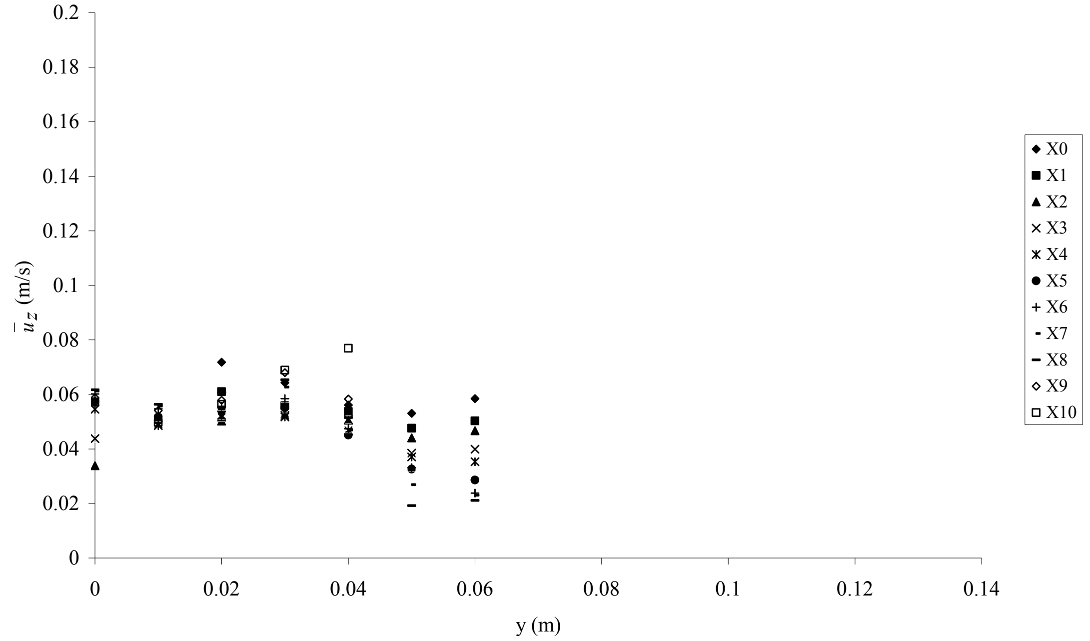

Figure 4.1 (f) Transverse variation of the depth averaged longitudinal velocity, $\bar{u}_z$ for 3.90SL. X0 relates to the most upstream cross-section and X10 relates to the most downstream cross-section.

The transverse profiles of normalised depth-averaged velocity for each test are shown in Figures 4.2(a) to 4.2 (f); depth-averaged values have been normalised by the cross-sectional area velocity so that direct comparison can be made between each test.

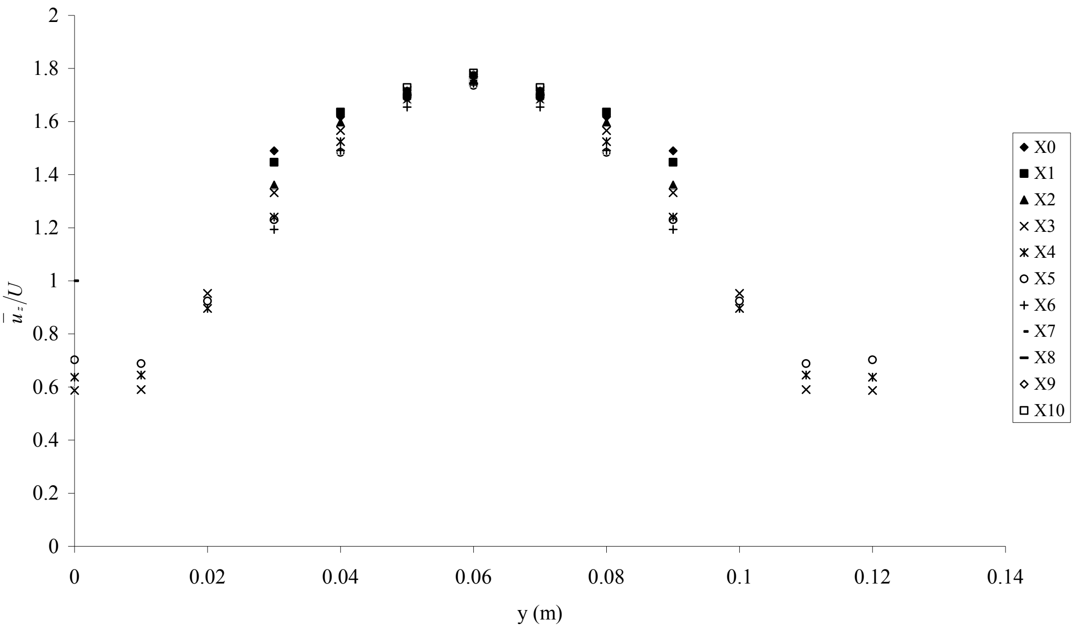

Figure 4.2 (a) Normalized depth-averaged velocity $\overline{u}_z/U$ for test 3.90A. The depth-averaged velocity is normalised by the cross-sectional area velocity.

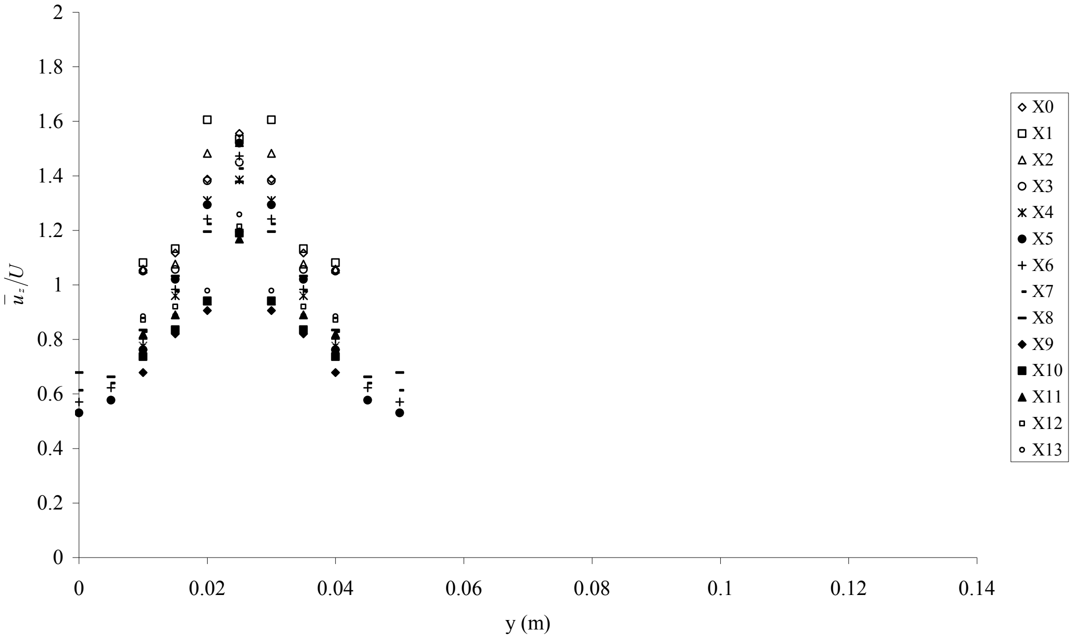

Figure 4.2 (b) Normalized depth-averaged velocity $\overline{u}_z/U$ for 7.79A. The depth-averaged velocity is normalised by the cross-sectional area velocity.

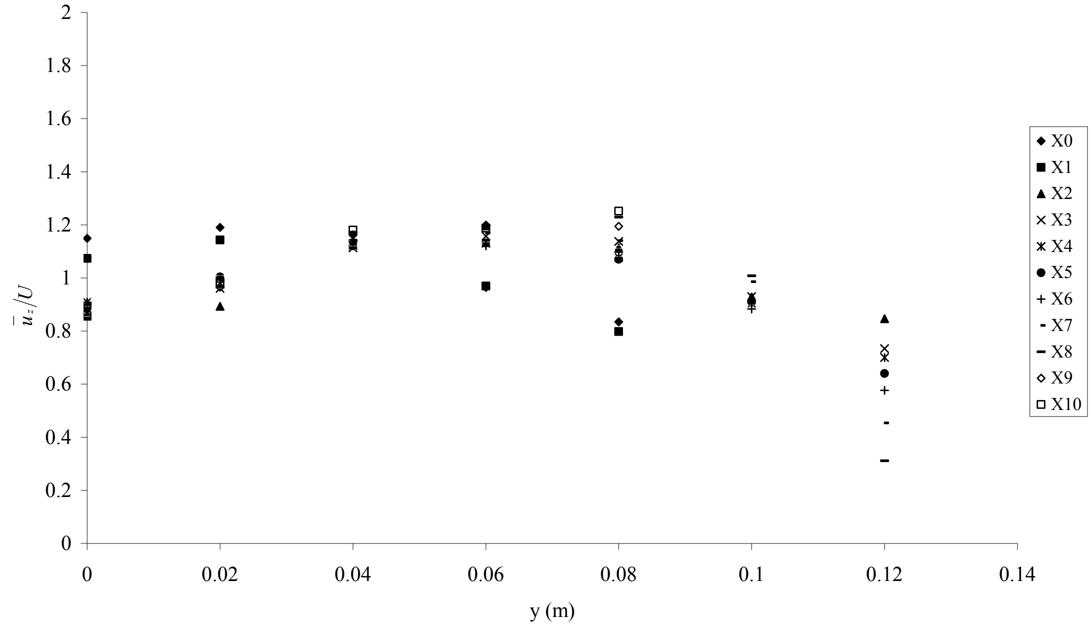

Figure 4.2 (c) Normalized depth-averaged velocity $\bar{u}_z/U$ for 0.97SL. The depth-averaged velocity is normalised by the cross-sectional area velocity.

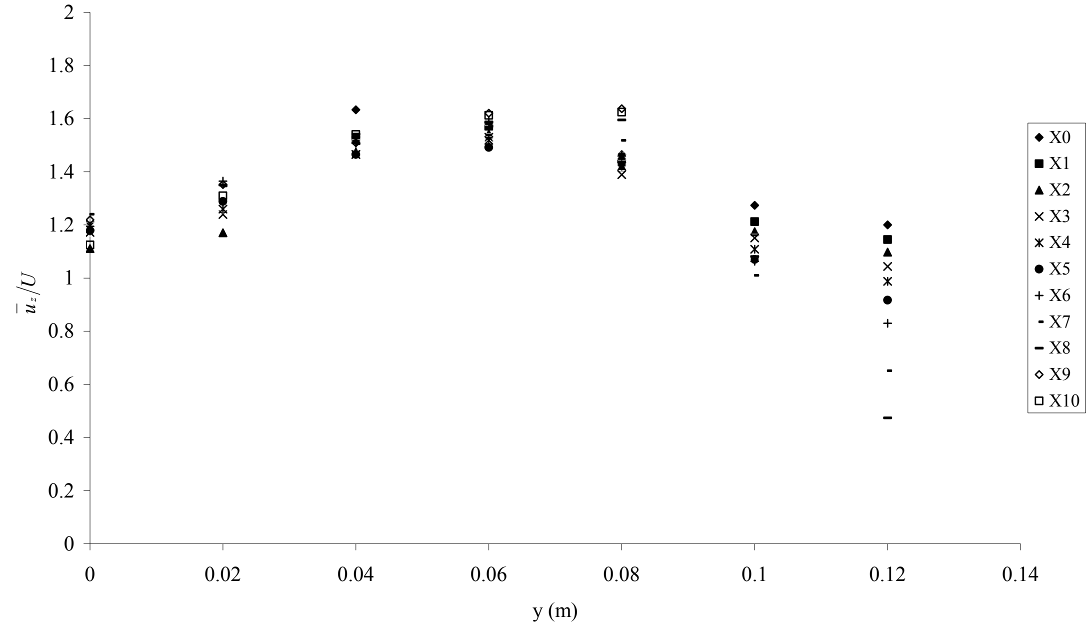

Figure 4.2 (d) Normalized depth-averaged velocity $\bar{u}_z/U$ for 0.97SH. The depth-averaged velocity is normalised by the cross-sectional area velocity.

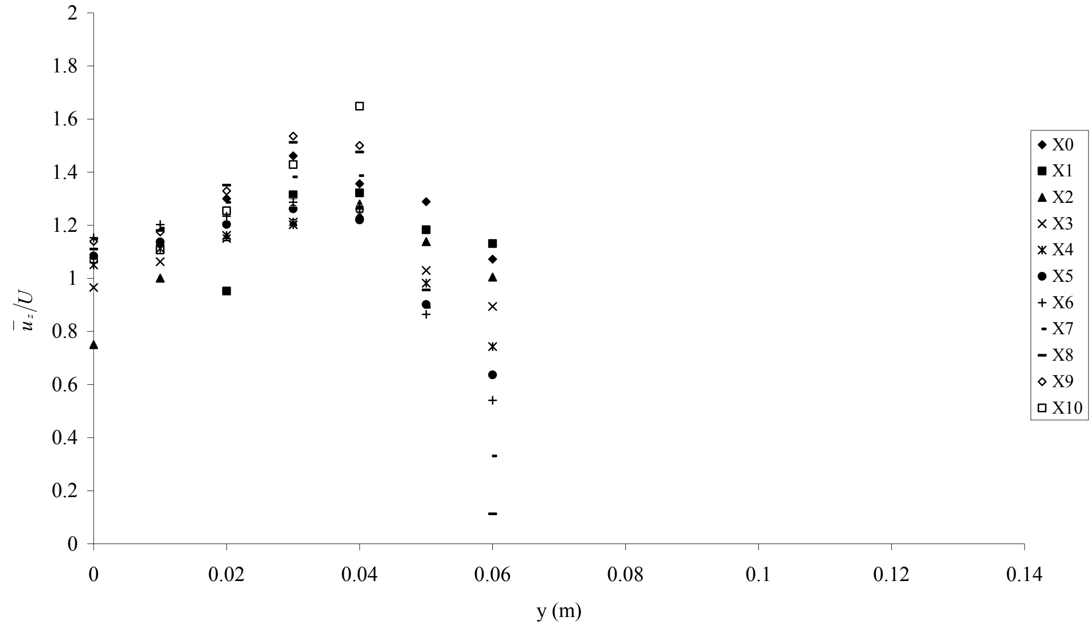

Figure 4.2 (e) Normalized depth-averaged velocity $\bar{u}_z/U$ for 3.90SH. The depth-averaged velocity is normalised by the cross-sectional area velocity.

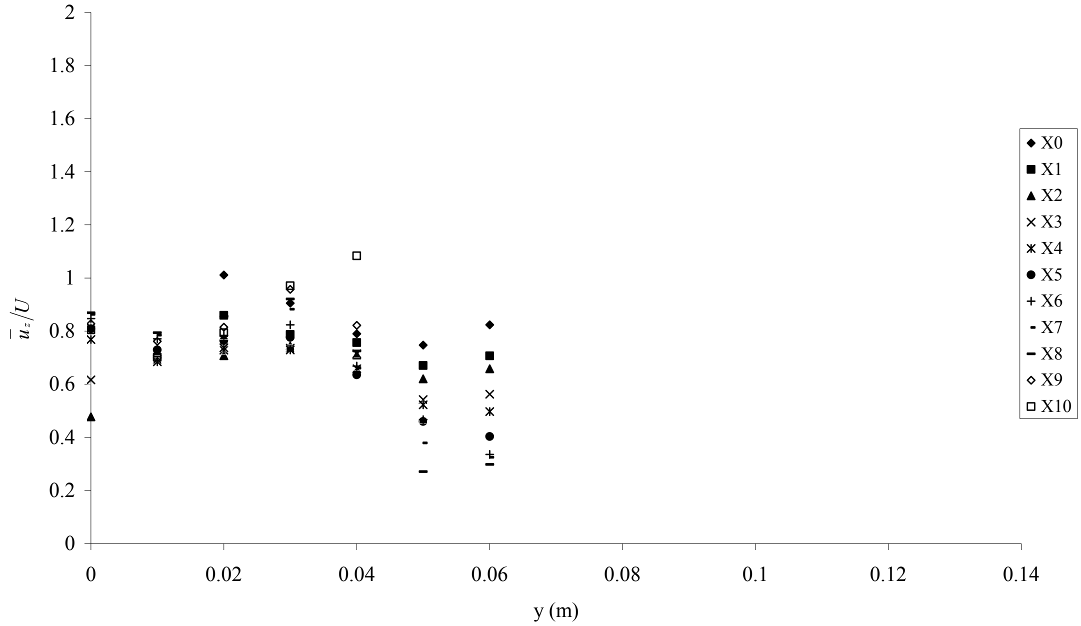

Figure 4.2 (f) Normalized depth-averaged velocity $\bar{u}_z/U$ for 3.90SL. The depth-averaged velocity is normalised by the cross-sectional area velocity.

For each point across the section (labelled *Y* on Figure 3.14) the depth-averaged velocity was averaged in the longitudinal direction (i.e. over cross-sections X0 to X13) to give a spatially-averaged velocity in both the vertical and longitudinal directions $\bar{u}_{xz}$. These values are again normalised by the cross-sectional area velocity and are presented for all six tests in Figures 4.3 (a) and (b).

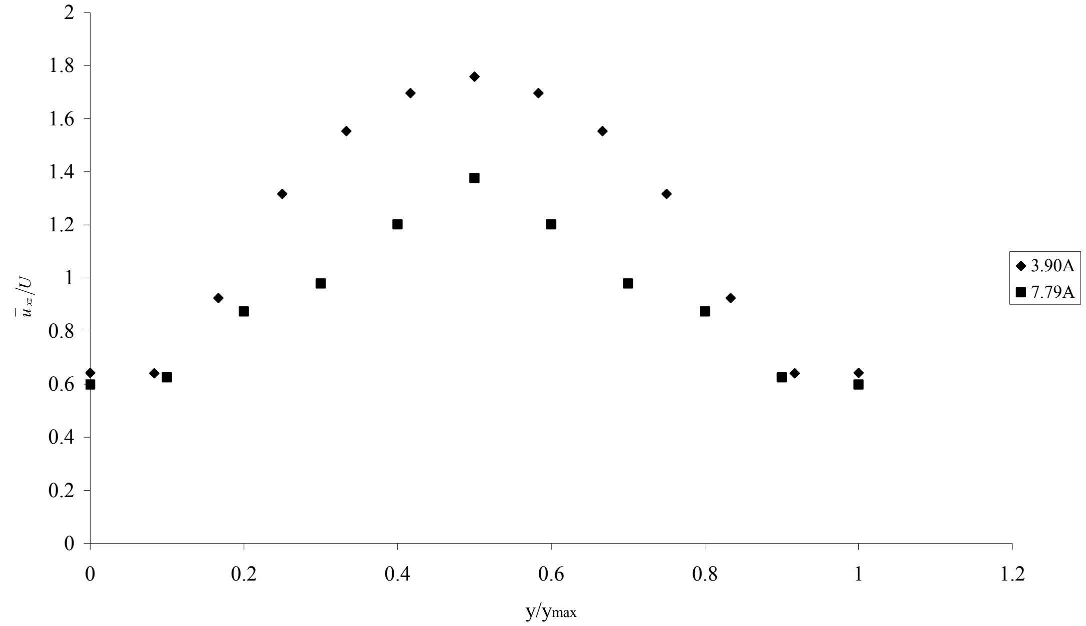

Figure 4.3 (a) Transverse variation of normalized longitudinal velocity $\bar{u}_{xz}/U$ for the aligned vegetation arrangements (tests 3.90A and 7.79A). ymax refers to the last point measurement on the right hand side of the control volume.

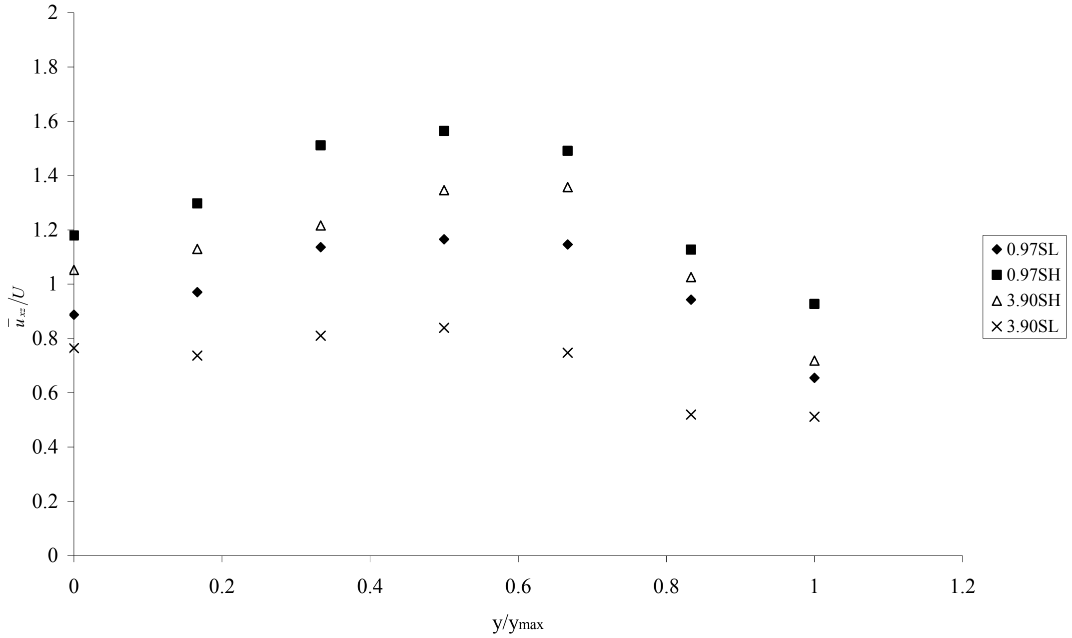

Figure 4.3 (b) Transverse variation of normalized longitudinal velocity $\overline{u}_{xz}/U$ for the staggered vegetation arrangements (tests 0.97S and 3.90S). y_{max} refers to the last point measurement on the right hand side of the control volume.

Figure 4.3 (a) presents the transverse profile for normalized longitudinal velocity $\overline{u}_{xz}/U$ for aligned vegetation arrangement. There is approximately 50 % to 60 % reduction in velocity, as the vegetation double in density from 3.90A to 7.79A. At y/y_{max} equal to 0 and 1, normalized velocities decreased about 40 % to 50 % compared to velocity in the middle section of the control volume.

The transverse profile for normalized longitudinal velocity $\overline{u}_{xz}/U$ for the staggered vegetation arrangement is presented in Figure 4.3 (b). 0.97SH created highest normalized velocity profile, followed by 3.90SH, then 0.97SL and 3.90SL produced the lowest normalized velocity profiles. Between the same densities, vegetation with higher water level generated greater velocity.

The highest longitudinal velocity for the aligned rod arrangement is located at the centreline between the two cylinders (labelled *Y6* for test 3.90A and *Y5* for test 7.79A see section 3.4.3, Figure 3.14) and the lowest velocity is located near the dowels either left and right hand side of the control volume (i.e. *Y0* and *Y12* for

3.90A; *Y0* and *Y10* for 7.79A). For the staggered arrangement the highest velocity is located at *Y3* which is along the longitudinal centreline between the cylinders and the lowest velocity is located at longitudinal section *Y6*, the longitudinal section closest to the cylinders.

In relation to above observations, Nepf (2004) and White and Nepf (2003) divide the velocity field into three regions. First is the recirculation zone of width d (stem diameter) and length γd where γ is a function stem Reynolds number. Second is the wake area downstream of the recirculation zone, where the velocity is positive but diminished from the spatially average velocity. The drag imposed by the surrounding arrays cause the wake profile to decay over length scale of $C_d a^{-1}$. Finally the flow in the gaps between the wakes area and recirculation zone, by conservation of mass must be greater than U.

Velocity deficit (i.e. $\overline{u}_{xz}/U$ lower than 1) in wake zones and velocity enhancement (i.e. $\overline{u}_{xz}/U$ greater than 1) zone can be observed in the experimental results. However experiment did not able to capture the recirculation zone due to instrument limitation. The nearest possible sampling measurement was about 3 cm or approximately *1d* (one diameter space) immediate after a dowel. According to Gerrard (1978) the size of recirculation zone γd is Reynolds number dependent.

Another observation is that for the same solid volume fraction for example test 3.90A and 3.90S with different arrangement vegetation it was found that aligned vegetation contained higher longitudinal velocity relative to staggered arrangement for the same density. This is according to Li and Shen (1973) staggered pattern generates more resistance than aligned configuration because the flow has to follow a more tortuous path.

4.1.2 Vertical Profiles of Longitudinal Velocity

In the *x-y* plane, the time-averaged longitudinal velocity was averaged longitudinally $\overline{u_x}$ for each control volume and each vertical level. The vertical profiles of longitudinal-averaged for each test and rod arrangement are presented in Figures 4.4 (a) to 4.4 (f). For the aligned vegetation *Y0* refers to longitudinal section nearest to the cylinders on the left hand side of the control volume and *Y6* (for 3.90A test) or *Y5* (for 7.79A test) refers to longitudinal centreline in the control volume. For the staggered arrangement *Y0* refers to the longitudinal section furthest from the upstream cylinder and *Y6* refers to the longitudinal section closest to the upstream cylinder (see section 3.4.3, Figure 3.14).

Vertical profiles of the longitudinal velocity display in Figures 4.4 (a) to (f) do not follow the universal logarithmic law and this also been observed by Wilson et. al (2003), Lightbody and Nepf (2006), Shucksmith (2008) and Liu (2008). Instead velocity within aligned and staggered dowels is observed to be almost constant with depth. According to Lightbody and Nepf (2006) velocity profile varies inversely with canopy morphology (i.e. velocity is minimum where the frontal area is maximum). Since this experimental work used dowels which have the same frontal area for the whole vertical length, therefore it is expected for the velocity profile to be constant with depth. Figure 4.4 (c) to 4.4 (f) show there are velocity deficit between velocity for the staggered configuration at 0.0075 m near bed and second level velocity reading at 0.0275 m, beyond that, the velocity profiles were nearly uniform. However this velocity deficit is not captured in aligned vegetation as the lowest level of velocity measurement was 0.01 m from the flume bed recommending that the boundary layer is thinner than 0.01 m from the bed. White and Nepf (2003) suggested that thin boundary layers are observed near the bed (below about 0.03h) in the vertical profiles.

According to Zavistoski (1994) the velocity deficit regime is cause by the difference in wake structure due to the absence of vortex shedding. In the absence of vortex the wake grows linearly and the velocity deficit decreases linearly as the distance from the cylinder increases. The velocity deficit regime is most prominent at 3 diameters downstream of the nearest dowel at the low density. Zavistoski (1994) commented that in the experiment vortex shedding does not occur for z < 40 mm. Experiment was conducted with 6 mm diameter hardwood to model *Spartina alterniflora* using flow with low stem Reynolds number (360 to 380).

Lui (2008) used the term velocity spike which is most pronounce immediately downstream of a dowel and decreases as the flow progresses. Lui (2008) explained that the velocity spike is probably caused by a horseshoe or junction vortex that forms at the base. The horseshoe vortex draws the faster moving fluid from the surrounding region into the base of the dowel causing a spike in the velocity near the bed. Lui (2008) used 6.35 mm acrylic dowels in staggered and aligned arrangement within range of *S*/*d* (i.e. *S* is the centre to centre distance between two rows of dowels and *d* is the diameter) between 8 (high vegetation density) to 16 (low vegetation density). The flow rates for the emergent and submerged experiments were 0.0057 m^3/s and 0.0114 m^3/s respectively (stem Reynolds number is about 1000).

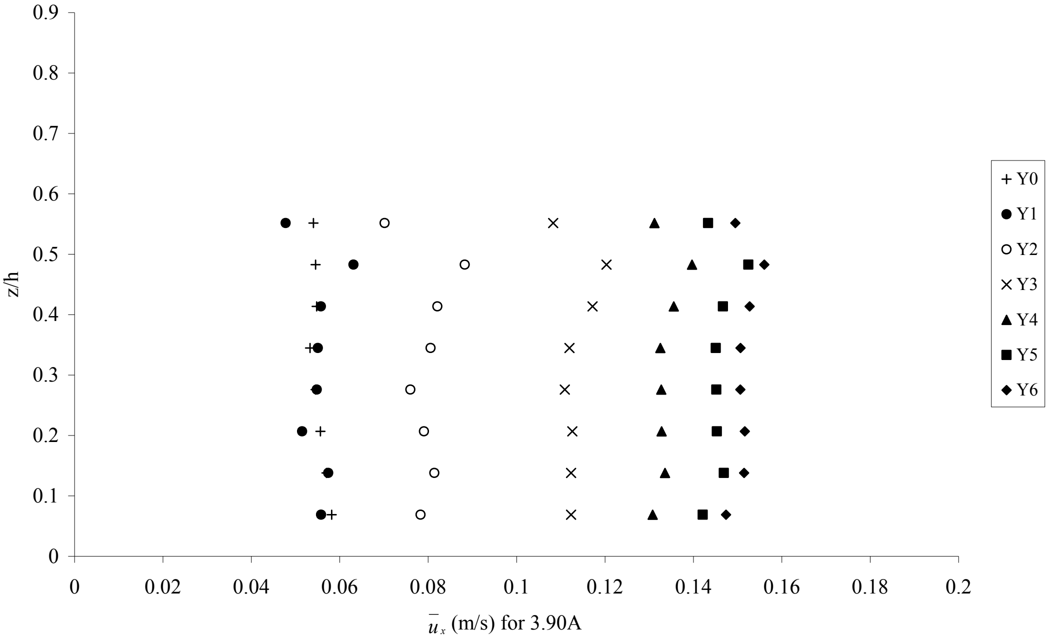

Figure 4.4 (a) Profiles of the longitudinally-averaged velocity, $\overline{u_x}$ for test 3.90A. *Y0* refers to longitudinal section nearest to the cylinders on the left hand side of the control volume and *Y6* refers to the longitudinal centreline in the control volume.

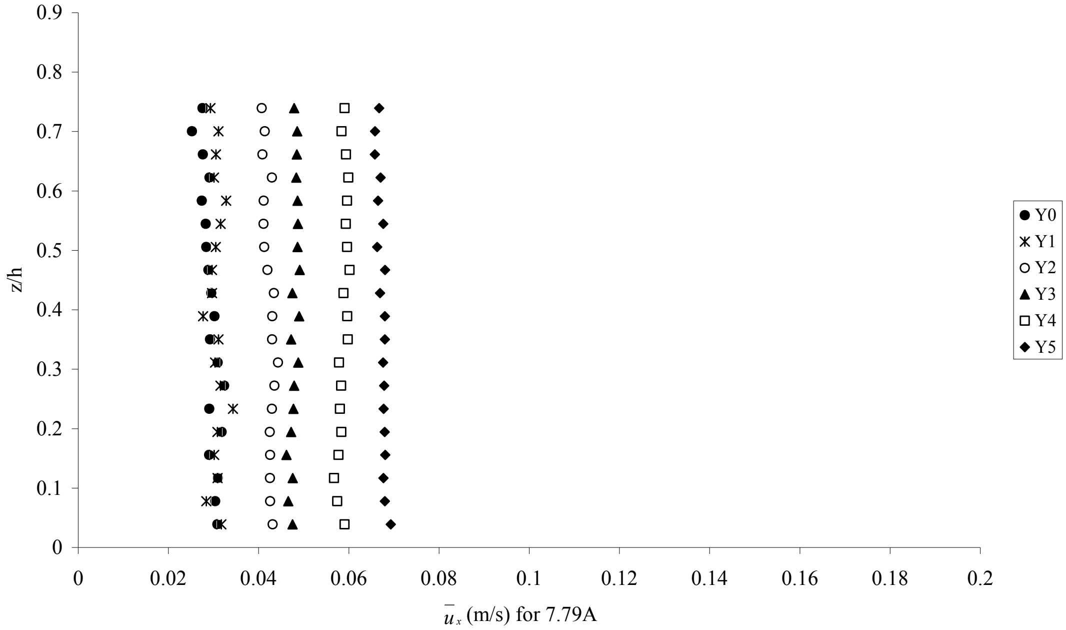

Figure 4.4 (b) Profiles of the longitudinally-averaged velocity, $\overline{u_x}$ for test 7.79A. *Y0* refers to longitudinal section nearest to the cylinders on the left hand side of the control volume and *Y5* refers to the longitudinal centreline in the control volume.

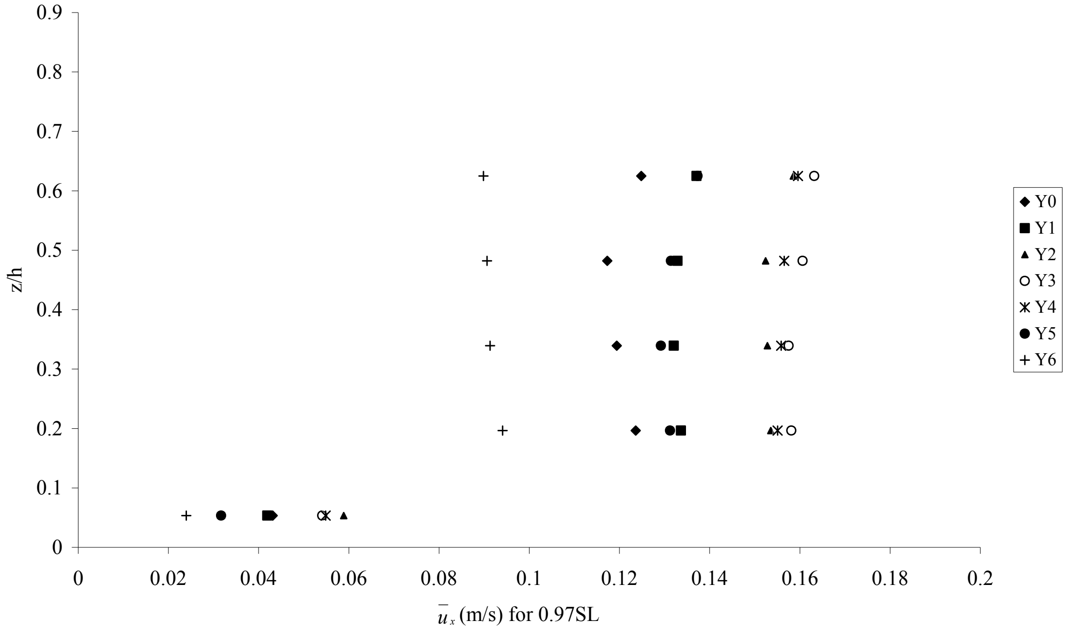

Figure 4.4 (c) Profiles of the longitudinally-averaged velocity, $\overline{u_x}$ for test 0.97SL. *Y0* refers to the longitudinal section furthest from the upstream cylinder and *Y6* refers to the longitudinal section closest to the upstream cylinder.

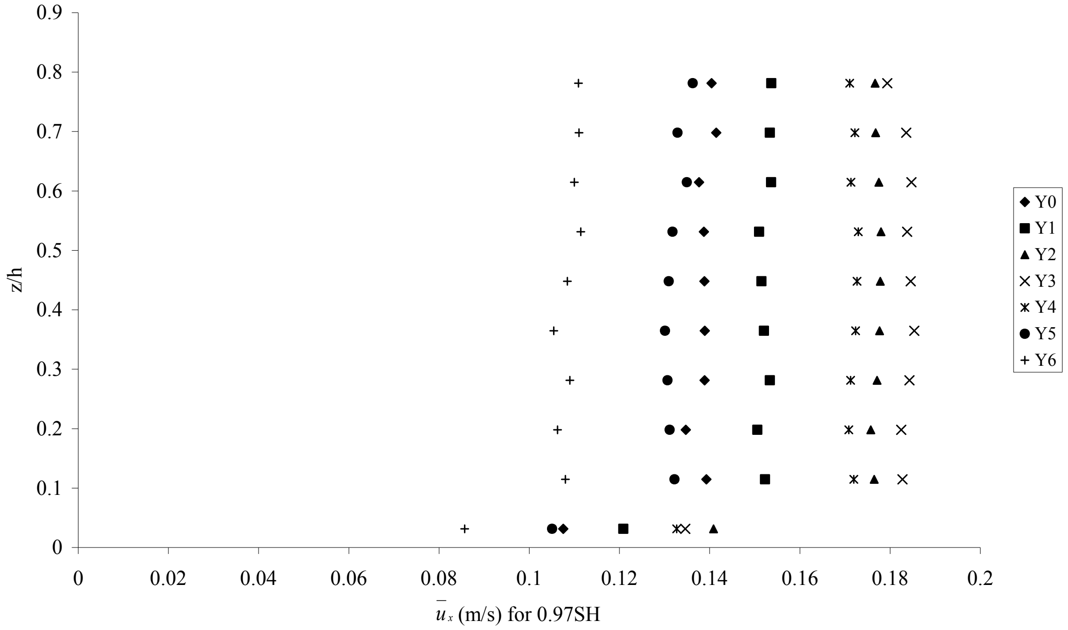

Figure 4.4 (d) Profiles of the longitudinally-averaged velocity, $\overline{u_x}$ for test 0.97SH. *Y0* refers to the longitudinal section furthest from the upstream cylinder and *Y6* refers to the longitudinal section closest to the upstream cylinder.

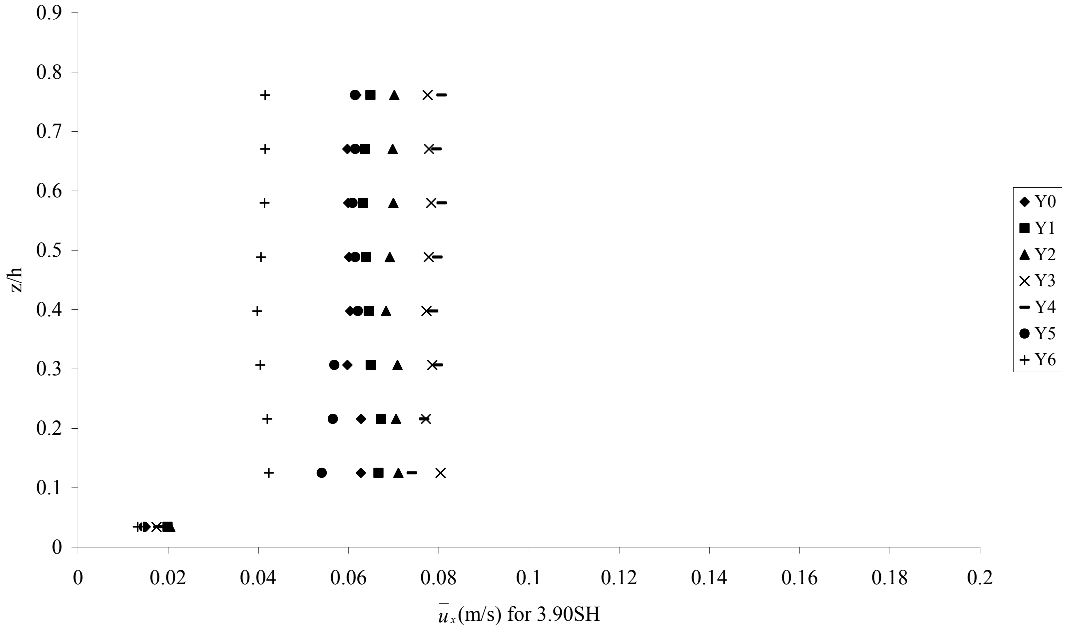

Figure 4.4 (e) Profiles of the longitudinally-averaged velocity, $\overline{u_x}$ for test 3.90SH. *Y0* refers to the longitudinal section furthest from the upstream cylinder and *Y6* refers to the longitudinal section closest to the upstream cylinder.

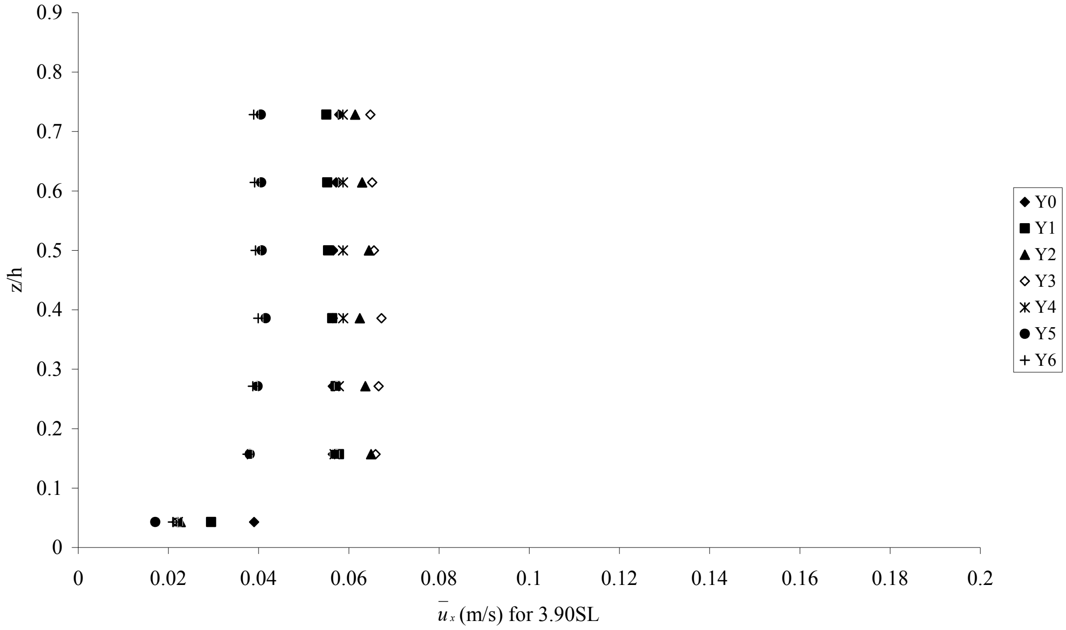

Figure 4.4 (f) Profiles of the longitudinally-averaged velocity, $\overline{u_x}$ for test 3.90SL. *Y0* refers to the longitudinal section furthest from the upstream cylinder and *Y6* refers to the longitudinal section closest to the upstream cylinder.

The longitudinal velocities were spatially-averaged both in the longitudinal and transverse directions, $\bar{u}_{xy}$ and each velocity was then normalised by the cross-sectional area velocity, *U*. The resulting spatially-averaged profiles for each test are presented in Figures 4.5 (a) and 4.5 (b).

Figure 4.5 (a) shows the vertical variation for aligned configuration and there is a reduced of 30 % to 40 % of longitudinal velocity, *u* by the increase in cylinder density from 3.90 % to 7.79 %. Another observation is that above 0.01 m (or z/h = 0.069 for 3.90A test and z/h = 0.039 for 7.79A) from the flume bed, the velocity profiles were relatively uniform.

Figure 4.5 (b) displays the vertical variation for staggered configuration. The lowest velocity is produced at 3.90SL, followed by 0.97SL, then 3.90SH and 0.97SH presents the highest velocity for staggered vegetation. Results indicate that, lower water level created more resistance to reduce the velocity.

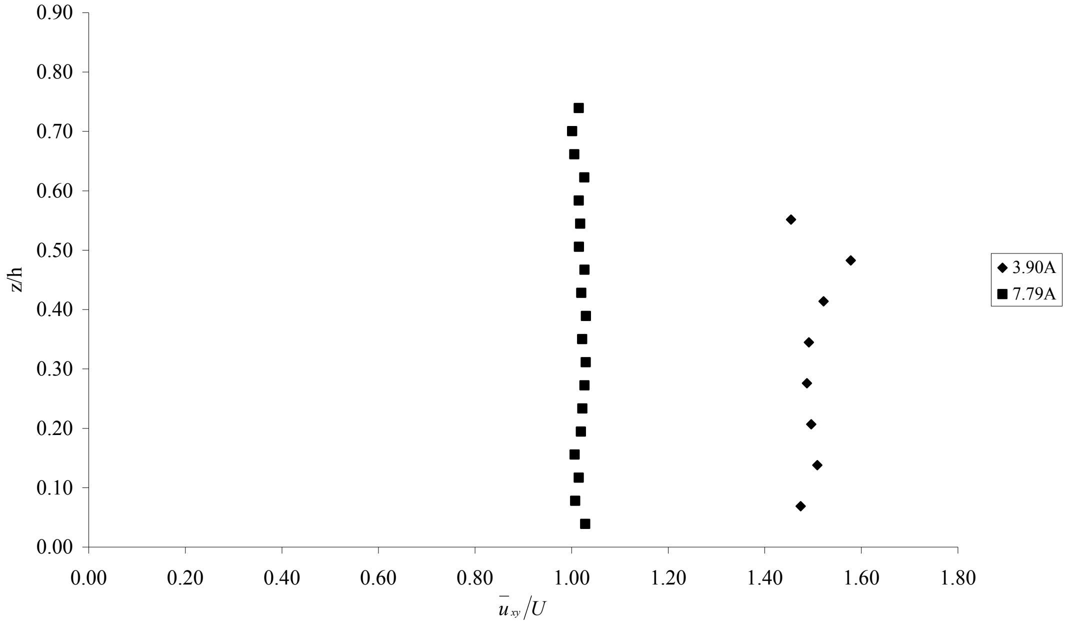

Figure 4.5 (a) Profiles of the normalised spatially-averaged velocity $\overline{u}_{xy}$ for aligned configurations

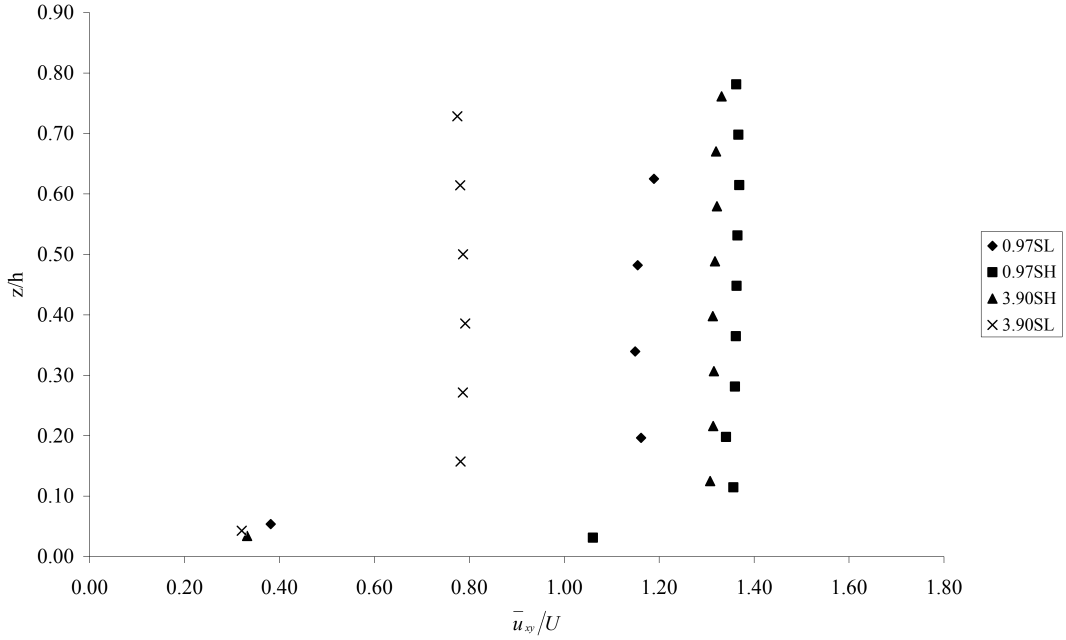

4.5 (b) Profiles of the normalised spatially-averaged velocity $\overline{u}_{xy}$ for staggered configurations

4.1.3 Vertical Variation in the Transverse Velocity

In the *x*-*y* plane, the transverse velocity was spatially-averaged over each longitudinal section $\bar{v}_x$ and then normalised by the cross-sectional area velocity. It is good to highlight that averaging transverse velocity involves positive and negative values of the transverse velocity. Therefore spatial averaging process may suppress the true magnitude of the transverse velocity. Hence a tactful interpretation or analysis of the one dimensional figures or results is definitely required. Vertical profiles of transverse velocities for each cylinder density and arrangement presented in Figures 4.6 (a) to 4.6 (f) are based on regular averaging process, nevertheless the display results will give some indication on the vertical variation of the transverse velocity across the control volume.

The difference in the magnitude and direction of the transverse velocity in the vertical direction reflects the transverse shear within the control volume that will give effect to the transverse mixing process. According to Zong (2011), the positive transverse velocity represents the flow diversion away from the vegetation and the negative transverse velocity indicating a flux towards the centre of the wake. Zong (2011) conducted an experimental study on interaction between flow and sediment deposition in vegetated channel. The first study investigates the flow structure and deposition pattern within partially vegetated channel. In the second study, a circular patch of emergent model vegetation located in the middle of the channel was examined. This experimental work was conducted in a low flow regime with stem Reynolds number between 6 and 84.

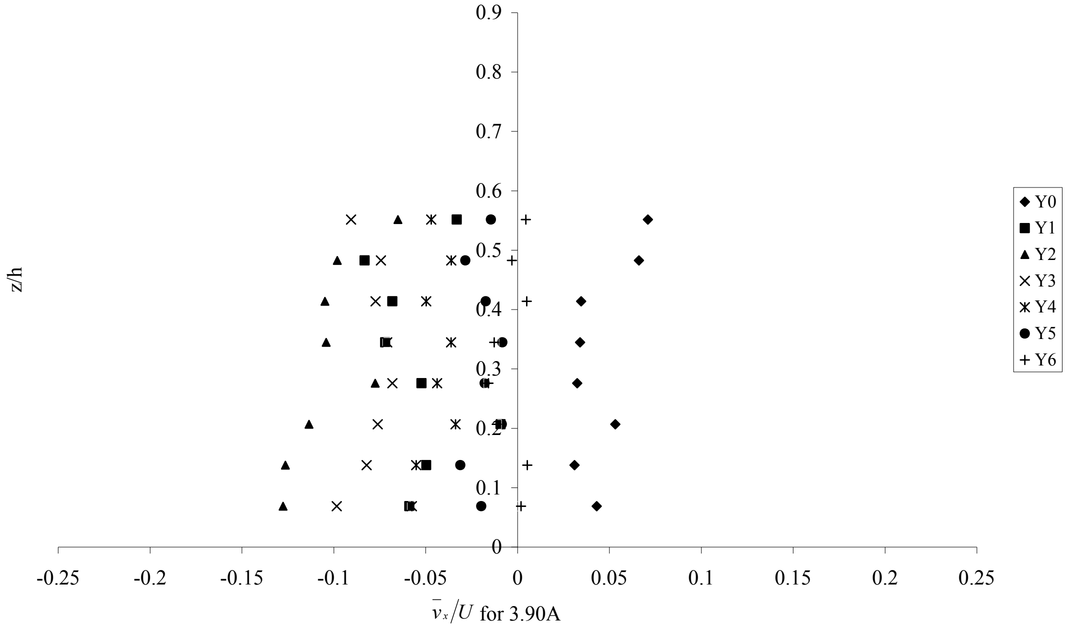

Figure 4.6 (a) Profiles of the normalised spatially-averaged transverse velocity $\bar{v}_x/U$ for test 3.90A. *Y0* refers to longitudinal section nearest to the cylinders on the left hand side of the control volume and *Y6* refers to the longitudinal centreline in the control volume.

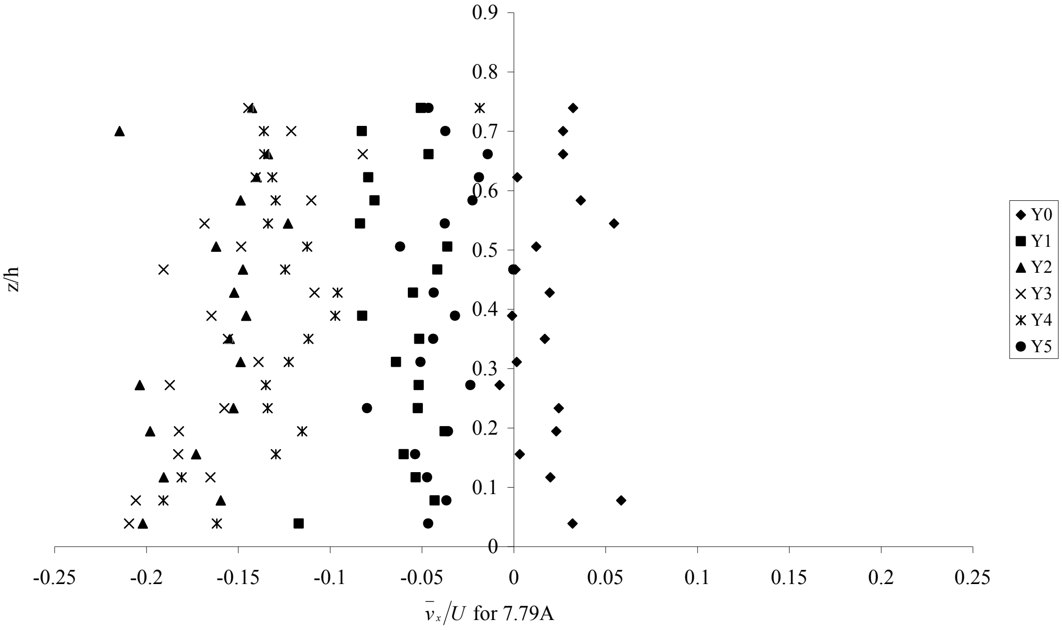

Figure 4.6 (b) Profiles of the normalised spatially-averaged transverse velocity $\bar{v}_x/U$ for test 7.79A. *Y0* refers to longitudinal section nearest to the cylinders on the left hand side of the control volume and *Y5* refers to the longitudinal centreline in the control volume.

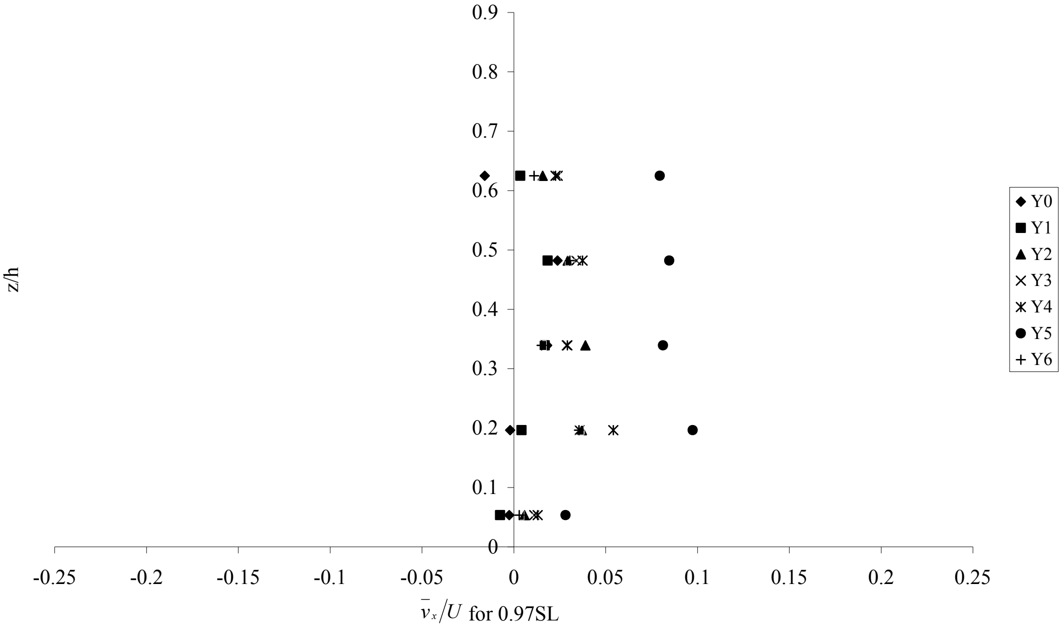

Figure 4.6 (c) Profiles of the normalised spatially-averaged transverse velocity $\bar{v}_x/U$ for test 0.97SL. *Y0* refers to the longitudinal section furthest from the upstream cylinder and *Y6* refers to the longitudinal section closest to the upstream cylinder.

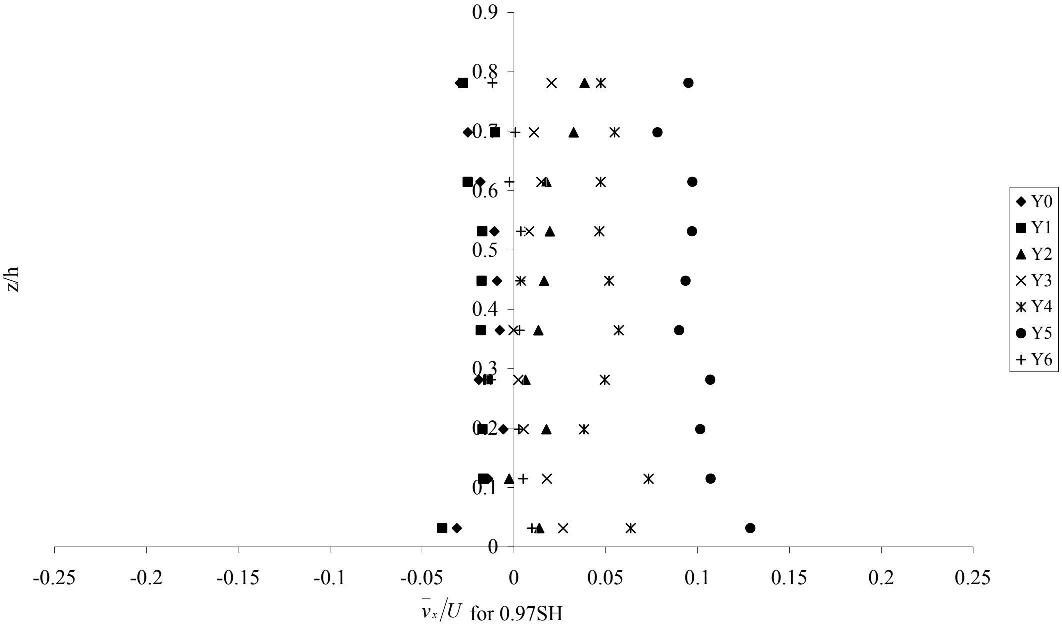

Figure 4.6 (d) Profiles of the normalised spatially-averaged transverse velocity $\bar{v}_x/U$ for test 0.97SH. *Y0* refers to the longitudinal section furthest from the upstream cylinder and *Y6* refers to the longitudinal section closest to the upstream cylinder.

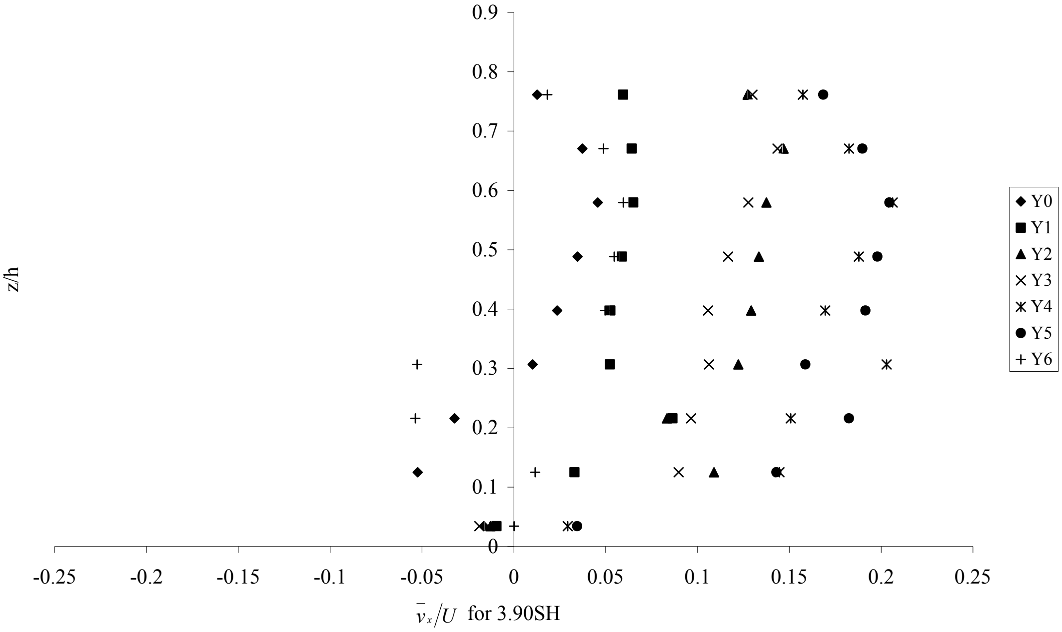

Figure 4.6 (e) Profiles of the normalised spatially-averaged transverse velocity $\bar{v}_x/U$ for test 3.90SH. *Y0* refers to the longitudinal section furthest from the upstream cylinder and *Y6* refers to the longitudinal section closest to the upstream cylinder.

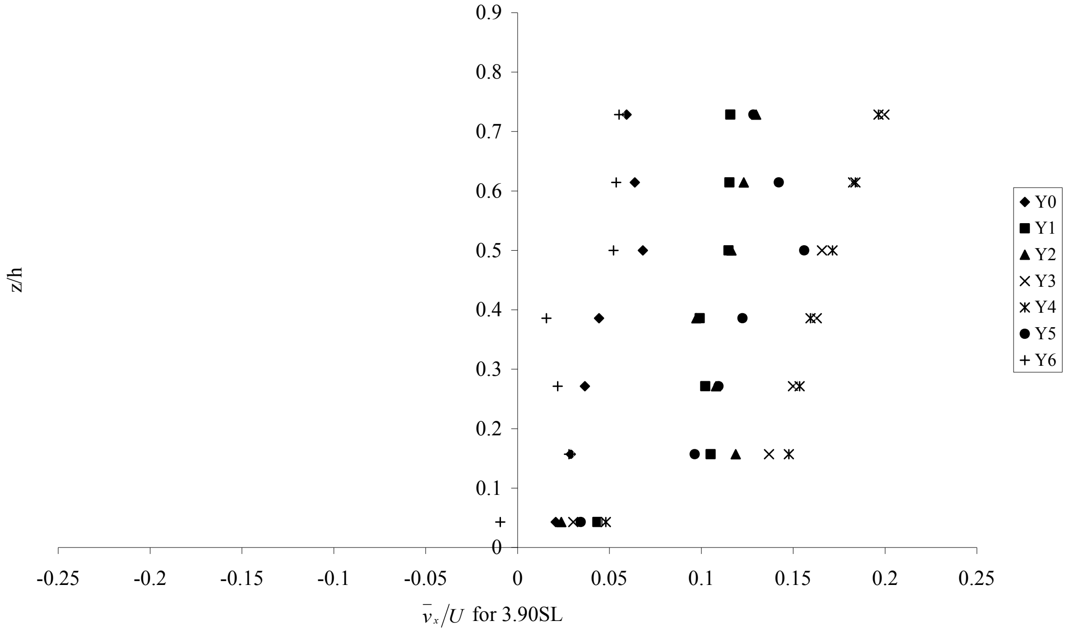

Figure 4.6 (f) Profiles of the normalised spatially-averaged transverse velocity $\bar{v}_x/U$ for test 3.90SL. *Y0* refers to the longitudinal section furthest from the upstream cylinder and *Y6* refers to the longitudinal section closest to the upstream cylinder.

Transverse velocity for test 3.90A and 7.79A (see Figures 4.6 (a) and 4.6 (b)) in aligned arrangement are mostly negative compared to transverse velocity for test 0.97S and 3.90S (see Figures 4.6 (c) to 4.6 (f)) in staggered arrangement. This is probably because in aligned arrangement the wake area is contributing to both left and right hand side of the control volume. Possibly due to the difference pressure within the wake area which is lower compared to the middle section of the control volume, therefore the transverse velocity will be driven towards the wake area. As previously mention by Zong (2011) the negative transverse velocity indicating the movement of flux to the centre of wake. Meanwhile in staggered arrangement where the farthest cylinder is located on the left hand side of the control volume and the nearest cylinder is located on right hand side of the control volume (looking downstream). Therefore, it is suspected that recovery wake area is on the left hand side of the control volume and the wake deficit area is in the right hand side of the control volume and the faster velocity area within the middle section of the control volume. For that reason probably there is more positive transverse velocity in the staggered arrangement compared to aligned arrangement.

Figures 4.7 (a) and (b) shows the standard deviation of transverse velocity as a function of solid volume fraction and stem Reynolds number respectively. For each vertical profile (including staggered and aligned vegetation) the average standard deviation of the absolute transverse velocity in the vertical profile was evaluated. These figures include the standard deviation from 0.97SH (staggered and high water level) and 0.97SL (staggered and low water level); 3.90A (aligned), 3.90SH (staggered and high water level) and 3.90SL (staggered and low water level); 7.79A (aligned). The average standard deviation for every test is resulted from the range difference of 60 % to 90 % between the minimum and the maximum standard deviation. The large variation of standard deviation maybe because in a control volume there are wake recovery area, wake deficit area and fast velocity area that contribute to the heterogeneous velocity condition. However as displayed in Figure 4.7 (a) and 4.7 (b) there is no direct correlation between the transverse velocity shear in the vertical and solid volume fraction or stem Reynolds number. Therefore more data is required to make this finding more conclusive.

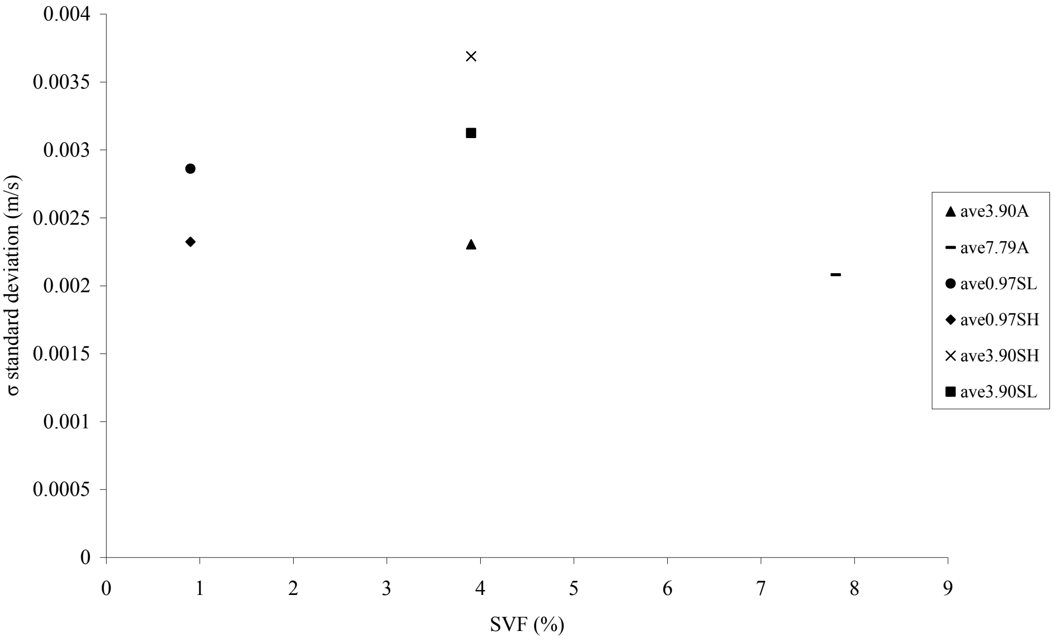

Figure 4.7 (a) Standard deviation σ of transverse velocity against solid volume fraction

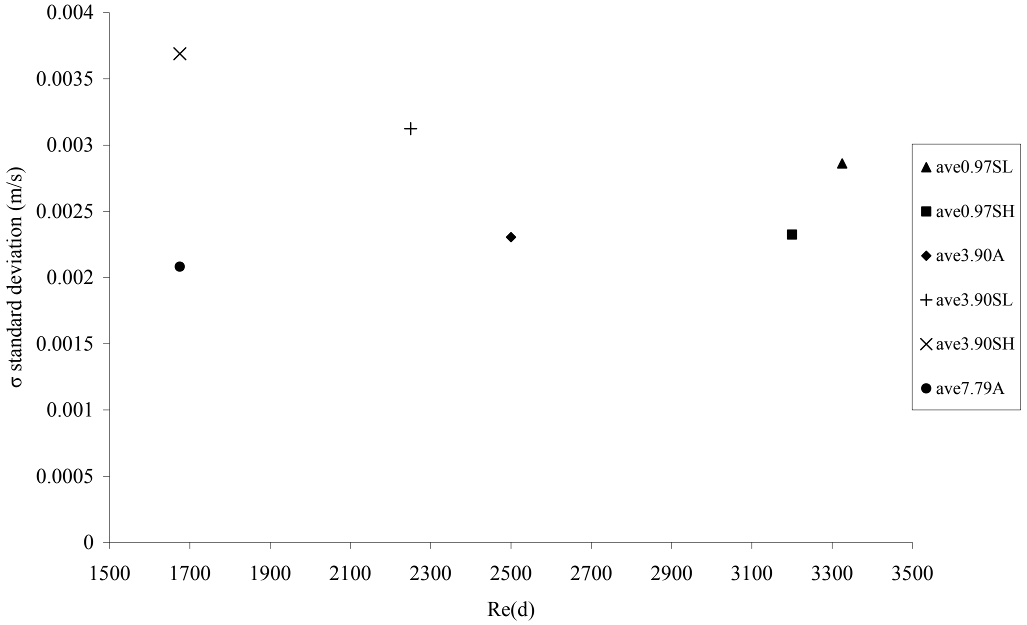

Figure 4.7 (b) Standard deviation of transverse velocity against Reynolds number

The variance of each vertical profile of transverse velocities can also be used to show the variation of the transverse velocities over the flow depth within the control volume. Figure 4.8 (a) and (b) show the variance of the transverse velocities in the vertical direction for aligned and staggered vegetation. The overall variation of the transverse velocities over the depth varies little except for tests 3.90SH and 3.90SL which have a slightly higher variance compared to other density arrangement. This is likely to happen because for tests 3.90SH and 3.90SL there is a velocity deficit of transverse velocity near the flume bed compared to other tests which are more uniform throughout the flow depth (as shown Figures 4.6 (a) to (f)). Therefore, variance results indicate that there is more transverse shear in 3.90SH and 3.90SL tests compared to others.

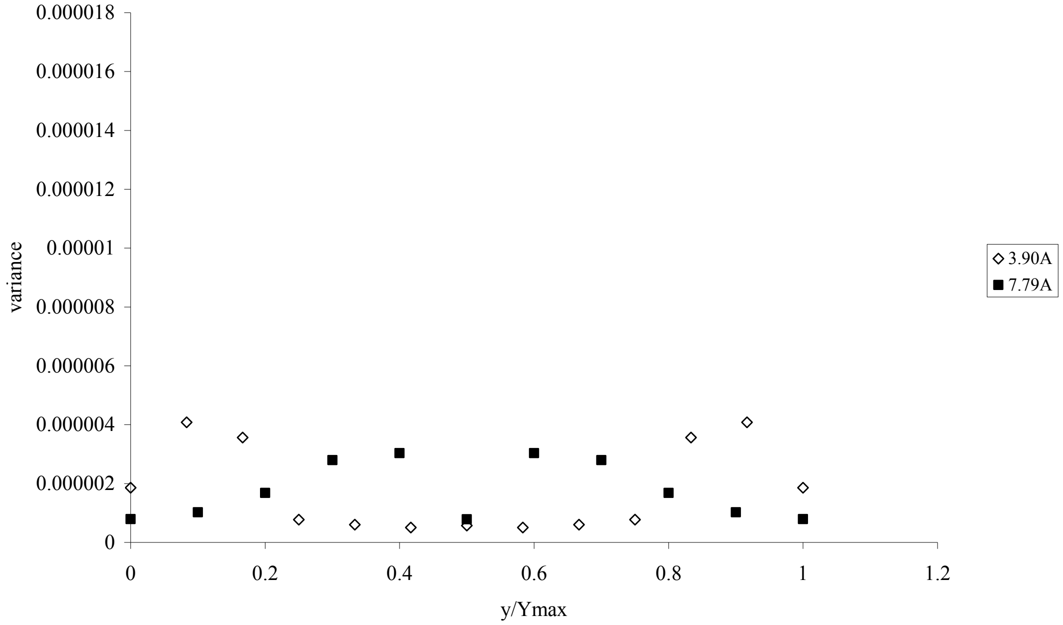

Figure 4.8 (a) Transverse profile of transverse velocity variance for aligned vegetation

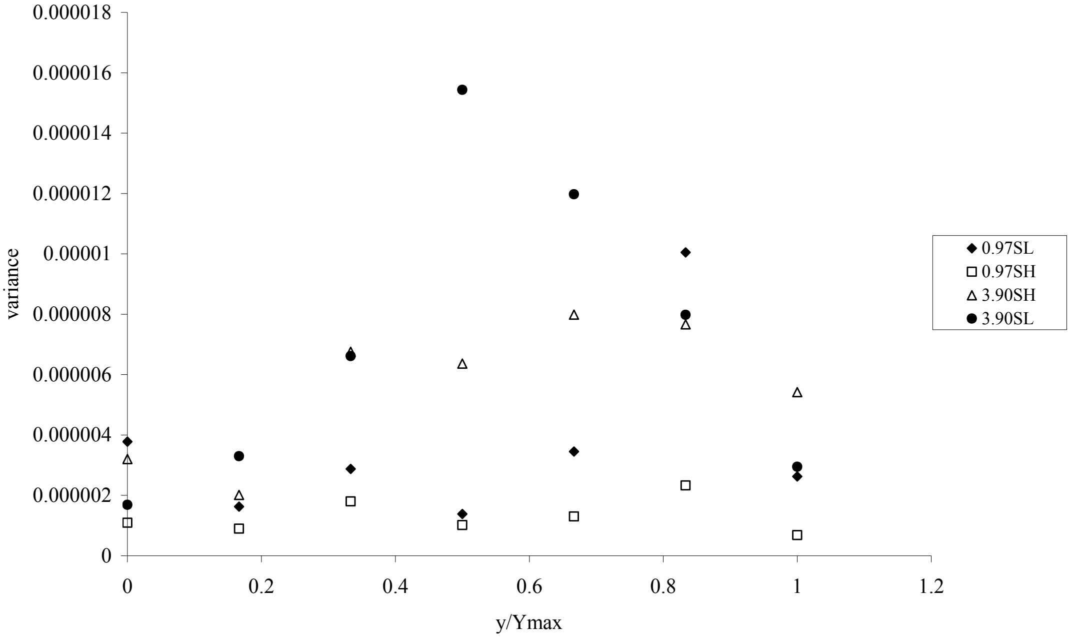

Figure 4.8 (b) Transverse profile of transverse velocity variance for staggered vegetation

4.2 Turbulence profiles

4.2.1 Vertical Variation of Turbulence Intensity

Turbulent intensities in the *x-y* plane (labelled *Y* in Figure 3.14) were spatially-averaged over each longitudinal section $\sqrt{\overline{u_x'^2}}$ and then normalized by the cross-sectional mean velocity, *U* and shown in Figures 4.9 (a) to 4.9 (f). For the aligned rod arrangement *Y0* located on the left hand side of the control volume and *Y6* (3.90A test) or *Y5* (7.79A test) is located at the centreline of the control volume. For the staggered arrangement *Y0* refers to the longitudinal section furthest from the upstream cylinders and *Y6* refers to the longitudinal section closest to upstream cylinders.

The spatially-averaged turbulent intensity $\sqrt{\overline{u_x'^2}}$ influenced by the variation of the vegetation parameter (i.e. density, vegetation arrangement) and hence will also affect the transverse mixing process. Figure 4.9 (a) present the vertical variation of normalized turbulence intensities for 3.90A test (SVF = 3.90 %, aligned). The highest turbulence intensity is located at *Y2* (see Figure 3.14 (c)) and there is possibly that *Y2* is situated within the boundary of the wake area and the fast flowing region. Zavistoski (1994) used the term wake edges where the turbulence intensity peaks occurs at the locations corresponding to the largest velocity gradient (*du/dy*). The lowest turbulence intensity for 3.90A is position at *Y6* at the middle section of the control volume with the fastest longitudinal velocity for the aligned vegetation arrangement (see Figure 4.3 (a)). Figure 4.9 (b) shows the results for the normalized turbulence intensity over the flow depth of 7.79A test (SVF = 7.79 %, aligned). Results for 7.79A test display some similarity with the 3.90A test, where the highest normalized turbulence intensity is situated at *Y3* which is between the wake and the fast flowing areas (see Figure 3.14 (d)) and *Y5* at the middle section of the control having the lowest normalized turbulence as expected. However, *Y1* which is situated within the wake area display slightly odd results when having same low turbulence intensity as *Y5*.

Figures 4.9 (a) and (b) show that for aligned arrangement larger vegetation density (SVF = 7.79 %) generated more turbulence intensities compared to the lower vegetation density (SVF = 3.90 %). Zavistoski (1994) also found similar results where the turbulence intensity also increases as the vegetation density increases. Meanwhile in Figures 4.9 (c) to (f) present that the staggered vegetation with higher water level for the same vegetation density produces more turbulent intensities relative to staggered vegetation with lower water level. However in Toth et al. (2011) found the opposite where the vertical averaged of turbulence intensity increases with flow depth of given site. Toth et al. (2011) study the turbulent energy dissipation rate based on instrumentally monitored turbulence intensity under different water levels in relation to zooplankton community of Lake Balaton, Hungary.

Figure 4.9 (c) shows the vertical variation for the normalized turbulence intensities for 0.97SL test (SVF = 0.97 %, staggered, low water level) and Figure 4.9 (d) present the results for 0.97SH test (SVF = 0.97 %, staggered, high water level). In these two test it was observed that turbulence intensities at *Y5* (0.97SH) and at *Y6* (0.97SL) which was situated at the longitudinal section near to the upstream cylinders produced the highest normalized turbulence intensities. Meanwhile *Y3* at the middle section of the control volume present the lowest normalized turbulence intensities. In 3.90SH test (SVF = 3.90 %, staggered, high water level) as shown in Figure 4.9 (e) and 3.90SL (SVF = 3.90 %, staggered, low water level) as shown in Figure 4.9 (f) where position *Y5* creating highest normalized turbulence intensities. However for 3.90SH test and 3.90SL test the lowest turbulence intensities were located at the *Y0* and *Y1* which were situated at the longitudinal section furthest from the upstream cylinders. Lui (2008) also observed the same situation where the highest turbulence intensities are found immediately downstream of a dowel and the weakest ones are in the free stream region. The former is caused by eddies shedding from the side of the cylinder in an alternating fashion.

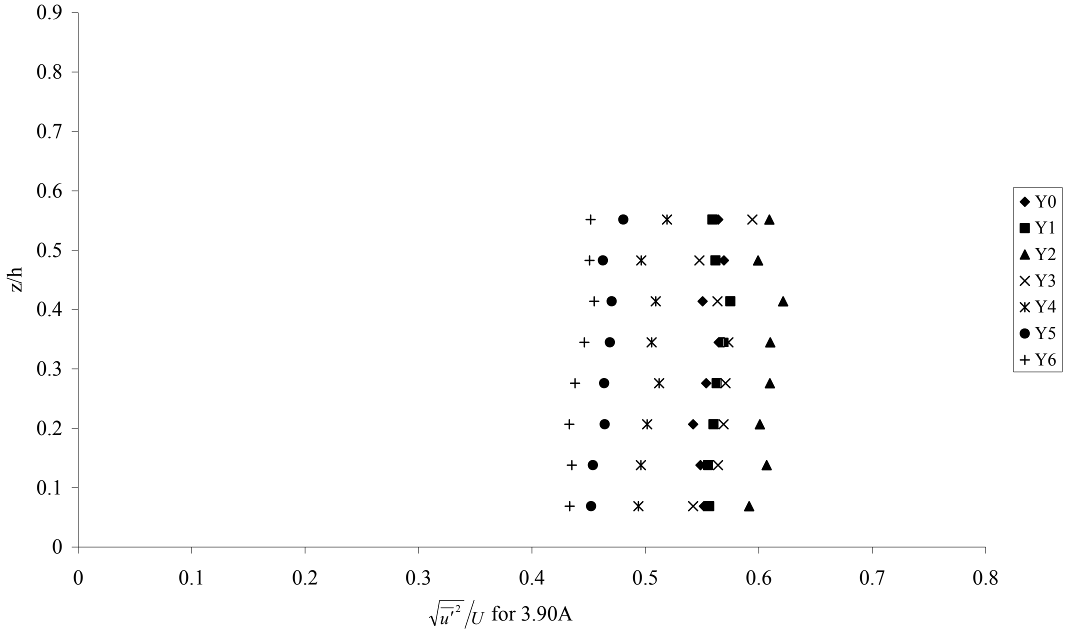

Figure 4.9 (a) Normalized turbulent intensities for vegetation density of 3.90A. *Y0* refers to longitudinal section nearest to the cylinders on the left hand side of the control volume and *Y6* refers to the longitudinal centreline in the control volume.

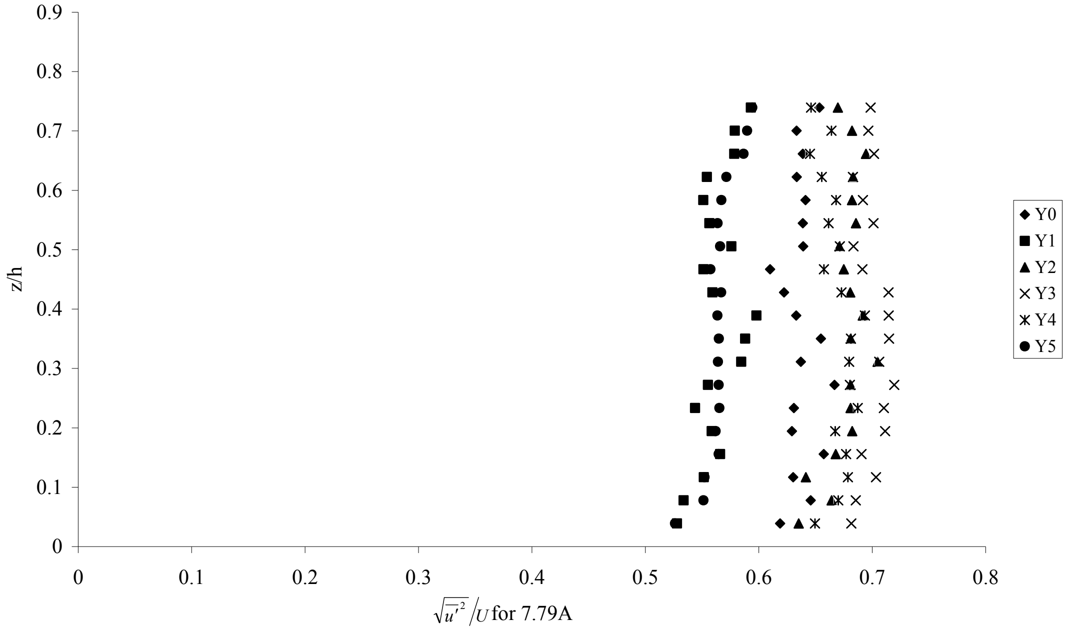

Figure 4.9 (b) Normalized turbulent intensities for vegetation density of 7.79A. *Y0* refers to longitudinal section nearest to the cylinders on the left hand side of the control volume and *Y5* refers to the longitudinal centreline in the control volume.

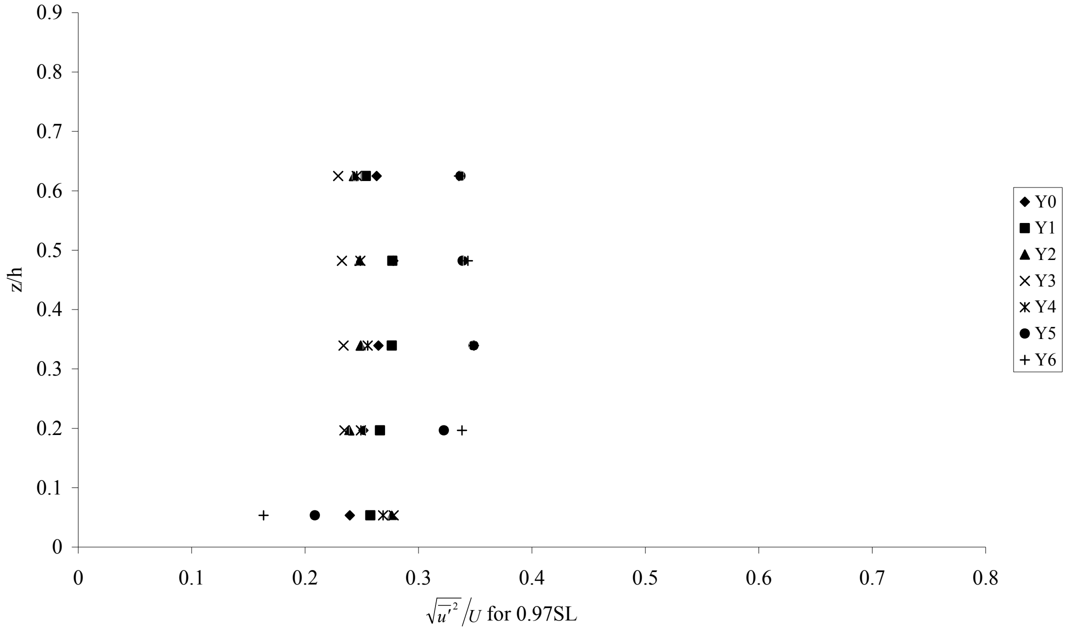

Figure 4.9 (c) Normalized turbulent intensities for vegetation density of 0.97SL. *Y0* refers to the longitudinal section furthest from the upstream cylinder and *Y6* refers to the longitudinal section closest to the upstream cylinder.

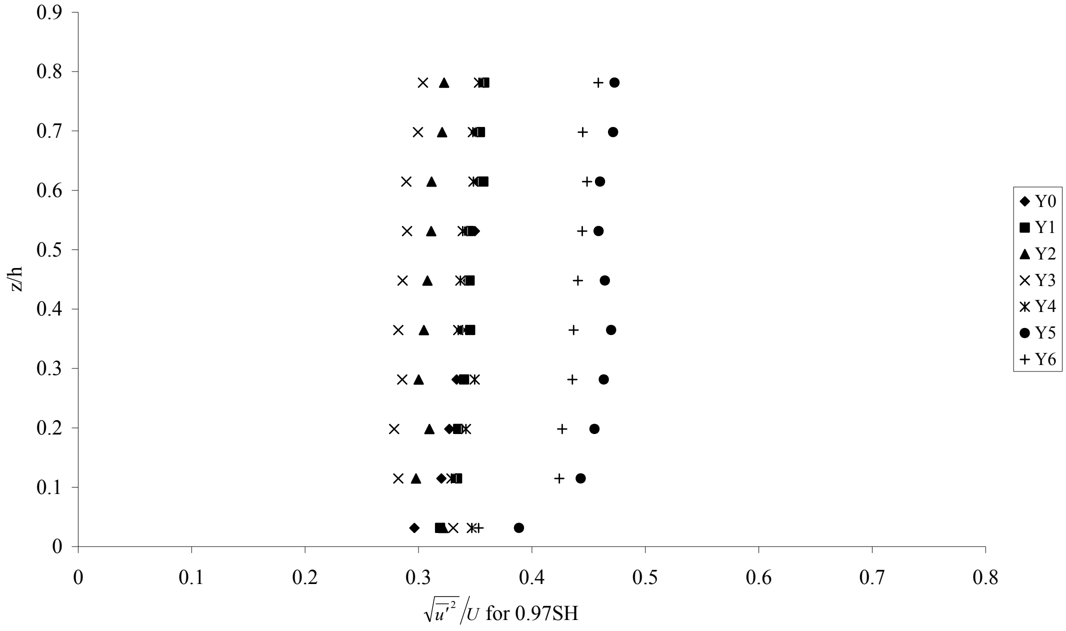

Figure 4.9 (d) Normalized turbulent intensities for vegetation density of 0.97SH. *Y0* refers to the longitudinal section furthest from the upstream cylinder and *Y6* refers to the longitudinal section closest to the upstream cylinder.

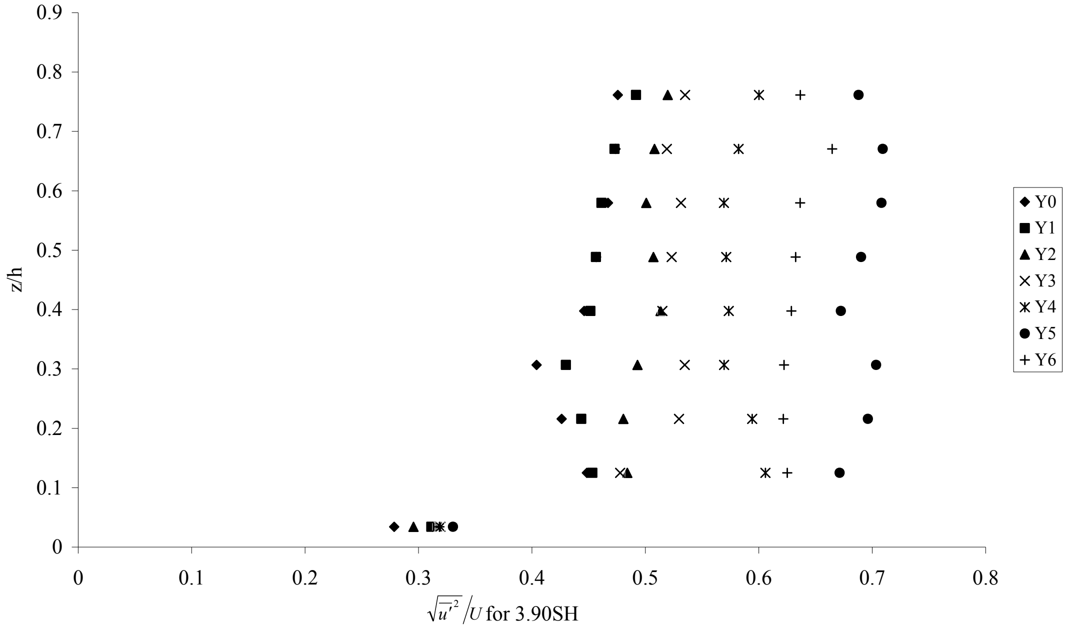

Figure 4.9 (e) Normalized turbulent intensities for vegetation density of 3.90SH. *Y0* refers to the longitudinal section furthest from the upstream cylinder and *Y6* refers to the longitudinal section closest to the upstream cylinder.

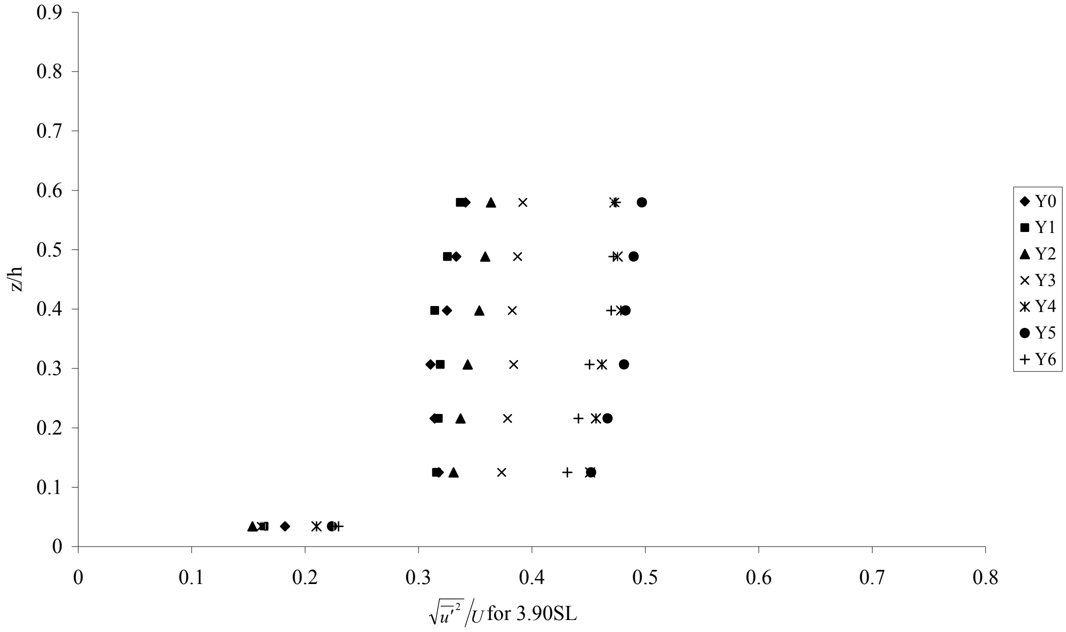

Figure 4.9 (f) Normalized turbulent intensities for vegetation density of 3.90SL. *Y0* refers to the longitudinal section furthest from the upstream cylinder and *Y6* refers to the longitudinal section closest to the upstream cylinder.

Figure 4.10 presents the averaged of normalized turbulent intensities against vegetation density where the turbulent intensities were spatially-averaged in the longitudinal, transverse and vertical directions and each turbulence intensity was then normalised by the cross-sectional area velocity $\sqrt{\overline{u'^2_{xyz}}}\big/U$. Figure 4.10 indicates there is a positive relation between turbulent intensity and vegetation density, where the turbulent intensities increases with vegetation density. As previously discussed this results similar to Zavistoski (1994) and Stoesser et al. (2010) results where the spatially-averaged turbulence intensity increases with vegetation density because there is more wakes present to generate more turbulence (Nepf, 2004).

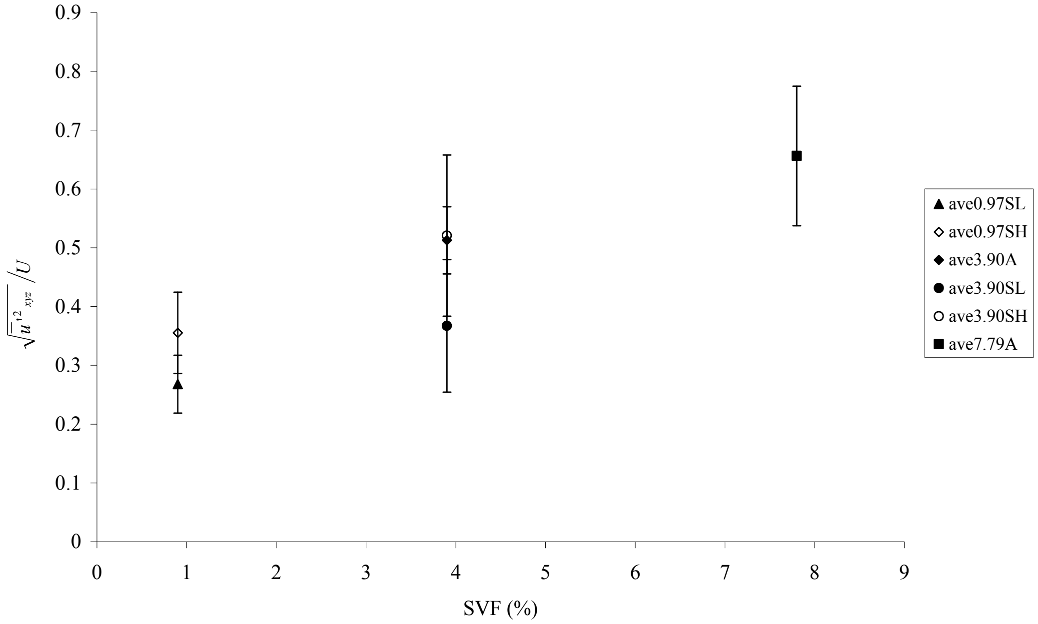

Figure 4.10 Averaged of normalized turbulent intensities plotted against solid volume fraction

Figure 4.11 displays the relation between the averaged normalized turbulent intensities $\sqrt{\overline{u'^2_{xyz}}}\big/U$ and stem Reynolds number where turbulent intensities decreases with the increment of stem Reynolds number. In this experiment the stem Reynolds number were between 1000 and 3000 and based on flow structure past a single emergent cylinder, for stem Reynolds number up to 1000, an increase in

Reynolds number corresponds to an increase in the turbulence level within both the free stream and the cylinder wake but as the turbulence levels in the free stream increases (up to stem Reynolds number 200000) the contribution of the cylinder wake to the total turbulence level of the flow decreases (Malki, 2009; Schlithting, 1955; Douglas et al., 1979).

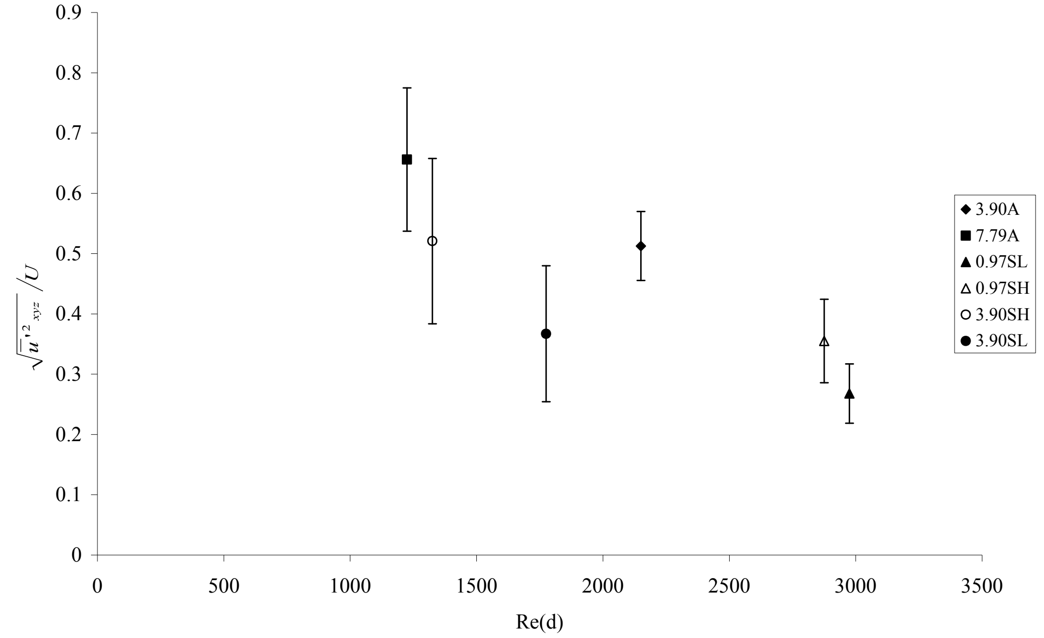

Figure 4.11 Averaged of normalized turbulent intensities plotted against stem Reynolds number

Figure 4.12 shows there is a weak positive relation between the averaged normalized turbulent intensities $\sqrt{\overline{u'^2_{xyz}}}/U$ and flow depth, *h*. Flow depth is often used in open channel study as characteristic length scale because the flow depth determines the size of the turbulence eddies which transport mass (Shucksmith, 2008). However according to Nepf (2012) and Tanino and Nepf (2008) the integral length scale of turbulence is set by canopy scale; i.e. the stems diameter (*d*) and the nearest-neighbour stems spacing (*S*). If the stems diameter is smaller than the nearest-neighbour stems spacing, then the integral length scale is stems diameter. Likewise if the stems diameter is larger that nearest-neighbour stems spacing, the integral length scale is nearest-neighbour stems spacing.

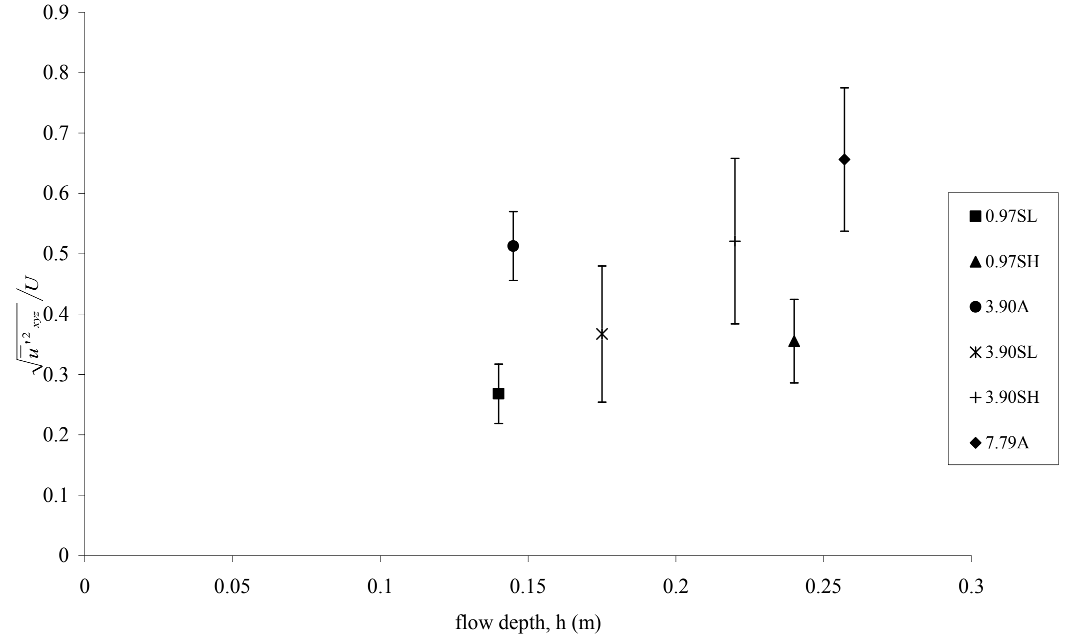

Figure 4.12 Averaged of normalized turbulent intensities plotted with flow depth

4.2.2 Vertical Variation of Turbulent Kinetic Energy

In the *x-y* plane the turbulent kinetic energy $\left(\overline{u'}^2 + \overline{v'}^2 + \overline{w'}^2\right)/2$ was averaged longitudinally (TKE_x) for every vertical level and this was repeated for each control volume. Figures 4.13 (a) to (e) present the vertical profiles of longitudinal-averaged turbulent kinetic energy for each test and rod arrangement. Please note that profile of longitudinal-averaged turbulent kinetic energy (TKE_x) for 0.97SH test was removed because of suspected erroneous data. For the aligned configuration (i.e. 3.90A and 7.79A tests), *Y0* refers to the dowels location on the left hand side of the control volume (looking downstream) and *Y6* (3.90A test) or *Y5* (7.79A test) refers to the middle section of the control volume. For staggered arrangement (i.e. 0.97SL, 0.97SH, 3.90SH, 3.90SL tests), *Y0* refers to the longitudinal sections furthest from the upstream cylinder and *Y6* refers to the longitudinal section closest to the upstream cylinder.

The vertical profiles of longitudinal-averaged turbulent kinetic energy (TKE_x) for aligned vegetation are shown in Figure 4.13 (a) to 4.13 (b). The lowest turbulence kinetic energy for aligned arrangement located at the centre section of the control volume (*Y6* for 3.90A test and *Y5* for 7.79A test) and the magnitude of turbulent kinetic energy increases towards the dowels at *Y0*. Meanwhile for the staggered arrangement (i.e. 0.97SL, 0.97SH, 3.90SH, and 3.90SL), the vertical profiles of the longitudinal-averaged turbulent kinetic energy (TKE_x) are displayed in Figures 4.13 (c) to (f). For the vegetation density of 0.97SL and 0.97SH (see Figures 4.13 (c) and (d)), *Y6* which was located at the longitudinal section closest to the upstream cylinder present the highest turbulent kinetic energy within the control volume and *Y3* at the middle section of the control volume displayed the lowest turbulent kinetic energy. Similar to 3.90SH and 3.90SH tests (see Figures 4.13 (e) and (f)) the highest turbulent kinetic energy is located at *Y6* for 3.90SH test or *Y5* for 3.90SL which were located at the longitudinal section closest to the upstream cylinder. However the lowest turbulence kinetic energy for vegetation density of 3.90SL and 3.90SH were not at the centre line of the control volume but shifted to *Y1* which is more to the left hand side of the control volume (looking downstream).

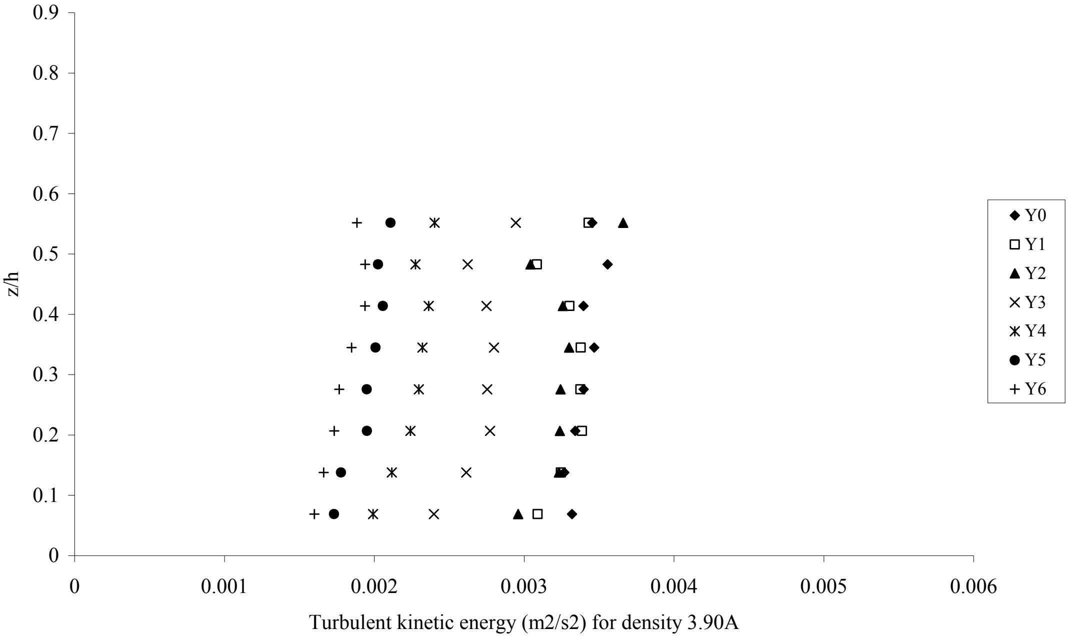

Figure 4.13 (a) Profiles of the longitudinal-averaged turbulent kinetic energy (TKE_x) for 3.90A test. *Y0* refers to longitudinal section nearest to the cylinders on the left hand side of the control volume and *Y6* refers to the longitudinal centreline in the control volume.

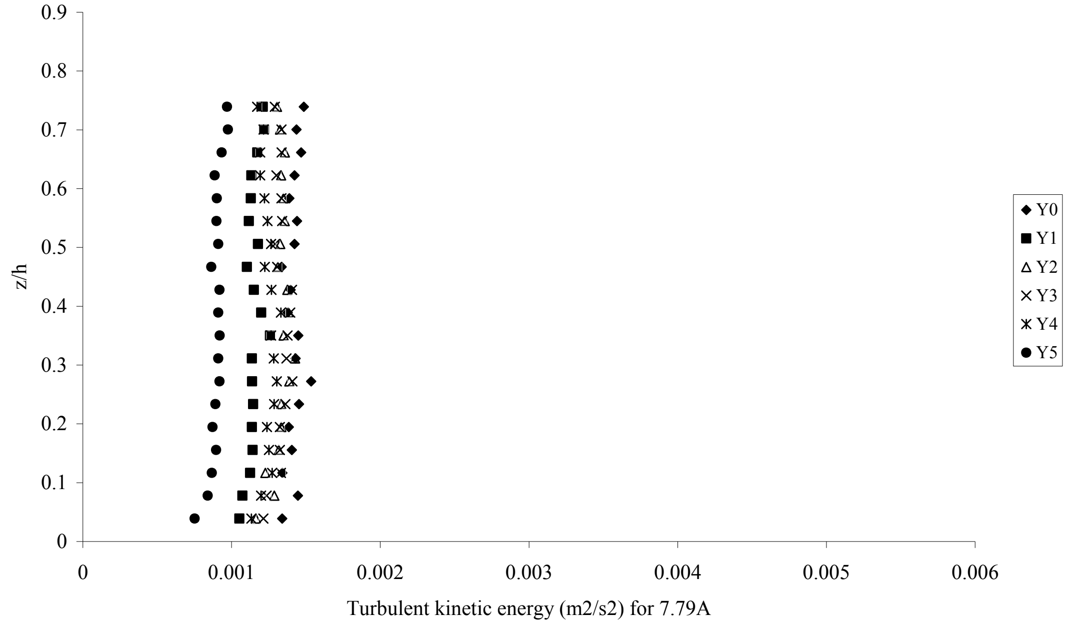

Figure 4.13 (b) Profiles of the longitudinal-averaged turbulent kinetic energy (TKE_x) for 3.90A test. *Y0* refers to longitudinal section nearest to the cylinders on the left hand side of the control volume and *Y5* refers to the longitudinal centreline in the control volume.

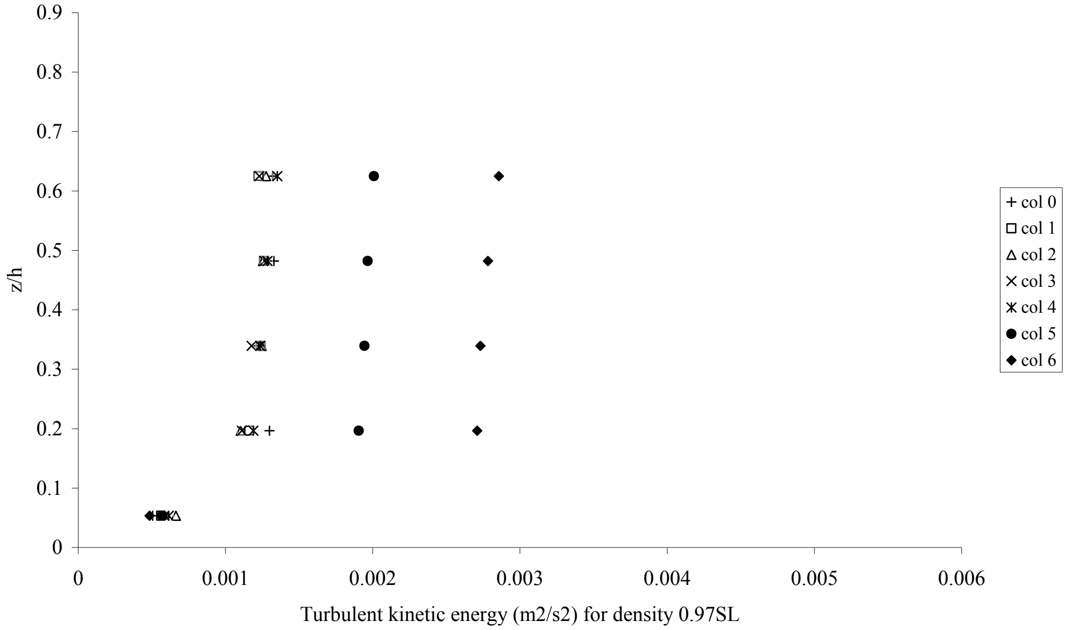

Figure 4.13 (c) Profiles of the longitudinal-averaged turbulent kinetic energy (TKE_x) for 0.97SL test. *Y0* refers to the longitudinal section furthest from the upstream cylinder and *Y6* refers to the longitudinal section closest to the upstream cylinder.

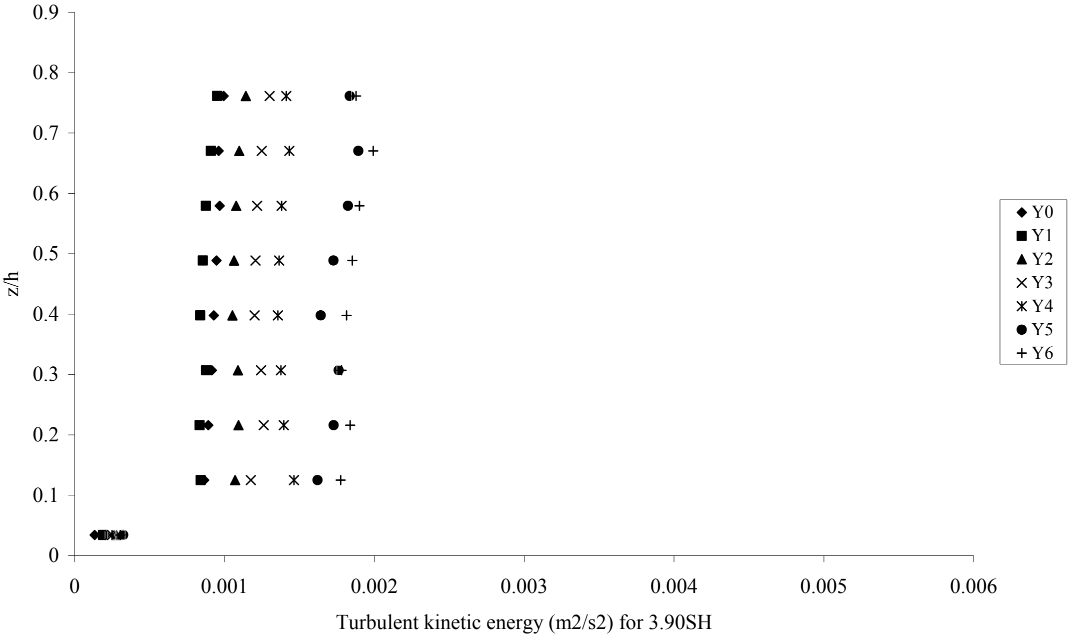

Figure 4.13 (d) Profiles of the longitudinal-averaged turbulent kinetic energy (TKE_x) for 3.90SH test. *Y0* refers to the longitudinal section furthest from the upstream cylinder and *Y6* refers to the longitudinal section closest to the upstream cylinder.

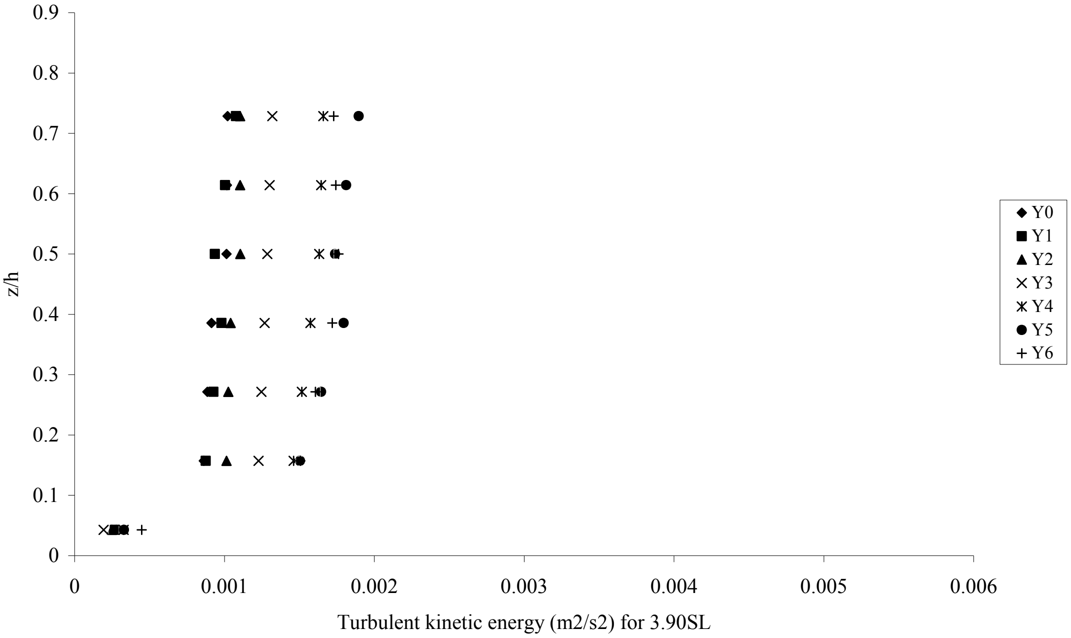

Figure 4.13 (e) Profiles of the longitudinal-averaged turbulent kinetic energy (TKE_x) for 3.90SL test. *Y0* refers to the longitudinal section furthest from the upstream cylinder and *Y6* refers to the longitudinal section closest to the upstream cylinder.

Turbulent kinetic energy is spatially-averaged in the longitudinal, transverse and vertical directions (TKE_{xyz}) for each vegetation density and is shown in Figures 4.14 to 4.16. Figure 4.14 present the spatially-averaged turbulent kinetic energy against the solid volume fraction and results display a weak negative relation (turbulence kinetic energy decreases as the solid volume fraction increases) between spatially-averaged turbulent kinetic energy and vegetation density. According to Nepf (1999) changes in turbulent kinetic energy reflect the competing effects of reduced velocity and increased turbulence production. These opposing tendencies produce a nonlinear response in which the turbulence levels initially increase with increasing stems density, but eventually decrease as vegetation density increases further.

Figure 4.15 shows the spatially-averaged turbulent kinetic energy (TKE_{xyz}) against stem Reynolds number which reflects a weak positive correlation (turbulent kinetic energy increases as the stem Reynolds number increases) between turbulent kinetic energy and stem Reynolds number. This positive correlation would be expected as higher stem Reynolds number associates with higher turbulence level. Meanwhile

Figure 4.16 plots the spatially-averaged turbulent kinetic energy (TKE_{xyz}) against flow depth and there is no observable trends can be captured between TKE_{xyz} and flow depth. In unobstructed open channel flow turbulent length scale are set by flow depth, however in vegetated channel the stems impinge on the channel scale eddies and these eddies are broken apart and the turbulence is then rescale to the stems geometry (Nepf, 1999).

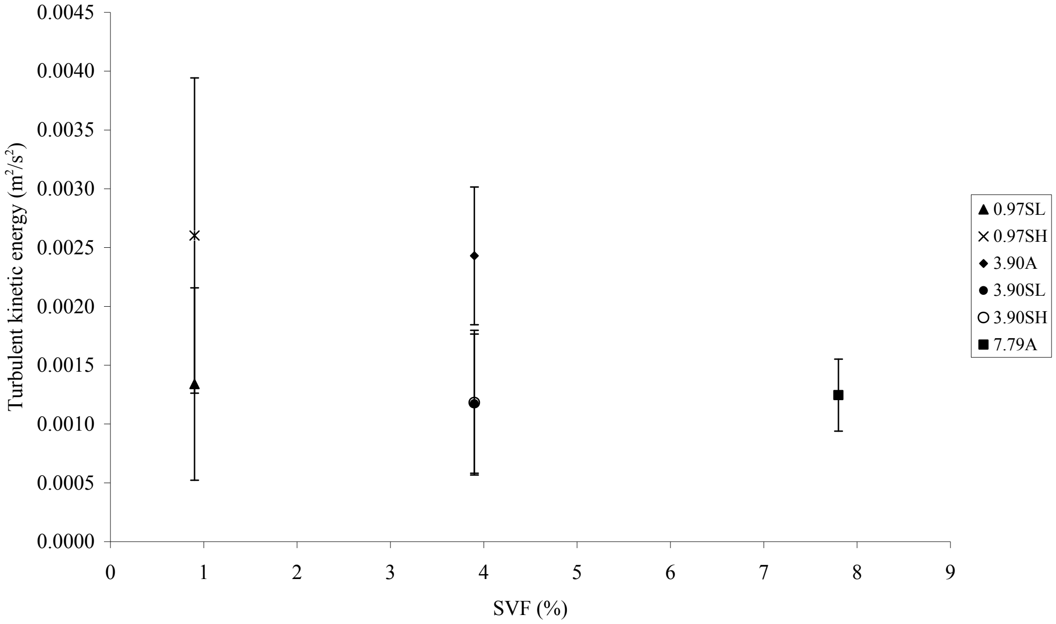

Figure 4.14 Spatially-averaged turbulent kinetic energy (TKE_{xyz}) plotted against solid volume fraction.

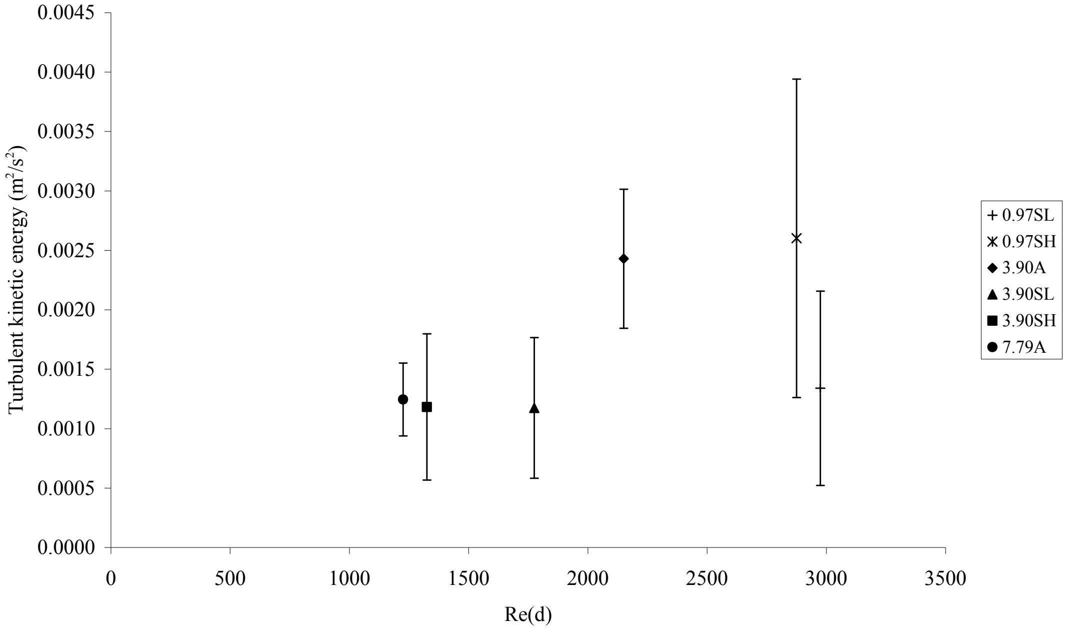

Figure 4.15 Spatially-averaged turbulent kinetic energy (TKE_{xyz}) plotted against stem Reynolds number.

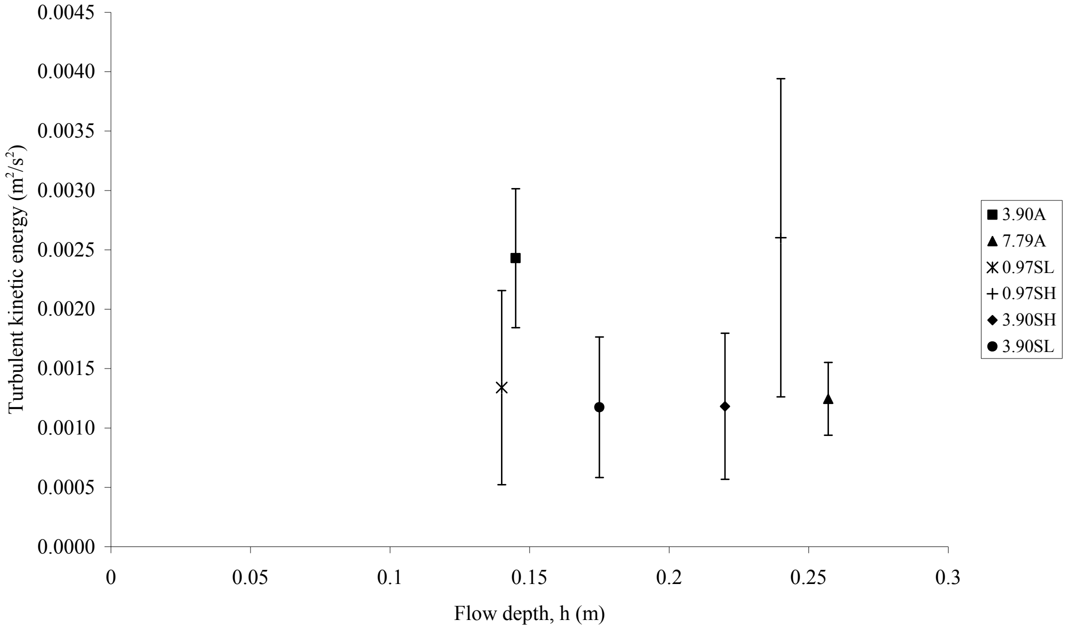

Figure 4.16 Spatially-averaged turbulent kinetic energy (TKE_{xyz}) against flow depth

4.3 Bulk Drag Coefficient

Table 4.3 list the calculated drag coefficient from equation (4.1) which is an extension from equation (2.16). For densely vegetated channel the drag exerted on the boundaries is not significant compared to the drag on vegetal elements implies that in uniform flow the drag force (F_d) is equal to gravitational force (F_g) (Jarvela, 2004). The gravitational force is defined as $Fg = \rho g(A_b h)S_e$, where S_e is the energy slope, A_b is the bottom area and h = flow depth. Therefore drag coefficient in vegetated area can be estimated using equation (4.1).

$$C_D = \frac{2ghS}{U^2}\left(\frac{A_b}{A_p}\right) \tag{4.1}$$

where A_p is the projected plant area perpendicular to the direction of the incident flow.

Table 4.3 List of the drag coefficient and the drag force component for each vegetation density test

SVF (%)	U (m/s)	Re(d)	H (m)	A_b (m^2)	A_p (m^2)	C_d
0.51S	0.157	2,826	0.09	0.0252	0.0016	1.1144
0.97S	0.099	2,475	0.135	0.0252	0.0034	2.0179
2.96AM	0.078	1,677	0.064	0.0126	0.0014	1.8899
3.90A	0.086	2,150	0.145	0.0126	0.0036	1.3370
5.92AM	0.041	882	0.121	0.0063	0.0026	3.4201
7.79A	0.049	1,225	0.257	0.0063	0.0064	2.0592

Figure 4.17 shows the positive trends whereby the drag coefficient increases as the solid volume fraction increases. However this is not what have been discussed by previous researchers (Righetti and Armanini, 2002) where an increase of the vegetation density leads to a reduction of the drag coefficient. According to Nepf (1999) drag coefficient is a function of upstream velocity acting upon vegetation

whereby the downstream vegetation experiences a lower pressure and thus lower the drag coefficient.

As in the current results where the drag coefficient increases with solid volume fraction is because in sparse vegetation (SVF less than 10 %) the turbulence intensities increases with solid volume fraction as shown in Figure 4.10. According to Dunn et al. (1996) and Nepf (1999) drag coefficients increases with turbulence intensities and therefore in relation with present results for sparse vegetation (SVF less than 10 %) and staggered and aligned vegetation the increment of vegetation density will induced greater turbulence intensity and contribute to higher drag coefficient. However more data is required to understand further this relation between turbulence intensity and drag coefficient.

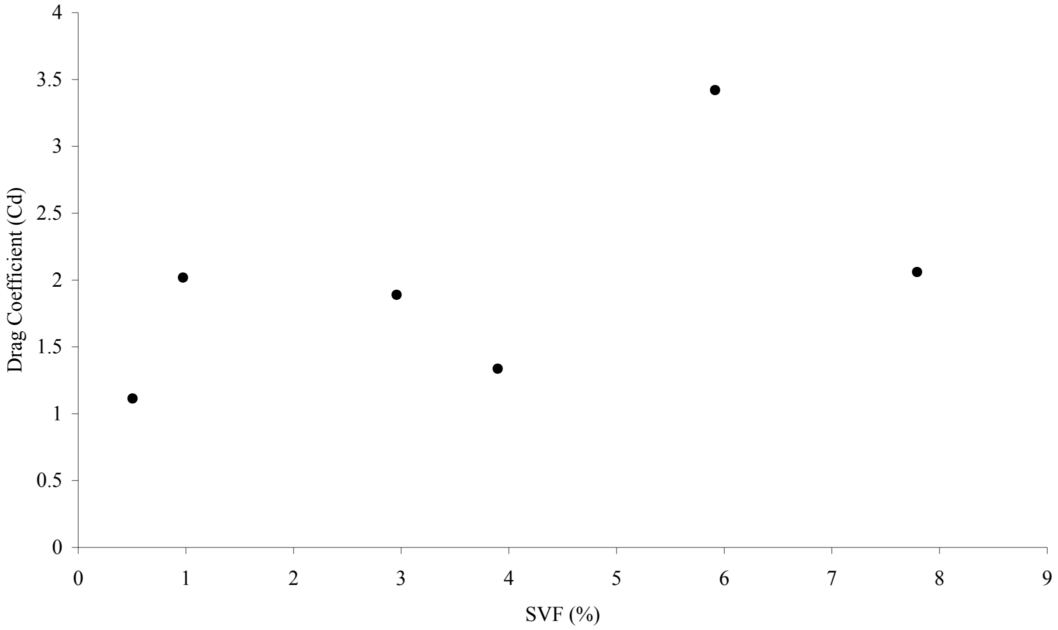

Figure 4.17 Drag coefficients plotted against solid volume fraction

Figure 4.18 shows drag coefficient decreases with stem Reynolds number. This is coincides with Cheng and Nguyen (2011) which experimentally shows that drag coefficient decreases monotonically with increasing pore Reynolds number. Cheng and Nguyen (2011) conducted the experiment using staggered vegetation arrangement with dowels diameter from 0.0032 m to 0.0083 m for vegetation density from 0.4 % to 12 %. Tanino and Nepf (2008) used randomly arranged rigid rods in their experimental work with a diameter of 0.0064 m diameter and solid volume fractions from 0.1 % to 35 % also observed the temporally and cross-sectional-averaged drag coefficient decreases with increasing pore Reynolds number. The reduction of drag coefficient could be due to the movement of flow separation point behind a cylinder with increasing stem Reynolds number; the separation point moves further around the downward-facing side of the cylinder as the Reynolds number increases, therefore creating a smaller wake area and hence lower drag coefficient.

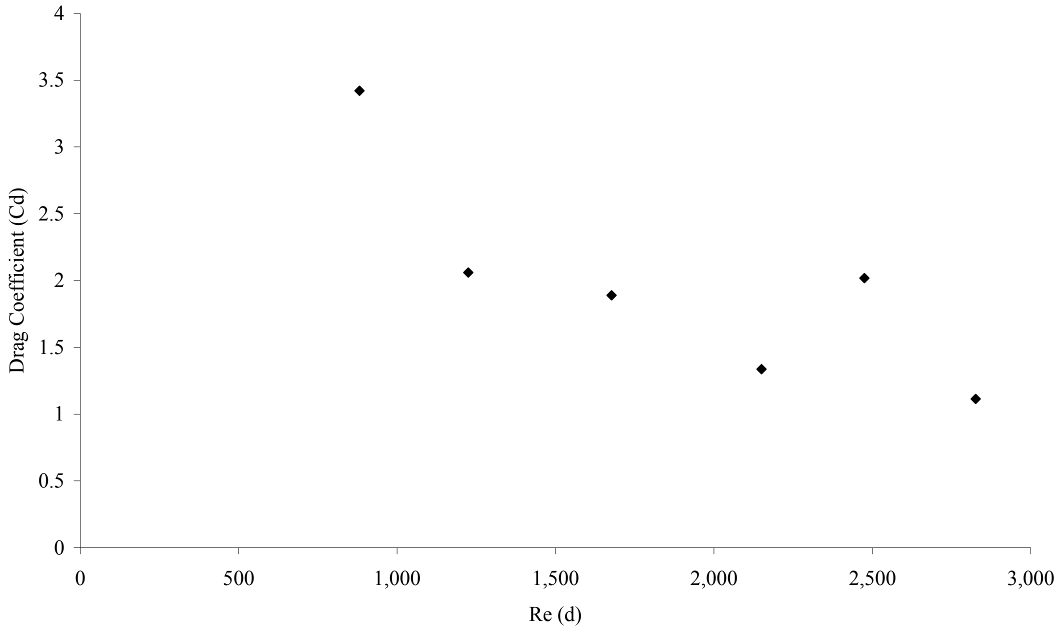

Figure 4.18 Drag coefficients plotted against stem Reynolds number

4.4 Summary

In this chapter the analysis of velocities and turbulence data are presented. Spatially-averaged longitudinal velocity was plotted in vertical and transverse profile to examine the effect of the vegetation density and vegetation arrangement on the velocities and turbulence data. Vertical variation of spatially-averaged transverse velocity was examined to quantify the standard deviation as an indication of transverse shear as one of the main contributions to transverse mixing was found to have low correlation with solid volume fraction and stem Reynolds number.

Apart from transverse shear, turbulence intensity is also known to drive the process of transverse mixing. It was shown there is a positive correlation between the normalized spatially-averaged turbulent intensity and solid volume fraction and a negative correlation with stem Reynolds number. Furthermore analysis of turbulent kinetic energy presents a somewhat weaker correlation with solid volume fraction, stem Reynolds number and flow depth. This result gives an indication that turbulence intensity in longitudinal direction plays a greater role in transverse mixing than the total turbulence in all three directions.

Bulk drag coefficients from one dimensional equation was calculated and analyse against solid volume fraction and stem Reynolds number. Results show that drag coefficient for sparse vegetation increases with vegetation whilst decreases stem Reynolds number. Next is Chapter 5 will present and discuss on the transverse mixing experiment with the variation of vegetation density and flow condition.

Chapter 5 – Transverse Mixing

5.0 Introduction

The first part of this chapter presents relationship between the transverse mixing coefficient and parameters which may influence the transverse mixing characteristics in vegetated open channel flow. As outlined in Section 2.3.8 transverse mixing is dominated by turbulence and secondary currents, and it has been postulated that secondary currents may be damped by the presence of vegetation and increased flow resistance (Shucksmith, 2008). In this chapter the degree of turbulence will be quantified in terms of the stem Reynolds number while the magnitude of the secondary currents will be examined by quantifying the degree of transverse shearing. Other parameters known to influence the turbulence length scale such as flow depth, stem diameter, stem spacing, vegetation density and shear velocity will also be examined. The second part of this chapter is a discussion of the results whereby the performance of the turbulence diffusion model proposed by Nepf (1999) and net lateral dispersion model proposed by Tanino and Nepf (2008) were examined. Both models were developed from data sets relating to randomly arranged emergent cylinders and the suitability and validity of the models were examined when applied to flow through a regular array of emergent cylinders in a staggered and aligned arrangements. Furthermore the data from the present study is also compared against the data from other researchers in this field.

The calculation of the transverse mixing coefficient was conducted in collaboration with Dr James Shucksmith of Sheffield University based on the method outlined in section 3.6 of this thesis. Transverse mixing method of moment (see equation 3.10) was used to establish initial transverse mixing coefficient (Ky). However according to Shucksmith (2008) the initial coefficient usually provides a poor description of the transverse mixing. This is because the method of moments is susceptible to an error due to uncertain level of trace cut off (please refer to section 3.6.2). Therefore the optimisation procedure was used to improve the accuracy of the transverse mixing coefficient. The principles of optimisation was based on a routing procedure to give an optimum fit between dispersion coefficient derived from the theoretical and experimental method (please refer to section 2.4.8 in Shucksmith, 2008). Figure 5.1 shows an example of the optimisation procedure used for 7.79A test 3 reach 1. Please refer to Appendix I for more results.

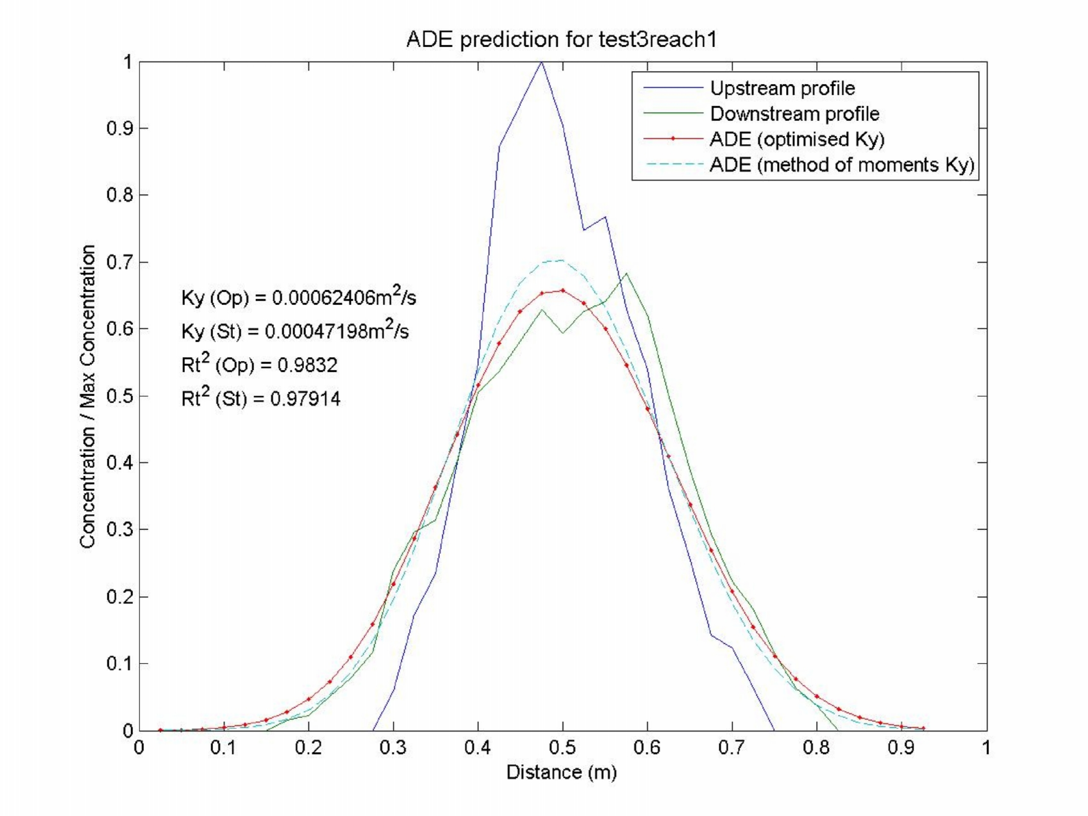

Figure 5.1 Example of the optimisation procedures used to calculate the transverse mixing coefficient for 7.79A test 3 reach 1. The parameter Ky(St) is computed from advection diffusion equation (ADE method of moments Ky) (equation 3.10) and Ky(Op) is the transverse mixing coefficient after the optimisation procedure (ADE optimised Ky). Upstream and downstream profiles show the raw concentration profile before analysis and optimisation and Rt^2 shows the goodness of fit between the predicted and measured values.

The results for the transverse mixing analysis using the method outlined in section 3.6 are presented in Tables 5.1 (a) to (f). The tracer tests were repeated five to six times for each vegetation density and are denoted by t1 to t6. The transverse variation in tracer concentration at each cross-section was measured using

Fluorometer 10-AU at discrete samples located at equal intervals across the section and were measured at three cross-sections, denoted as C1, C2 and C3, as outlined in section 3.2. If the mass balance was below 95 % or above 105 % and if a trace contained erroneous data, the data was removed (see Appendix II). The standard deviation of the mixing coefficient is shown for each test (Tables 5.1).

Table 5.1 (a) List of transverse mixing coefficient for six tracer tests for test 0.51S (SVF = 0.505 %; rod arrangement is staggered)

Test name	SVF (%)	d (m)	test/cross-section	Ky (m^2/s)	Average Ky (m^2/s)	Standard deviation	Re(d)	h (m)	U (m/s)
0.51S	0.505	0.018	t1c1	0.00186008	0.00067480	0.00062	2970	0.09	0.157
			t2c1	0.00060083					
			t3c1	0.00050540					
			t4c1	0.00062040					
			t5c1	0.00043740					
			t6c1	0.00002469					

Table 5.1 (b) List of transverse mixing coefficient for six tracer tests of 0.97S (SVF = 0.974 %; rod arrangement is staggered)

Test name	SVF (%)	d (m)	test/cross-section	Ky (m^2/s)	Average Ky (m^2/s)	Standard deviation	Re(d)	h (m)	U (m/s)
0.97S	0.974	0.025	t1c1	0.00014046	0.00039583	0.0002	2650	0.135	0.099
			t2c1	0.00045484					
			t3c1	0.00021975					
			t4c1	0.00057162					
			t5c1	0.00066584					
			t6c1	0.00032246					

Table 5.1 (c) List of transverse mixing coefficient for three dye tracer tests of 2.96AM (SVF = 2.958 %; arrangement is aligned)

Test name	SVF (%)	d (m)	test/cross-section	Ky (m^2/s)	Average Ky (m^2/s)	Standard deviation	Re(d)	h (m)	U (m/s)
2.96 AM	2.958	0.0215	t1c1	0.00042294	0.00051197	0.00024	1914	0.064	0.078
			t2c1	0.00059852					
			t3c1	0.00086776					
			t1c2	0.00058446					
			t2c2	0.00000038					
			t3c2	0.00060283					
			t1c3	0.00049969					
			t2c3	0.00051919					

Table 5.1 (d) List of transverse mixing coefficient for four tracer tests of 3.90A (SVF = 3.896 %; arrangement is aligned)

Test name	SVF (%)	d (m)	test/cross-section	Ky (m^2/s)	Average Ky (m^2/s)	Standard deviation	Re(d)	h (m)	U (m/s)
3.90A	3.896	0.025	t1c1	0.00167794	0.00102428	0.00056	2500	0.145	0.086
			t2c1	0.00031052					
			t3c1	0.00113383					
			t4c1	0.00097484					

Table 5.1 (e) List of transverse mixing coefficient for six dye tracer tests of 5.92AM (SVF = 5.915 %; arrangement is aligned)

Test name	SVF (%)	d (m)	test/cross-section	Ky (m^2/s)	Average Ky (m^2/s)	Standard deviation	Re(d)	h (m)	U (m/s)
5.92 AM	5.915	0.0215	t1c1	0.00013831	0.00028616	0.00019	1161	0.121	0.041
			t2c1	0.00015017					
			t3c1	0.00020994					
			t4c1	0.00020566					
			t5c1	0.00028590					
			t6c1	0.00019724					
			t1c2	0.00082252					
			t2c2	0.00048345					
			t5c2	0.00015260					
			t1c3	0.00027243					
			t2c3	0.00029581					
			t5c3	0.00021991					

Table 5.1 (f) List of transverse mixing coefficient for six tracer tests of 7.79A (SVF = 7.792 %; arrangement is aligned)

Test name	SVF (%)	d (m)	test/cross-section	Ky (m^2/s)	Average Ky (m^2/s)	Standard deviation	Re(d)	h (m)	U (m/s)
7.79A	7.792	0.025	t1c1	0.00029645	0.00051036	0.00012	1675	0.257	0.049
			t2c1	0.00041673					
			t3c1	0.00048504					
			t4c1	0.00065871					
			t5c1	0.00056943					
			t6c1	0.00055397					
			t3c2	0.00059220					

The transverse mixing coefficients for test 0.51S were shown to have the highest standard deviation while the coefficients for test 7.79A were shown to have the lowest standard deviation (see Tables 5.1(a) to 5.1(f)).

5.1 Effect of Vegetation on Transverse Mixing

5.1.1 Transverse Mixing and Vegetation Density

Figure 5.2 (a) shows the transverse mixing coefficient plotted against the vegetation density parameterised using the solid volume fraction. There is no clear correlation between the transverse mixing coefficient and the solid volume fraction. In Figure 5.2 (b) the normalised transverse mixing coefficient (normalised using the cross-sectional mean velocity (U) and stems diameter (d)) is plotted against the solid volume fraction and data sets from the Nepf et al. (1997) and Tanino and Nepf (2008) studies are presented together with data from the present study. Please note that Tanino and Nepf (2008) used pore velocity (U_p) instead of cross-sectional mean velocity in their calculation of the normalised transverse dispersion coefficient. As described in Section 2.4.1 Nepf et al.'s study (1997) was conducted in random arrays of cylinders with diameters of 0.006 m or 0.012 m and with solid volume fractions ranging from 0.6 % to 5.3 %. Stem Reynolds numbers (Re_d) ranged from 66 to 1800, so hence were performed at lower Reynolds numbers than in current experiments. While in the study by Tanino and Nepf (2008), solid volume fractions in the range of

1 % to 35 % were examined. Again random arrays of cylinders were examined using stem diameter of 0.0064 m. Experiments were performed at stem Reynolds numbers from 60 to 770. The experiments presented in this thesis were performed at stem Reynolds numbers of 1100 to 3000, using generally larger diameter cylinders (0.018m or 0.025m) arranged in an aligned or staggered configuration. Some experiments were performed with two different diameter cylinders.

Nepf et al. (1997) showed that the normalized transverse mixing coefficient increases with increasing solid volume fraction and this is most significant from the non-vegetated flume (SVF = 0 %) to vegetated flume with solid volume fraction 0.6%. Tanino and Nepf (2008) results showed that the normalized transverse mixing coefficient rapidly increased with increasing SVF from 0 % to 3.1 %, then decreases with increasing SVF from 3.1 % to 20 %, before gradually increasing again when the SVF increases from SVF of 20 % to 35 %.

Normalised transverse mixing coefficient values from the current study are slightly higher in magnitude than the values reported in Nepf et al. (1997) and Tanino and Nepf (2008). This is probably because the experimental work presented herein used bigger stem diameters and was conducted at relatively higher cross-sectional mean velocities. As would be expected bigger vegetation leads to greater turbulent transport and together with higher are mean velocities leads to higher stem Reynolds numbers. As previously mentioned the stem Reynolds numbers were between 1000 and 3000.

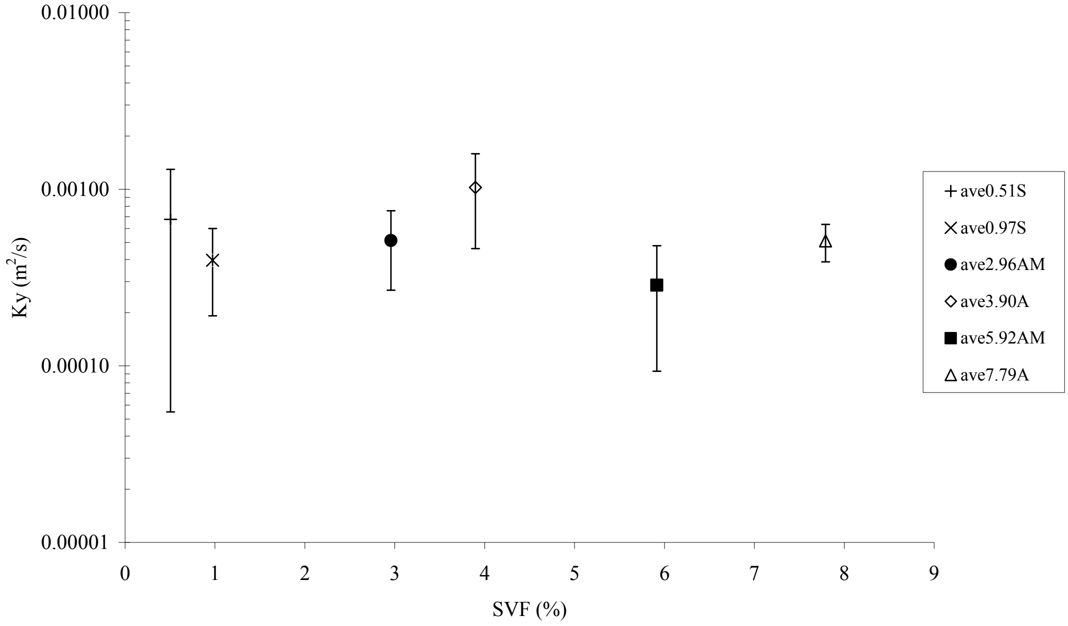

Figure 5.2 (a) Transverse mixing coefficient plotted on a logarithmic scale as a function of the solid volume fraction for different vegetation configurations. The bar denotes the one standard deviation and the marker denotes the mean transverse mixing coefficient for each vegetation density test.

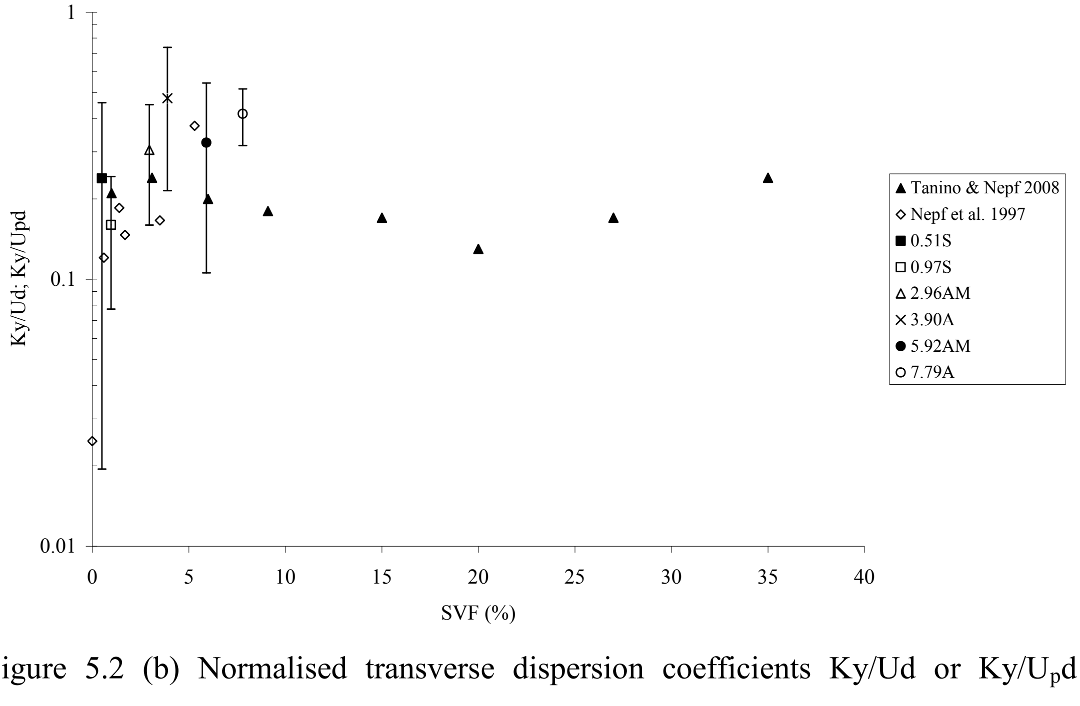

Figure 5.2 (b) Normalised transverse dispersion coefficients Ky/Ud or Ky/U_pd plotted on a logarithmic scale as a function of the solid volume fraction. Data from studies by Nepf et al. (1997) and Tanino and Nepf (2008) are included. For the

Tanino and Nepf (2008), Ky/U_pd is used. The bar denotes the one standard deviation and the marker denotes the mean of transverse mixing coefficients for each vegetation density test.

5.1.2 Transverse Mixing and the Stem Reynolds Number

In Figure 5.3 (a) the transverse mixing coefficient against stem Reynolds number is presented. It is shown that the transverse mixing coefficient increases with increasing stem Reynolds number. Please note that this finding is based on a small data sample. However data sets from the studies by Serra et al. (2004) (Re_d between 10 to 100), Nepf et al. (1997) (Re_d between 66 to 1800), Shucksmith (2008) with emergent reeds (Re_d between 210 to 290) and Shucksmith (2008) with emergent carex (Re_d between 4210 to 5500) are plotted in Figure 5.3 (b) with data from the present supported previous findings in Figure 5.3(a). Data from the present study extends the range of stem Reynolds numbers that have been studied previously and therefore suggests that for sparse vegetation, this trend exists at the higher stem Reynolds numbers.

As mentioned in section 2.4.1 within sparse arrays of cylinders (SVF < 10%) vortex shedding is thought to be delayed until the stem Reynolds number is greater than 200 (Nepf et al., 1997) compared to flow past a single cylinder where vortex shedding occurs at stem Reynolds number of around 90 (Douglas et al. 1979). Therefore it would seem that the trend of increasing transverse mixing coefficient with increasing stem Reynolds number holds for stem Reynolds numbers in the range of 10 to 5500 and is regardless of the stage of turbulent wake development.

Since transverse mixing is driven by turbulence and secondary currents, it would be expected that the transverse mixing coefficient increases with increasing stem Reynolds number. Furthermore according to Nepf (2012) for solid volume fraction less than 10% (sparse), turbulent diffusion is the dominant component of the diffusion and the velocity scale controlling turbulent diffusion is the spatial and temporal average velocity. The spatial averaging volume is thin in the vertical direction, to preserve vertical variation in the canopy density, and large enough in the horizontal plane to include several stems (>_*S*) (Nepf, 2012).

In Serra et al's study (2004) higher solid volume fractions were employed (SVF between 10 % and 35 %) and because the experiments were conducted at considerably lower stem Reynolds numbers (i.e. Re_d ranged from 10 and 100), the diffusion process is dominated by mechanical diffusion (Nepf, 1999; Serra et al 2004) rather than by the turbulent diffusion in the wake region. Nepf (1999) suggested that channel scale (i.e. flow depth) eddies can persist in sparse vegetation when stem diameter much smaller than flow depth (d << h). However Serra et al. (2004) who examined two ratios of diameter to flow depth 0.212 and 0.294, observed a dependency of $(K_y/Ud)(S/d)$ with stem Reynolds number but no disconcernable relationship with the stem diameter to flow depth ratio. Serra et al. (2004) (as previously mentioned in section 2.4.2) noted that the transverse diffusion coefficient K_y was related to stem Reynolds number but was also influenced by the ratio of the stem diameter to the characteristic distance between the stems (d/S)..

If the results from the emergent reed experiments (Shucksmith, 2008) are compared against those from similar experiments conducted with cylinders (Nepf et al., 1997) it can be observed that higher transverse mixing coefficients were observed for the similar stem Reynolds numbers in the range of 219 to 290 (see Figure 5.3 b). Quantitatively the normalized transverse mixing coefficient for emergent reeds by Shucksmith (2008) is five times greater than normalized transverse mixing coefficient reported by Nepf et al. (1997b) for asimilar range of stem Reynolds number. However, it should be noted that Nepf et al. (1997) examined a vegetation density estimated to be approximatley 415 stems/m^2 for the stem Reynolds number range 240 to 300, compared to Shucksmith vegetation density of approximately 150 to 333 stems/m^2. The high transverse mixing in emergent reeds for Shucksmith (2008) may be explained by the higher frontal area for the same number of stems per unit area associated with the reed array and the variation in plant area with plant height due to the leaf blades. Therefore for 'sparse' vegetation configurations (solid volume fraction less than 10 %), the greater blockage contributes to higher horizontal diffusivities due to the wake shear dispersion. Shucksmith (2008) also examined arrays of Carex plants. In contrast to the reed arrays the Carex array was a denser plant in terms of the number of leaves and was shorter in plant height and more flexible.. It is thought that as a consequence of the Carex plant's flexibility for similar Reynolds numbers the flexibility contributed to a lower the transverse mixing coefficient compared to that generated by rigid cylinder arrays examined in this thesis (see Figure 5.3 b).

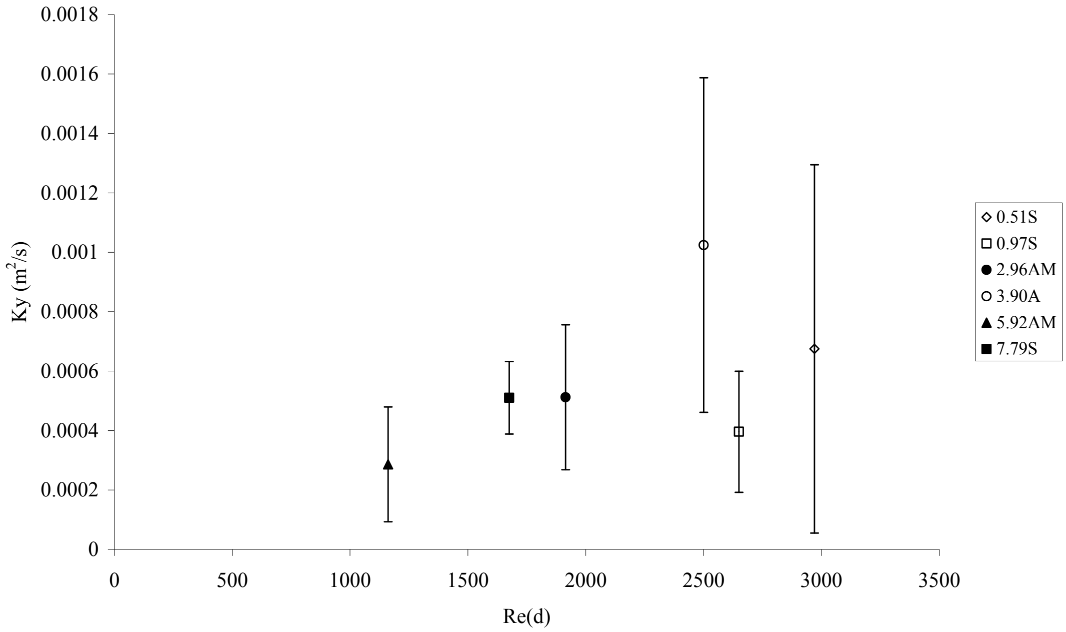

Figure 5.3 (a) Transverse mixing coefficient *Ky* as a function stem Reynolds number. The bar denotes the one standard deviation for the average transverse mixing coefficient for each vegetation density test.

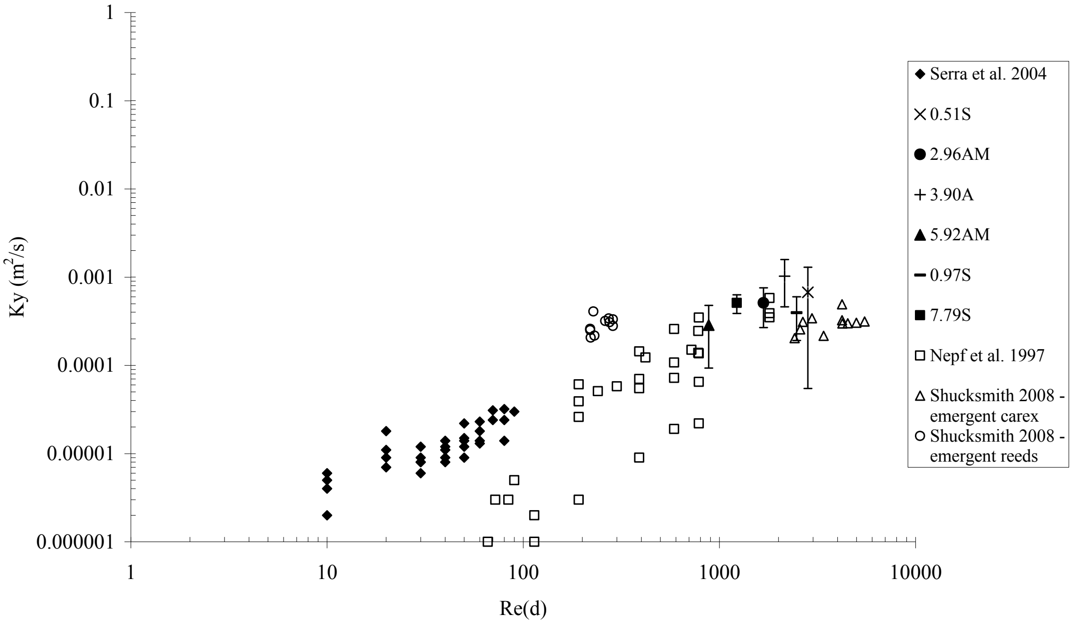

Figure 5.3 (b) Transverse mixing coefficient variation as a function of stem Reynolds data plotted with data from the studies by Serra et al. (2004), Nepf et al. (1997) and Shucksmith (2008). Logarithmic scales are used on both axes and the bar denotes the one standard deviation for the average transverse mixing coefficient for each vegetation density test.

5.1.3 Transverse Mixing and Flow Depth

The variation in the transverse mixing coefficient with flow depth for the current study is presented in Figure 5.4 (a). As discussed in Section 2.4.2 for uniform flow conditions the presence of vegetation will dampen the secondary flow and increase the flow depth (Shucksmith 2008). Furthermore as previously discussed the flow depth is often used to scale the transverse mixing coefficient since in a wide straight channel the flow depth will determine the maximum length scale of the turbulence which will transport mass. Figure 5.4 (a) shows that there is no obvious correlation between transverse mixing and the flow depth. This is consistent with the work conducted by Shucksmith (2008) using emergent reeds with stem Reynolds numbers in the range of 219 to 290 and carex with stem Reynolds number between 2400 and 5500 as shown in Figure 5.4 (b) and further substantiated by the work conducted by

Fischer and Hanamura (1975) whereby vertical strips of galvanized metal were used to simulate vegetation for stem Reynolds numbers in the range of 2300 to 7700.

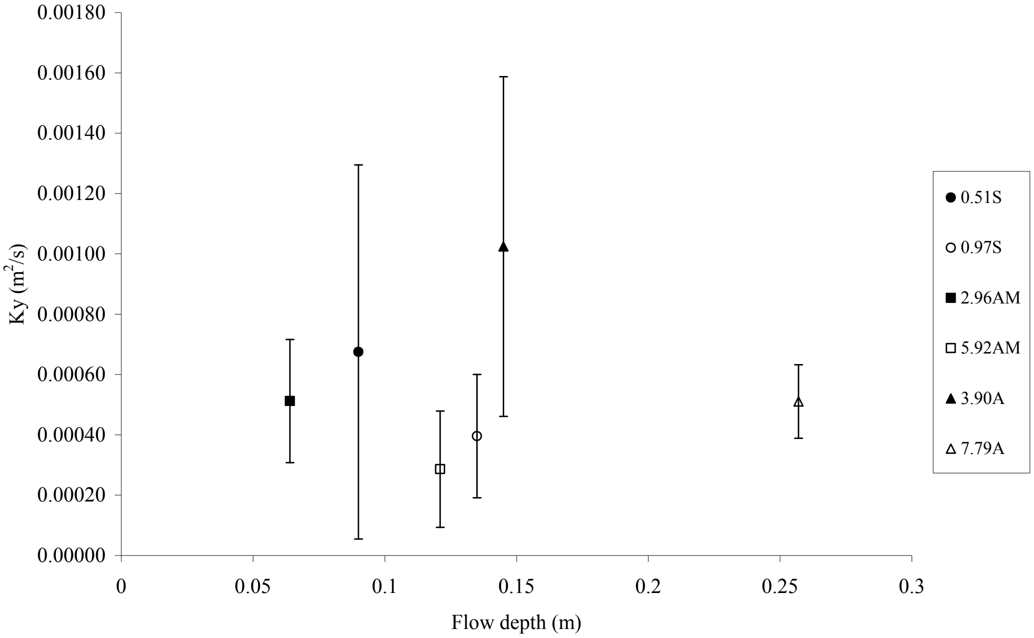

Figure 5.4 (a) Transverse mixing coefficient as a function of flow depth. The bar denotes the one standard deviation for the mean transverse mixing coefficient for each vegetation density test.

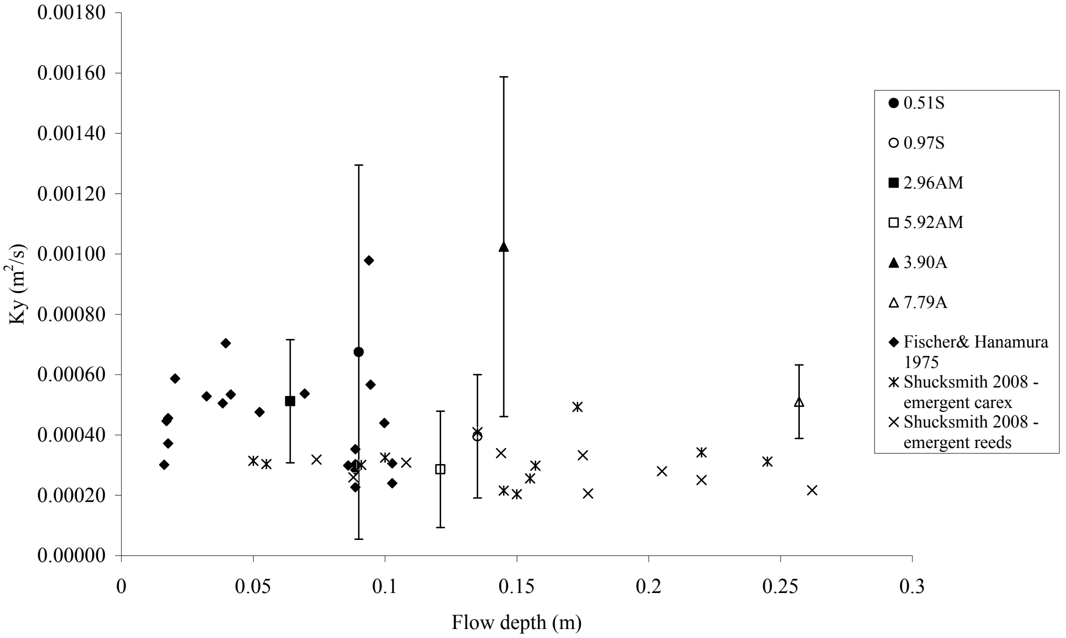

Figure 5.4 (b) Transverse mixing coefficients as a function of flow depth. Results from the studies conducted by Fischer and Hanamura (1975) and Shucksmith (2008) are included. The bar denotes the one standard deviation for the mean transverse mixing coefficient for each vegetation density test.

5.1.4 Transverse Mixing and Shear Velocity

Figure 5.5 presents the transverse mixing coefficient as a function of shear velocity. As mentioned in section 2.3.8 shear velocity is commonly used to scale transverse mixing and this is suitable for wide open channel because the turbulence which drives transverse mixing is generated by vertical velocity shear due to the bed friction. Shear velocity here is calculated using equation (2.73b) based on the assumption of one-dimensional flow. Figure 5.5 shows that there is no apparent relationship between the shear velocity and transverse mixing coefficient. Furthermore Shucksmith (2008) also showed that there was no observable trend between the transverse mixing coefficient and shear velocity. This is probably because in vegetated turbulent flow for certain flow depth to stem ratios the contribution of the turbulence generated by bed shear to the overall turbulence production is less dominant compared to the wake turbulence generated at the stem scale. For carex the flow depth to stems diameter (h/d) is about 0.9 to 4.6, meanwhile for emergent reeds the h/d ratio is in the range of 29 to 105 and for present study the ratio of h/d is between 2.9 to 10.3. Based on results from Figure 5.4, therefore at h/d ratio between 0.9 and 105, it seems that there will be small or less preeminent turbulence generated by bed shear relative to wake turbulence generated at the stem scale.

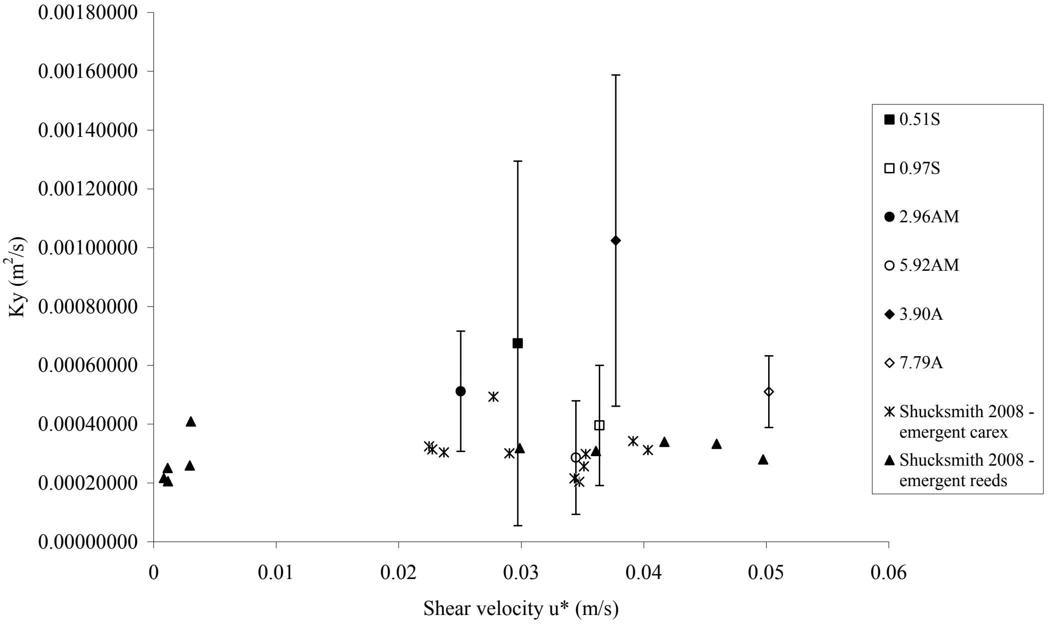

Figure 5.5 Transverse mixing coefficients as a function of shear velocity plotted with results from Shucksmith (2008). The bar denotes the one standard deviation for the mean transverse mixing coefficient for each vegetation density test.

5.1.5 Transverse Mixing and Mean Area Velocity

The variation in transverse mixing coefficient with the product of mean area velocity and stem diameter (*Ud*) is presented in Figure 5.6 (a). Since the data sample is small, caution should be taken however it can be seen that the transverse mixing coefficient increases with increasing values of the product of the area mean velocity and diameter (*Ud*). This trend is further supported by the data set presented by Nepf et al. (1997), the carex and reeds data sets presented by Shucksmith (2008) and the data set presented by Serra et al. (2004) as shown in Figure 5.6 (b). The transverse mixing coefficients for emergent reeds (Shucksmith, 2008) are somewhat higher than those presented by Nepf et al. (1997) for the rigid rods for the same range of *Ud.* As previously explained in section 5.1.2, the morphology and variation in plant area with plant height together with the flexibility of real vegetation affects the mixing process and this is an obvious interesting area for further research.

Figure 5.6 (c) present the transverse mixing coefficients normalized by the product of cross-sectional mean velocity and stems diameter as a function of stem Reynolds number. Data sets from currents research with Nepf et al. (1997), Serra et al. (2004) and Shucksmith (2008) are plotted in Figure 5.6 (c) and it shows relatively scattered plots. Serra et al. (2004) commented for Nepf et al. (1997) data sets corresponding to stem Reynolds number less than 100, do not collapsed with the data from their research and this is also shown in Figure 5.3 (b). This discrepancy might due to the mismatch in the solid volume fraction (i.e. 10 % to 35 % for Serra et al (2004) and 0.6 % to 5.3 % for Nepf et al. (1997)).

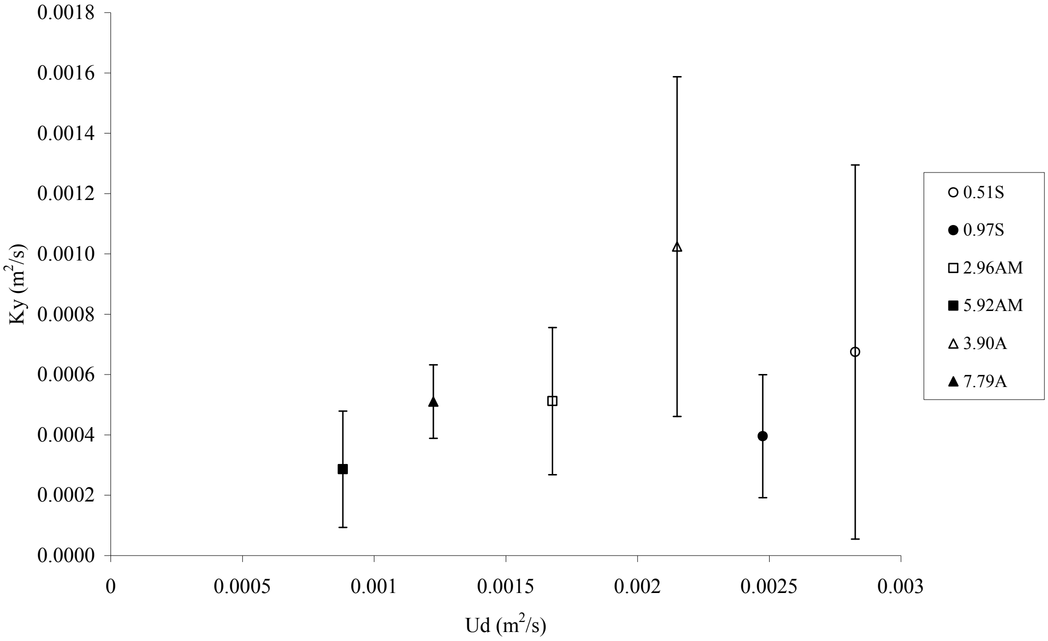

Figure 5.6 (a) Transverse mixing coefficient as a function of the product of cross-sectional mean velocity and stem diameter. The bar denotes the one standard deviation for the mean transverse mixing coefficient for each vegetation density test.

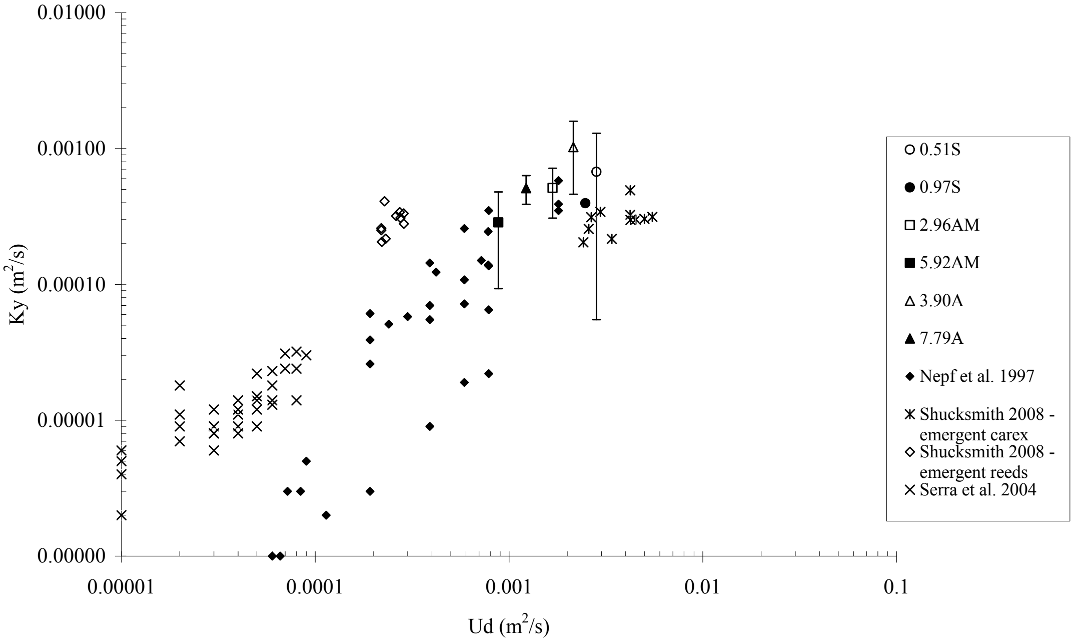

Figure 5.6 (b) Transverse mixing coefficient as a function of the product of cross-sectional mean velocity and diameter (*Ud*) plotted with results from Nepf et al. (1997) and Shucksmith (2008). Logarithmic scales are used on both axes and the bar denotes the one standard deviation for the mean transverse mixing coefficient for each vegetation density test.

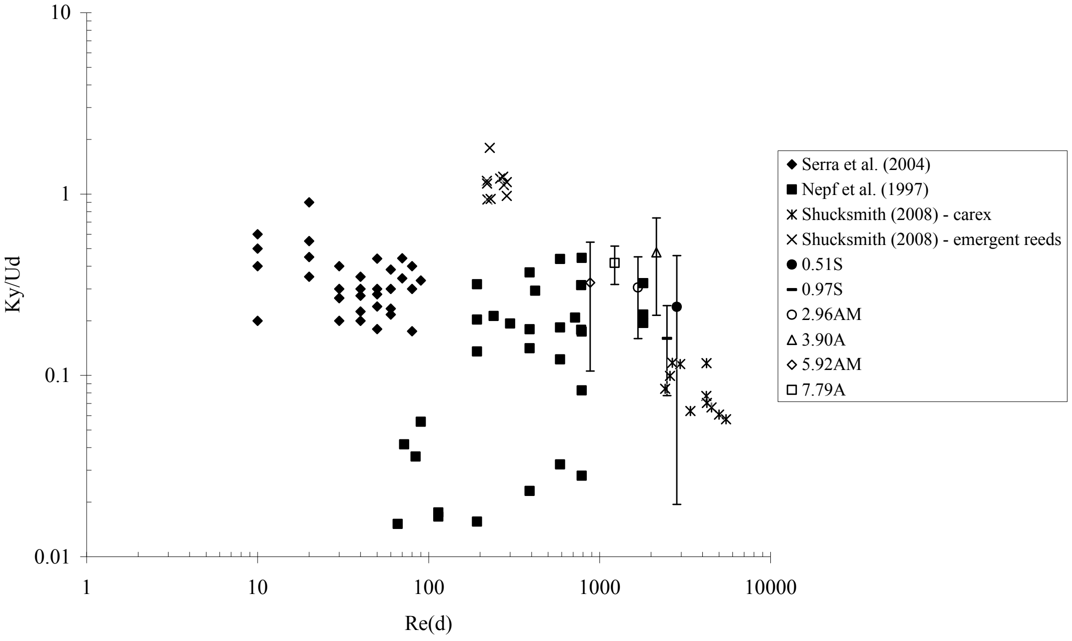

Figure 5.6 (c) Normalised transverse mixing coefficient (normalised by *Ud*) as a function of stem Reynolds data plotted with data from the studies by Serra et al. (2004), Nepf et al. (1997) and Shucksmith (2008). Logarithmic scales are used on both axes and the bar denotes the one standard deviation for the mean transverse mixing coefficient for each vegetation density test.

5.1.6 Transverse Mixing and Turbulence Intensity

In Figure 5.2 (b) it can be observed that the transverse mixing coefficient increases with increasing solid volume fraction and meanwhile in Figure 5.7 shows that for a given stem Reynolds number (1000 to 3000) the normalized spatially-averaged turbulence intensity in the longitudinal direction also increases with solid volume fractions. Therefore this research would like to relate that transverse mixing coefficient is also expected to increase with turbulence intensity. However more data is required to support this finding.

In the diffusion model developed by Nepf (1999) described in section 2.3.2, it was suggested that turbulence intensity increases with the introduction of sparse vegetation (solid volume fraction less than 10 %) because of the addition wake production (relative to non vegetated flow) but for a given flow rate turbulence intensity decreases with increasing population density as the mean velocity is reduced due to the increase in hydraulic resistance. Therefore according to Nepf (1999) increasing the vegetation density results in a reduction in the diffusion rate because of the reduced velocity and reduced eddy scale relative to non vegetated region. This finding is highly relevant to the current results where solid volume fractions of less than 10 % were used.

Tanino and Nepf (2008) proposed that only turbulent eddies with a characteristic mixing length greater than the stem diameter and the distance between two neighbouring cylinder centres farther than the distance of two diameters (*2d*) from each other to contain eddies that can contribute to the net transverse dispersion. It follows therefore that if the distance between stems is less than *2d,* even though turbulence intensity increases monotonically with stem density the contribution of turbulent diffusion to the net lateral dispersion decreases. This is illustrated above in Figure 5.2 (b) whereby Tanino and Nepf (2008) results of normalized transverse mixing coefficient increased from SVF of 0 % to 3.1 %, then decreases from SVF of 3.1 % to 20 %, before gradually increases again from SVF of 20 % to 35 %.

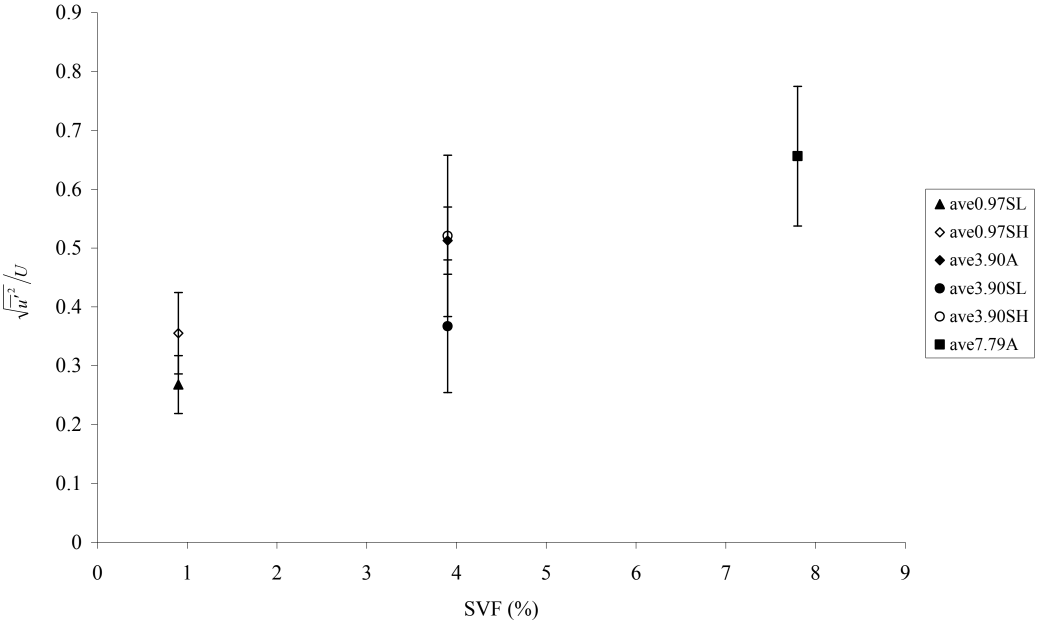

Figure 5.7 Variation of the normalized turbulent intensity in the longitudinal direction with solid volume fraction. The bar denotes one standard deviation and the marker denotes the mean of the normalized turbulence intensity for each vegetation density test.

5.1.7 Transverse Mixing and Turbulent Kinetic Energy

Based on the assumption that turbulence production in emergent vegetation within stem wakes dominates the production of turbulence through bed shear, the turbulent kinetic energy budget can be reduced to a balanced between the wake production and viscous dissipation (Nepf, 1999). If it is assumed that the characteristic length of turbulence is set by the stem diameter (*d*) and Nepf (1999) suggested that the dissipation rate should scale as $\varepsilon \sim k^{3/2} d^{-1}$ where *k* is turbulent kinetic energy. Therefore based on this hypothesis and the fact that transverse mixing is driven by turbulence and secondary currents, one would expect that the magnitude of turbulent kinetic energy should be related to the transverse mixing coefficient.

Figure 5.8 presents that turbulent kinetic energy decreases with solid volume fraction and it has been shown in Figure 5.2 (b) that the normalized transverse mixing coefficient increases with increasing solid volume fraction. Therefore in relation to results in Figure 5.7, this study try to suggest that turbulence intensity in the longitudinal direction correlates better to the transverse mixing coefficient than the turbulent kinetic energy. However more data is required to support this finding.

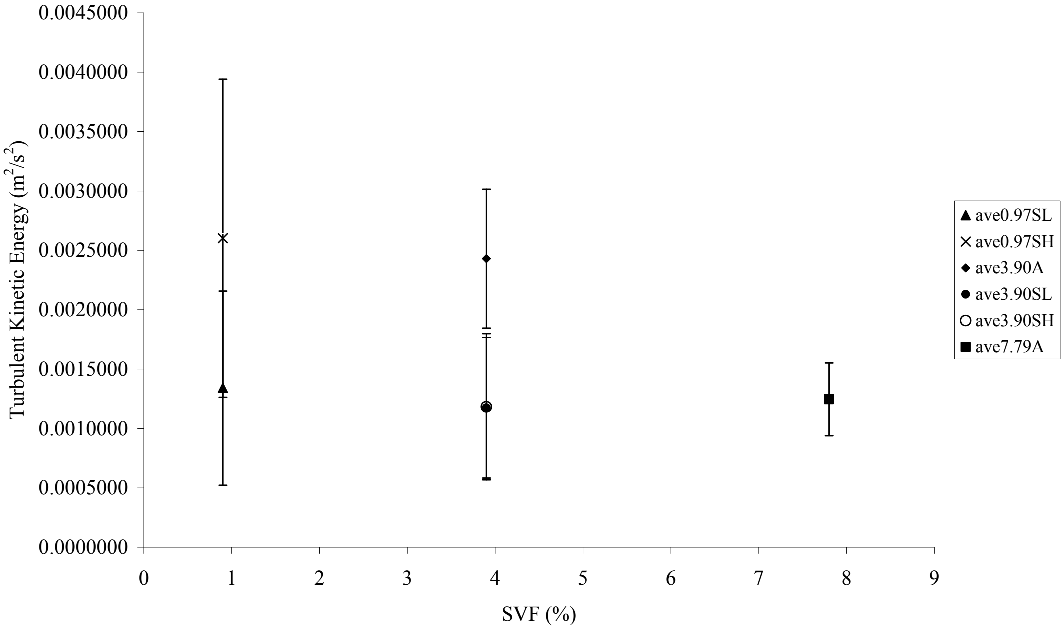

Figure 5.8 Spatially-averaged turbulent kinetic energy (TKE_{xyz}) against solid volume fraction. The bar denotes one standard deviation and the marker denotes the mean of the normalized turbulence intensity for each vegetation density test.

5.1.8 Transverse Mixing and Vertical Variation of Transverse Velocity

Transverse mixing is driven by both turbulence and vertical variations in the transverse velocity. The variance or standard deviation of the vertical variation of the transverse velocity profile can be used to quantify the strength of the secondary currents (Shucksmith, 2008). The standard deviation of the normalized transverse mixing coefficient as a function of solid volume fraction is shown in Figure 5.9. It can be seen from Figure 5.9 that there is only small variation of standard deviation between the normalized transverse mixing which indicates that the normalized transverse mixing coefficient is not dependent with the vertical variation of the transverse velocity. Shucksmith (2008) commented on the observation of the standard deviation of the vertical variation of transverse velocity with carex porosity (that reflects carex age; high porosity presenting young plant) which shows that standard deviation varies little with plants porosity. In comparison with the results from the turbulence intensity as shown in Figure 5.7 (b) with the vertical variation of transverse velocity in Figure 5.9, reflect that the turbulence intensity correlates better to transverse mixing compared to the vertical variation of transverse velocity. However more data is required to supports this finding.

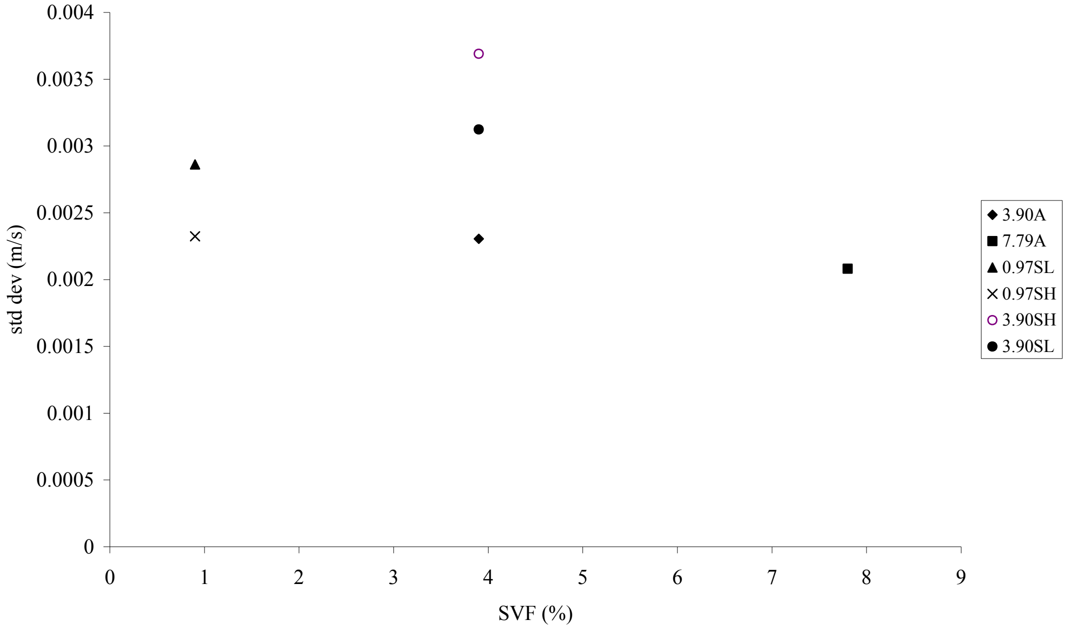

Figure 5.9 Normalized transverse mixing coefficients against the standard deviation in the vertical transverse velocity profile

5.2 Transverse Mixing Models

The following part of this chapter present prediction of transverse mixing coefficient from two models: the turbulence diffusion model proposed by Nepf (1999) and the net lateral dispersion model by Tanino and Nepf (2008). These models have been described in section 2.3.2. Comparison is made between the predictions from both models and the suitability of the models for staggered and aligned vegetation arrangement is discussed.

5.2.1 Nepf's Model (1999)

As previously mentioned in section 2.4.2, Nepf (1999) proposed the total lateral diffusion model given by

$$\frac{K_y}{Ud} = \alpha\left(C_D ad\right)^{1/3} + \left(\frac{\beta^2}{2}\right)ad \qquad (2.97)$$

where d = stem diameter; a = the projected vegetated area per unit volume and α = scale factor. In an array of emergent cylinders, Nepf (2004) suggested a value of 0.8 for the scale factor (α) and α = 0.2 for vertical diffusion and Serra et al. (2004) experimentally shown β approximately equal to 1. The bulk drag coefficient C_d was estimated based on the wake interference model proposed by Nepf (1999) (see Figure 6, page 483, Nepf, 1999) and it was computed from a numerical model used to extrapolate the observations made for cylinder pairs (Bokaian and Geoola, 1984; Re_d = 2600) to estimate the cumulative sheltering and bulk drag within a randomly arranged array (please refer Nepf (1999) Section 2.1 page 480). For sparse or low solid volume fractions (SVF < 10 %) with stem spacing greater than the stem diameter ($S > d$), Nepf (2012) further suggested that $ad \approx (d^2/s^2)$. Table 5.2 lists the predicted normalized turbulent dispersion coefficient using Nepf's model (1999) against the observed normalized transverse mixing coefficient for the current experimental work.

Table 5.2 and Figure 5.10 show the comparison between the predicted normalized transverse mixing coefficient and the observed normalized transverse mixing coefficient. There are two predicted normalized transverse mixing which one is using drag coefficient proposed by Nepf (1999) and the other refer to one dimensional drag coefficient (see section 2.17). Table 5.2 shows that the percentage difference between predicted and observed normalized transverse mixing using Nepf (1999) proposed C_d and one dimensional C_d gave a similar results with percentage difference ranges from 3 % to 55 %, within the context of dispersion coefficients this is a reasonably good prediction. Since the total lateral diffusion model developed by Nepf (1999) was based on random cylinder arrangement with solid volume fraction of 0.6 %, 2 % and 6 % for stem Reynolds numbers in the range of 4000 to 10000 it seems that proposed model by Nepf (1999) to certain degree has the ability to capture the transverse mixing pattern within staggered vegetation. Total lateral diffusion model (Nepf, 1999) require an estimation of scale factor (α for turbulence diffusion model and β for mechanical diffusion model) which may affect the predicted transverse mixing coefficient. This aspect of estimating scale factor involves a certain degree of subjectivity and needs further investigation in relation to random, staggered or aligned arrangements.

Table 5.2 Prediction and observed values of the normalised dispersion coefficient using Nepf's model (1999).

Test	C_d Nepf (1999)	1D C_d	Predicted Ky/Ud from C_d Nepf (1999)	Predicted Ky/Ud from 1D C_d	Observed Ky/Ud	% difference Ky/Ud from C_d Nepf (1999)	% difference Ky/Ud from 1D C_d
0.51S	1.2	0.56	0.1575	0.1537	0.2388	-34.05	55.32
0.97S	1.15	1.01	0.1979	0.2375	0.1599	23.74	-32.65
2.96AM	0.75	1.33	0.2634	0.3516	0.3053	-13.73	-13.16
3.90A	0.3	1.34	0.2241	0.3524	0.4764	-52.96	35.21
5.92AM	0.7	2.41	0.3371	0.5458	0.3246	3.83	-40.52
7.79A	0.7	2.06	0.3829	0.5266	0.4166	-8.10	-20.88

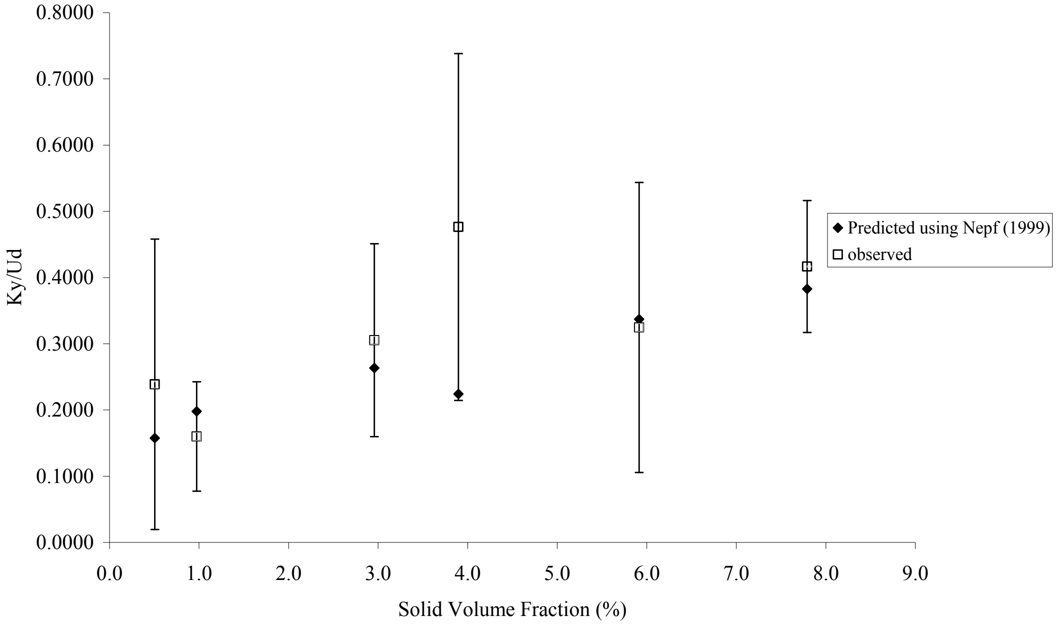

Figure 5.10 Predicted and observed values of the normalized transverse mixing coefficient against solid volume fraction. The bar denotes the one standard deviation for the mean observed transverse mixing coefficient for each vegetation density test.

5.2.2 Tanino and Nepf's Model (2012)

As previously shown in section 2.4.2, Tanino and Nepf (2008) proposed a net transverse dispersion model which is a linear superposition of turbulent diffusion and dispersion from the spatially heterogeneous velocity field and this model is given by equation (2.106). For dispersion from spatially heterogeneous velocity field, Tanino and Nepf (2008) consider two models including Nepf (1999) model and Koch and Brady (1986). Nepf (1999) model is based on one dimensional random walk which describes the lateral deflection of fluid particles (equal probability of either being in the positive or negative y direction) due to the presence of the cylinders. Tanino and Nepf (2008) make an adjustment to Koch and Brady (1986) model which is based mechanical dispersion due to two cylinders interaction with nearest neighbour sufficiently close to permit cylinder to cylinder interaction. Analytical solution is by averaging the governing equation of Fickian dispersion over an ensemble of arrays with different cylinder configurations.

Calculated parameters as used by the model are presented in Table 5.3 including C_D^{form} (form drag coefficient), $\left\langle \sqrt{k_t} \middle/ \langle \bar{u} \rangle \right\rangle$ (turbulence intensities), $P_{s_{nc}>r*}$ (probability that a cylinder in the random array has its nearest neighbour farther than $r = r^*=2d$), $P_{sn_c<5d}$ (probability that a cylinder has its neighbour within $r = 5d$), $\langle s_n^2 \rangle_{s_{nc}>r^*}$ (distance surface to surface of the nearest neighbour farther than $r^* =2d$), λ (number of random coordinates generated per unit area), A_L (circular invalid area for a cylinder) and $k^{\perp}$ (permeability). The scaling constants γ_1 and γ_2 are derived from the least square method and taken as $\gamma_1 = 1.48$ and $\gamma_2 = 2.41$. The parameter $r*$ has been taken as *2d* as suggested in Tanino and Nepf (2008) where *2d* is the minimum distance between cylinder centres that permits the pore space to contain eddies with mixing length scale that contribute to the net lateral dispersion. More details of the equation and parameter derivation can be found in section 2.4.2 and Tanino and Nepf (2008).

Table 5.3 Calculated parameters used in equation (2.105) please note that the definition of each parameter is given in section 2.4.2 in Table 2.2

Test	C_D^{form}	$\left\langle \dfrac{\sqrt{k_t}}{\langle \bar{u} \rangle} \right\rangle$	$P_{s_{nc}>r*}$	$P_{sn_c<5d}$	$\langle s_n^2 \rangle_{s_{nc}>r^*}$ (m^2)	λ (m^{-2})	A_L (m^2)	$k^{\perp}$ (m)
0.51S	0.9584	0.1237	0.9467	0.3805	0.0501	19.8413	0.0013	0.0501
0.97S	0.9940	0.1600	0.8997	0.6030	0.0470	19.8413	0.0025	0.0470
2.96AM	1.1448	0.2686	0.7315	0.9350	0.0070	79.3651	0.0019	0.0070
3.90A	1.2161	0.3138	0.6553	0.9752	0.0064	79.3651	0.0025	0.0064
5.92AM	1.3695	0.4090	0.5352	0.9958	0.0015	158.7302	0.0019	0.0015
7.79A	1.5122	0.3987	0.4294	0.9994	0.0012	158.7302	0.0025	0.0012

Table 5.4 List of predicted and observed normalized transverse mixing coefficient from the Tanino and Nepf's model (2008)

Test	Predicted K_y/U_pd	Observed K_y/U_pd	% difference
0.51S	0.18672	0.23697	-21.2
0.97S	0.21663	0.15881	36.4
2.96AM	0.19801	0.29581	-33.1
3.90A	0.18953	0.45676	-58.5
5.92AM	0.16464	0.30319	-45.7
7.79A	0.15122	0.38737	-61.0

Table 5.4 and Figure 5.11 present the predicted normalized mixing coefficient from the net lateral dispersion model and the observed normalized transverse mixing coefficient. The difference between the predicted and observed coefficient ranges between 21 % and 61 % which is reasonably good and within similar degree of error to that given by the Nepf's model (1999). Again values are generally under-predicted by this model. Interesting to note is that the model predicts first an increase of normalized transverse mixing coefficient from 0.5 % to 1 % SVF, than a decrease in the normalized transverse mixing coefficient with increasing solid volume fraction from 1 % to 7.8 %. This coincides with the findings of Tanino and Nepf (2008) who find that the normalized transverse mixing coefficient increases rapidly from SVF 0 % to 3.1 % and decreases from SVF 3.1 % to 20 %. Even though the percentage difference between predicted normalized transverse mixing coefficients from Nepf (1999) is in the similar range with the predicted results from Tanino and Nepf (2008), however result shows model from Tanino and Nepf (2008) has slightly a tendency of biasness. Therefore more data is required to explore further the model proposed by Tanino and Nepf (2008).

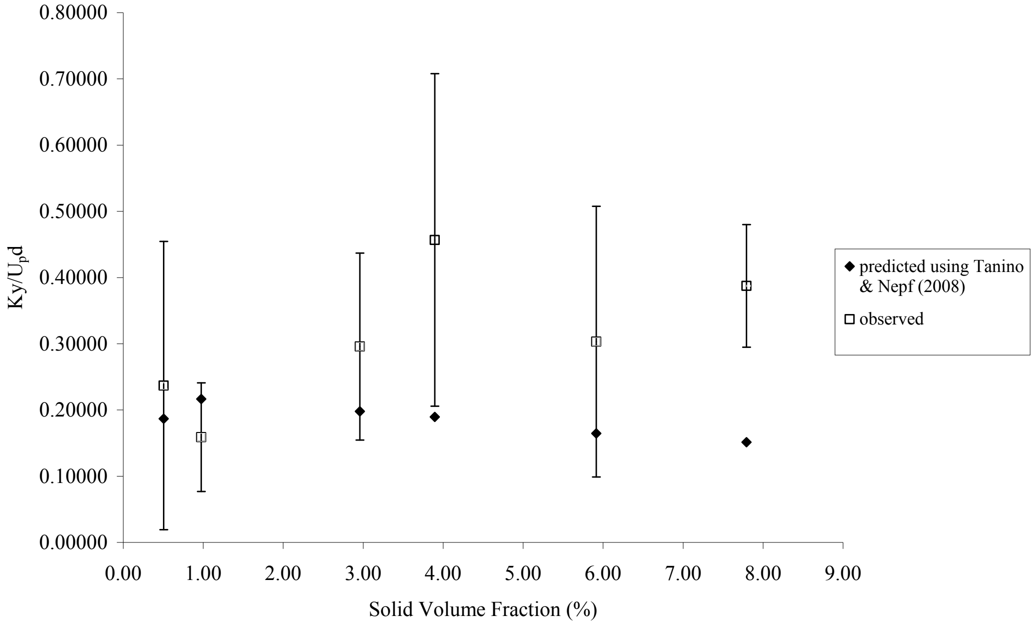

Figure 5.11 Observed and predicted normalized transverse mixing coefficients against solid volume fraction. The bar denotes the one standard deviation for the mean observed transverse mixing coefficient for each vegetation density test.

5.3 Summary

This chapter present results from dye tracing study which has examined the effect of sparse vegetation (whereby the SVF < 10%) on the transverse mixing characteristics for stem Reynolds number in the range of 1000 to 3000. Result shows that the transverse mixing coefficient increases with solid volume fraction and this is due to the increase in wake turbulence generation and shear dispersion associated with the stem wake region.

The transverse mixing coefficient was also shown to increase with increasing stem Reynolds number and with increasing area mean velocity multiplied by the stem diameter. Both trends are supported by results from previous studies (Nepf et al., 1997; Shucksmith, 2008).

For a given stem Reynolds number it was shown that the dispersion coefficient was higher for a reed array compared to rigid cylinder array but lower for Carex plants compared to rigid cylinder array. Stem diameter for emergent reeds is about 0.002 m to 0.003 which is smaller than cylinder diameter (0.025 and 0.018 m) used in the current study. However there were 150 to 333 stems/m^2 compare to 19 to 163 stems/m^2 cylinders per metre used in the current study. Therefore higher frontal area would be expected for emergent reeds compare to the cylinder array which generated higher transverse mixing coefficient in the emergent reed array. Stem diameter at the base of carex was 0.05 m to 0.056 m which is greater than cylinder diameter used in current experimental work, but since carex is a leafy and flexible plant, therefore the flexibility of carex reduced the drag coefficient relative to rigid cylinders. For this reason lower transverse mixing coefficient could be expected for carex array compared to rigid cylinder array.

Furthermore the current study suggests that dispersion coefficient has a stronger correlation with turbulence intensity in the longitudinal direction than the kinetic turbulent energy. This suggests that turbulence in the longitudinal direction plays a greater contribution to the overall transverse dispersion than the contribution of turbulence when considered in all three directions. With regard to the vertical variation in transverse velocity which is indicative of the transverse shear, it was found that there was a weak correlation with the transverse mixing coefficient and hence this shows that for the flow regimes examined in the current study transverse dispersion in sparse vegetated flow is driven predominated by turbulence rather than secondary currents or transverse shear. However more data is required to substantiate this finding.

The total lateral diffusion model by Nepf (1999) and net transverse dispersion model by Tanino and Nepf (2008) predicted reasonably well within 3 % to 61 %. However more data is required to test the Tanino and Nepf (2008) model because results show the possibility of biasness in the prediction of transverse mixing coefficient.

Chapter 6 – Conclusion

6.0 Introduction

The aim of this thesis is to investigate the influence of the emergent vegetation canopies on velocity and turbulence fields in order to have a better understanding of the effect vegetation on the transverse mixing processes. To achieve this aim, there are four objectives that have been outlined including; first to study the impact of stem density on the velocity and turbulence structure in emergent vegetated flows. Second is to understand which hydrodynamic processes are most influential in driving transverse dispersion in emergent vegetated flows at high stem Reynolds numbers (1000 to 3000). Third to examine which pertinent vegetation canopy parameters can be used to scale the transverse dispersion coefficient for sparse vegetation densities (solid volume less than 10 %) which are arranged in both staggered and aligned arrangements and fourth to test the applicability and performance of proposed transverse mixing models in the literature with the results from this study. To achieve these objectives a detailed laboratory study was conducted which measure the velocity, turbulence and transverse mixing through six different vegetation densities with staggered or aligned vegetation arrangement. Results were compared against the data from other researchers in this field. After completing the study and analysing the results the following conclusions have been made.

6.1 Velocity and turbulence profiles

Experimental works confirmed studies by other researchers that longitudinal velocity reduces with the increment of vegetation density. There is approximately 50 % reduction in longitudinal velocity as the vegetation double in density. Experiment results demonstrate that aligned vegetation arrangement contained higher longitudinal velocity relative to staggered arrangement for the same density. Furthermore experiment observation also shows that lower water level for the same vegetation creates more resistance to reduce the velocity.

It is known that vertical variation of transverse velocity contributes to transverse mixing process. Therefore, this thesis has evaluated the vertical variation of spatially-averaged transverse velocity to quantify the standard deviation as an indication of transverse shear. The standard deviation was plotted as a function of solid volume fraction and stem Reynolds number which shows low correlation with both parameters.

Transverse mixing process is also arises by the influence of turbulence, hence experiment measures two turbulence parameters including turbulence intensity and turbulent kinetic energy. Turbulence intensity is plotted vertically to study the impact of the vegetation density and results indicate there is a positive relationship between averaged turbulent intensity with solid volume fraction. Furthermore experiment results also show that turbulence intensity decreases with stem Reynolds number and shows a weak relation with water depth. Present study also show that turbulent kinetic energy presents a weak correlation with solid volume fraction, stem Reynolds number and water depth.

Bulk drag coefficients from one dimensional equation was calculated and analyse against solid volume fraction and stem Reynolds number. Results show that drag coefficient for sparse vegetation increases with vegetation whilst decreases stem Reynolds number.

6.2 Transverse mixing

The normalized transverse mixing coefficient was shown to increase with higher vegetation density. Other analysis shows that transverse mixing coefficients increases with stem Reynolds number and there are no observable trends between transverse mixing coefficient with flow depth and shear velocity.

Experimental analysis shows that for a similar range of stem Reynolds number the transverse dispersion coefficient was higher for emergent reeds compared to rigid cylinders because higher frontal area would be expected for emergent reeds that contributed to produce higher transverse mixing coefficient in emergent reeds. In the case for carex plants, for similar range of stem Reynolds number, lower transverse dispersion coefficient was observed compared to rigid cylinders because carex is a leafy and flexible plant, therefore the flexibility of carex reduce the drag coefficient relative to rigid cylinders.

Furthermore the current study suggests that for sparse vegetation (SVF less than 10 %) transverse mixing coefficient has a stronger correlation with turbulence intensity in the longitudinal direction than the kinetic turbulent energy. This indicates that the turbulence in the longitudinal direction plays a greater contribution to the overall transverse dispersion than the contribution of turbulence from all three directions.

With regards to the vertical variation in transverse velocity which is indicative of the transverse shear, it was found that there is a weak correlation with the transverse mixing coefficient and hence this shows that for the flow regimes examined in the current study transverse dispersion in sparse vegetated flow is driven predominated by turbulence rather than secondary currents or transverse shear. However more data is required to substantiate this finding.

6.3 Transverse Mixing Models

This thesis examines two transverse mixing models including the total lateral diffusion model by Nepf (1999) and the net transverse dispersion model by Tanino and Nepf (2008). Both model predicted reasonably well within 3 % to 55 % for Nepf (1999) model and 21 % to 61 % for Tanino and Nepf (2008) model. However more data is required for Tanino and Nepf (2008) proposed model because results show the possibility of biasness in the prediction of transverse mixing coefficient.

6.4 Recommendations for Further Research

This research has looked into the influence of sparse emergent vegetation on the flow characteristics and transverse mixing processes. The following is a list of recommendations for future research.

1. Current research shows that for sparse and fully vegetated channel, turbulence intensity is more dominant relative to secondary flow in transverse mixing process. Therefore further study is required to investigate the therefore driver for transverse dispersion in a vegetated meandering channel.

2. Since this thesis only focused on sparse vegetation future research should examine the effect of high density of vegetation (i.e. SVF greater than 10 %) of turbulence intensity and secondary currents in transverse mixing process.

3. Future research should also examine the effect of flexible vegetation on the transverse mixing for emergent and submerged conditions either in straight or meandering channel as there have been few studies previously conducted.

4. Furthermore research should examine the effect of vegetation on the transverse mixing within a broader range ofstem Reynolds number that covers fromlow Reynolds numbers (i.e. less than 200) to high Reynolds number (i.e. more than 1000).

Appendix I

Test 0.51S

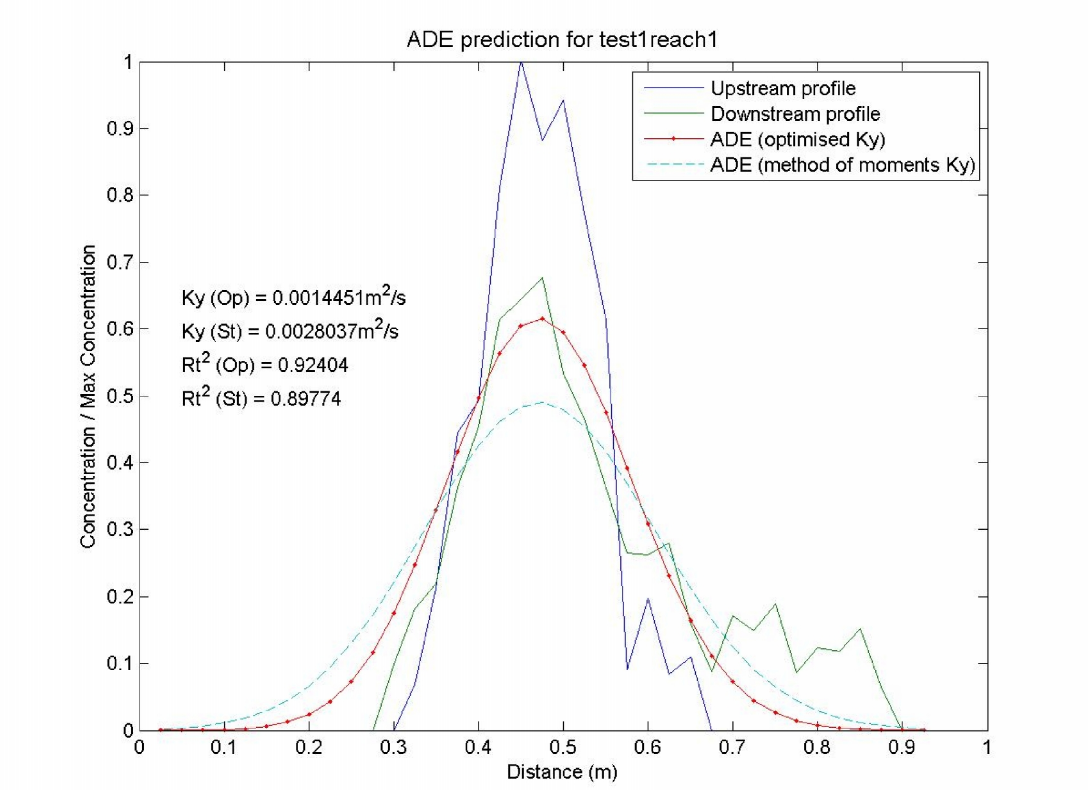

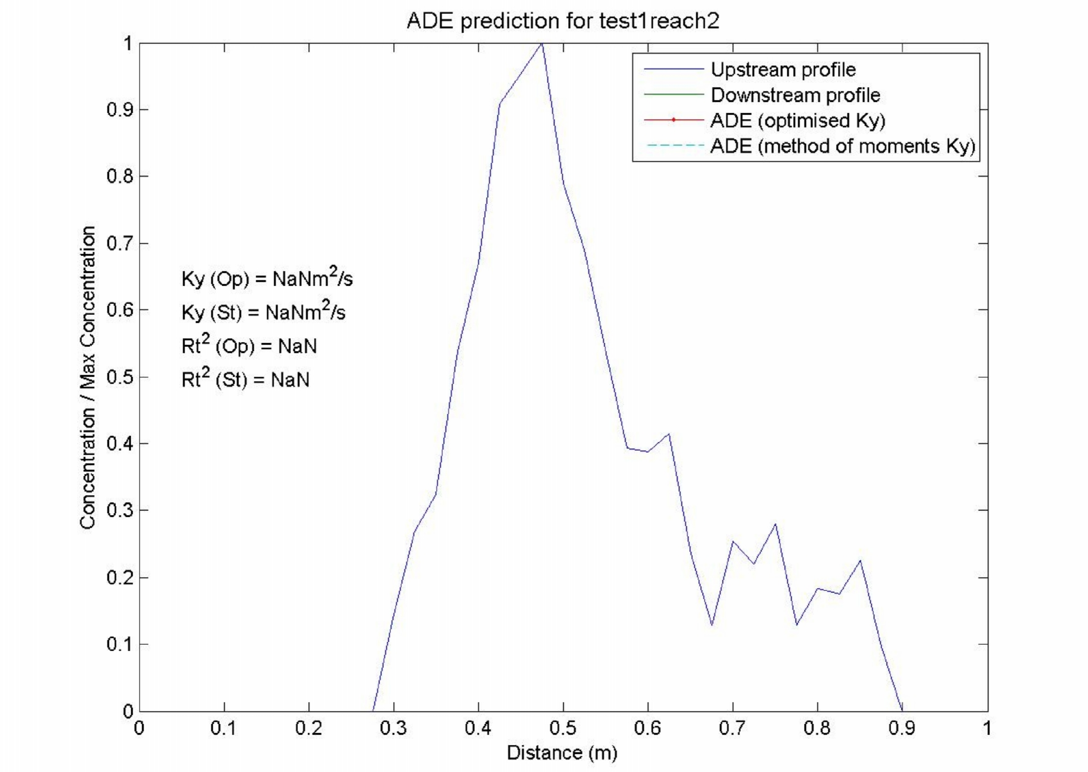

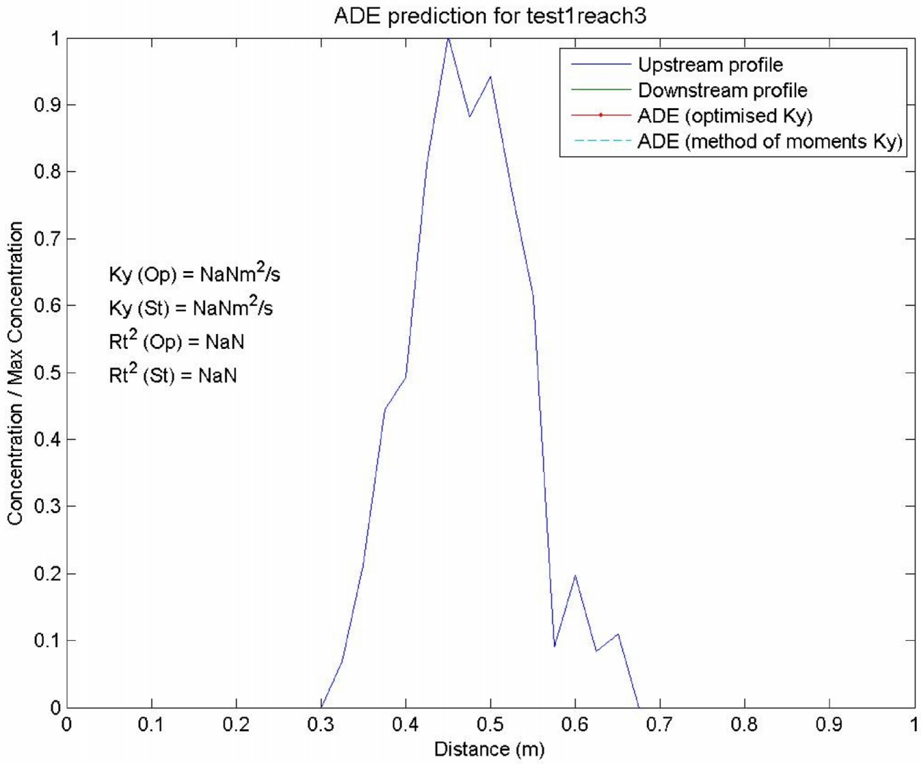
ADE prediction for test1reach3
Upstream profile
Downstream profile
ADE (optimised Ky)
ADE (method of moments Ky)
Ky (Op) = NaNm^2/s
Ky (St) = NaNm^2/s
Rt^2 (Op) = NaN
Rt^2 (St) = NaN
Concentration / Max Concentration
0
0.1
0.2
0.3
0.4
0.5
0.6
0.7
0.8
0.9
1
Distance (m)

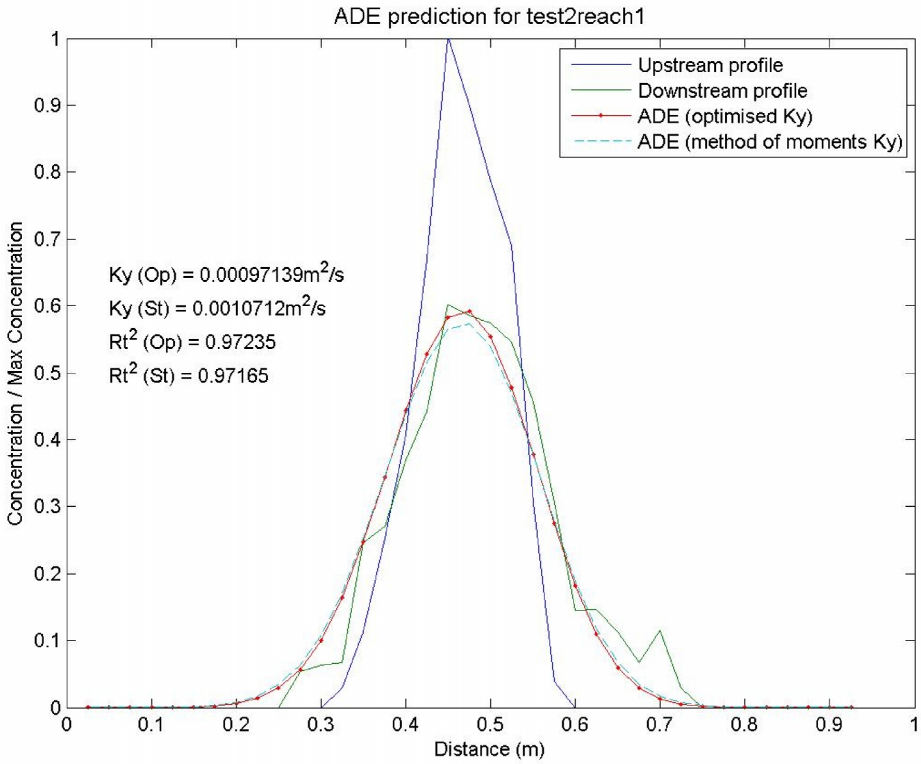
ADE prediction for test2reach1
Upstream profile
Downstream profile
ADE (optimised Ky)
ADE (method of moments Ky)
Ky (Op) = 0.00097139m^2/s
Ky (St) = 0.0010712m^2/s
Rt^2 (Op) = 0.97235
Rt^2 (St) = 0.97165
Concentration / Max Concentration
0
0.1
0.2
0.3
0.4
0.5
0.6
0.7
0.8
0.9
1
Distance (m)

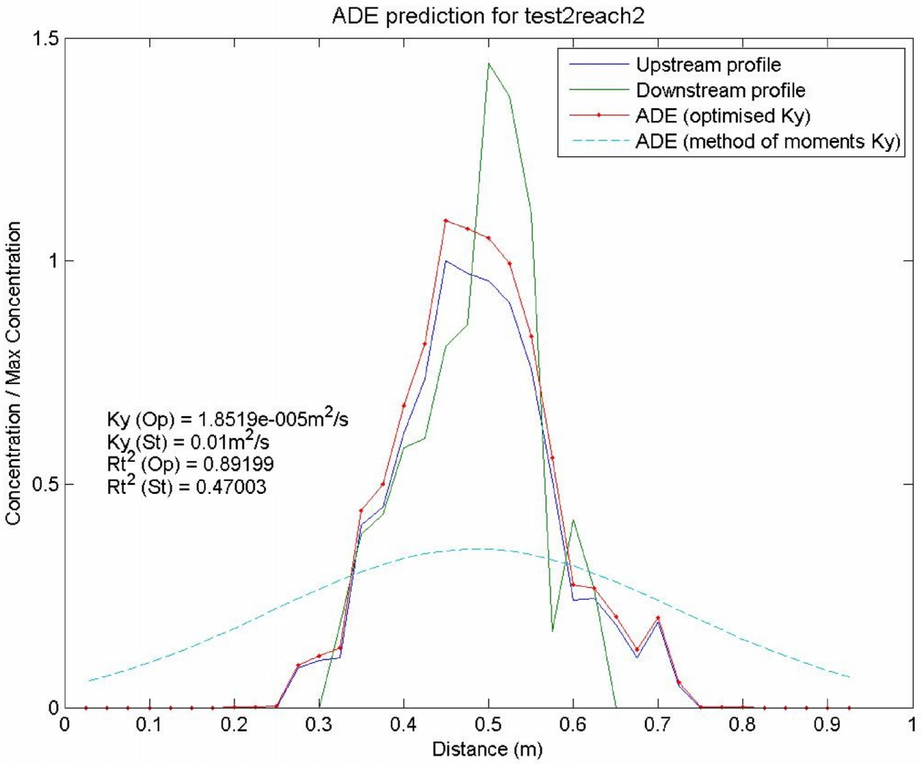
ADE prediction for test2reach2
Upstream profile
Downstream profile
ADE (optimised Ky)
ADE (method of moments Ky)
Ky (Op) = 1.8519e-005m^2/s
Ky (St) = 0.01m^2/s
Rt^2 (Op) = 0.89199
Rt^2 (St) = 0.47003
Concentration / Max Concentration
Distance (m)
0
0.5
1
1.5
0
0.1
0.2
0.3
0.4
0.5
0.6
0.7
0.8
0.9
1

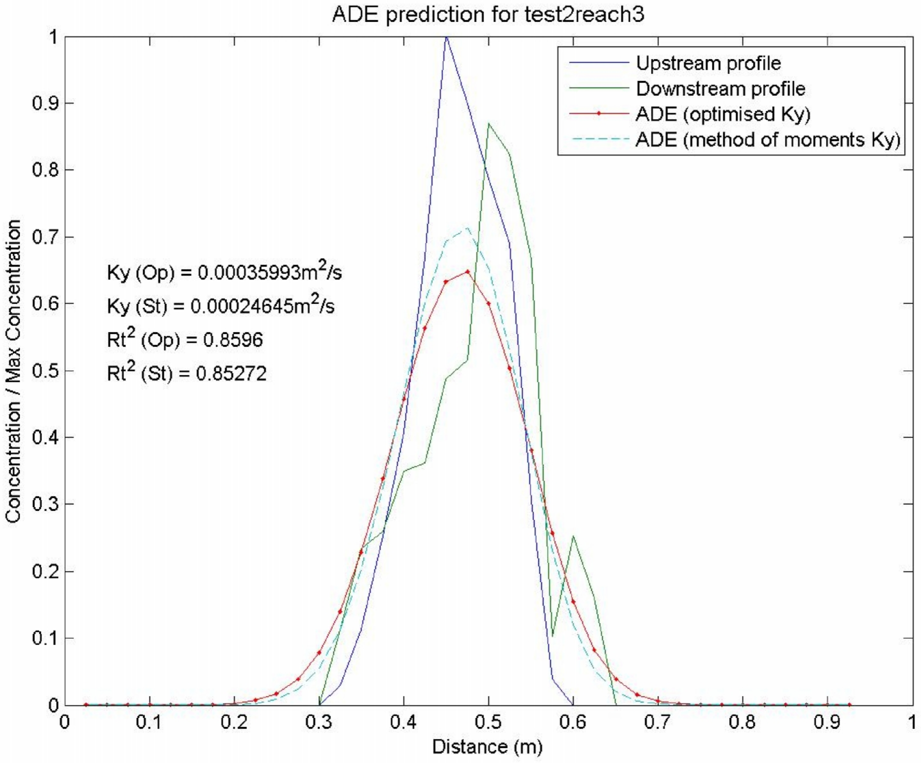
ADE prediction for test2reach3
Upstream profile
Downstream profile
ADE (optimised Ky)
ADE (method of moments Ky)
Ky (Op) = 0.00035993m^2/s
Ky (St) = 0.00024645m^2/s
Rt^2 (Op) = 0.8596
Rt^2 (St) = 0.85272
Concentration / Max Concentration
Distance (m)
0
0.1
0.2
0.3
0.4
0.5
0.6
0.7
0.8
0.9
1
0
0.1
0.2
0.3
0.4
0.5
0.6
0.7
0.8
0.9
1

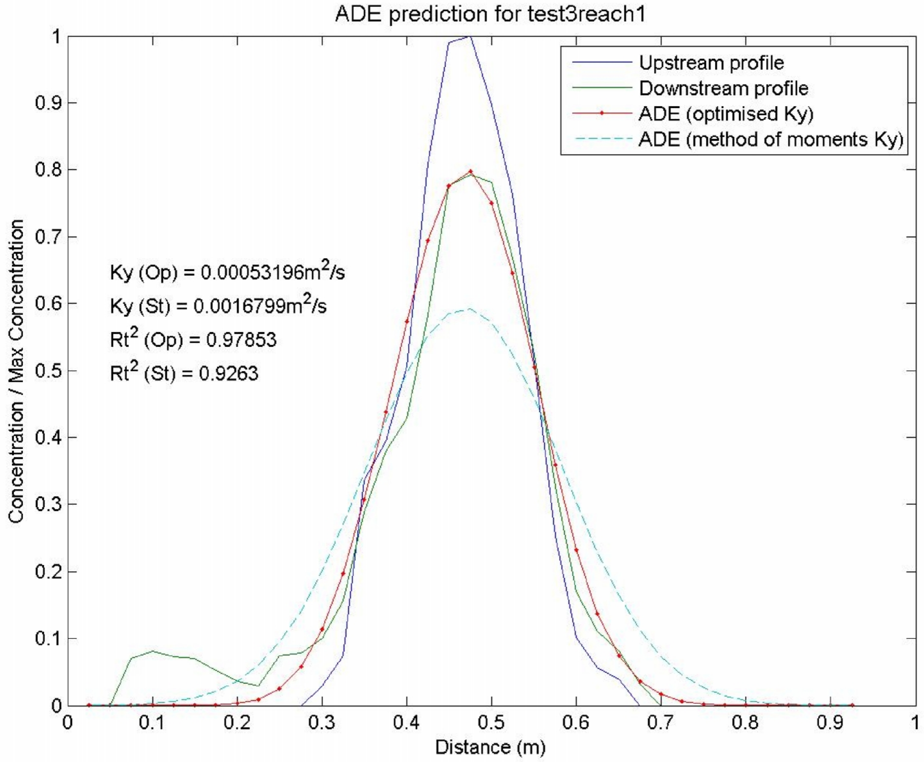
ADE prediction for test3reach1
Upstream profile
Downstream profile
ADE (optimised Ky)
ADE (method of moments Ky)
Ky (Op) = 0.00053196m^2/s
Ky (St) = 0.0016799m^2/s
Rt^2 (Op) = 0.97853
Rt^2 (St) = 0.9263
Concentration / Max Concentration
Distance (m)
0
0.1
0.2
0.3
0.4
0.5
0.6
0.7
0.8
0.9
1

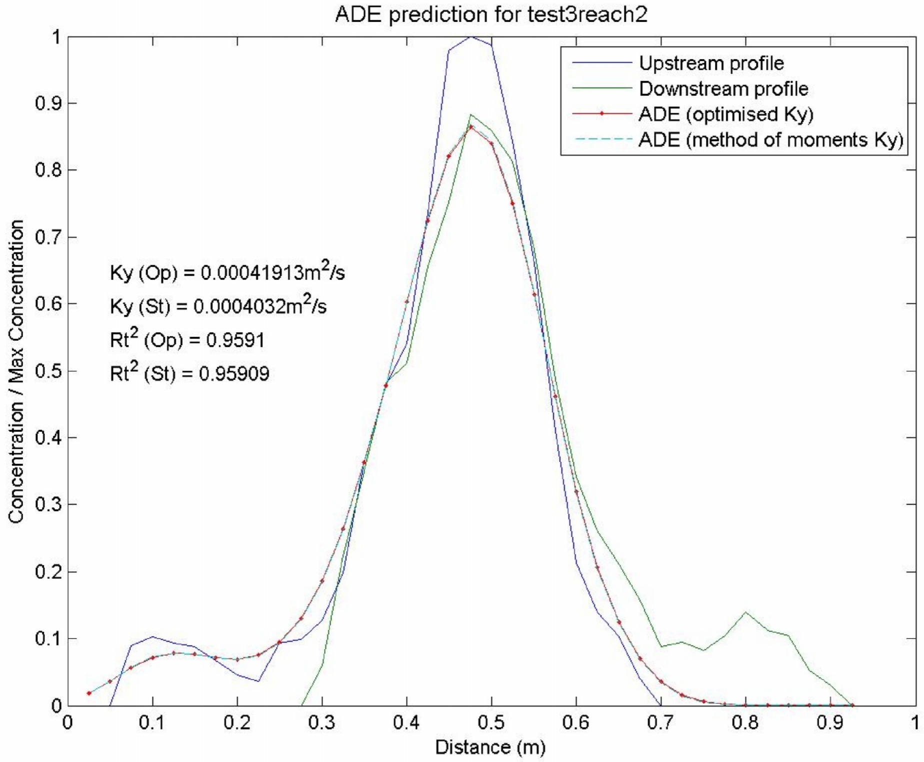
ADE prediction for test3reach2
Upstream profile
Downstream profile
ADE (optimised Ky)
ADE (method of moments Ky)
Ky (Op) = 0.00041913m^2/s
Ky (St) = 0.0004032m^2/s
Rt^2 (Op) = 0.9591
Rt^2 (St) = 0.95909
Concentration / Max Concentration
Distance (m)
0
0.1
0.2
0.3
0.4
0.5
0.6
0.7
0.8
0.9
1

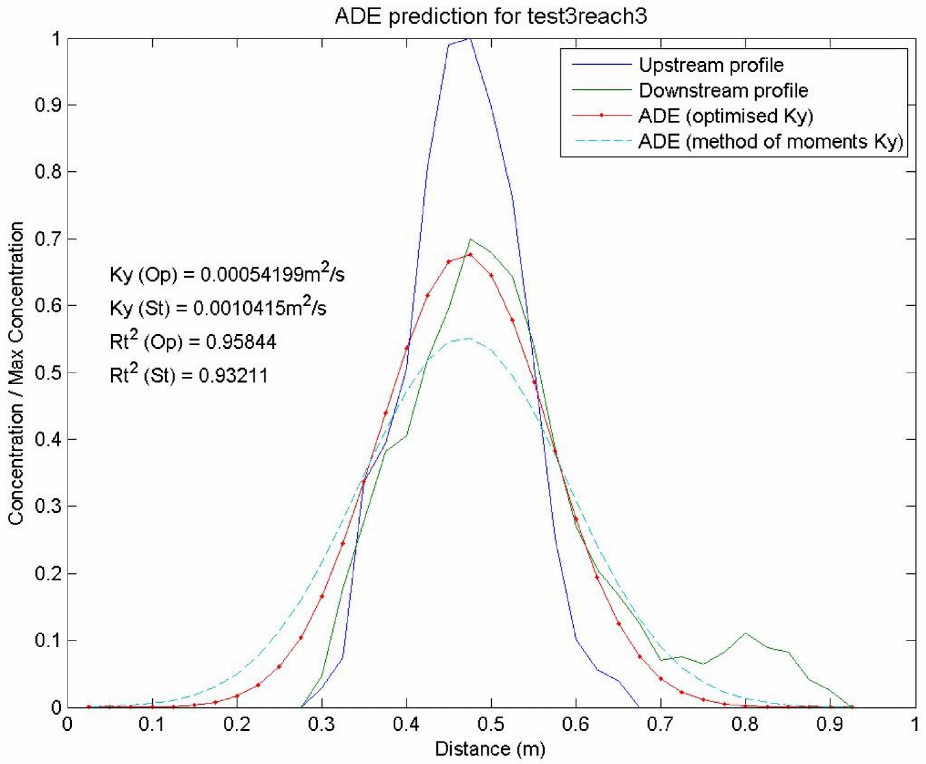
ADE prediction for test3reach3
Upstream profile
Downstream profile
ADE (optimised Ky)
ADE (method of moments Ky)
Ky (Op) = 0.00054199m^2/s
Ky (St) = 0.0010415m^2/s
Rt^2 (Op) = 0.95844
Rt^2 (St) = 0.93211
Concentration / Max Concentration
Distance (m)
0
0.1
0.2
0.3
0.4
0.5
0.6
0.7
0.8
0.9
1

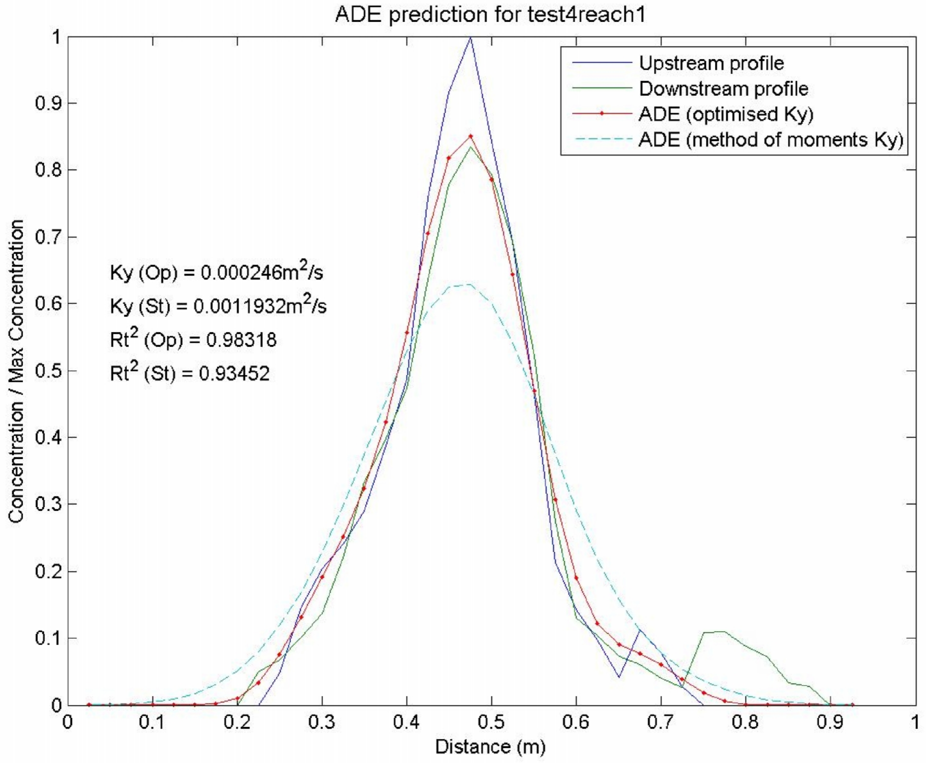
ADE prediction for test4reach1
Upstream profile
Downstream profile
ADE (optimised Ky)
ADE (method of moments Ky)
Ky (Op) = 0.000246m^2/s
Ky (St) = 0.0011932m^2/s
Rt^2 (Op) = 0.98318
Rt^2 (St) = 0.93452
Concentration / Max Concentration
Distance (m)
0
0.1
0.2
0.3
0.4
0.5
0.6
0.7
0.8
0.9
1

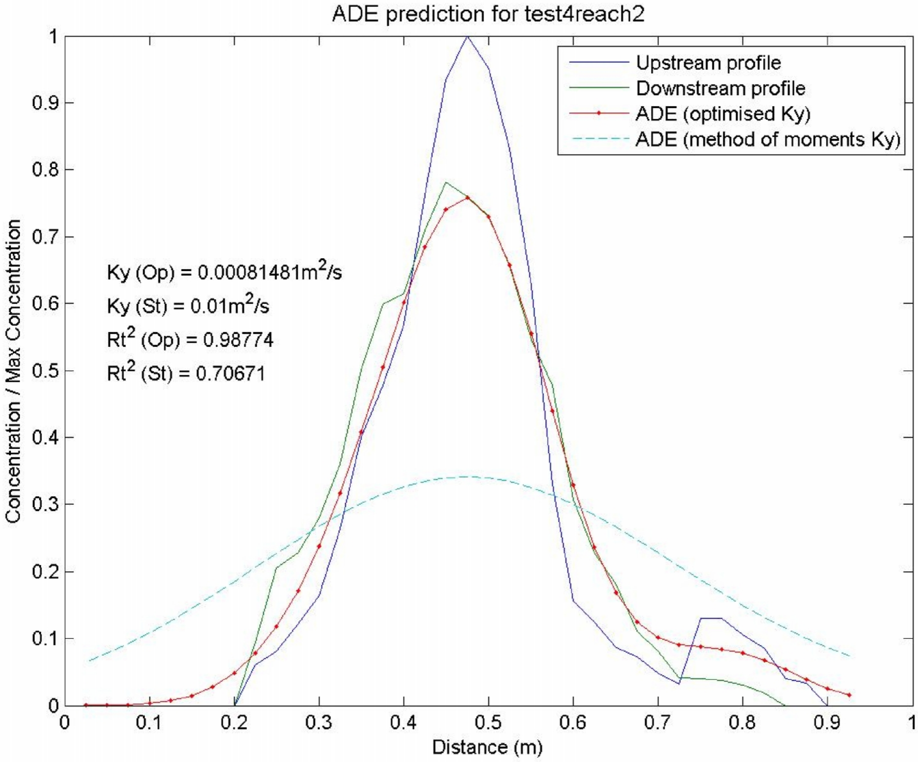
ADE prediction for test4reach2
Upstream profile
Downstream profile
ADE (optimised Ky)
ADE (method of moments Ky)
Ky (Op) = 0.00081481m^2/s
Ky (St) = 0.01m^2/s
Rt^2 (Op) = 0.98774
Rt^2 (St) = 0.70671
Concentration / Max Concentration
Distance (m)
0
0.1
0.2
0.3
0.4
0.5
0.6
0.7
0.8
0.9
1

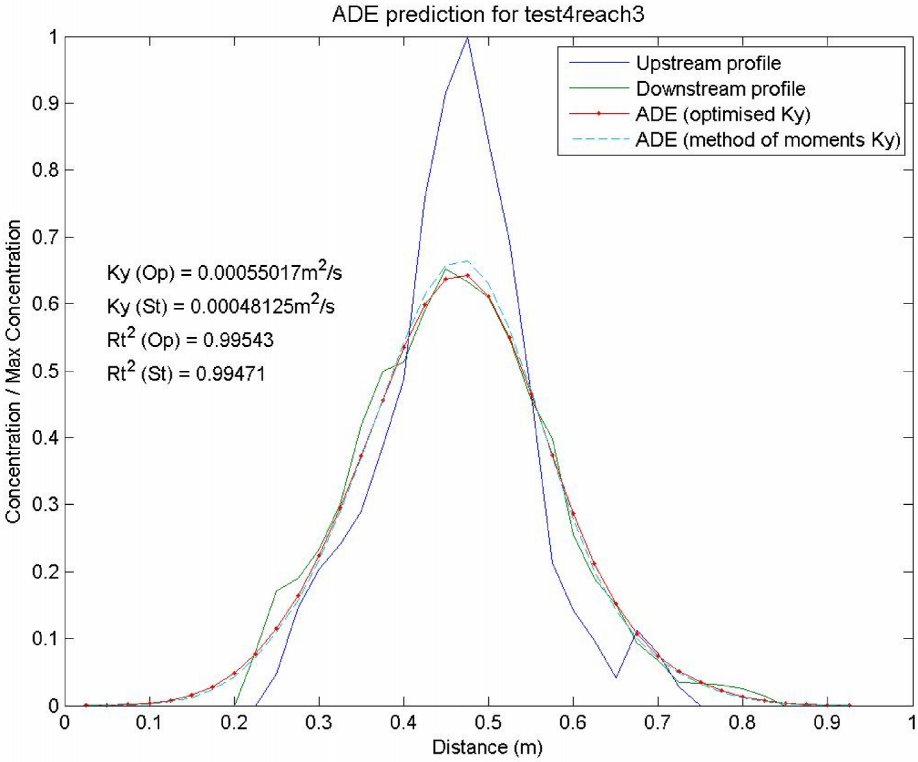
ADE prediction for test4reach3
Upstream profile
Downstream profile
ADE (optimised Ky)
ADE (method of moments Ky)
Ky (Op) = 0.00055017m^2/s
Ky (St) = 0.00048125m^2/s
Rt^2 (Op) = 0.99543
Rt^2 (St) = 0.99471
Concentration / Max Concentration
Distance (m)
0
0.1
0.2
0.3
0.4
0.5
0.6
0.7
0.8
0.9
1

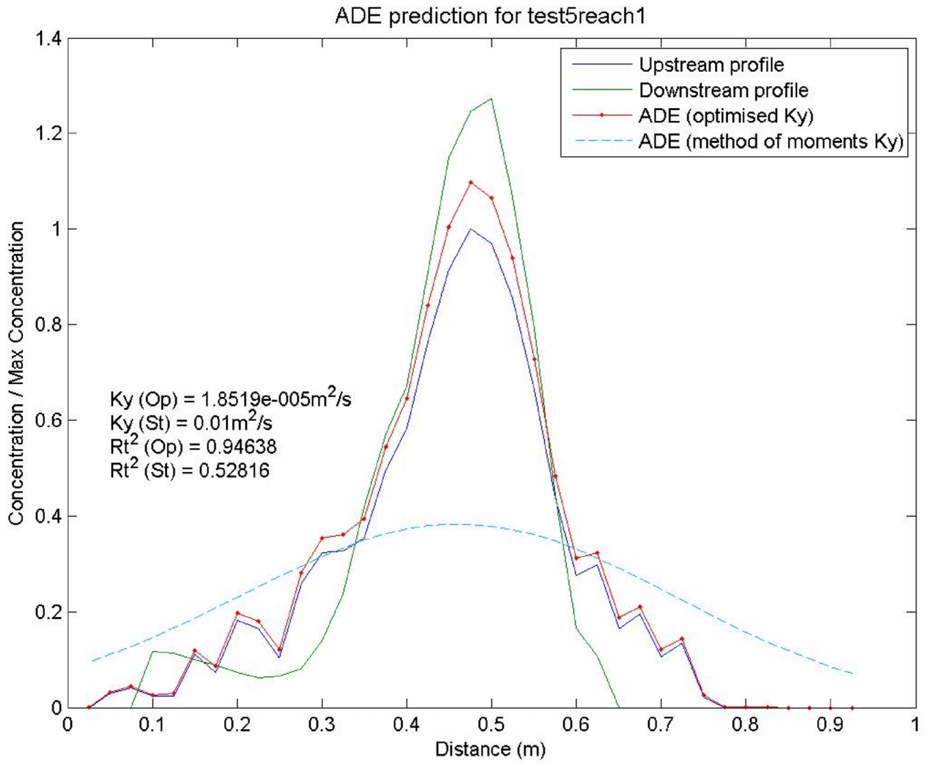
ADE prediction for test5reach1
Upstream profile
Downstream profile
ADE (optimised Ky)
ADE (method of moments Ky)
Ky (Op) = 1.8519e-005m^2/s
Ky (St) = 0.01m^2/s
Rt^2 (Op) = 0.94638
Rt^2 (St) = 0.52816
Concentration / Max Concentration
Distance (m)
0
0.2
0.4
0.6
0.8
1
1.2
1.4
0.1
0.2
0.3
0.4
0.5
0.6
0.7
0.8
0.9
1

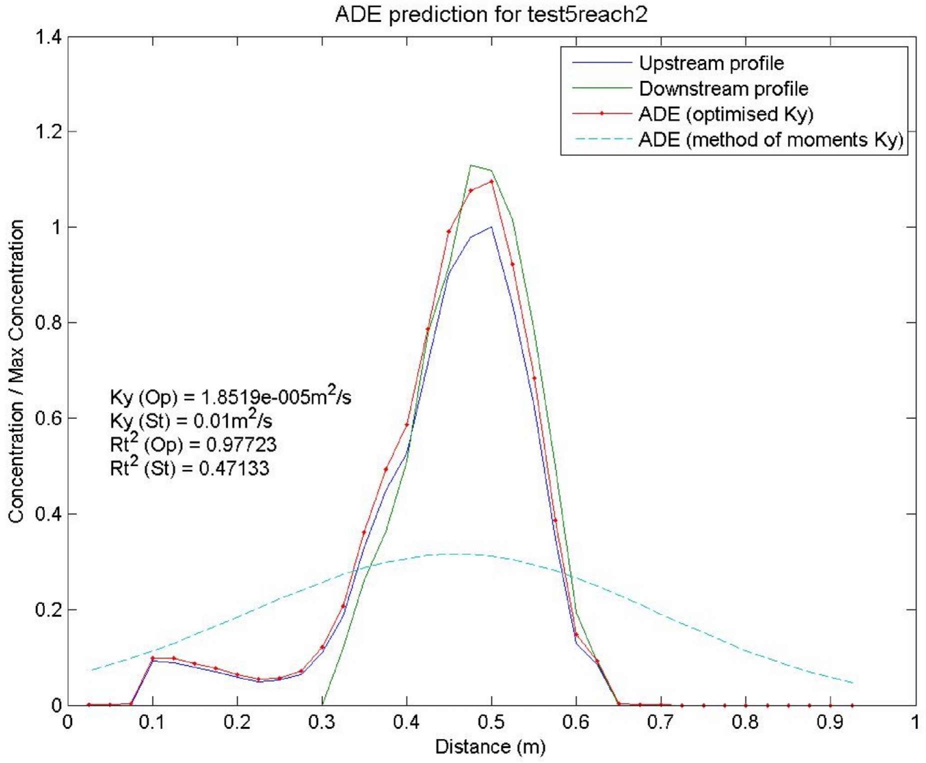
ADE prediction for test5reach2
Upstream profile
Downstream profile
ADE (optimised Ky)
ADE (method of moments Ky)
Ky (Op) = 1.8519e-005m^2/s
Ky (St) = 0.01m^2/s
Rt^2 (Op) = 0.97723
Rt^2 (St) = 0.47133
Concentration / Max Concentration
Distance (m)
0
0.2
0.4
0.6
0.8
1
1.2
1.4
0.1
0.2
0.3
0.4
0.5
0.6
0.7
0.8
0.9
1

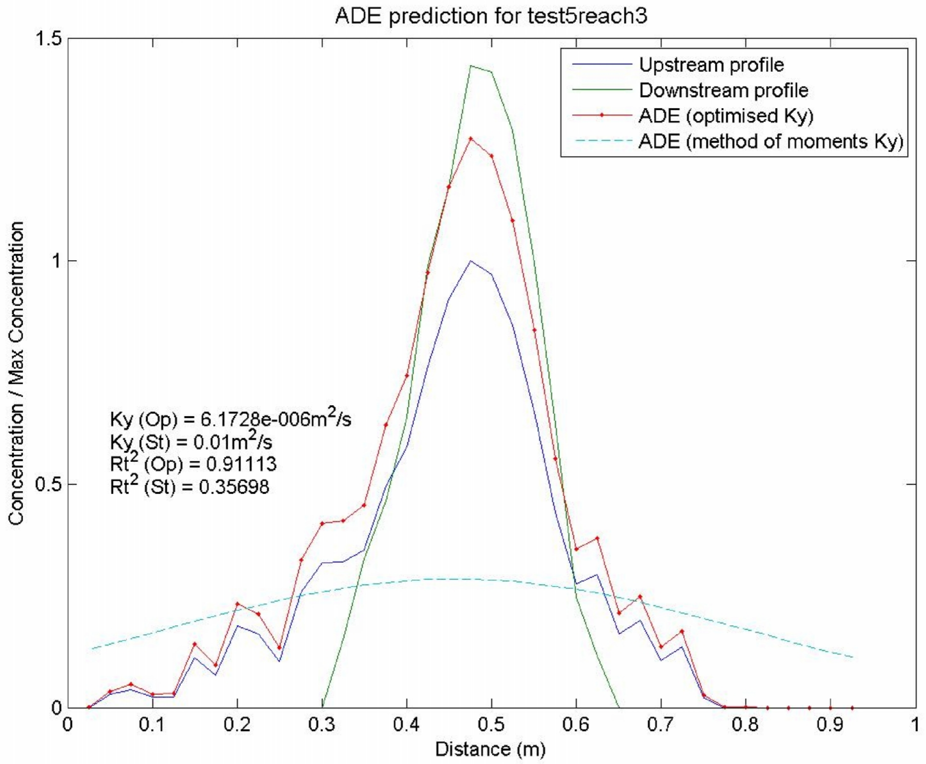
ADE prediction for test5reach3
Upstream profile
Downstream profile
ADE (optimised Ky)
ADE (method of moments Ky)
Ky (Op) = 6.1728e-006m^2/s
Ky (St) = 0.01m^2/s
Rt^2 (Op) = 0.91113
Rt^2 (St) = 0.35698
Concentration / Max Concentration
Distance (m)
0
0.5
1
1.5
0
0.1
0.2
0.3
0.4
0.5
0.6
0.7
0.8
0.9
1

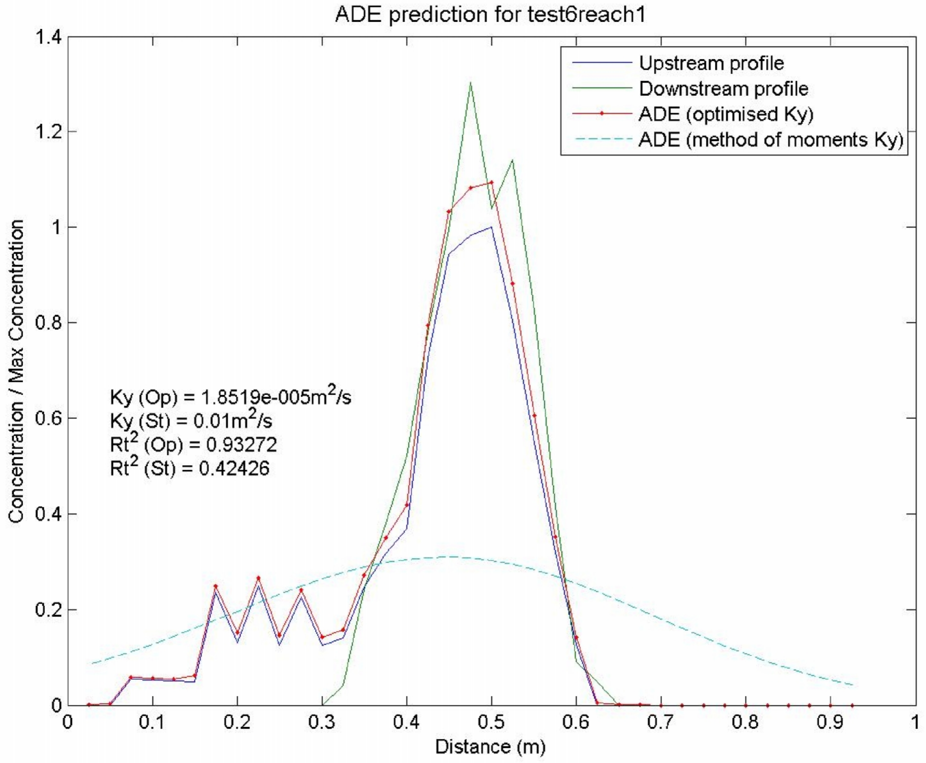
ADE prediction for test6reach1
Upstream profile
Downstream profile
ADE (optimised Ky)
ADE (method of moments Ky)
Ky (Op) = 1.8519e-005m^2/s
Ky (St) = 0.01m^2/s
Rt^2 (Op) = 0.93272
Rt^2 (St) = 0.42426
Concentration / Max Concentration
Distance (m)
0
0.2
0.4
0.6
0.8
1
1.2
1.4
0
0.1
0.2
0.3
0.4
0.5
0.6
0.7
0.8
0.9
1

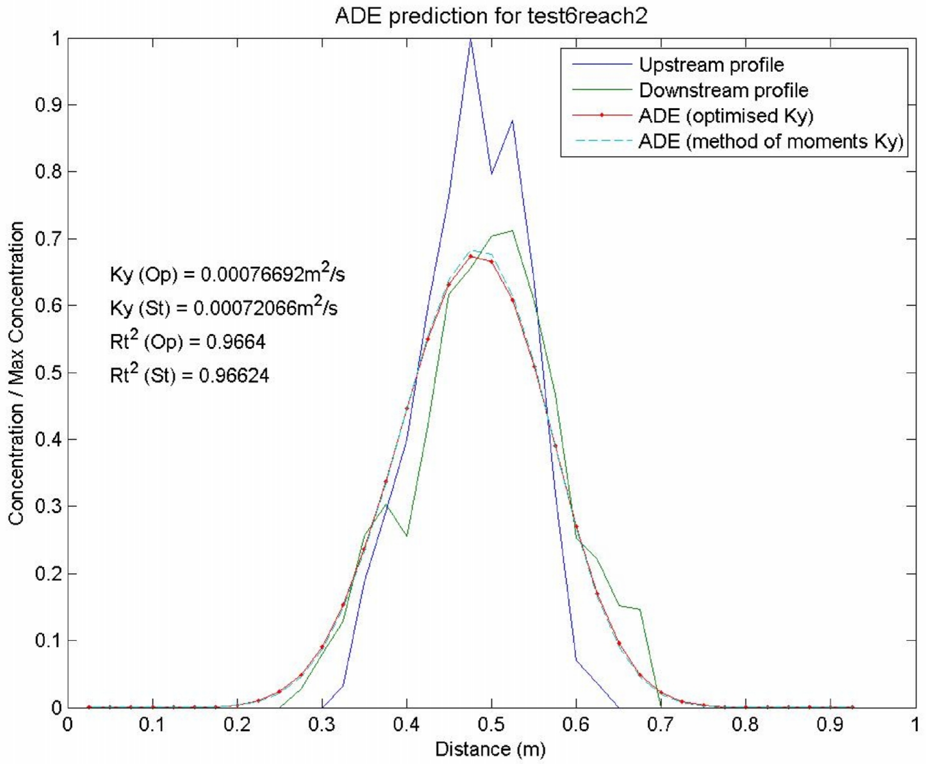

ADE prediction for test6reach2

Ky (Op) = 0.00076692m^2/s

Ky (St) = 0.00072066m^2/s

Rt^2 (Op) = 0.9664

Rt^2 (St) = 0.96624

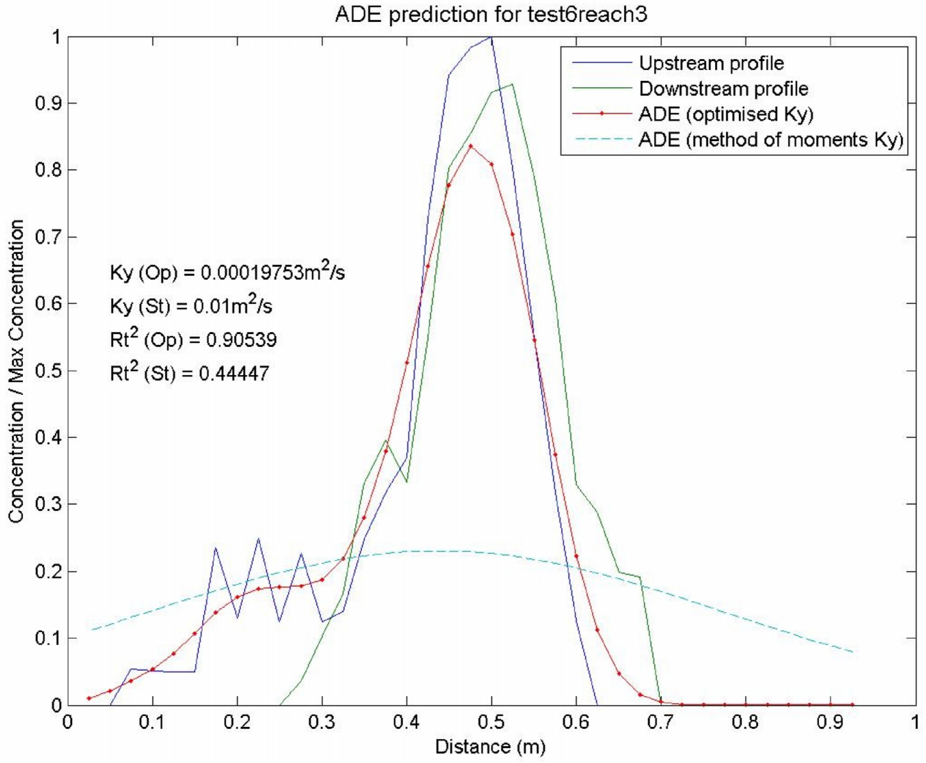

ADE prediction for test6reach3

Ky (Op) = 0.00019753m^2/s

Ky (St) = 0.01m^2/s

Rt^2 (Op) = 0.90539

Rt^2 (St) = 0.44447

Test 0.97S

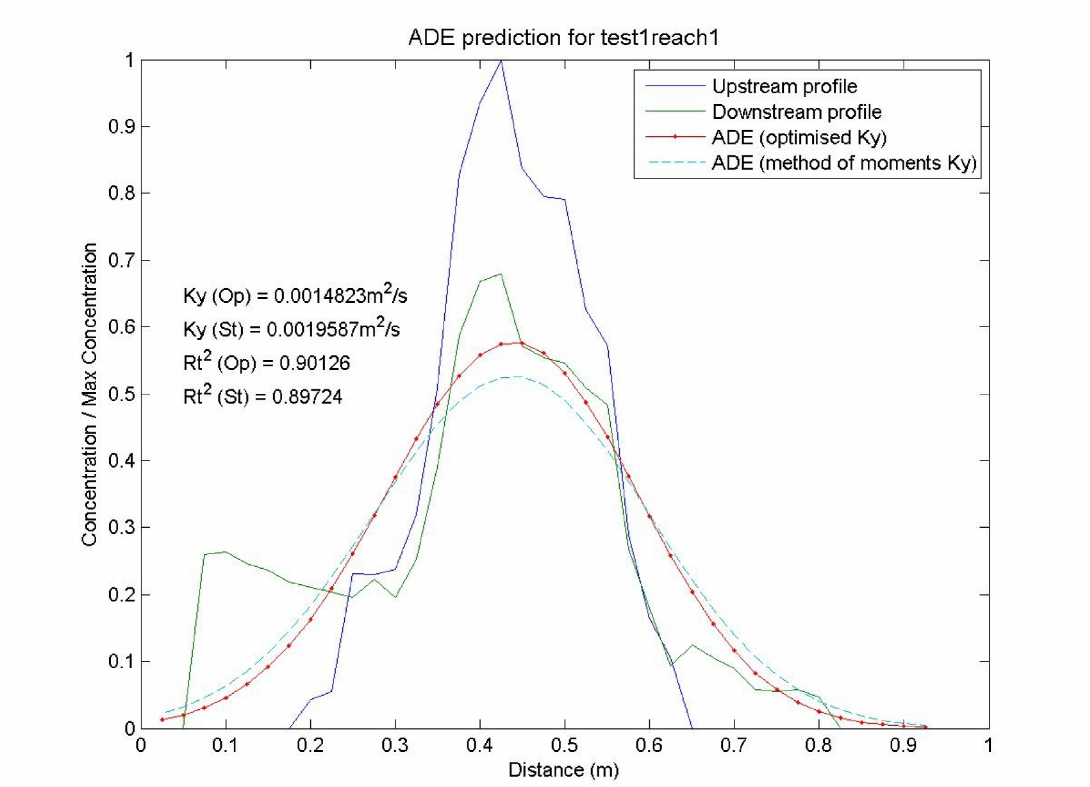

ADE prediction for test1reach1
Upstream profile
Downstream profile
ADE (optimised Ky)
ADE (method of moments Ky)
Ky (Op) = 0.0014823m^2/s
Ky (St) = 0.0019587m^2/s
Rt^2 (Op) = 0.90126
Rt^2 (St) = 0.89724
Concentration / Max Concentration
Distance (m)
0
0.1
0.2
0.3
0.4
0.5
0.6
0.7
0.8
0.9
1

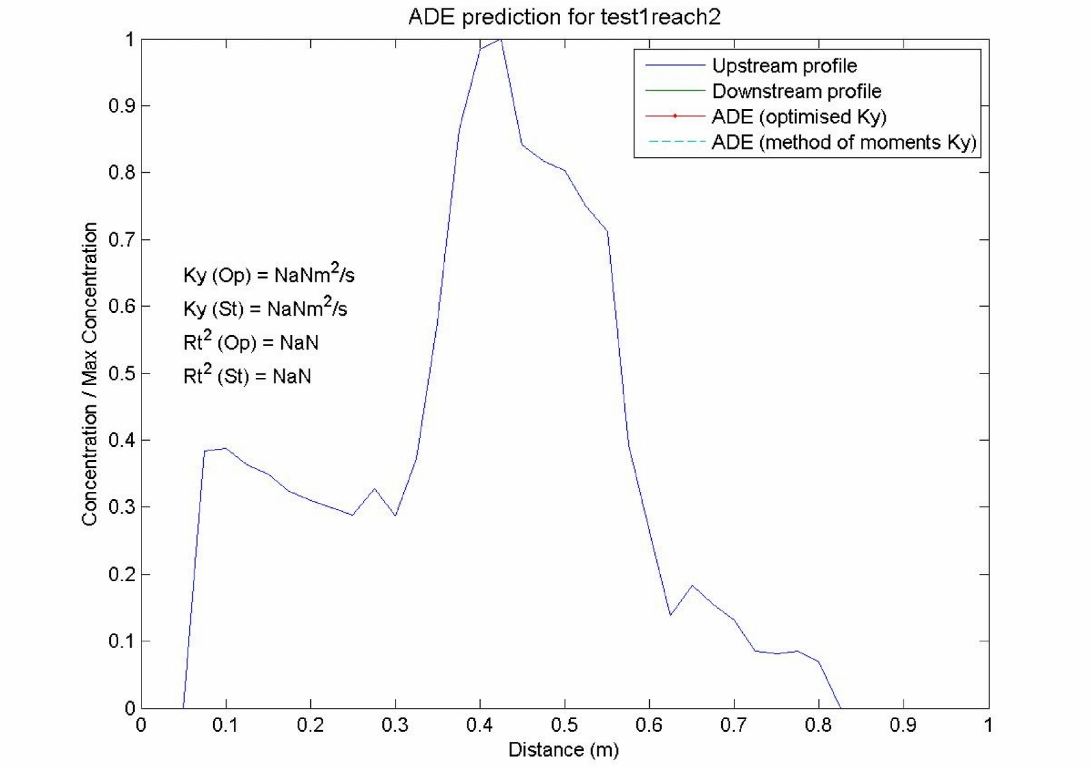

ADE prediction for test1reach2
Upstream profile
Downstream profile
ADE (optimised Ky)
ADE (method of moments Ky)
Ky (Op) = NaNm^2/s
Ky (St) = NaNm^2/s
Rt^2 (Op) = NaN
Rt^2 (St) = NaN
Concentration / Max Concentration
Distance (m)
0
0.1
0.2
0.3
0.4
0.5
0.6
0.7
0.8
0.9
1

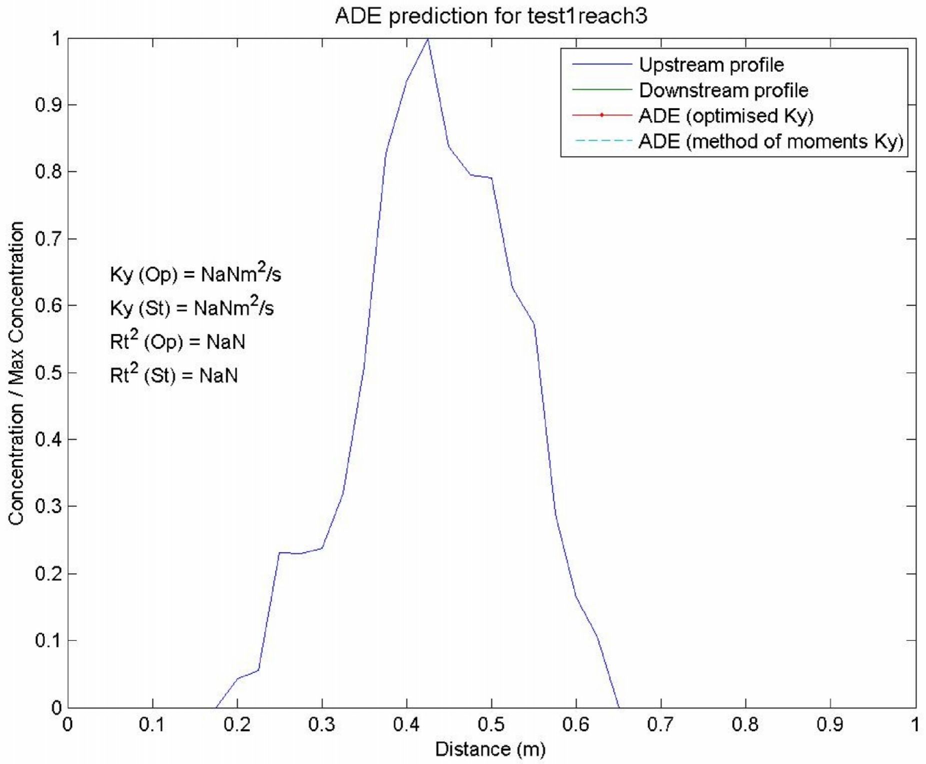

ADE prediction for test1reach3

Ky (Op) = NaNm^2/s

Ky (St) = NaNm^2/s

Rt^2 (Op) = NaN

Rt^2 (St) = NaN

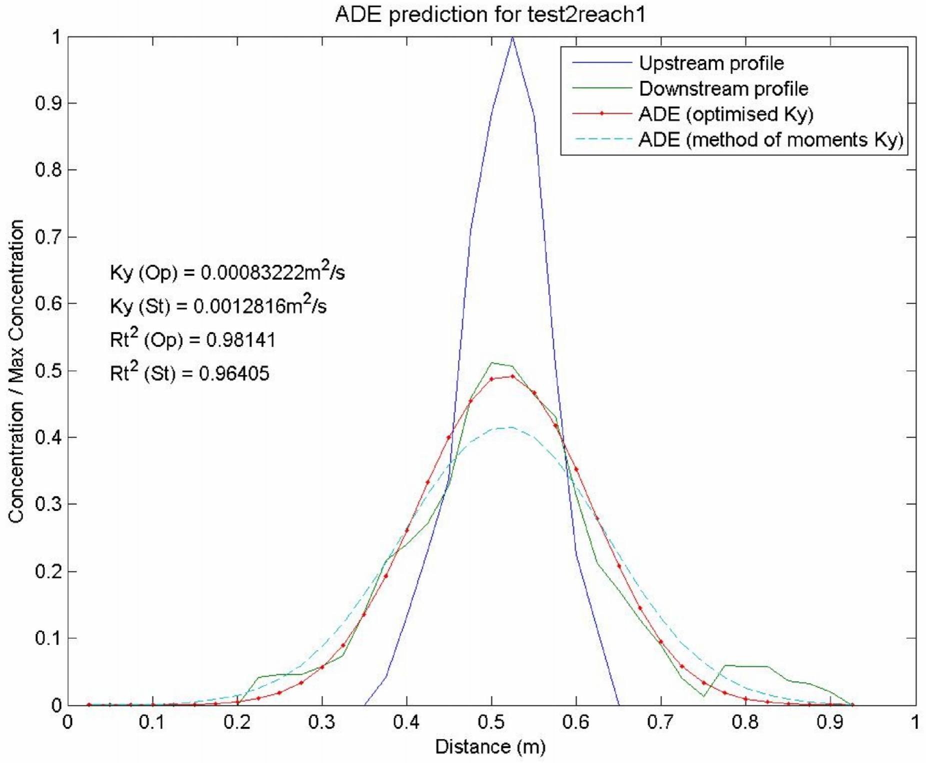

ADE prediction for test2reach1

Ky (Op) = 0.00083222m^2/s

Ky (St) = 0.0012816m^2/s

Rt^2 (Op) = 0.98141

Rt^2 (St) = 0.96405

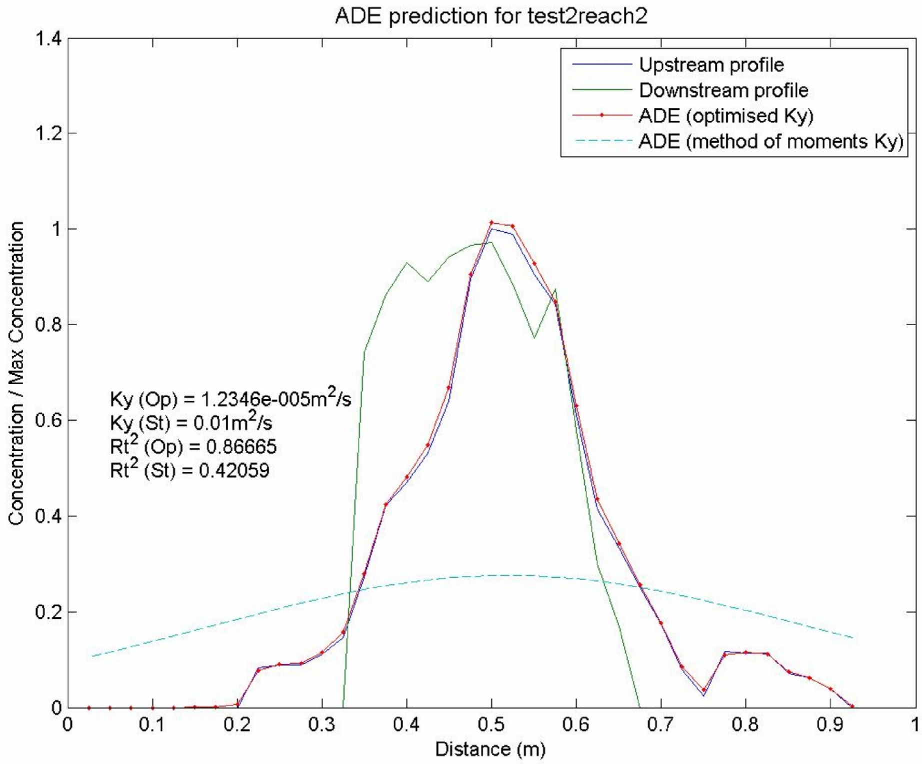
ADE prediction for test2reach2
Upstream profile
Downstream profile
ADE (optimised Ky)
ADE (method of moments Ky)
Ky (Op) = 1.2346e-005m^2/s
Ky (St) = 0.01m^2/s
Rt^2 (Op) = 0.86665
Rt^2 (St) = 0.42059
Concentration / Max Concentration
Distance (m)
0
0.2
0.4
0.6
0.8
1
1.2
1.4
0
0.1
0.2
0.3
0.4
0.5
0.6
0.7
0.8
0.9
1

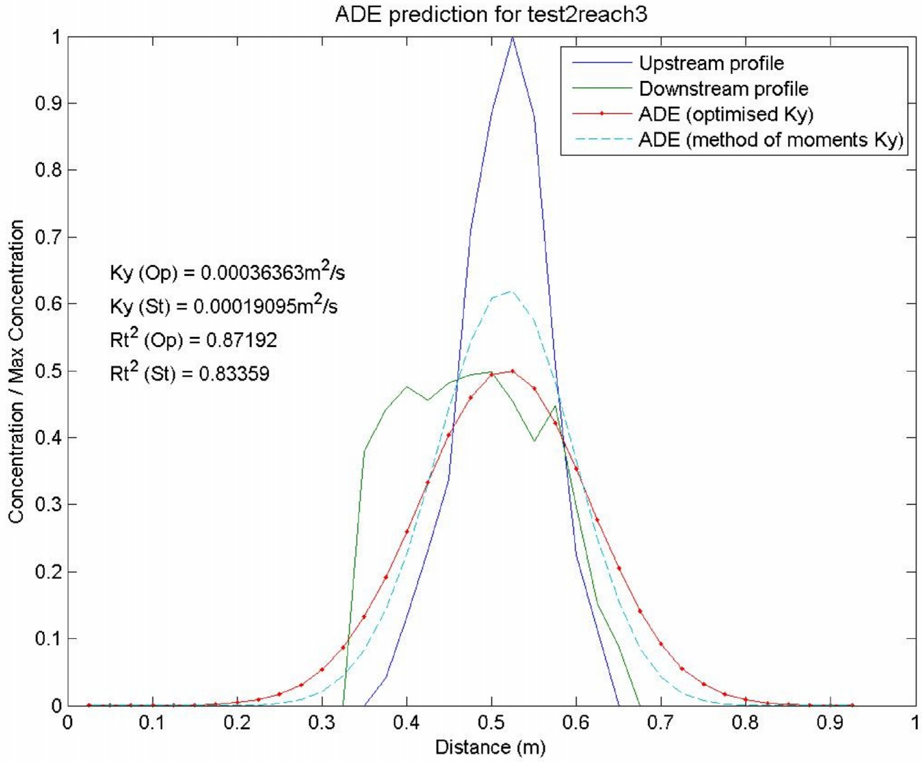
ADE prediction for test2reach3
Upstream profile
Downstream profile
ADE (optimised Ky)
ADE (method of moments Ky)
Ky (Op) = 0.00036363m^2/s
Ky (St) = 0.00019095m^2/s
Rt^2 (Op) = 0.87192
Rt^2 (St) = 0.83359
Concentration / Max Concentration
Distance (m)
0
0.1
0.2
0.3
0.4
0.5
0.6
0.7
0.8
0.9
1
0
0.1
0.2
0.3
0.4
0.5
0.6
0.7
0.8
0.9
1

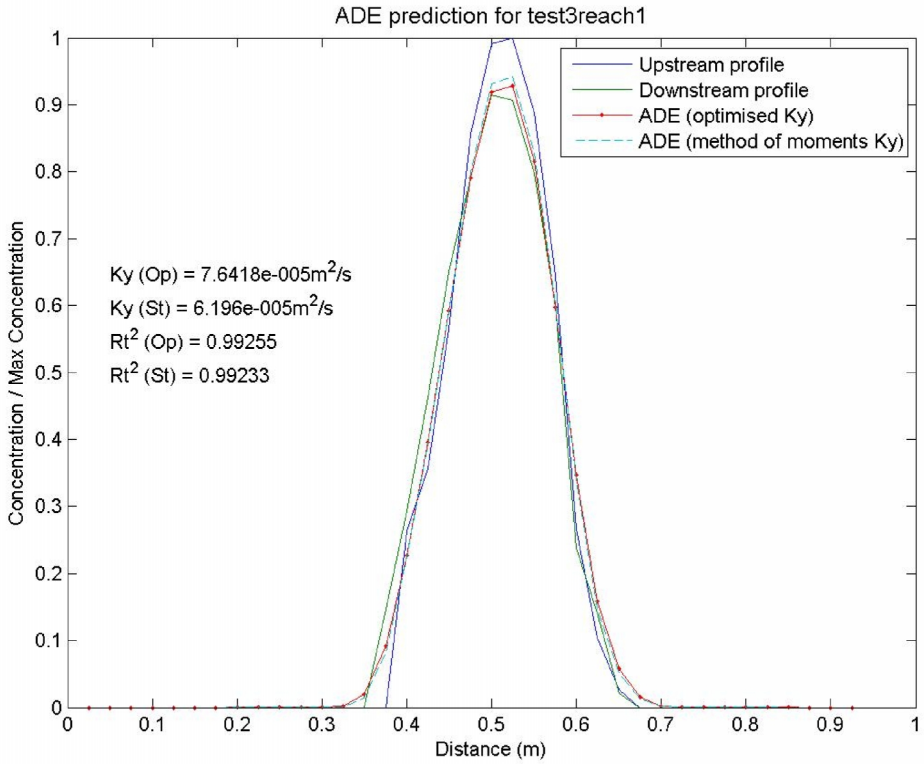
ADE prediction for test3reach1
Upstream profile
Downstream profile
ADE (optimised Ky)
ADE (method of moments Ky)
Ky (Op) = 7.6418e-005m²/s
Ky (St) = 6.196e-005m²/s
Rt² (Op) = 0.99255
Rt² (St) = 0.99233
Concentration / Max Concentration
Distance (m)
0
0.1
0.2
0.3
0.4
0.5
0.6
0.7
0.8
0.9
1

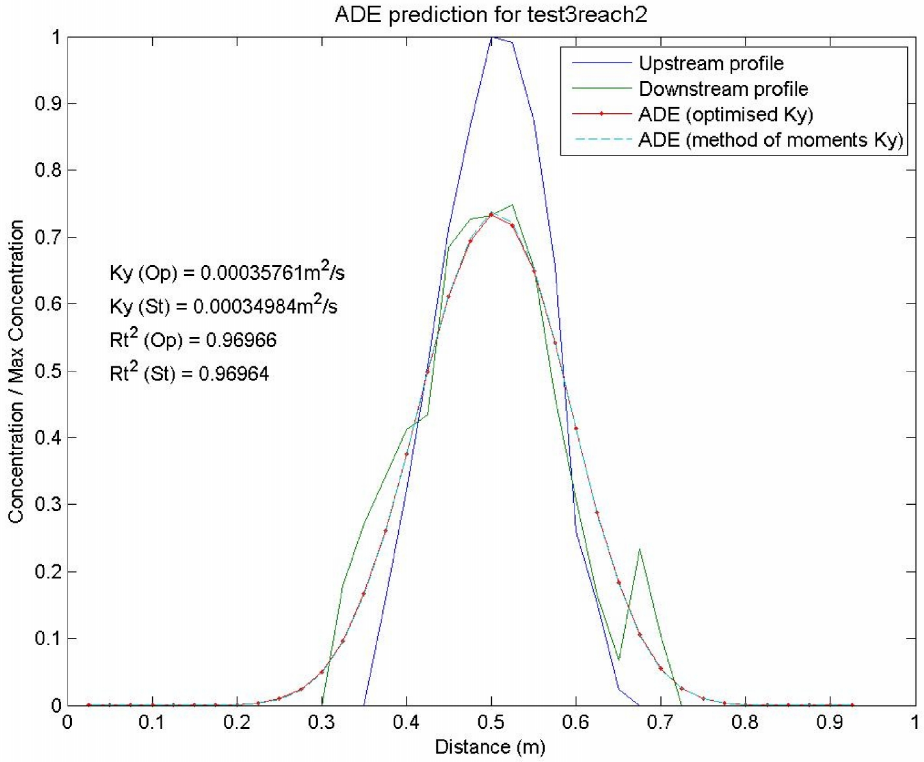
ADE prediction for test3reach2
Upstream profile
Downstream profile
ADE (optimised Ky)
ADE (method of moments Ky)
Ky (Op) = 0.00035761m²/s
Ky (St) = 0.00034984m²/s
Rt² (Op) = 0.96966
Rt² (St) = 0.96964
Concentration / Max Concentration
Distance (m)
0
0.1
0.2
0.3
0.4
0.5
0.6
0.7
0.8
0.9
1

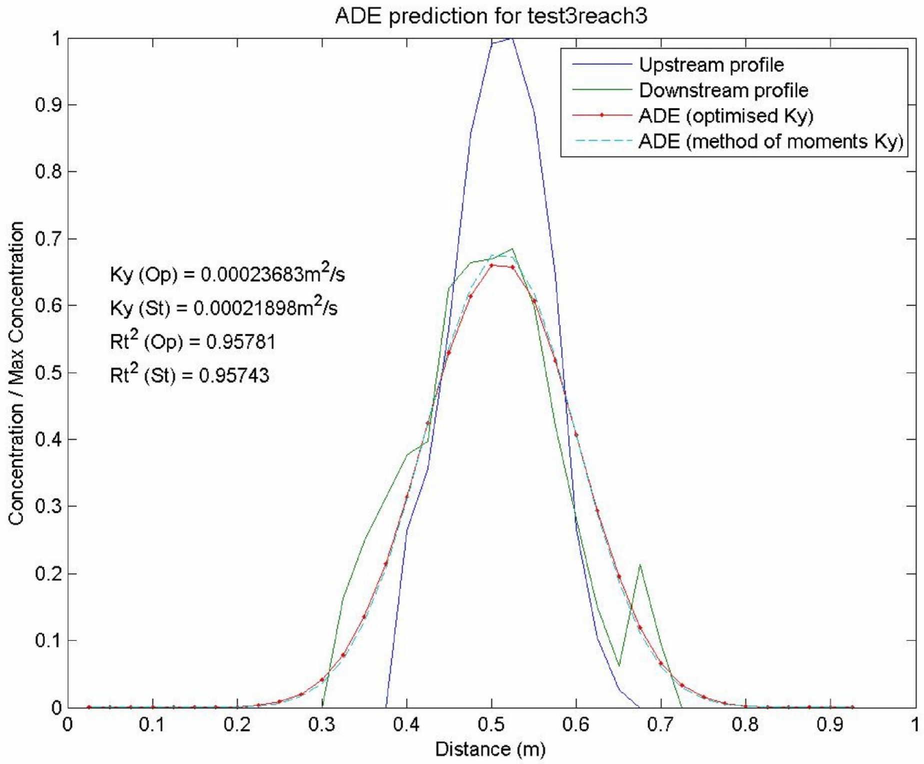
ADE prediction for test3reach3
Upstream profile
Downstream profile
ADE (optimised Ky)
ADE (method of moments Ky)
Ky (Op) = 0.00023683m²/s
Ky (St) = 0.00021898m²/s
Rt² (Op) = 0.95781
Rt² (St) = 0.95743
Concentration / Max Concentration
Distance (m)
0
0.1
0.2
0.3
0.4
0.5
0.6
0.7
0.8
0.9
1

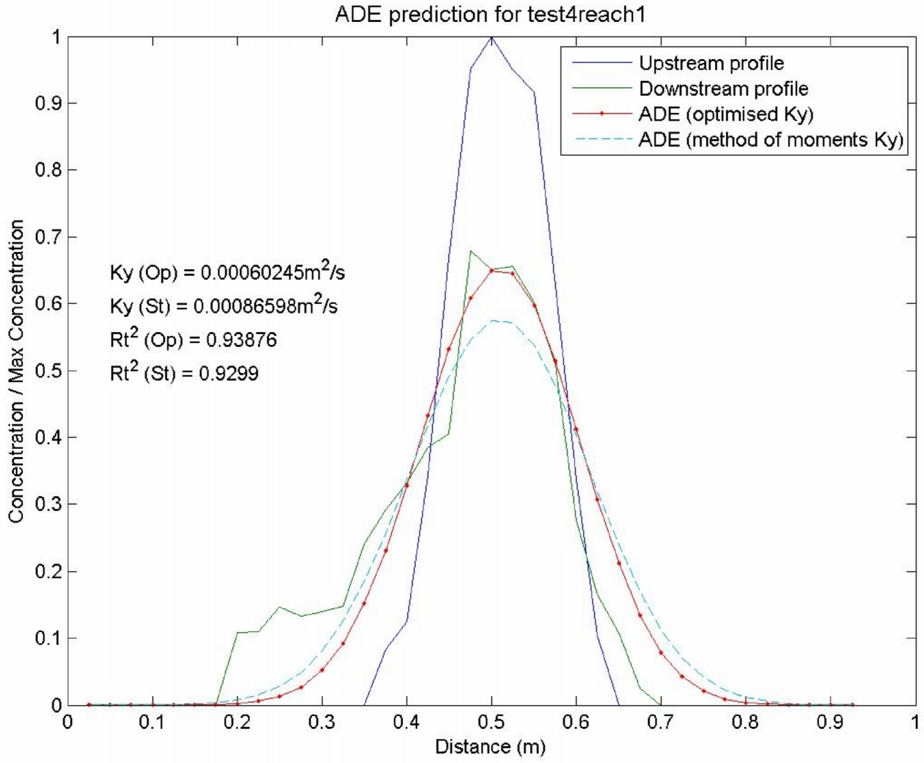
ADE prediction for test4reach1
Upstream profile
Downstream profile
ADE (optimised Ky)
ADE (method of moments Ky)
Ky (Op) = 0.00060245m²/s
Ky (St) = 0.00086598m²/s
Rt² (Op) = 0.93876
Rt² (St) = 0.9299
Concentration / Max Concentration
Distance (m)
0
0.1
0.2
0.3
0.4
0.5
0.6
0.7
0.8
0.9
1

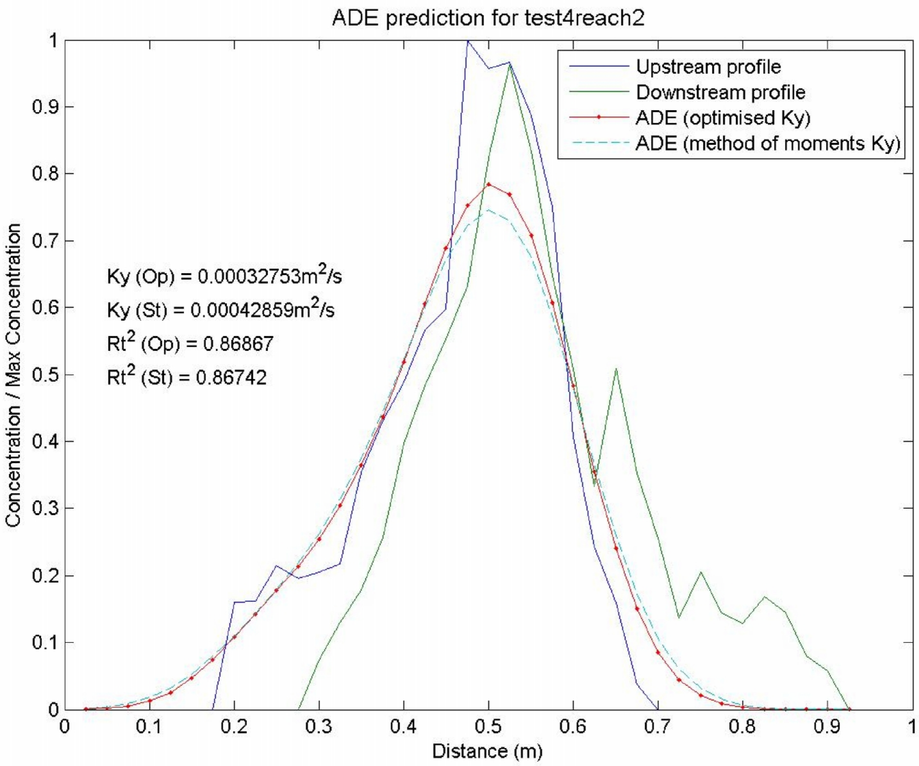
ADE prediction for test4reach2
Upstream profile
Downstream profile
ADE (optimised Ky)
ADE (method of moments Ky)
Ky (Op) = 0.00032753m^2/s
Ky (St) = 0.00042859m^2/s
Rt^2 (Op) = 0.86867
Rt^2 (St) = 0.86742
Concentration / Max Concentration
Distance (m)
0
0.1
0.2
0.3
0.4
0.5
0.6
0.7
0.8
0.9
1

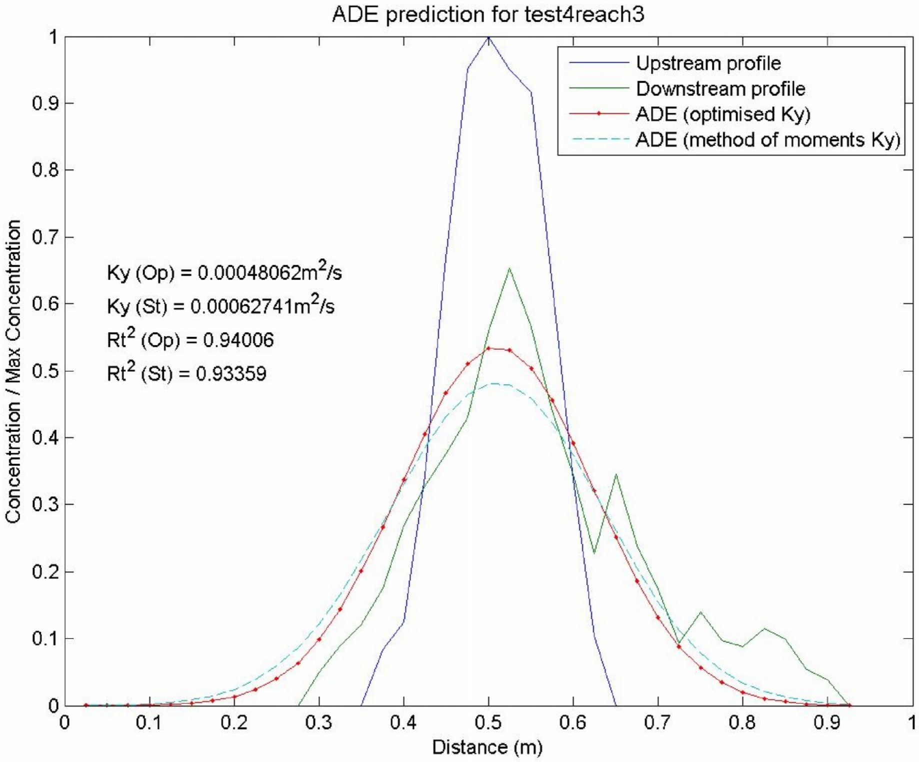
ADE prediction for test4reach3
Upstream profile
Downstream profile
ADE (optimised Ky)
ADE (method of moments Ky)
Ky (Op) = 0.00048062m^2/s
Ky (St) = 0.00062741m^2/s
Rt^2 (Op) = 0.94006
Rt^2 (St) = 0.93359
Concentration / Max Concentration
Distance (m)
0
0.1
0.2
0.3
0.4
0.5
0.6
0.7
0.8
0.9
1

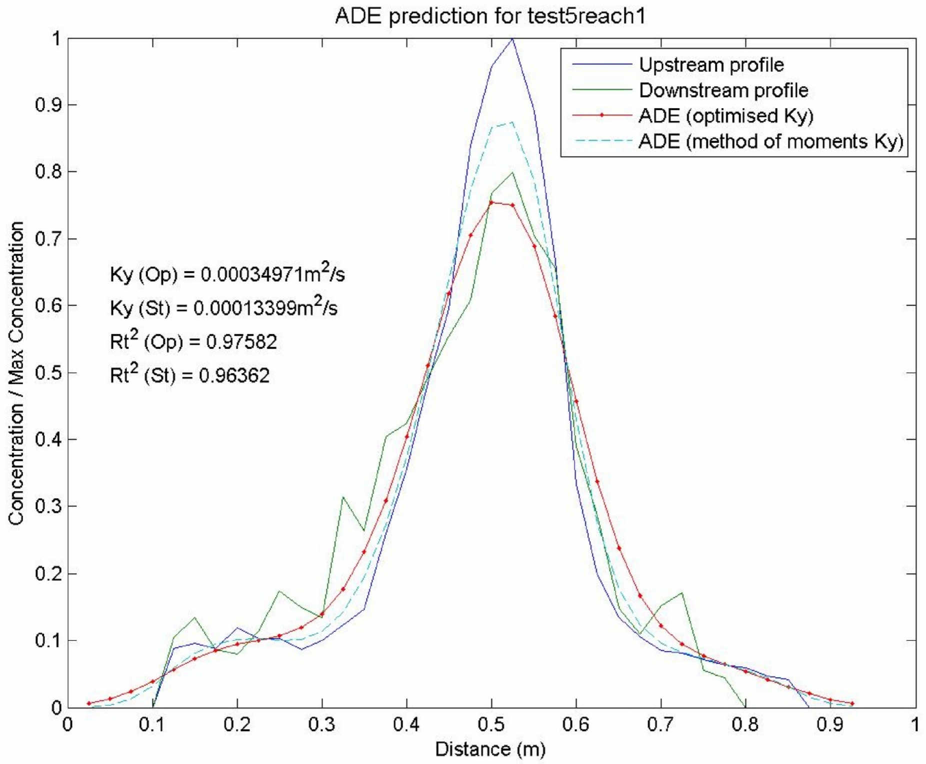
ADE prediction for test5reach1
Upstream profile
Downstream profile
ADE (optimised Ky)
ADE (method of moments Ky)
Ky (Op) = 0.00034971m^2/s
Ky (St) = 0.00013399m^2/s
Rt^2 (Op) = 0.97582
Rt^2 (St) = 0.96362
Concentration / Max Concentration
Distance (m)
0
0.1
0.2
0.3
0.4
0.5
0.6
0.7
0.8
0.9
1

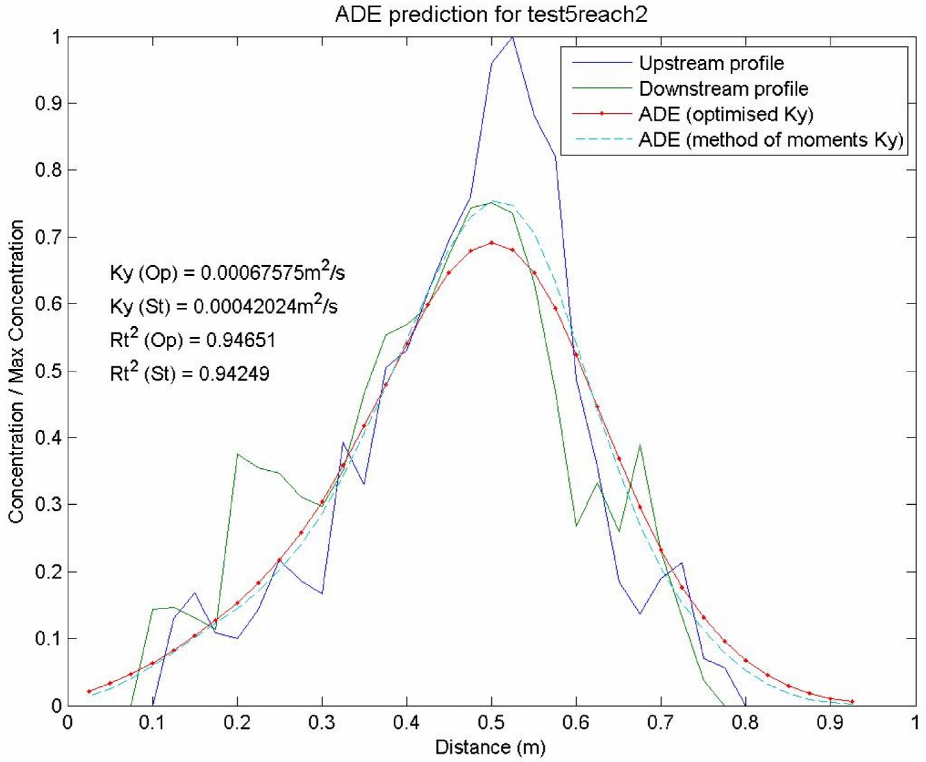
ADE prediction for test5reach2
Upstream profile
Downstream profile
ADE (optimised Ky)
ADE (method of moments Ky)
Ky (Op) = 0.00067575m^2/s
Ky (St) = 0.00042024m^2/s
Rt^2 (Op) = 0.94651
Rt^2 (St) = 0.94249
Concentration / Max Concentration
Distance (m)
0
0.1
0.2
0.3
0.4
0.5
0.6
0.7
0.8
0.9
1

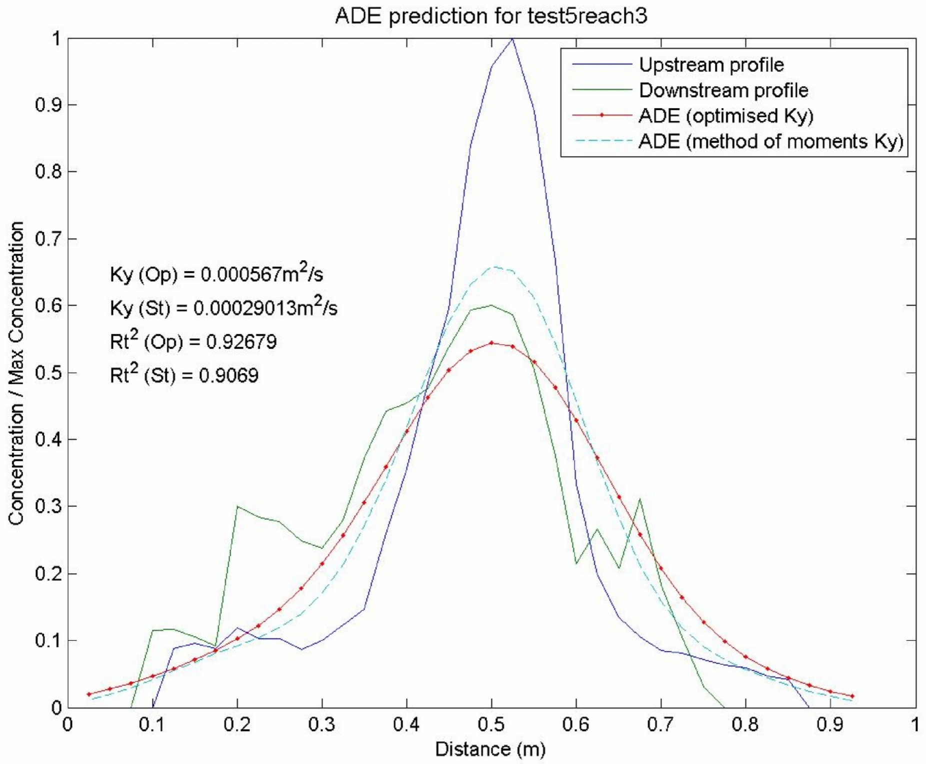
ADE prediction for test5reach3
Upstream profile
Downstream profile
ADE (optimised Ky)
ADE (method of moments Ky)
Ky (Op) = 0.000567m^2/s
Ky (St) = 0.00029013m^2/s
Rt^2 (Op) = 0.92679
Rt^2 (St) = 0.9069
Concentration / Max Concentration
Distance (m)
0
0.1
0.2
0.3
0.4
0.5
0.6
0.7
0.8
0.9
1

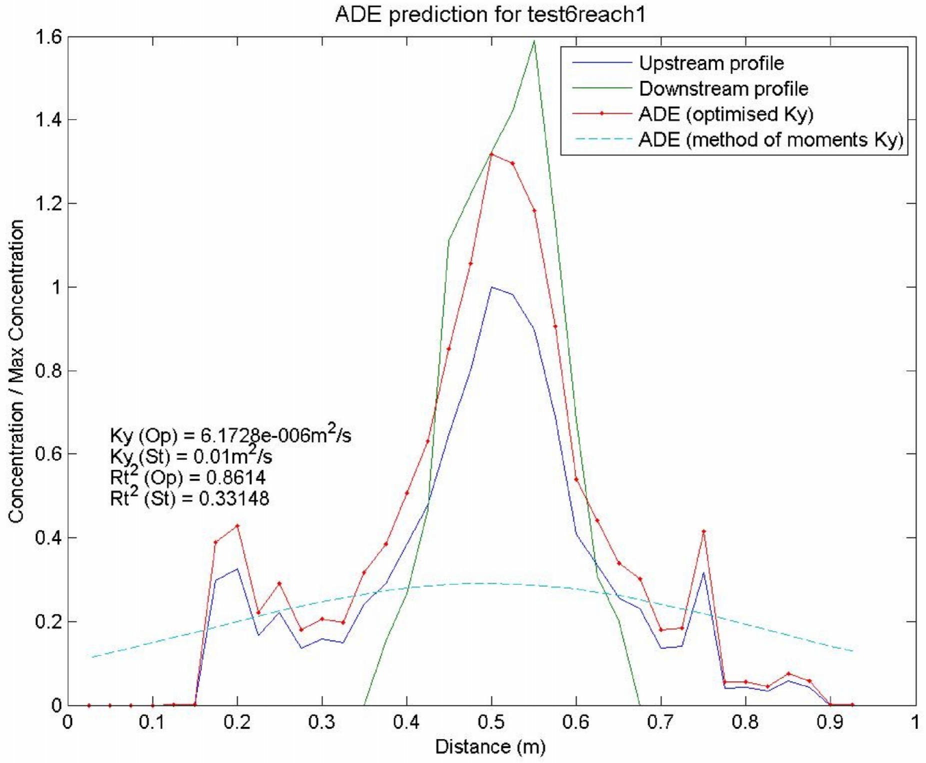
ADE prediction for test6reach1
Upstream profile
Downstream profile
ADE (optimised Ky)
ADE (method of moments Ky)
Ky (Op) = 6.1728e-006m^2/s
Ky (St) = 0.01m^2/s
Rt^2 (Op) = 0.8614
Rt^2 (St) = 0.33148
Concentration / Max Concentration
Distance (m)
0
0.2
0.4
0.6
0.8
1
1.2
1.4
1.6
0.1
0.2
0.3
0.4
0.5
0.6
0.7
0.8
0.9

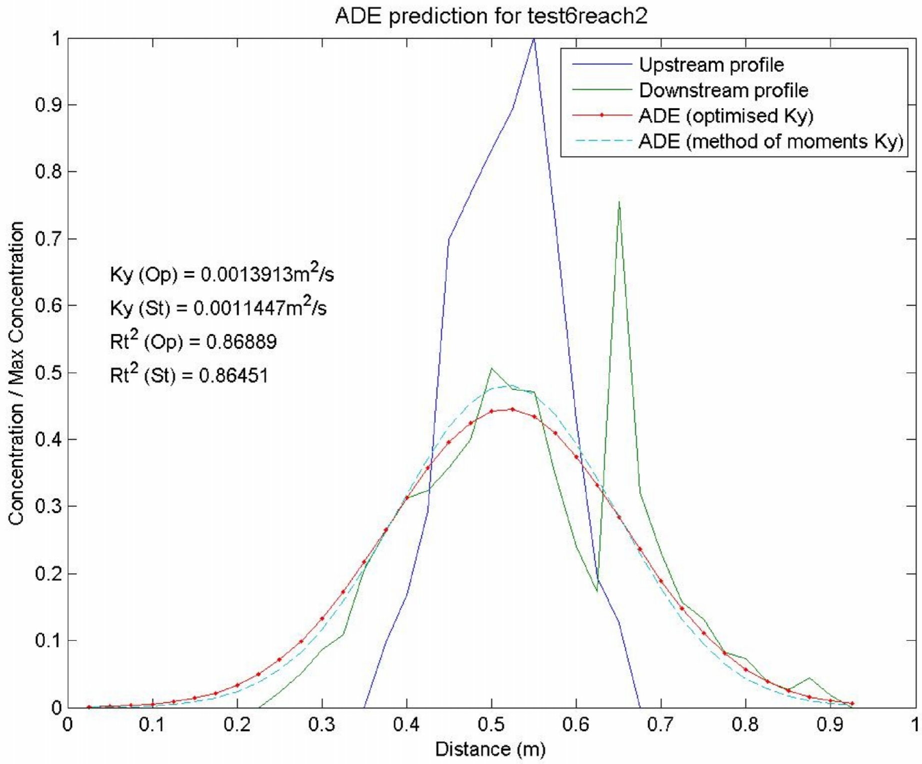
ADE prediction for test6reach2
Upstream profile
Downstream profile
ADE (optimised Ky)
ADE (method of moments Ky)
Ky (Op) = 0.0013913m^2/s
Ky (St) = 0.0011447m^2/s
Rt^2 (Op) = 0.86889
Rt^2 (St) = 0.86451
Concentration / Max Concentration
Distance (m)
0
0.1
0.2
0.3
0.4
0.5
0.6
0.7
0.8
0.9
1

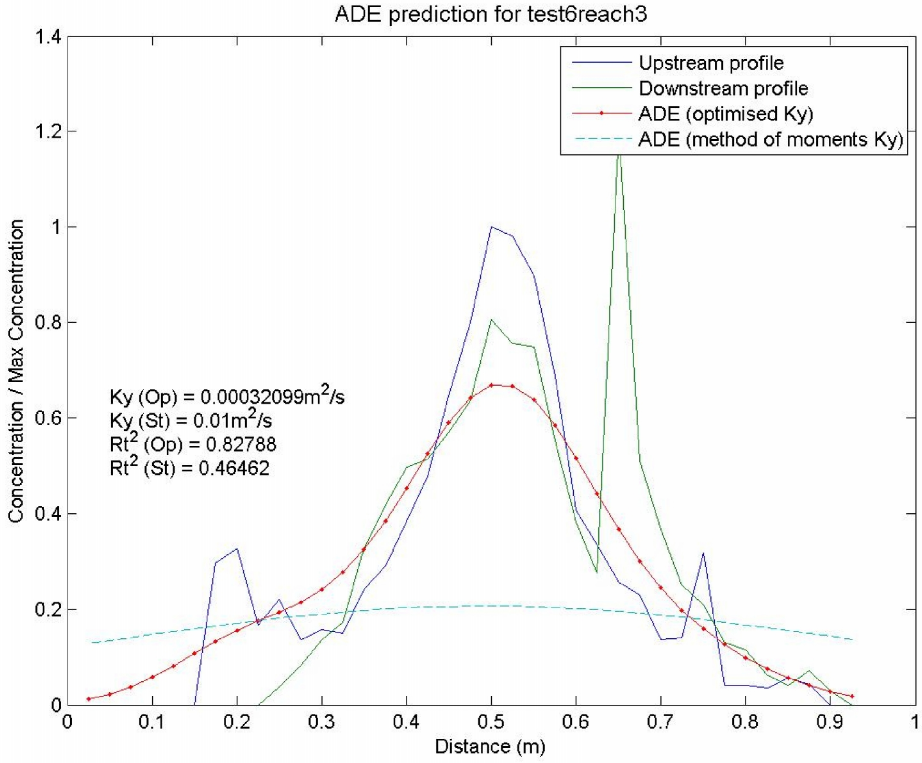
ADE prediction for test6reach3
Upstream profile
Downstream profile
ADE (optimised Ky)
ADE (method of moments Ky)
Ky (Op) = 0.00032099m^2/s
Ky (St) = 0.01m^2/s
Rt^2 (Op) = 0.82788
Rt^2 (St) = 0.46462
Concentration / Max Concentration
Distance (m)
0
0.2
0.4
0.6
0.8
1
1.2
1.4
0.1
0.3
0.5
0.7
0.9

Test 2.96AM

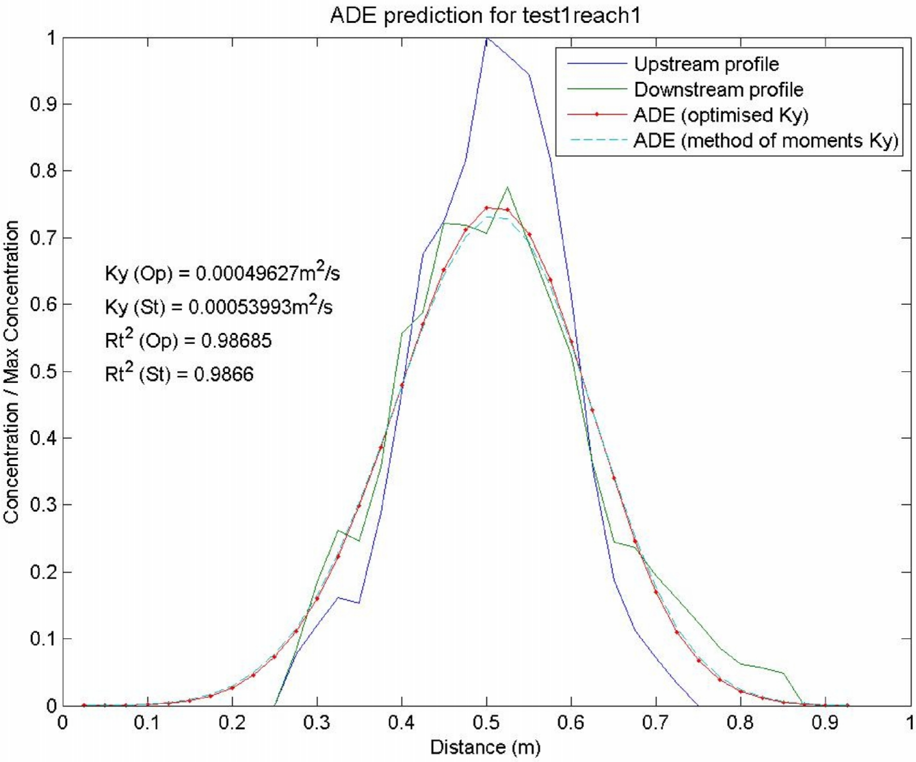
ADE prediction for test1reach1
Upstream profile
Downstream profile
ADE (optimised Ky)
ADE (method of moments Ky)
Ky (Op) = 0.00049627m^2/s
Ky (St) = 0.00053993m^2/s
Rt^2 (Op) = 0.98685
Rt^2 (St) = 0.9866
Concentration / Max Concentration
Distance (m)
0
0.1
0.2
0.3
0.4
0.5
0.6
0.7
0.8
0.9
1

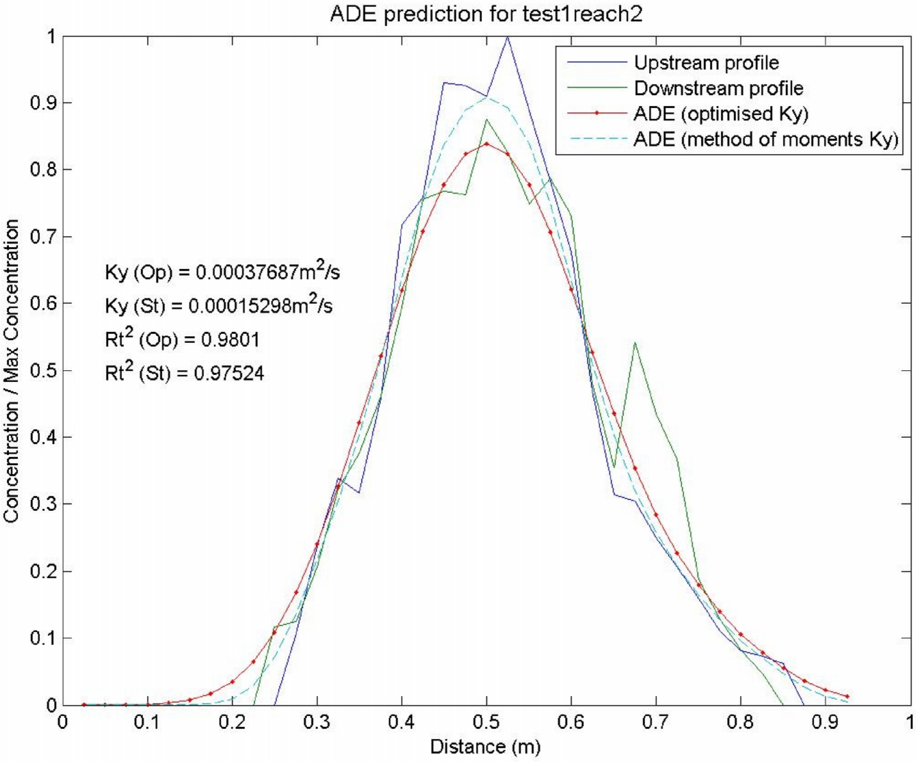
ADE prediction for test1reach2
Upstream profile
Downstream profile
ADE (optimised Ky)
ADE (method of moments Ky)
Ky (Op) = 0.00037687m^2/s
Ky (St) = 0.00015298m^2/s
Rt^2 (Op) = 0.9801
Rt^2 (St) = 0.97524
Concentration / Max Concentration
Distance (m)
0
0.1
0.2
0.3
0.4
0.5
0.6
0.7
0.8
0.9
1

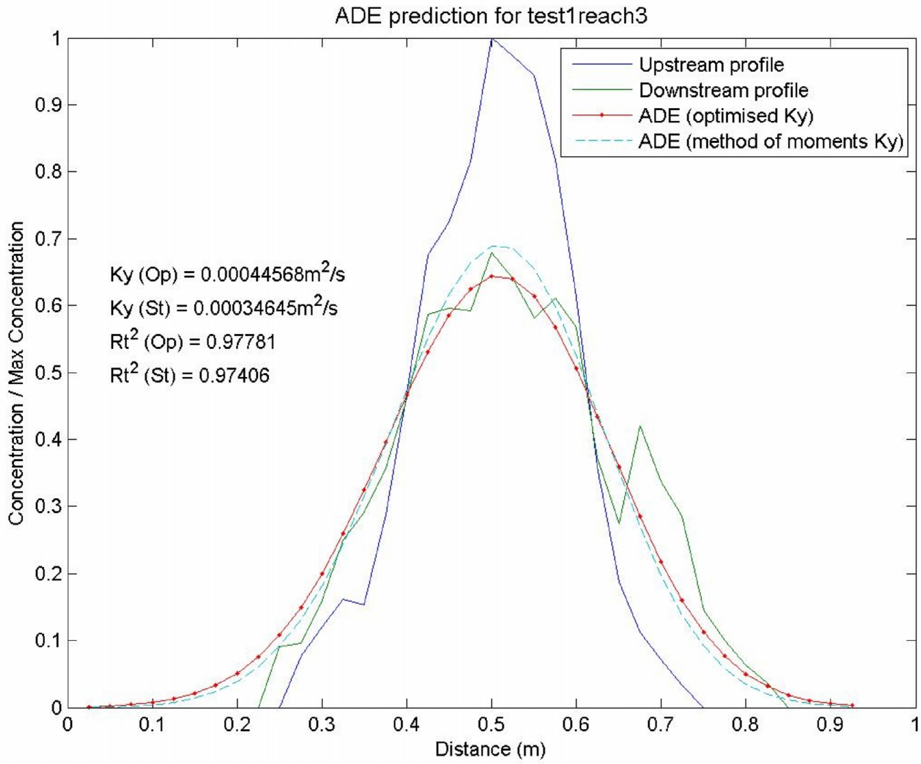
ADE prediction for test1reach3
Upstream profile
Downstream profile
ADE (optimised Ky)
ADE (method of moments Ky)
Ky (Op) = 0.00044568m^2/s
Ky (St) = 0.00034645m^2/s
Rt^2 (Op) = 0.97781
Rt^2 (St) = 0.97406
Concentration / Max Concentration
Distance (m)
0
0.1
0.2
0.3
0.4
0.5
0.6
0.7
0.8
0.9
1

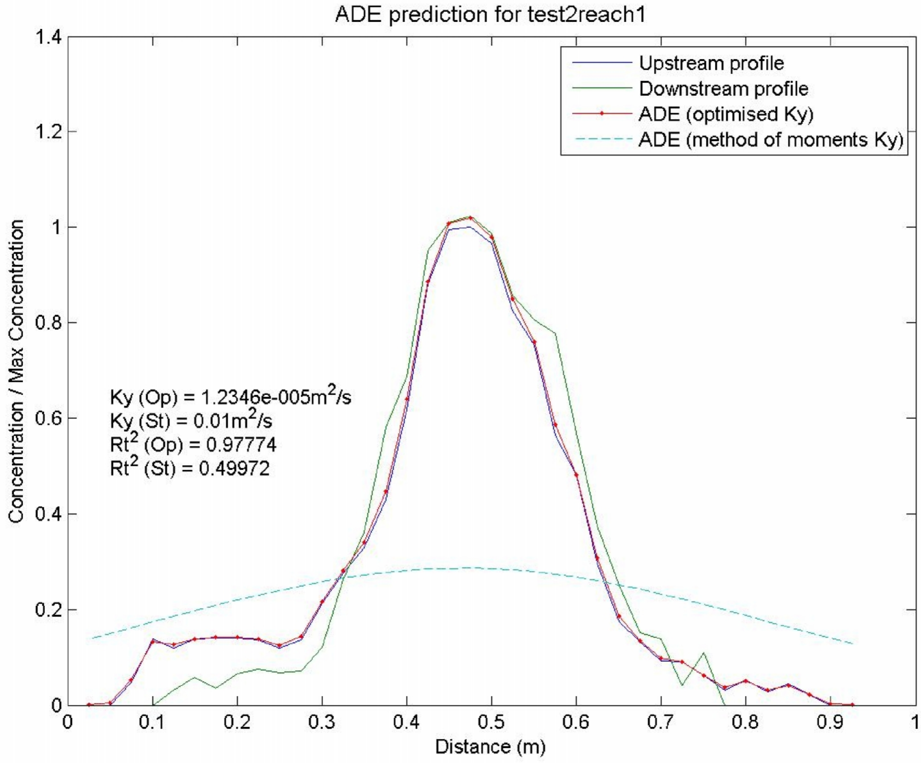
ADE prediction for test2reach1
Upstream profile
Downstream profile
ADE (optimised Ky)
ADE (method of moments Ky)
Ky (Op) = 1.2346e-005m^2/s
Ky (St) = 0.01m^2/s
Rt^2 (Op) = 0.97774
Rt^2 (St) = 0.49972
Concentration / Max Concentration
Distance (m)
0
0.2
0.4
0.6
0.8
1
1.2
1.4
0.1
0.3
0.5
0.7
0.9

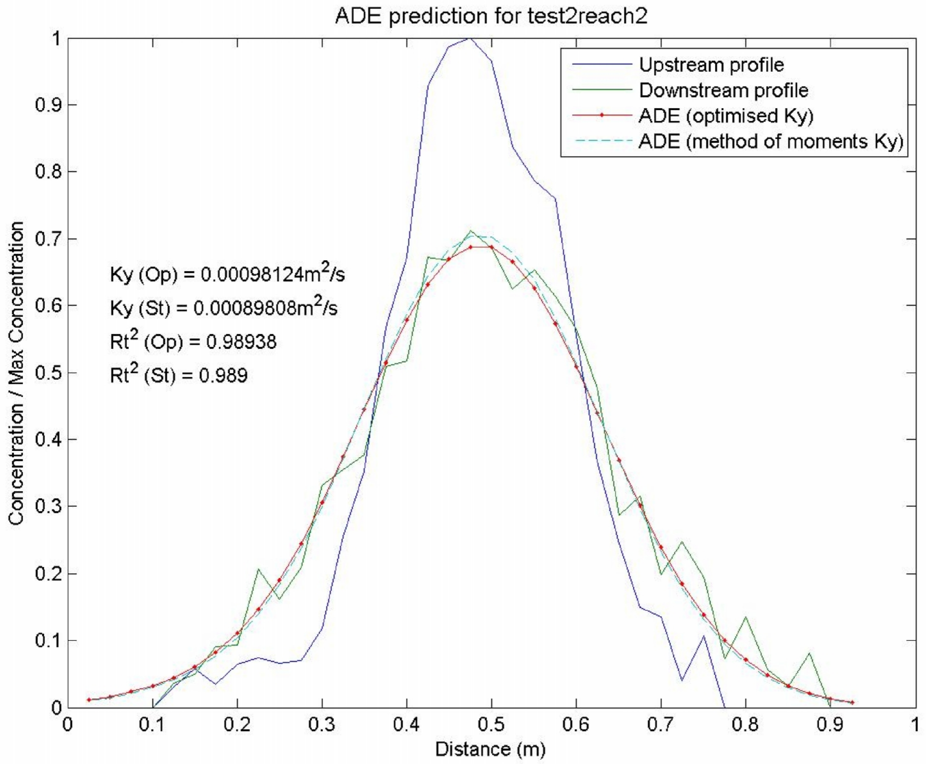
ADE prediction for test2reach2
Upstream profile
Downstream profile
ADE (optimised Ky)
ADE (method of moments Ky)
Ky (Op) = 0.00098124m^2/s
Ky (St) = 0.00089808m^2/s
Rt^2 (Op) = 0.98938
Rt^2 (St) = 0.989
Concentration / Max Concentration
Distance (m)
0
0.1
0.2
0.3
0.4
0.5
0.6
0.7
0.8
0.9
1

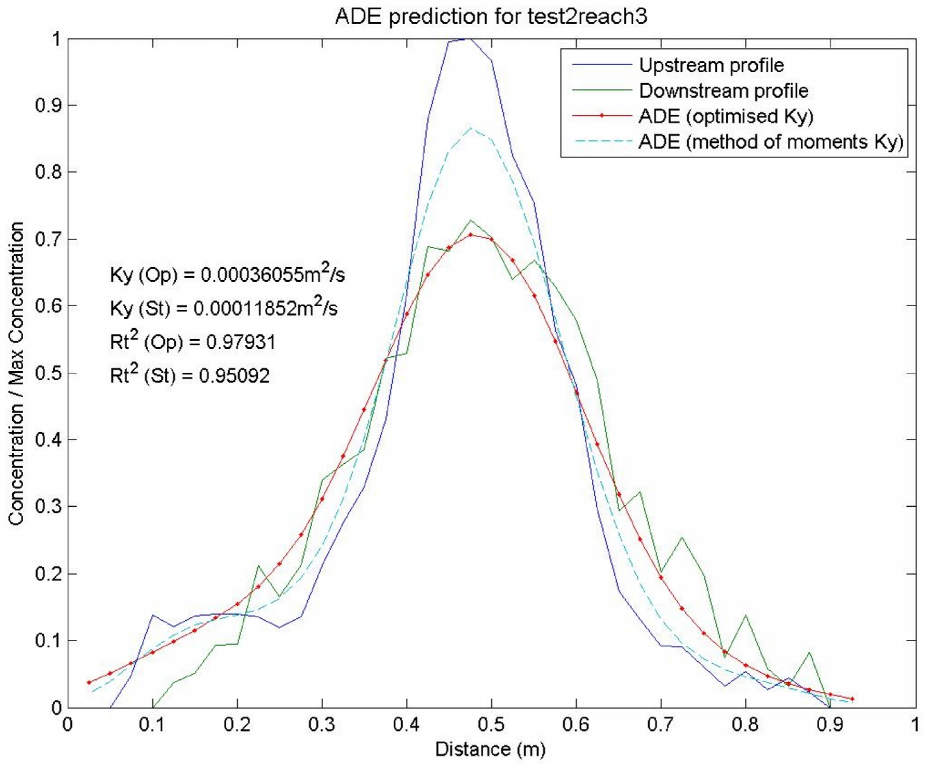
ADE prediction for test2reach3
Upstream profile
Downstream profile
ADE (optimised Ky)
ADE (method of moments Ky)
Ky (Op) = 0.00036055m^2/s
Ky (St) = 0.00011852m^2/s
Rt^2 (Op) = 0.97931
Rt^2 (St) = 0.95092
Concentration / Max Concentration
Distance (m)
0
0.1
0.2
0.3
0.4
0.5
0.6
0.7
0.8
0.9
1

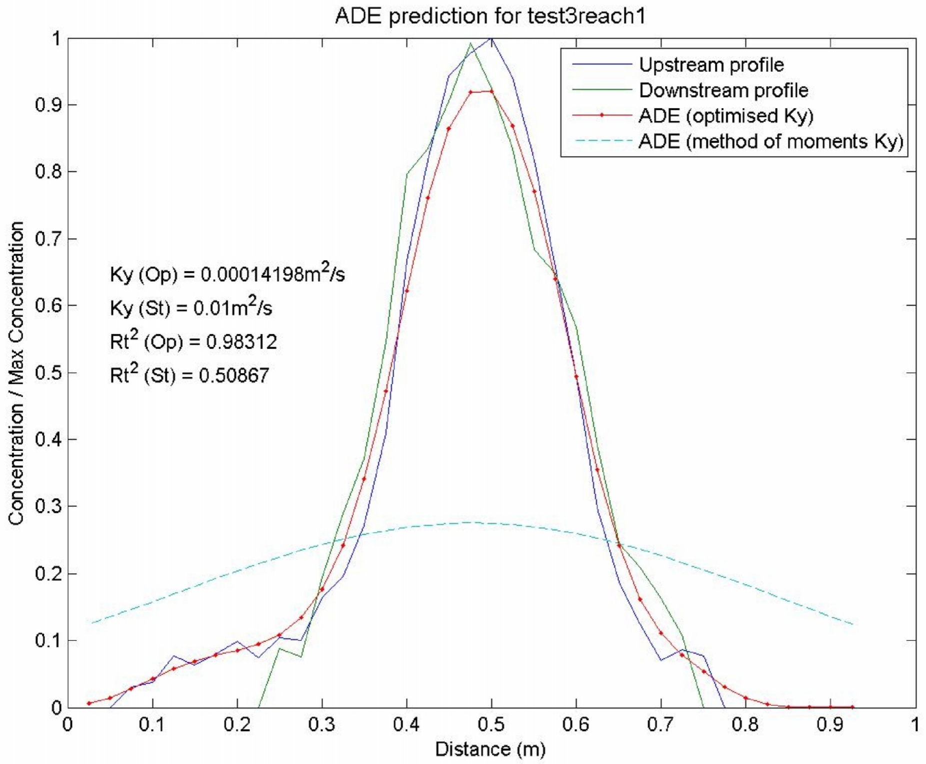
ADE prediction for test3reach1
Upstream profile
Downstream profile
ADE (optimised Ky)
ADE (method of moments Ky)
Ky (Op) = 0.00014198m^2/s
Ky (St) = 0.01m^2/s
Rt^2 (Op) = 0.98312
Rt^2 (St) = 0.50867
Concentration / Max Concentration
Distance (m)
0
0.1
0.2
0.3
0.4
0.5
0.6
0.7
0.8
0.9
1

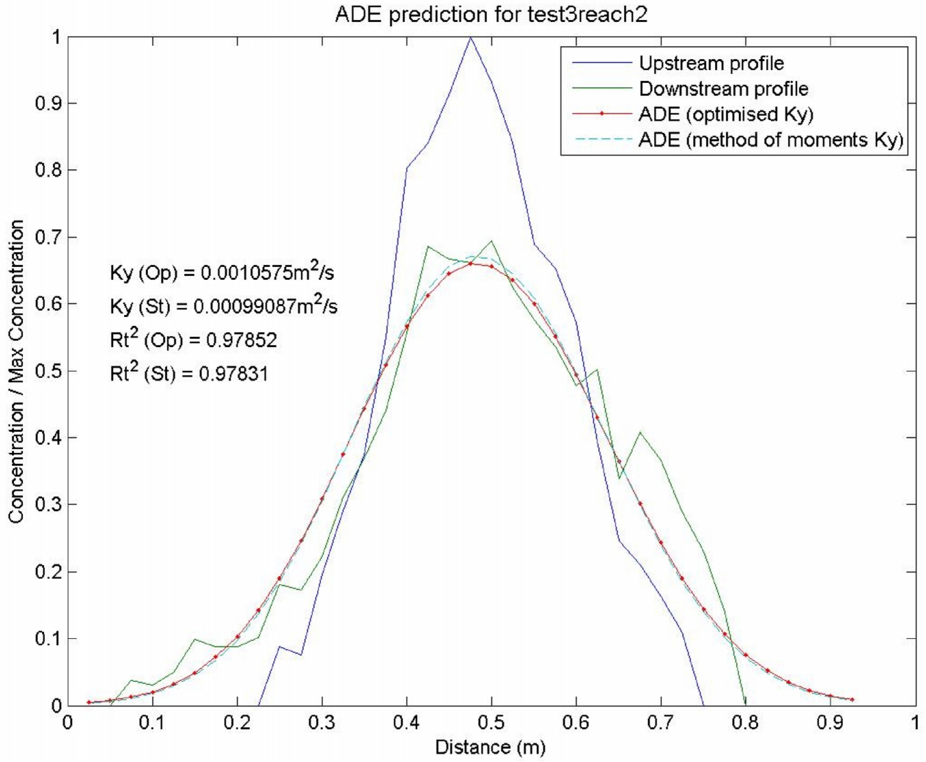
ADE prediction for test3reach2
Upstream profile
Downstream profile
ADE (optimised Ky)
ADE (method of moments Ky)
Ky (Op) = 0.0010575m^2/s
Ky (St) = 0.00099087m^2/s
Rt^2 (Op) = 0.97852
Rt^2 (St) = 0.97831
Concentration / Max Concentration
Distance (m)
0
0.1
0.2
0.3
0.4
0.5
0.6
0.7
0.8
0.9
1

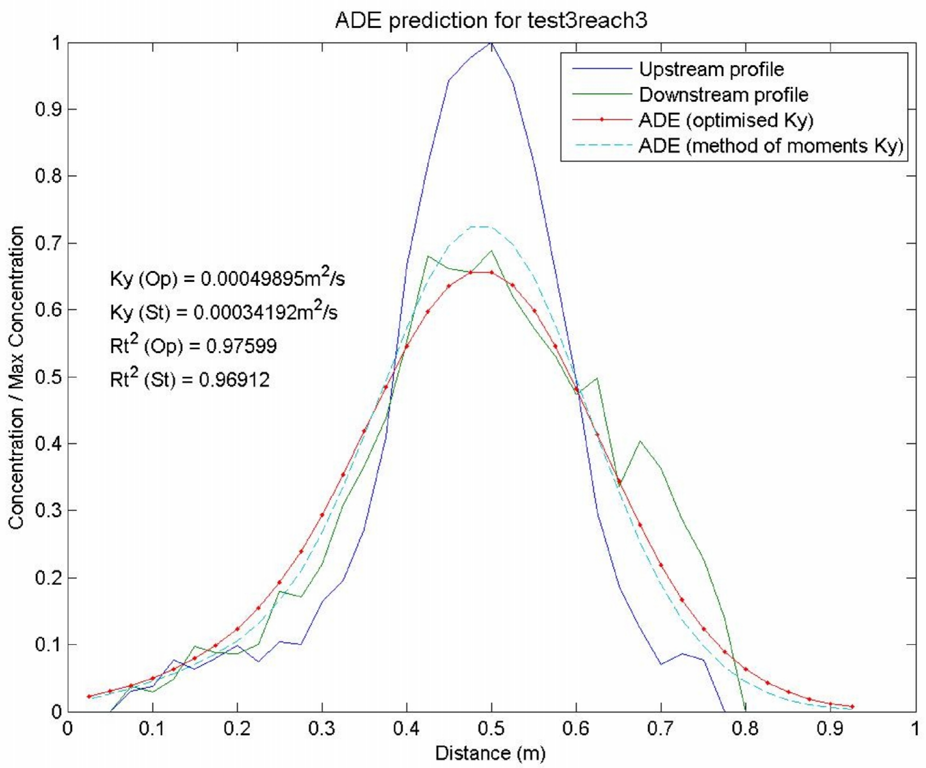
ADE prediction for test3reach3
Upstream profile
Downstream profile
ADE (optimised Ky)
ADE (method of moments Ky)
Ky (Op) = 0.00049895m^2/s
Ky (St) = 0.00034192m^2/s
Rt^2 (Op) = 0.97599
Rt^2 (St) = 0.96912
Concentration / Max Concentration
Distance (m)
0
0.1
0.2
0.3
0.4
0.5
0.6
0.7
0.8
0.9
1

Test 3.90A

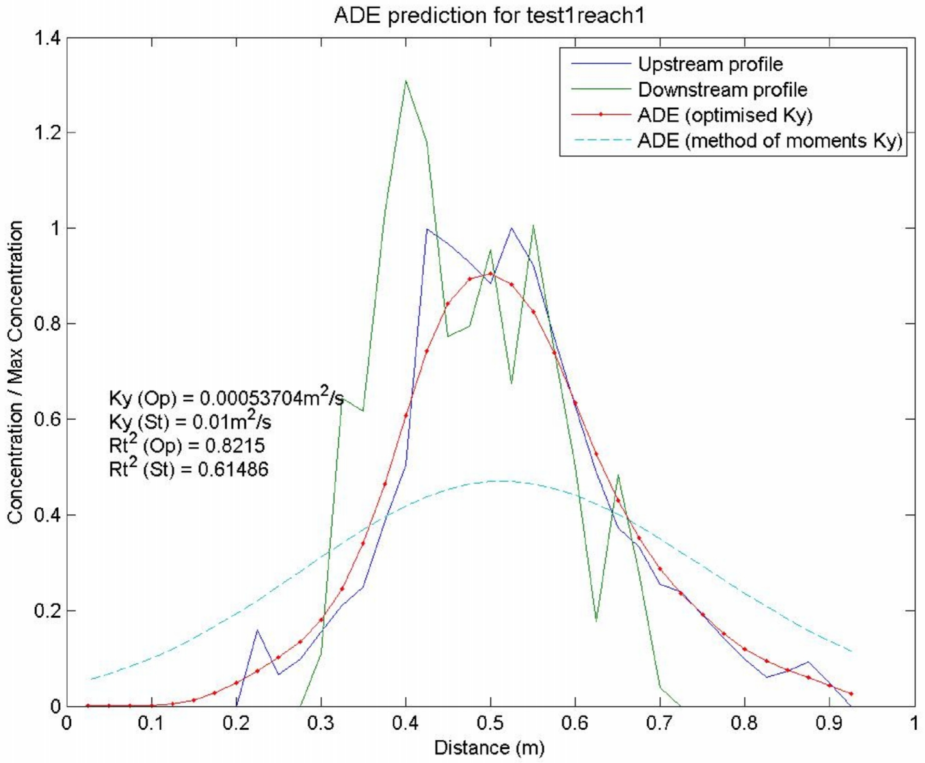
ADE prediction for test1reach1
Upstream profile
Downstream profile
ADE (optimised Ky)
ADE (method of moments Ky)
Ky (Op) = 0.00053704m^2/s
Ky (St) = 0.01m^2/s
Rt^2 (Op) = 0.8215
Rt^2 (St) = 0.61486
Concentration / Max Concentration
Distance (m)
0
0.2
0.4
0.6
0.8
1
1.2
1.4
0
0.1
0.2
0.3
0.4
0.5
0.6
0.7
0.8
0.9
1

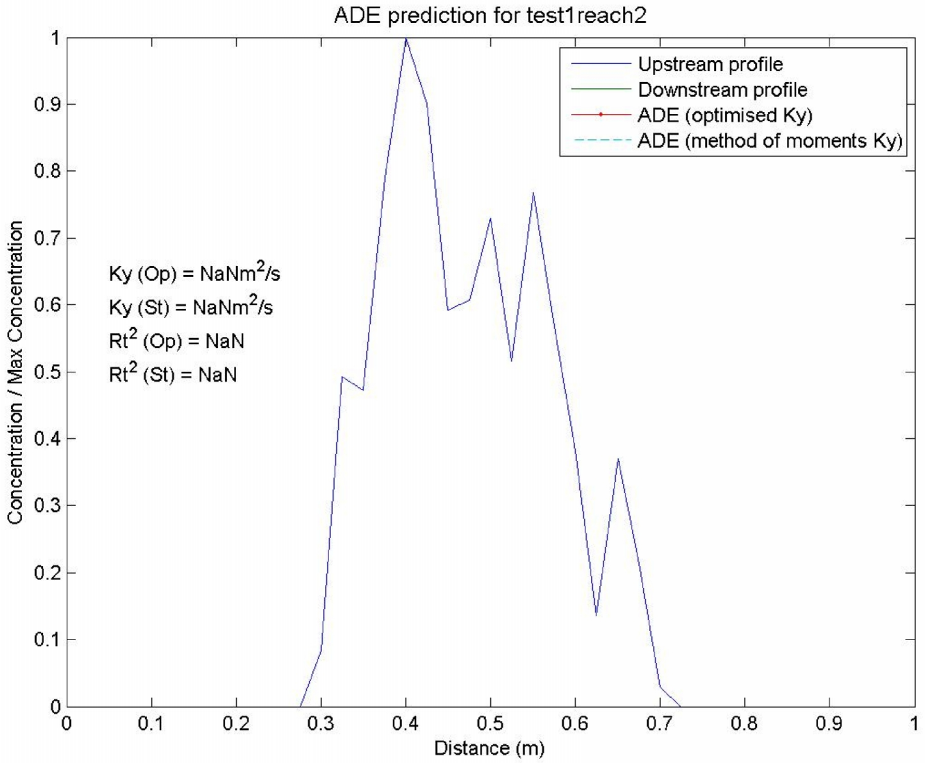
ADE prediction for test1reach2
Upstream profile
Downstream profile
ADE (optimised Ky)
ADE (method of moments Ky)
Ky (Op) = NaNm^2/s
Ky (St) = NaNm^2/s
Rt^2 (Op) = NaN
Rt^2 (St) = NaN
Concentration / Max Concentration
Distance (m)
0
0.1
0.2
0.3
0.4
0.5
0.6
0.7
0.8
0.9
1
0
0.1
0.2
0.3
0.4
0.5
0.6
0.7
0.8
0.9
1

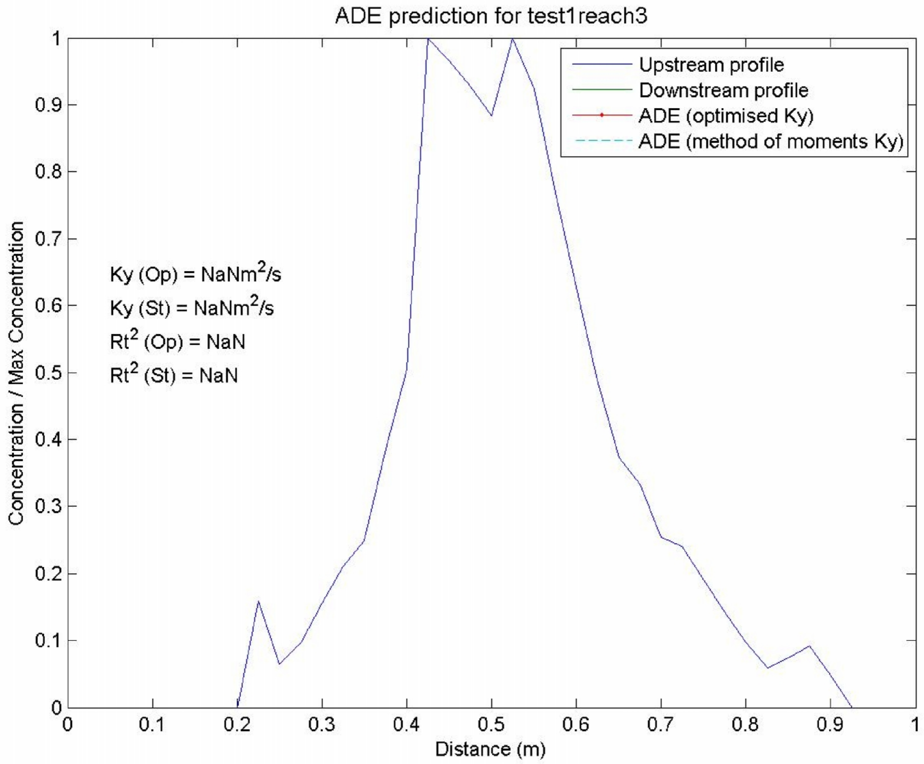
ADE prediction for test1reach3
Upstream profile
Downstream profile
ADE (optimised Ky)
ADE (method of moments Ky)
Ky (Op) = NaNm^2/s
Ky (St) = NaNm^2/s
Rt^2 (Op) = NaN
Rt^2 (St) = NaN
Concentration / Max Concentration
Distance (m)
0
0.1
0.2
0.3
0.4
0.5
0.6
0.7
0.8
0.9
1

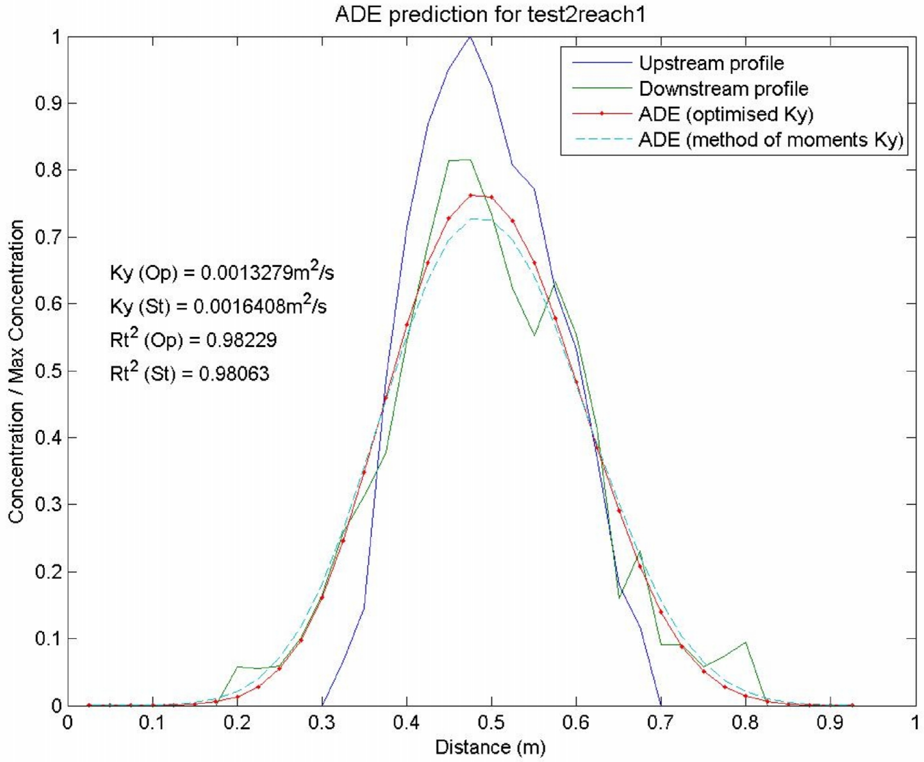
ADE prediction for test2reach1
Upstream profile
Downstream profile
ADE (optimised Ky)
ADE (method of moments Ky)
Ky (Op) = 0.0013279m^2/s
Ky (St) = 0.0016408m^2/s
Rt^2 (Op) = 0.98229
Rt^2 (St) = 0.98063
Concentration / Max Concentration
Distance (m)
0
0.1
0.2
0.3
0.4
0.5
0.6
0.7
0.8
0.9
1

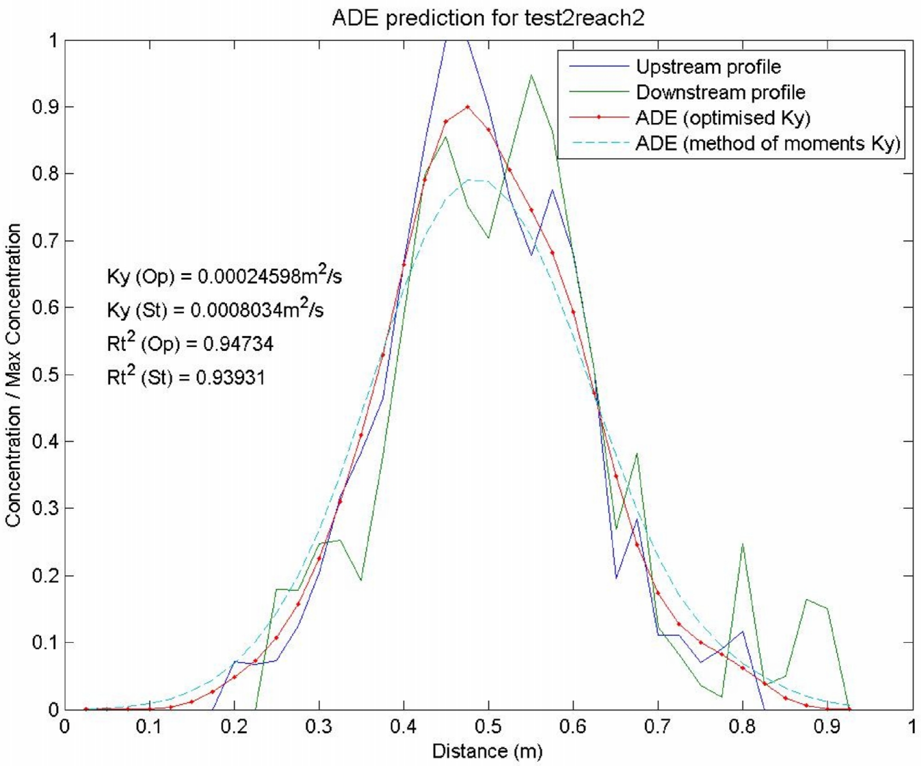
ADE prediction for test2reach2
Upstream profile
Downstream profile
ADE (optimised Ky)
ADE (method of moments Ky)
Ky (Op) = 0.00024598m^2/s
Ky (St) = 0.0008034m^2/s
Rt^2 (Op) = 0.94734
Rt^2 (St) = 0.93931
Concentration / Max Concentration
Distance (m)
0
0.1
0.2
0.3
0.4
0.5
0.6
0.7
0.8
0.9
1

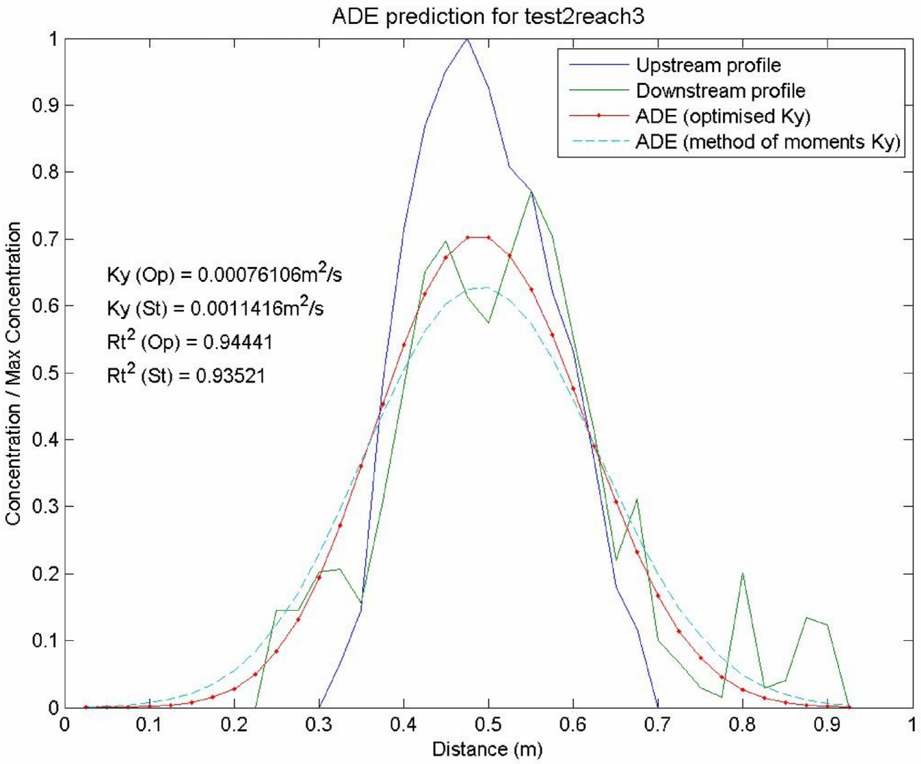
ADE prediction for test2reach3
Upstream profile
Downstream profile
ADE (optimised Ky)
ADE (method of moments Ky)
Ky (Op) = 0.00076106m^2/s
Ky (St) = 0.0011416m^2/s
Rt^2 (Op) = 0.94441
Rt^2 (St) = 0.93521
Concentration / Max Concentration
Distance (m)
0
0.1
0.2
0.3
0.4
0.5
0.6
0.7
0.8
0.9
1

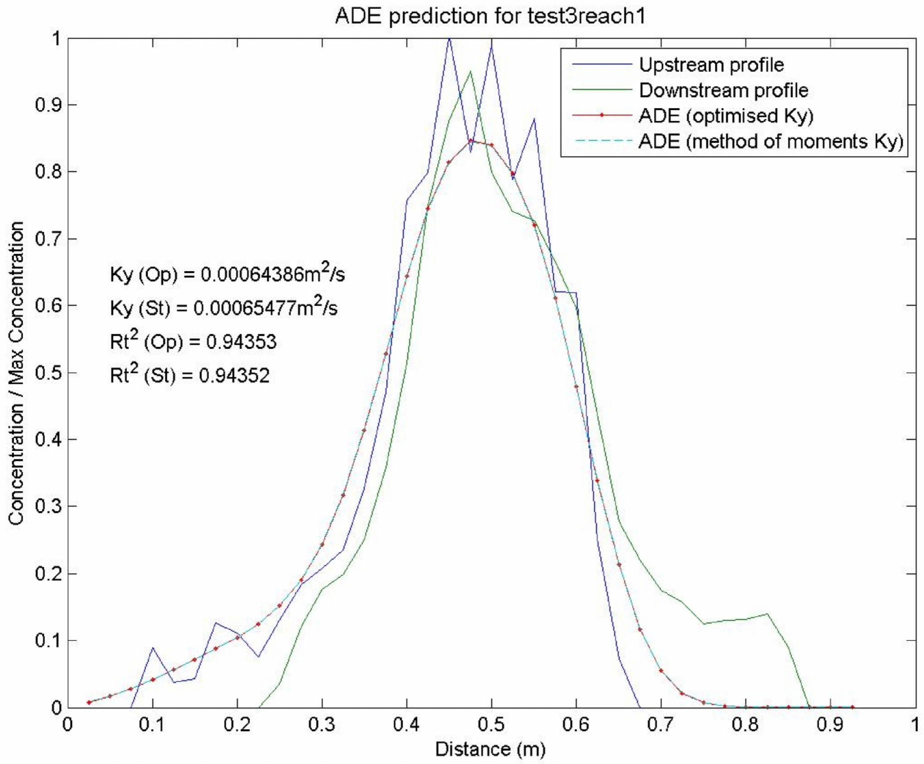
ADE prediction for test3reach1
Upstream profile
Downstream profile
ADE (optimised Ky)
ADE (method of moments Ky)
Ky (Op) = 0.00064386m^2/s
Ky (St) = 0.00065477m^2/s
Rt^2 (Op) = 0.94353
Rt^2 (St) = 0.94352
Concentration / Max Concentration
Distance (m)
0
0.1
0.2
0.3
0.4
0.5
0.6
0.7
0.8
0.9
1

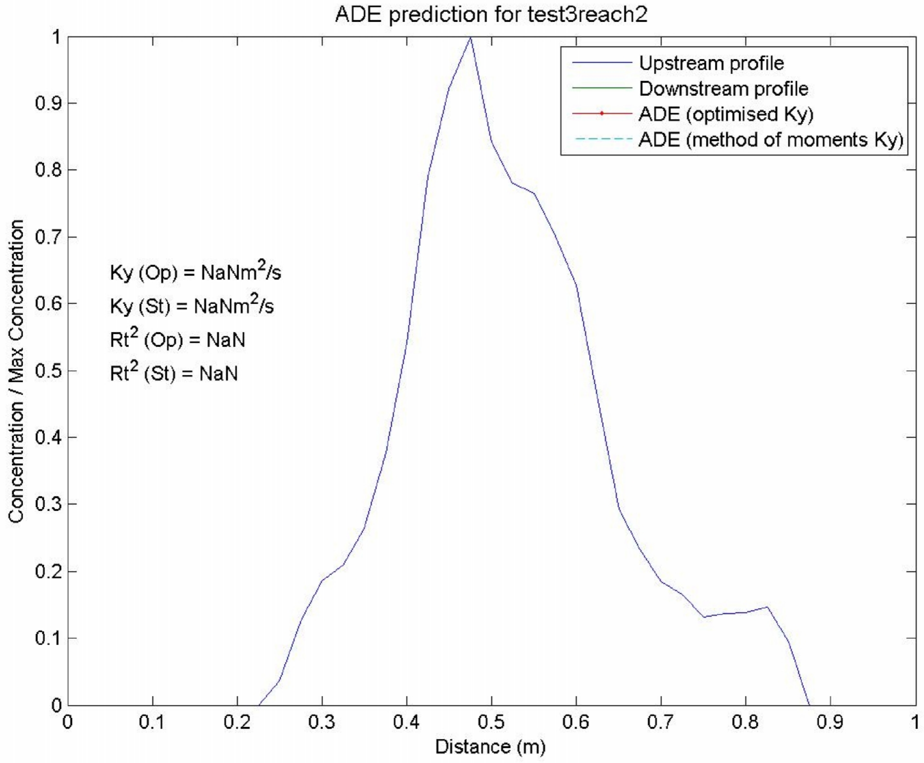
ADE prediction for test3reach2
Upstream profile
Downstream profile
ADE (optimised Ky)
ADE (method of moments Ky)
Ky (Op) = NaNm^2/s
Ky (St) = NaNm^2/s
Rt^2 (Op) = NaN
Rt^2 (St) = NaN
Concentration / Max Concentration
Distance (m)
0
0.1
0.2
0.3
0.4
0.5
0.6
0.7
0.8
0.9
1

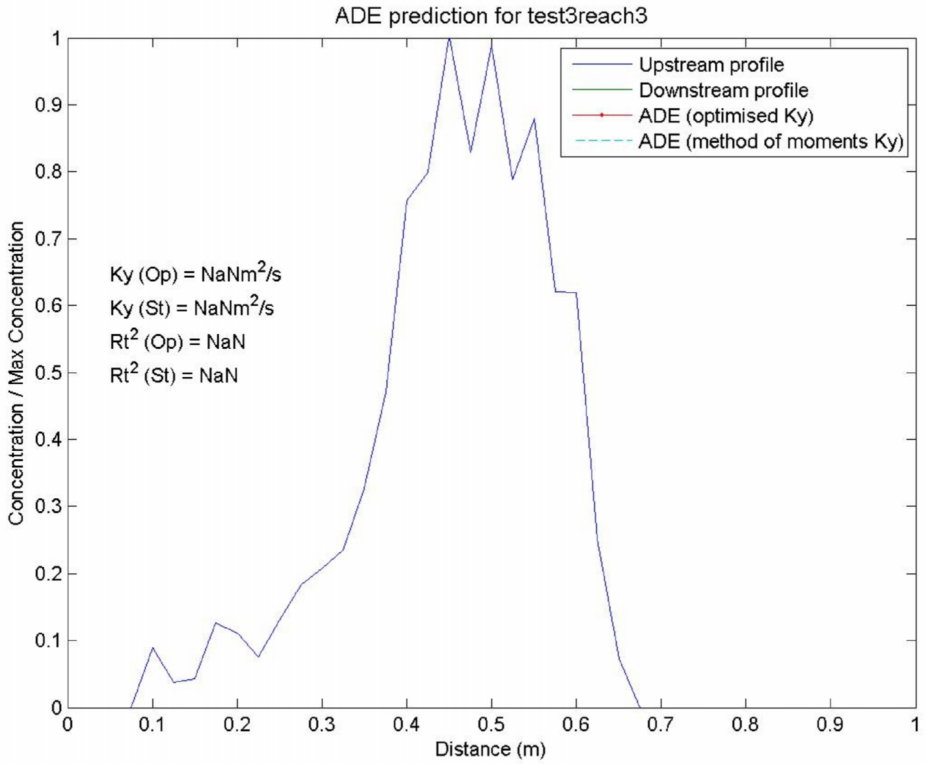
ADE prediction for test3reach3
Upstream profile
Downstream profile
ADE (optimised Ky)
ADE (method of moments Ky)
Ky (Op) = NaNm^2/s
Ky (St) = NaNm^2/s
Rt^2 (Op) = NaN
Rt^2 (St) = NaN
Concentration / Max Concentration
Distance (m)
0
0.1
0.2
0.3
0.4
0.5
0.6
0.7
0.8
0.9
1

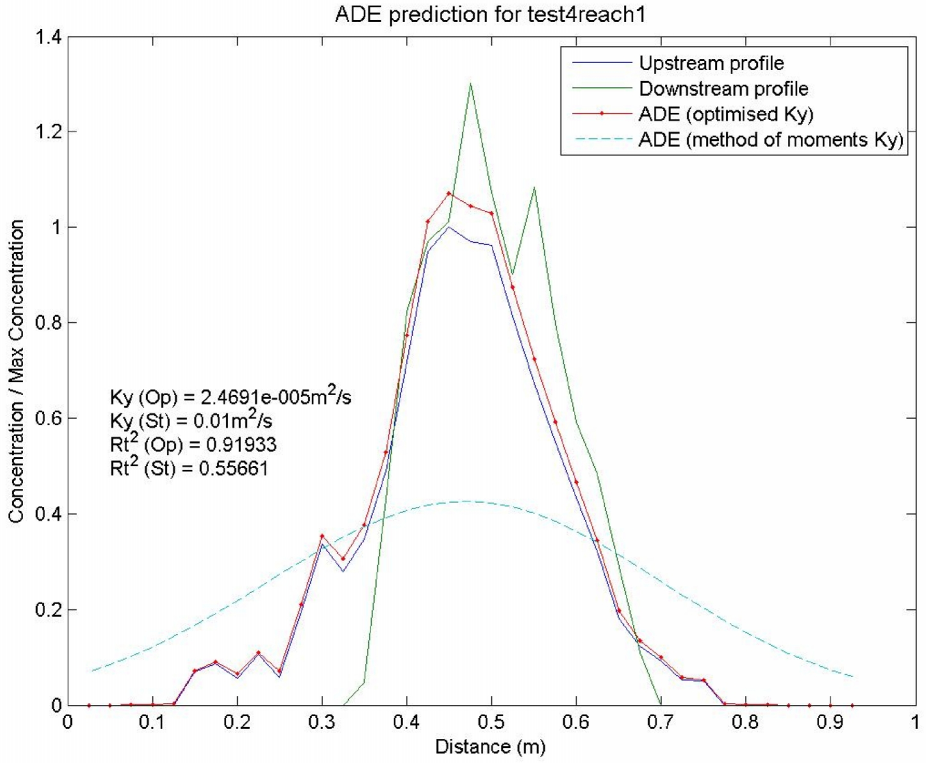
ADE prediction for test4reach1
Upstream profile
Downstream profile
ADE (optimised Ky)
ADE (method of moments Ky)
Ky (Op) = 2.4691e-005m^2/s
Ky (St) = 0.01m^2/s
Rt^2 (Op) = 0.91933
Rt^2 (St) = 0.55661
Concentration / Max Concentration
Distance (m)
0
0.2
0.4
0.6
0.8
1
1.2
1.4
0.1
0.3
0.5
0.7
0.9

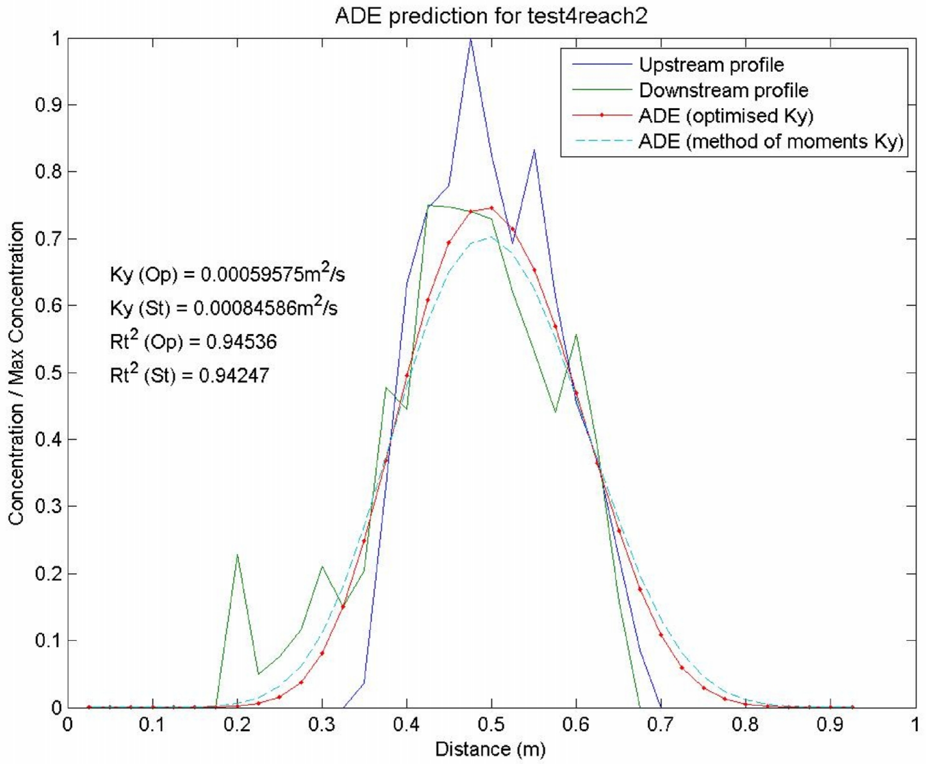
ADE prediction for test4reach2
Upstream profile
Downstream profile
ADE (optimised Ky)
ADE (method of moments Ky)
Ky (Op) = 0.00059575m^2/s
Ky (St) = 0.00084586m^2/s
Rt^2 (Op) = 0.94536
Rt^2 (St) = 0.94247
Concentration / Max Concentration
0
0.1
0.2
0.3
0.4
0.5
0.6
0.7
0.8
0.9
1
Distance (m)
0
0.1
0.2
0.3
0.4
0.5
0.6
0.7
0.8
0.9
1

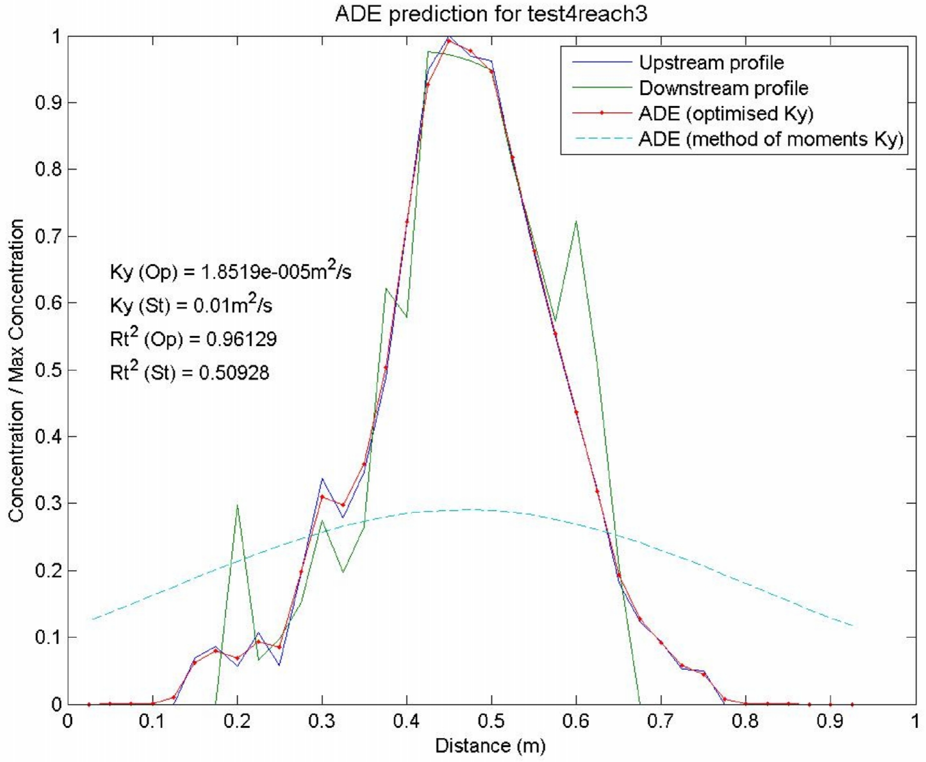
ADE prediction for test4reach3
Upstream profile
Downstream profile
ADE (optimised Ky)
ADE (method of moments Ky)
Ky (Op) = 1.8519e-005m^2/s
Ky (St) = 0.01m^2/s
Rt^2 (Op) = 0.96129
Rt^2 (St) = 0.50928
Concentration / Max Concentration
0
0.1
0.2
0.3
0.4
0.5
0.6
0.7
0.8
0.9
1
Distance (m)
0
0.1
0.2
0.3
0.4
0.5
0.6
0.7
0.8
0.9
1

Test 5.92AM

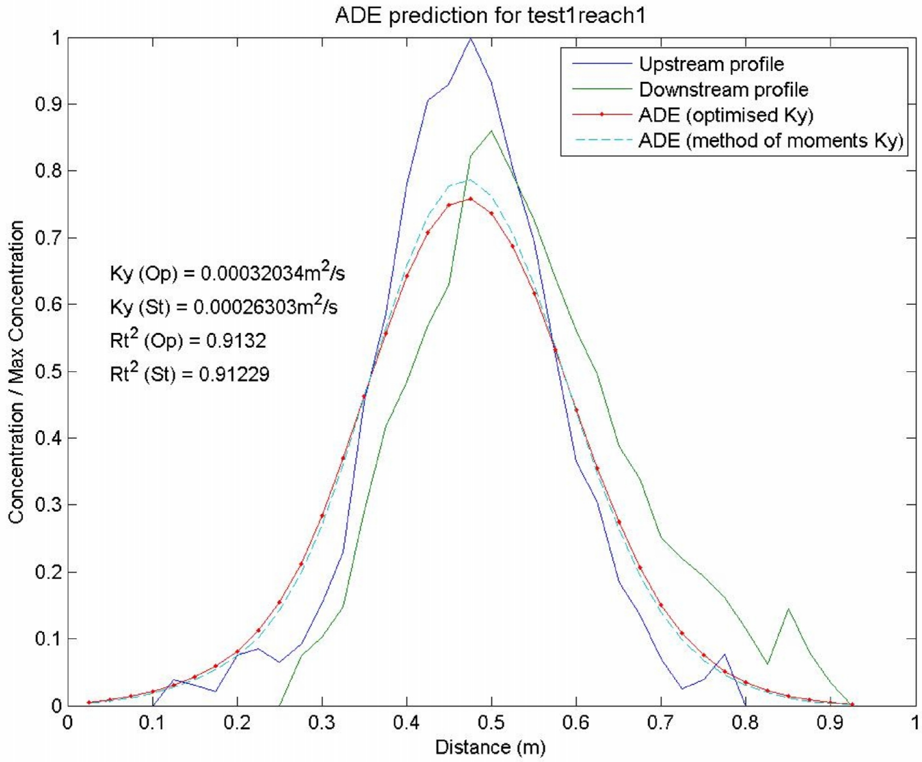
ADE prediction for test1reach1

Ky (Op) = 0.00032034m^2/s
Ky (St) = 0.00026303m^2/s
Rt^2 (Op) = 0.9132
Rt^2 (St) = 0.91229

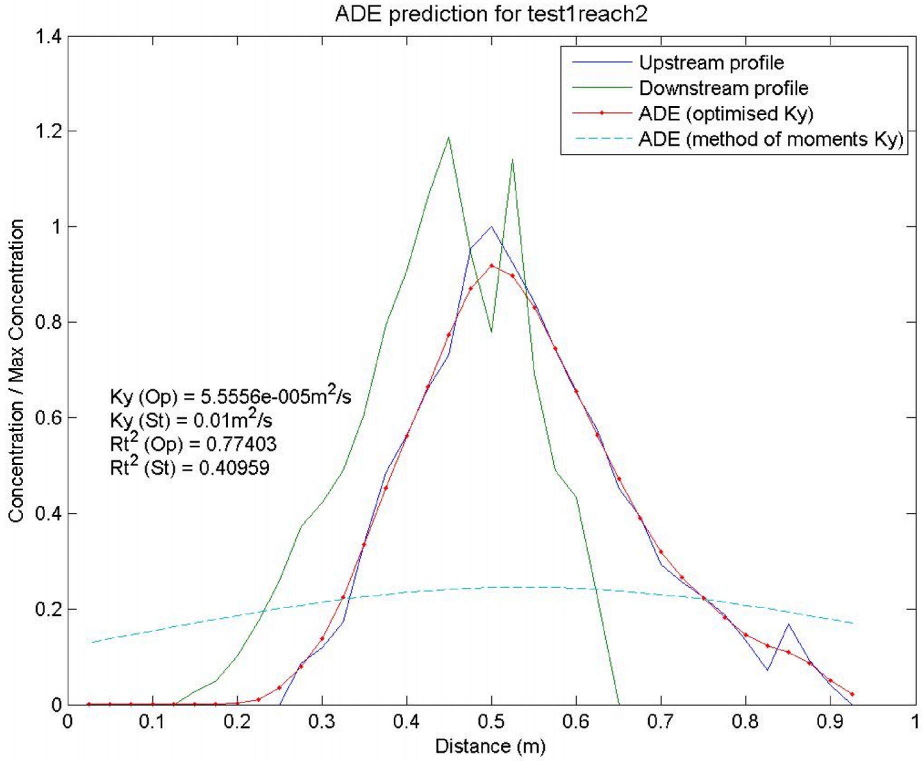
ADE prediction for test1reach2

Ky (Op) = 5.5556e-005m^2/s
Ky (St) = 0.01m^2/s
Rt^2 (Op) = 0.77403
Rt^2 (St) = 0.40959

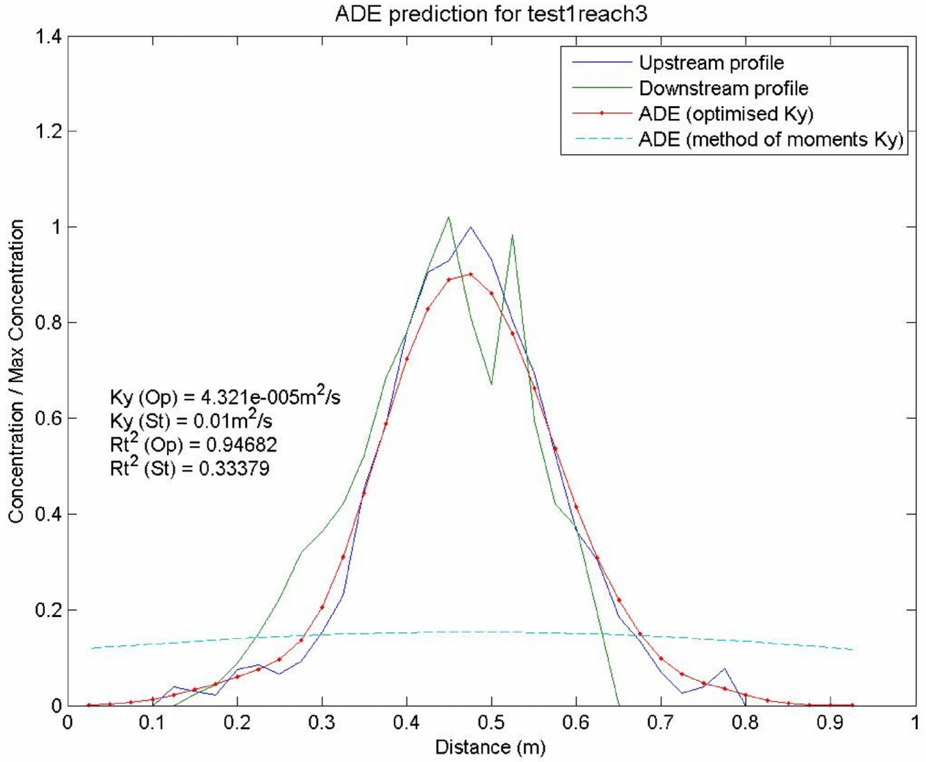
ADE prediction for test1reach3
Upstream profile
Downstream profile
ADE (optimised Ky)
ADE (method of moments Ky)
Ky (Op) = 4.321e-005m^2/s
Ky (St) = 0.01m^2/s
Rt^2 (Op) = 0.94682
Rt^2 (St) = 0.33379
Concentration / Max Concentration
Distance (m)
0
0.2
0.4
0.6
0.8
1
1.2
1.4
0
0.1
0.2
0.3
0.4
0.5
0.6
0.7
0.8
0.9
1

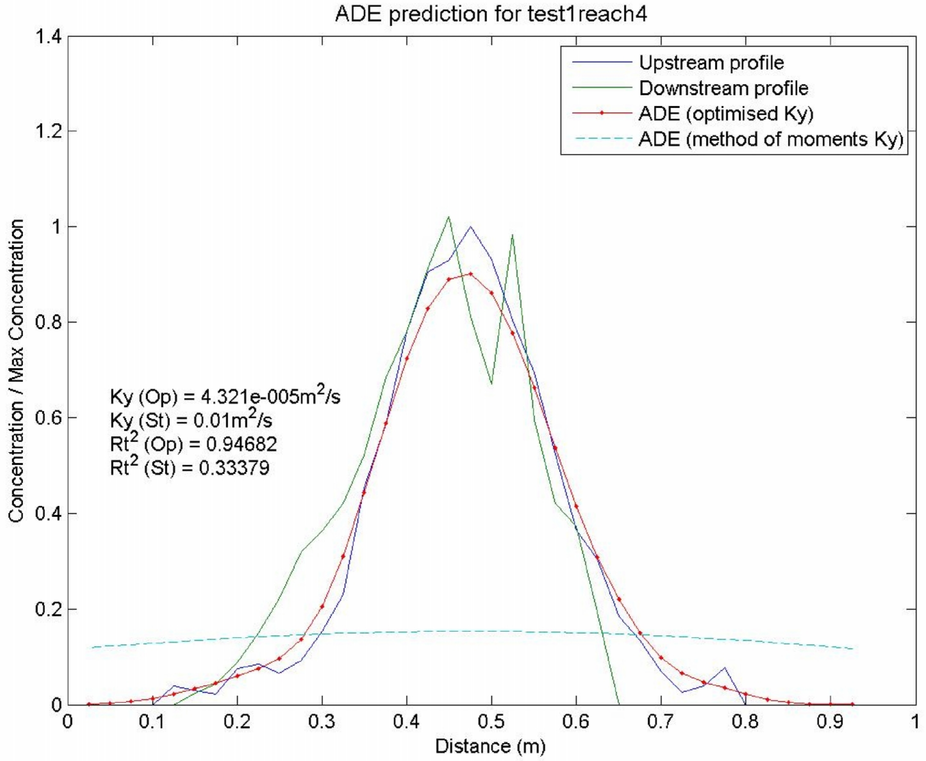
ADE prediction for test1reach4
Upstream profile
Downstream profile
ADE (optimised Ky)
ADE (method of moments Ky)
Ky (Op) = 4.321e-005m^2/s
Ky (St) = 0.01m^2/s
Rt^2 (Op) = 0.94682
Rt^2 (St) = 0.33379
Concentration / Max Concentration
Distance (m)
0
0.2
0.4
0.6
0.8
1
1.2
1.4
0
0.1
0.2
0.3
0.4
0.5
0.6
0.7
0.8
0.9
1

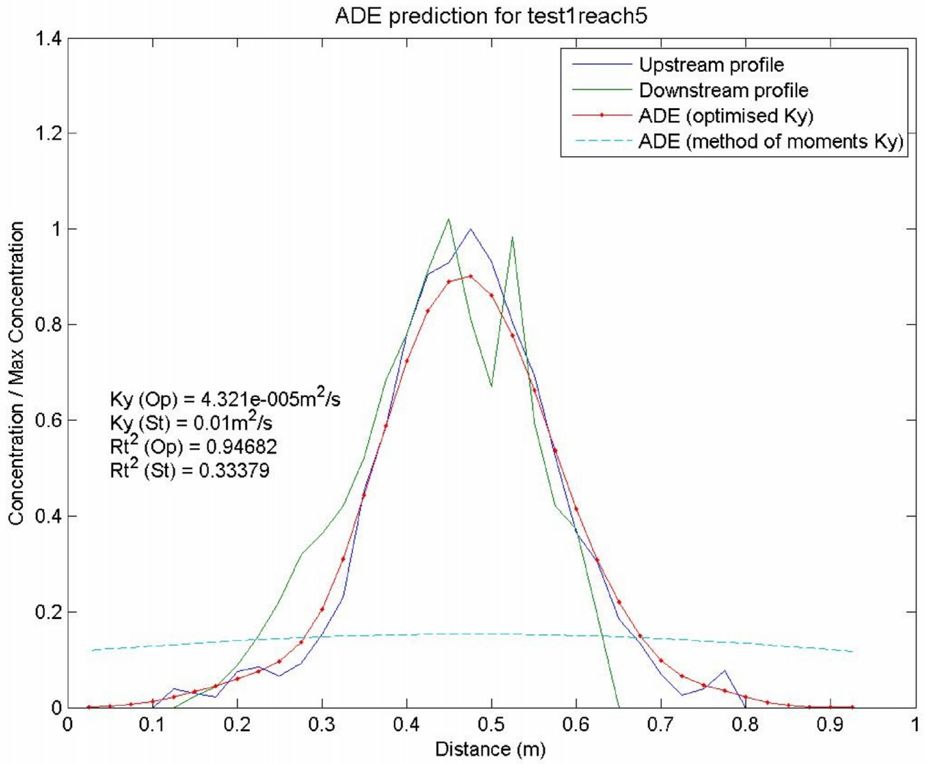

ADE prediction for test1reach5

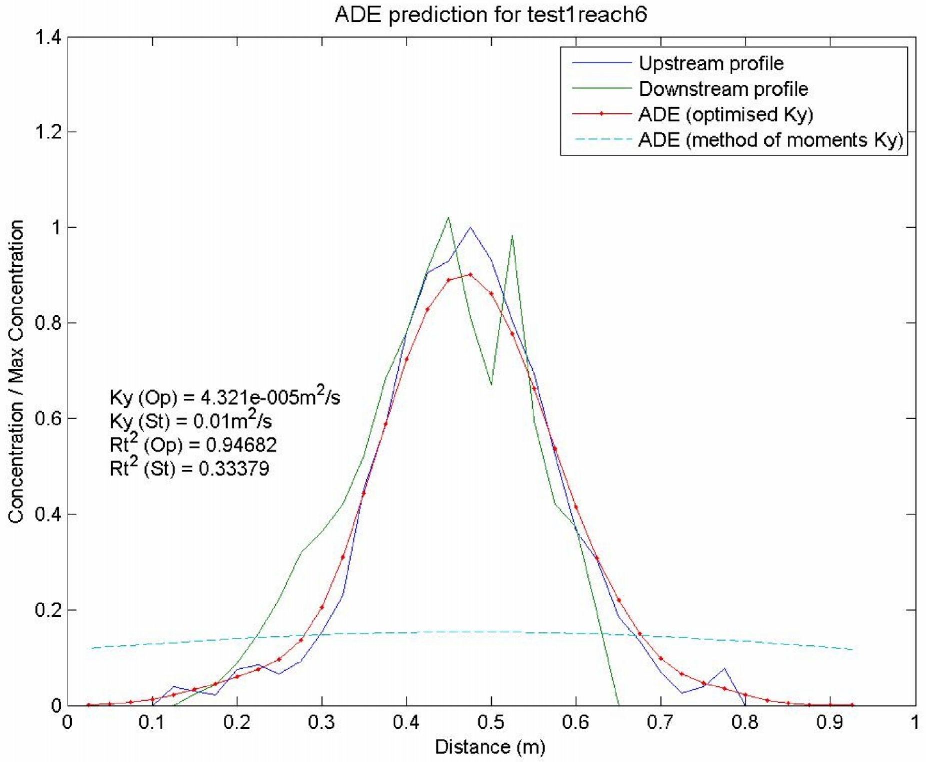

ADE prediction for test1reach6

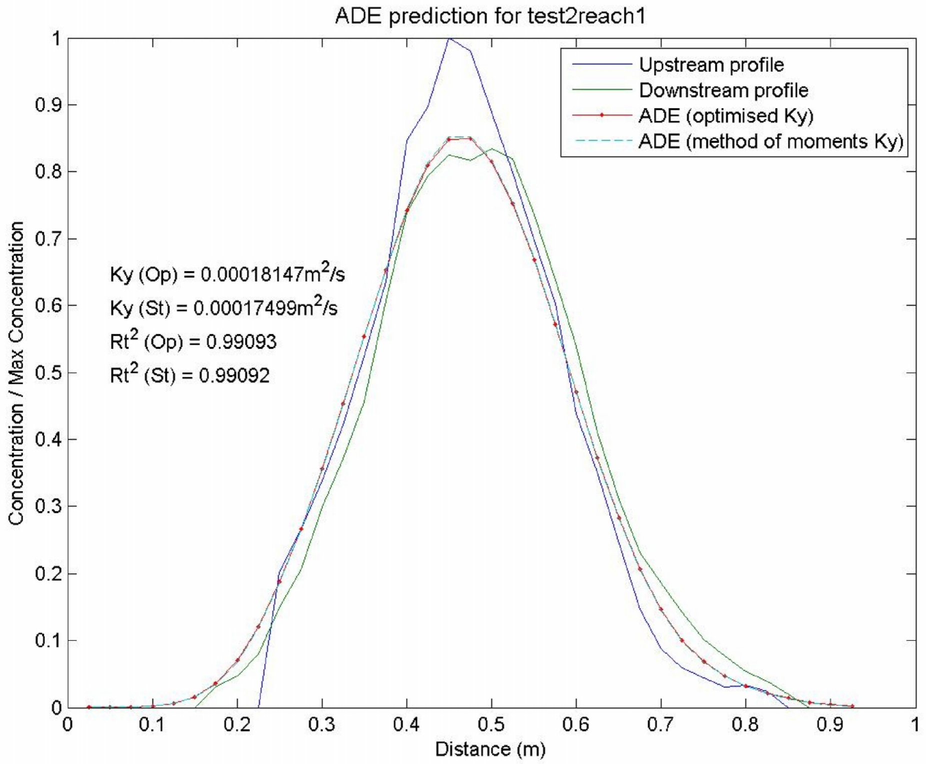
ADE prediction for test2reach1
Upstream profile
Downstream profile
ADE (optimised Ky)
ADE (method of moments Ky)
Ky (Op) = 0.00018147m^2/s
Ky (St) = 0.00017499m^2/s
Rt^2 (Op) = 0.99093
Rt^2 (St) = 0.99092
Concentration / Max Concentration
Distance (m)
0
0.1
0.2
0.3
0.4
0.5
0.6
0.7
0.8
0.9
1

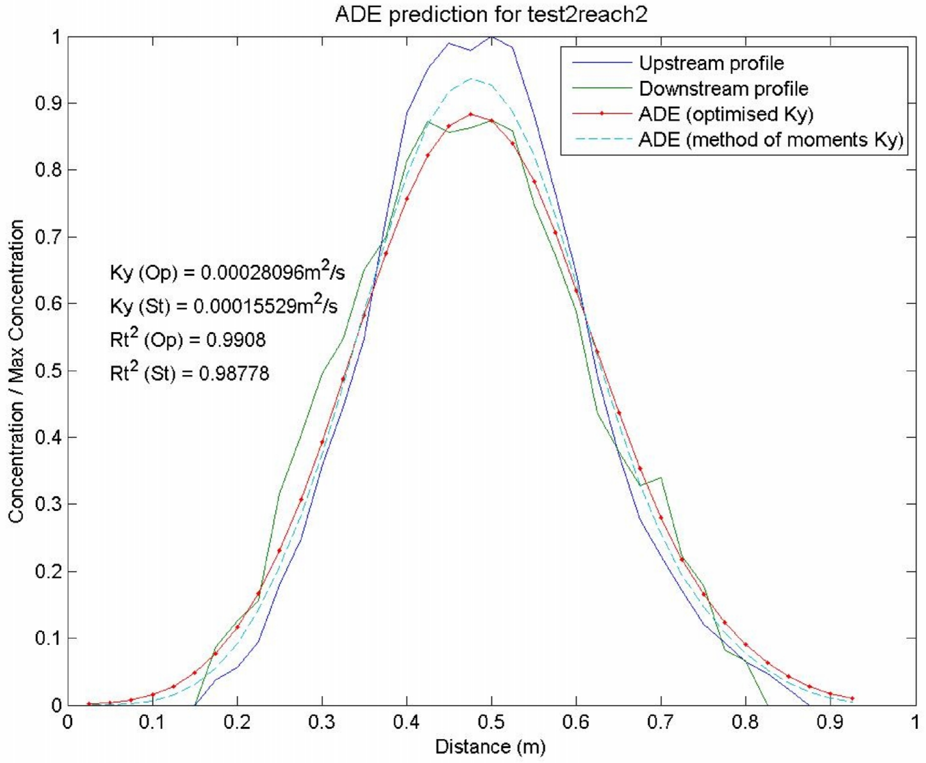
ADE prediction for test2reach2
Upstream profile
Downstream profile
ADE (optimised Ky)
ADE (method of moments Ky)
Ky (Op) = 0.00028096m^2/s
Ky (St) = 0.00015529m^2/s
Rt^2 (Op) = 0.9908
Rt^2 (St) = 0.98778
Concentration / Max Concentration
Distance (m)
0
0.1
0.2
0.3
0.4
0.5
0.6
0.7
0.8
0.9
1

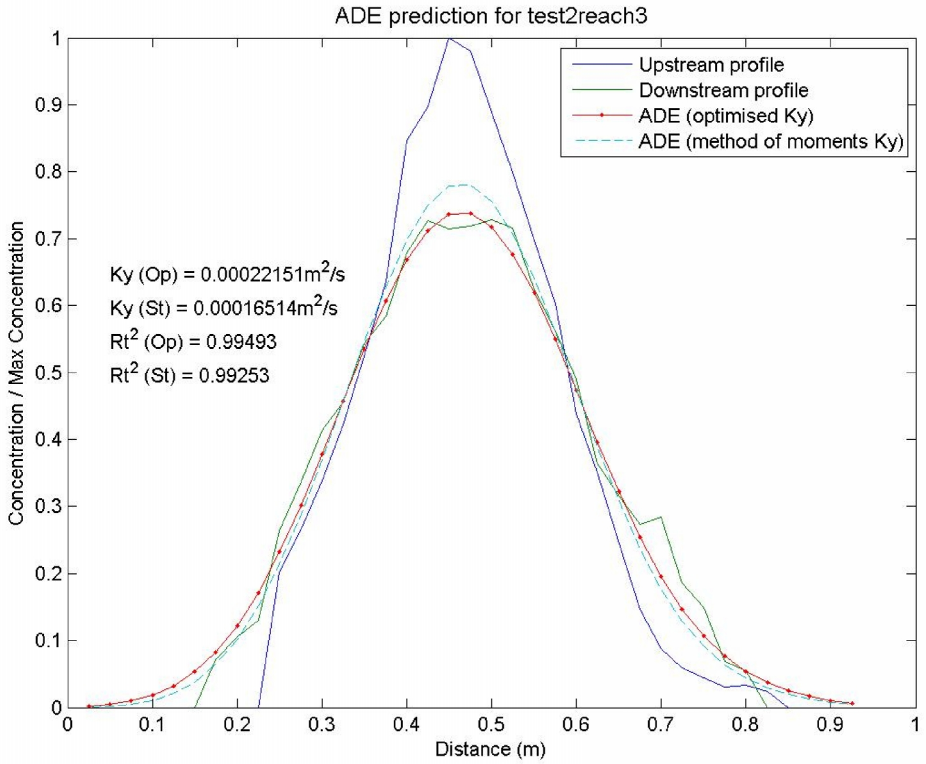
ADE prediction for test2reach3
Upstream profile
Downstream profile
ADE (optimised Ky)
ADE (method of moments Ky)
Ky (Op) = 0.00022151m^2/s
Ky (St) = 0.00016514m^2/s
Rt^2 (Op) = 0.99493
Rt^2 (St) = 0.99253
Concentration / Max Concentration
Distance (m)
0
0.1
0.2
0.3
0.4
0.5
0.6
0.7
0.8
0.9
1

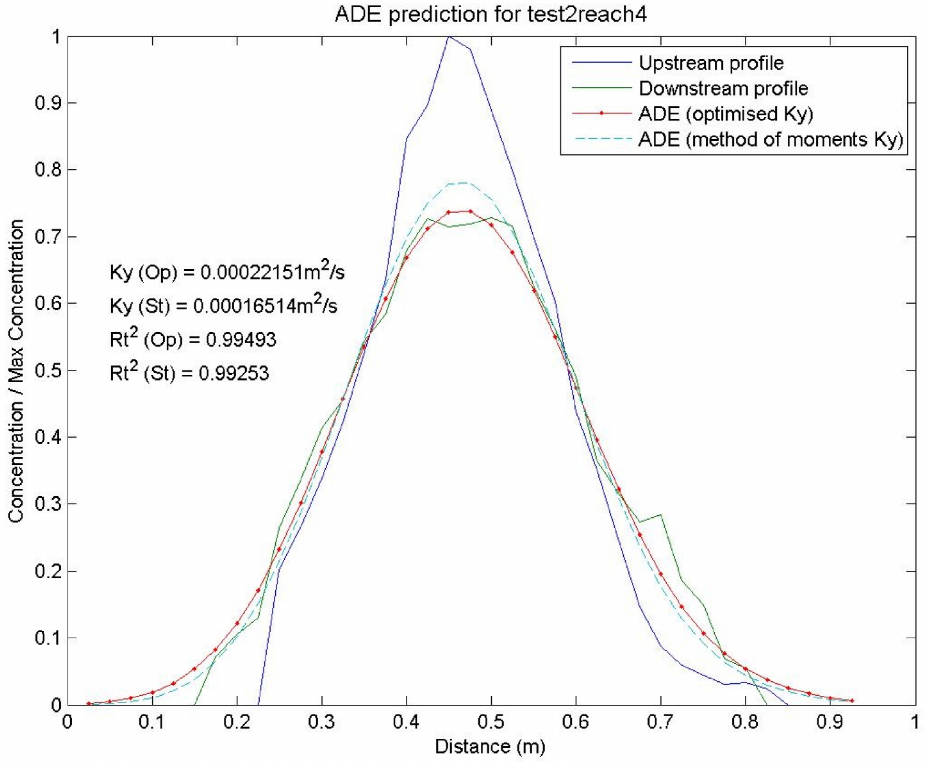
ADE prediction for test2reach4
Upstream profile
Downstream profile
ADE (optimised Ky)
ADE (method of moments Ky)
Ky (Op) = 0.00022151m^2/s
Ky (St) = 0.00016514m^2/s
Rt^2 (Op) = 0.99493
Rt^2 (St) = 0.99253
Concentration / Max Concentration
Distance (m)
0
0.1
0.2
0.3
0.4
0.5
0.6
0.7
0.8
0.9
1

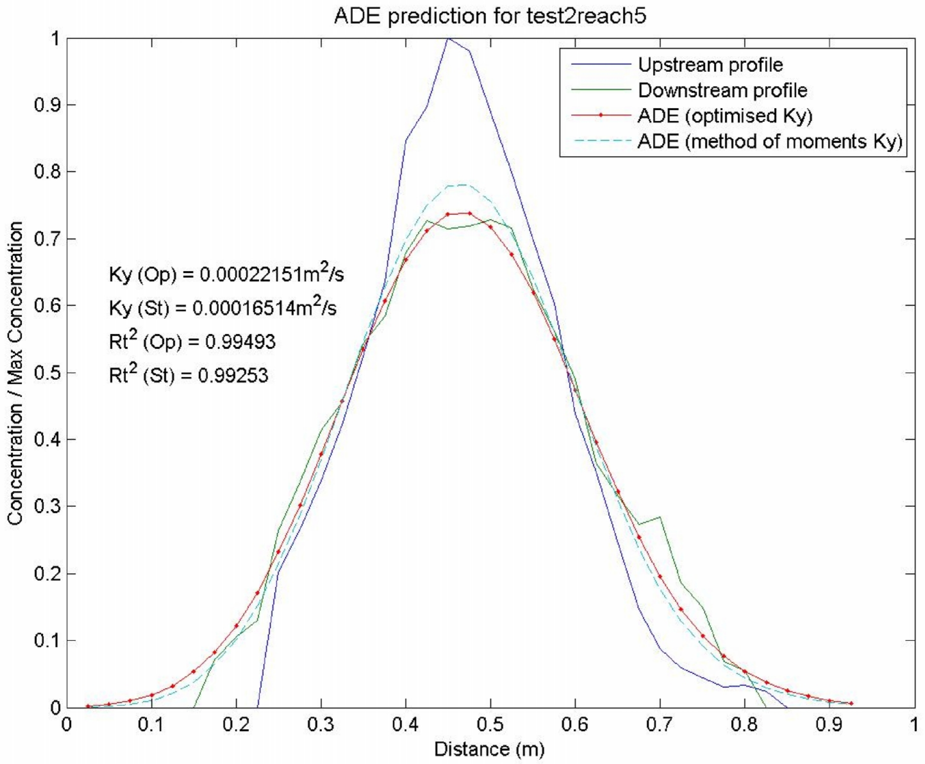
ADE prediction for test2reach5
Upstream profile
Downstream profile
ADE (optimised Ky)
ADE (method of moments Ky)
Ky (Op) = 0.00022151m^2/s
Ky (St) = 0.00016514m^2/s
Rt^2 (Op) = 0.99493
Rt^2 (St) = 0.99253
Concentration / Max Concentration
Distance (m)
0
0.1
0.2
0.3
0.4
0.5
0.6
0.7
0.8
0.9
1

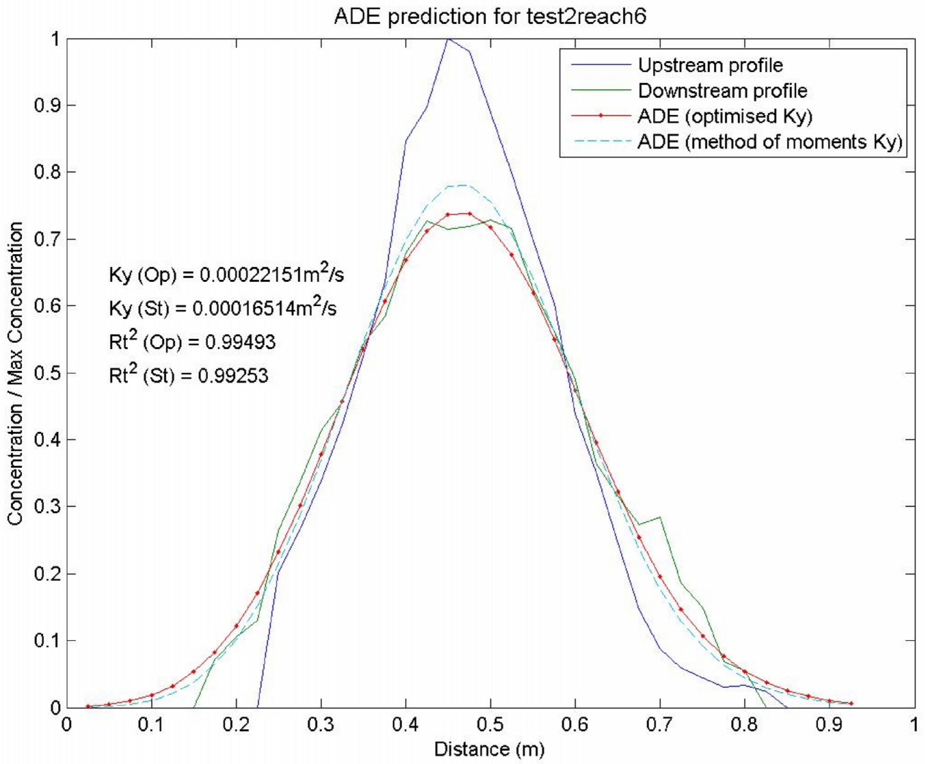
ADE prediction for test2reach6
Upstream profile
Downstream profile
ADE (optimised Ky)
ADE (method of moments Ky)
Ky (Op) = 0.00022151m^2/s
Ky (St) = 0.00016514m^2/s
Rt^2 (Op) = 0.99493
Rt^2 (St) = 0.99253
Concentration / Max Concentration
Distance (m)
0
0.1
0.2
0.3
0.4
0.5
0.6
0.7
0.8
0.9
1

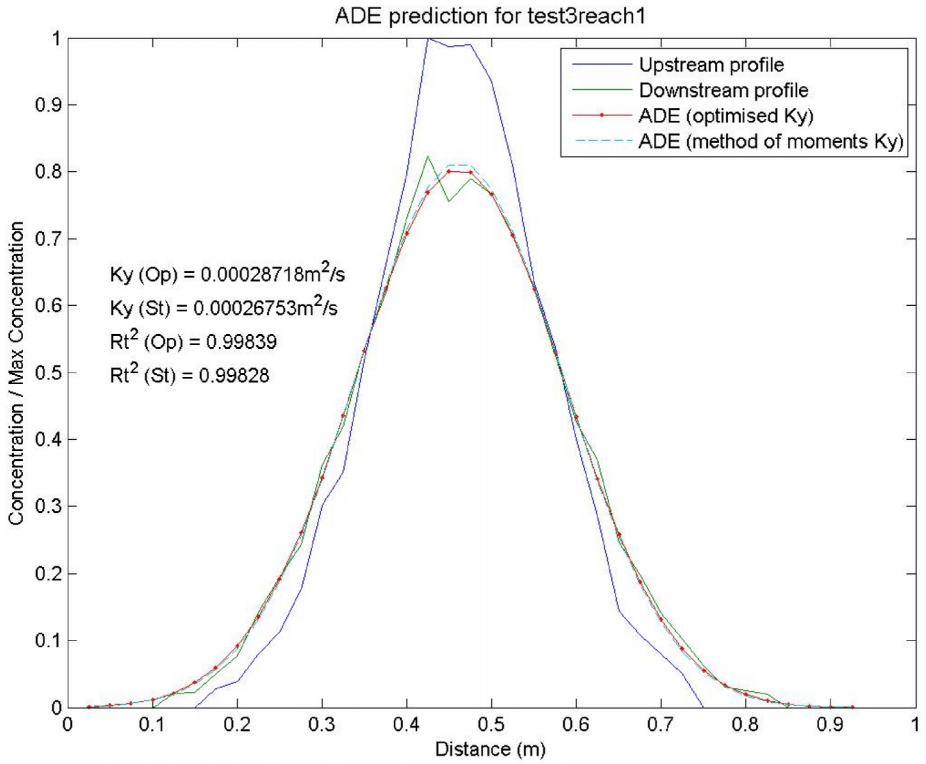
ADE prediction for test3reach1
Upstream profile
Downstream profile
ADE (optimised Ky)
ADE (method of moments Ky)
Ky (Op) = 0.00028718m^2/s
Ky (St) = 0.00026753m^2/s
Rt^2 (Op) = 0.99839
Rt^2 (St) = 0.99828
Concentration / Max Concentration
Distance (m)
0
0.1
0.2
0.3
0.4
0.5
0.6
0.7
0.8
0.9
1

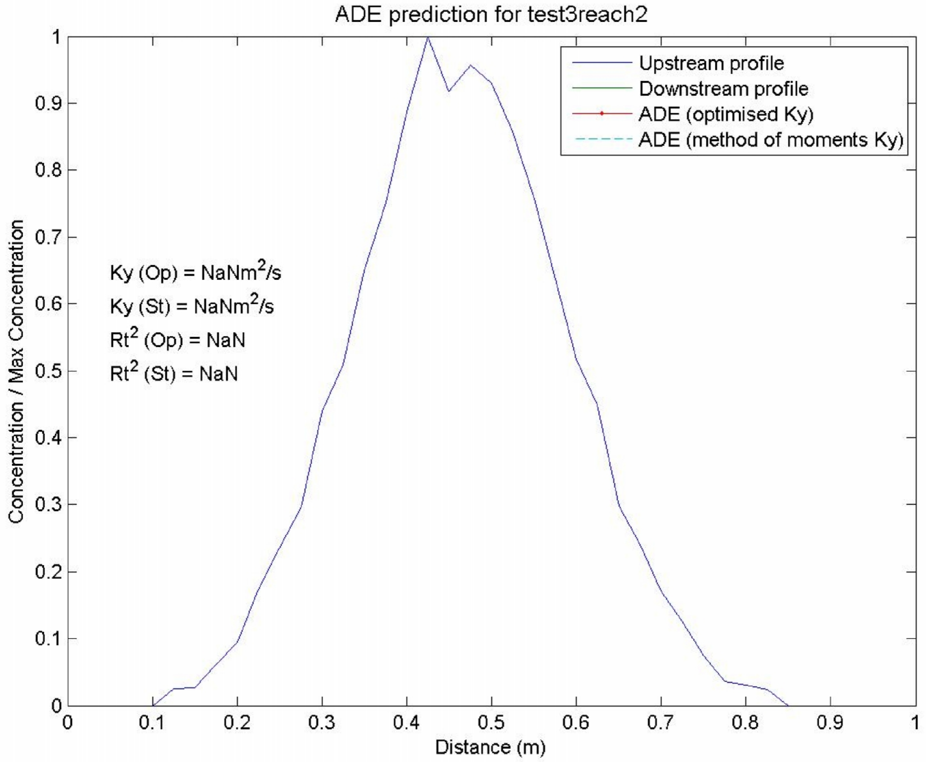
ADE prediction for test3reach2
Upstream profile
Downstream profile
ADE (optimised Ky)
ADE (method of moments Ky)
Ky (Op) = NaNm^2/s
Ky (St) = NaNm^2/s
Rt^2 (Op) = NaN
Rt^2 (St) = NaN
Concentration / Max Concentration
Distance (m)
0
0.1
0.2
0.3
0.4
0.5
0.6
0.7
0.8
0.9
1

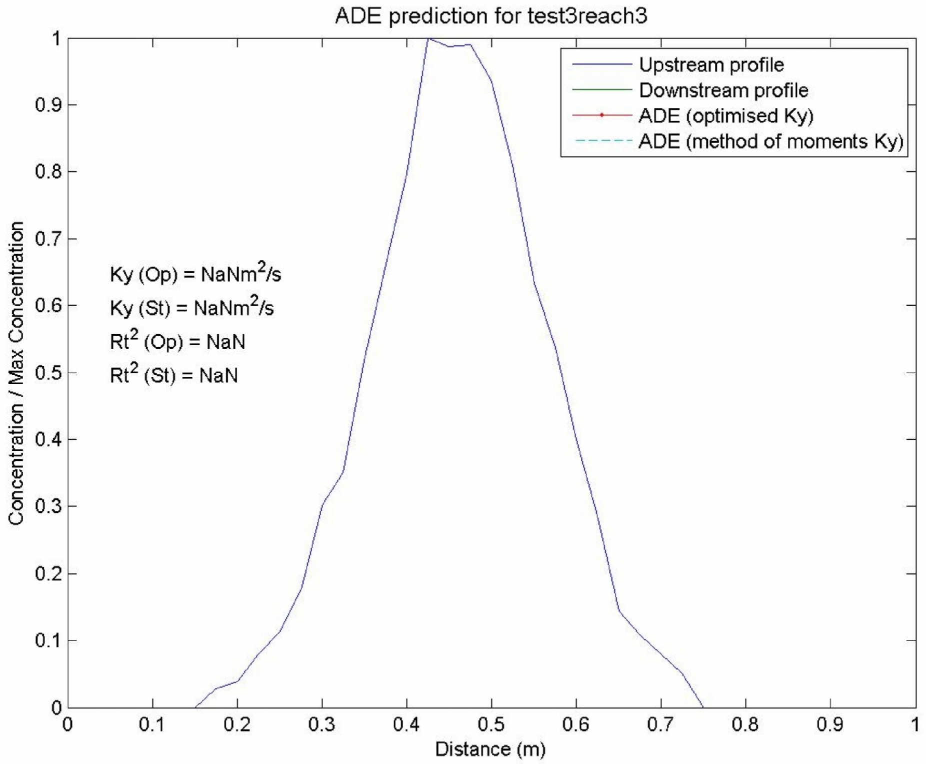
ADE prediction for test3reach3
Upstream profile
Downstream profile
ADE (optimised Ky)
ADE (method of moments Ky)
Ky (Op) = NaNm^2/s
Ky (St) = NaNm^2/s
Rt^2 (Op) = NaN
Rt^2 (St) = NaN
Concentration / Max Concentration
Distance (m)
0
0.1
0.2
0.3
0.4
0.5
0.6
0.7
0.8
0.9
1

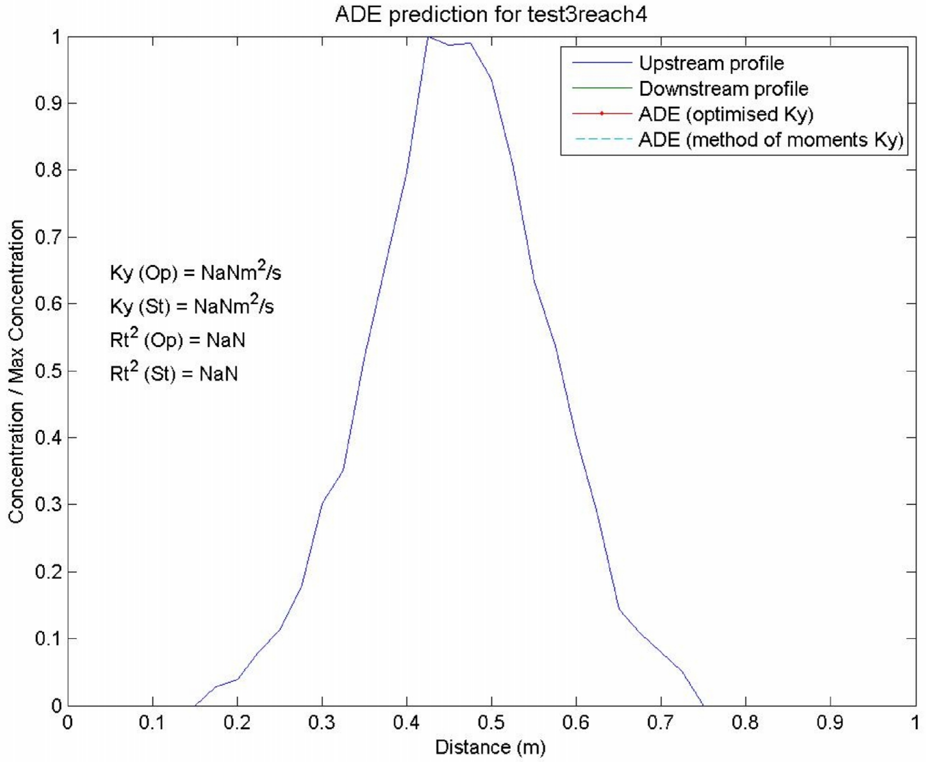
ADE prediction for test3reach4
Upstream profile
Downstream profile
ADE (optimised Ky)
ADE (method of moments Ky)
Ky (Op) = NaNm^2/s
Ky (St) = NaNm^2/s
Rt^2 (Op) = NaN
Rt^2 (St) = NaN
Concentration / Max Concentration
Distance (m)
0
0.1
0.2
0.3
0.4
0.5
0.6
0.7
0.8
0.9
1

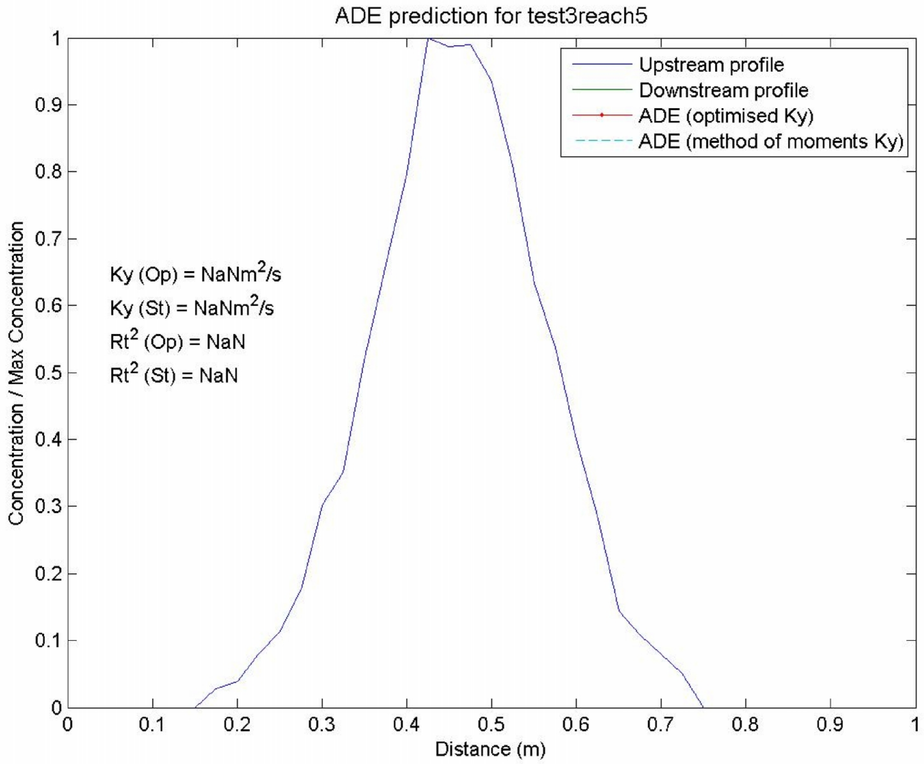
ADE prediction for test3reach5
Upstream profile
Downstream profile
ADE (optimised Ky)
ADE (method of moments Ky)
Ky (Op) = NaNm²/s
Ky (St) = NaNm²/s
Rt² (Op) = NaN
Rt² (St) = NaN
Concentration / Max Concentration
Distance (m)
0
0.1
0.2
0.3
0.4
0.5
0.6
0.7
0.8
0.9
1

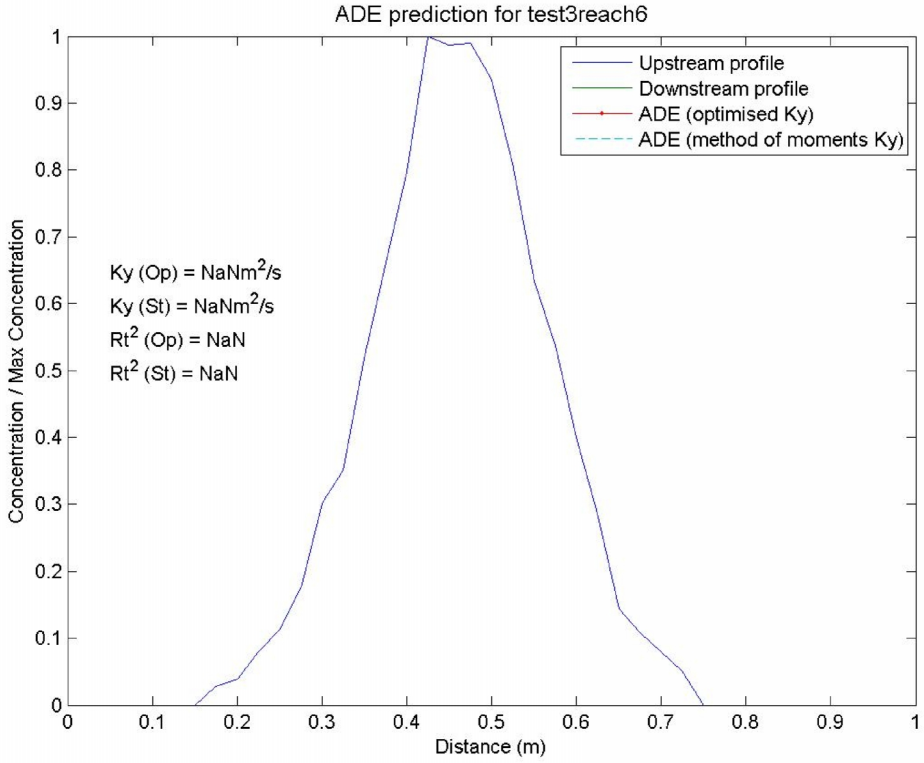
ADE prediction for test3reach6
Upstream profile
Downstream profile
ADE (optimised Ky)
ADE (method of moments Ky)
Ky (Op) = NaNm²/s
Ky (St) = NaNm²/s
Rt² (Op) = NaN
Rt² (St) = NaN
Concentration / Max Concentration
Distance (m)
0
0.1
0.2
0.3
0.4
0.5
0.6
0.7
0.8
0.9
1

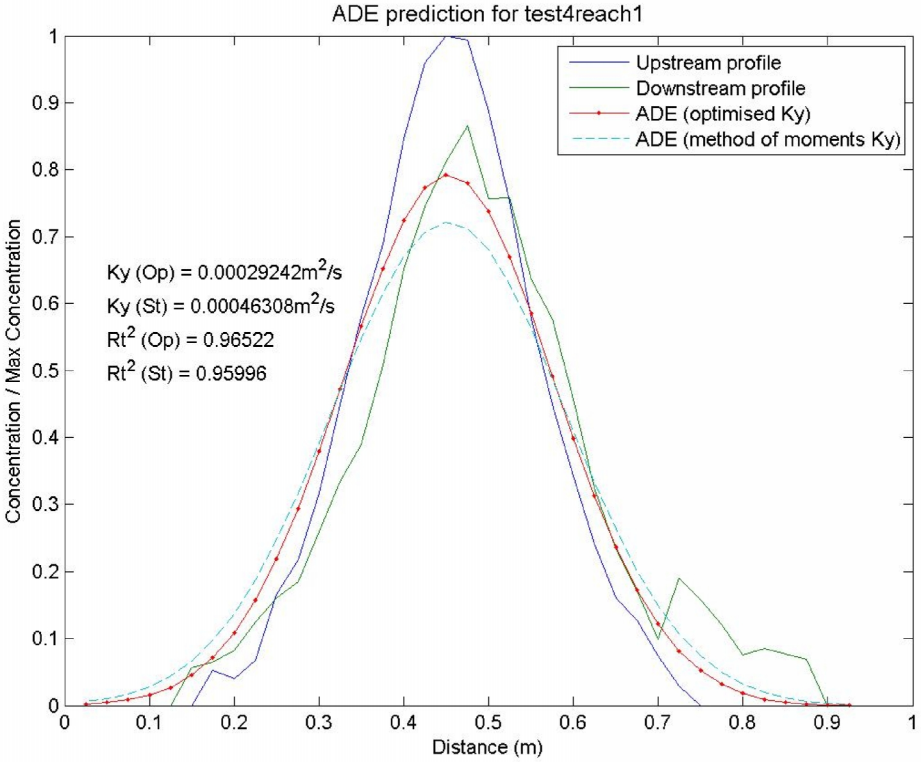
ADE prediction for test4reach1
Upstream profile
Downstream profile
ADE (optimised Ky)
ADE (method of moments Ky)
Ky (Op) = 0.00029242m^2/s
Ky (St) = 0.00046308m^2/s
Rt^2 (Op) = 0.96522
Rt^2 (St) = 0.95996
Concentration / Max Concentration
Distance (m)
0
0.1
0.2
0.3
0.4
0.5
0.6
0.7
0.8
0.9
1

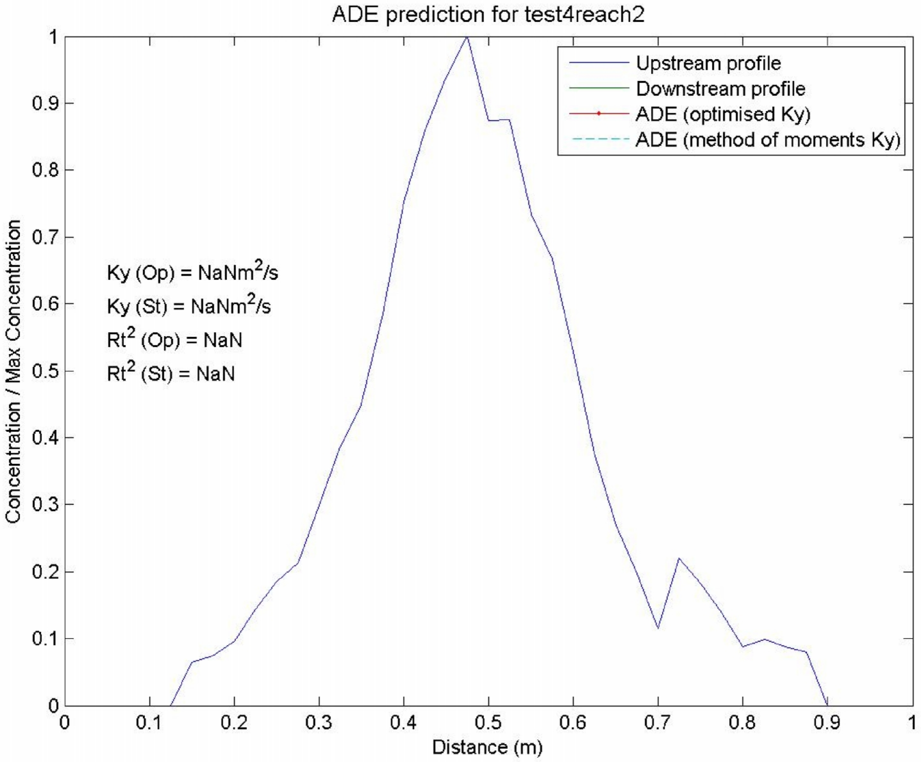
ADE prediction for test4reach2
Upstream profile
Downstream profile
ADE (optimised Ky)
ADE (method of moments Ky)
Ky (Op) = NaNm^2/s
Ky (St) = NaNm^2/s
Rt^2 (Op) = NaN
Rt^2 (St) = NaN
Concentration / Max Concentration
Distance (m)
0
0.1
0.2
0.3
0.4
0.5
0.6
0.7
0.8
0.9
1

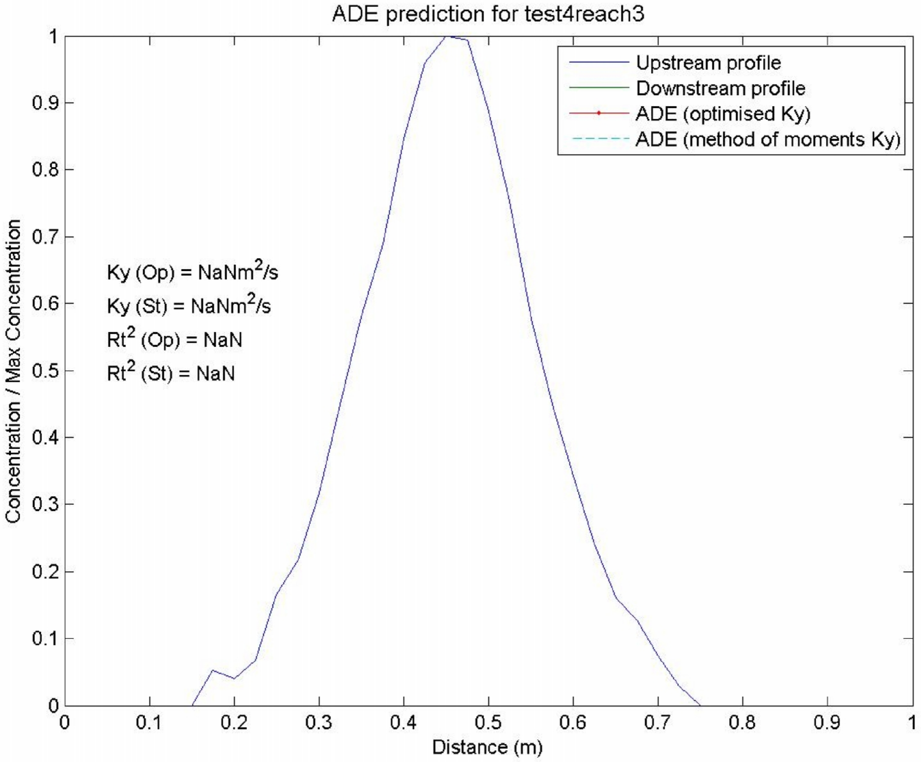
ADE prediction for test4reach3
Upstream profile
Downstream profile
ADE (optimised Ky)
ADE (method of moments Ky)
Ky (Op) = NaNm^2/s
Ky (St) = NaNm^2/s
Rt^2 (Op) = NaN
Rt^2 (St) = NaN
Concentration / Max Concentration
Distance (m)
0
0.1
0.2
0.3
0.4
0.5
0.6
0.7
0.8
0.9
1

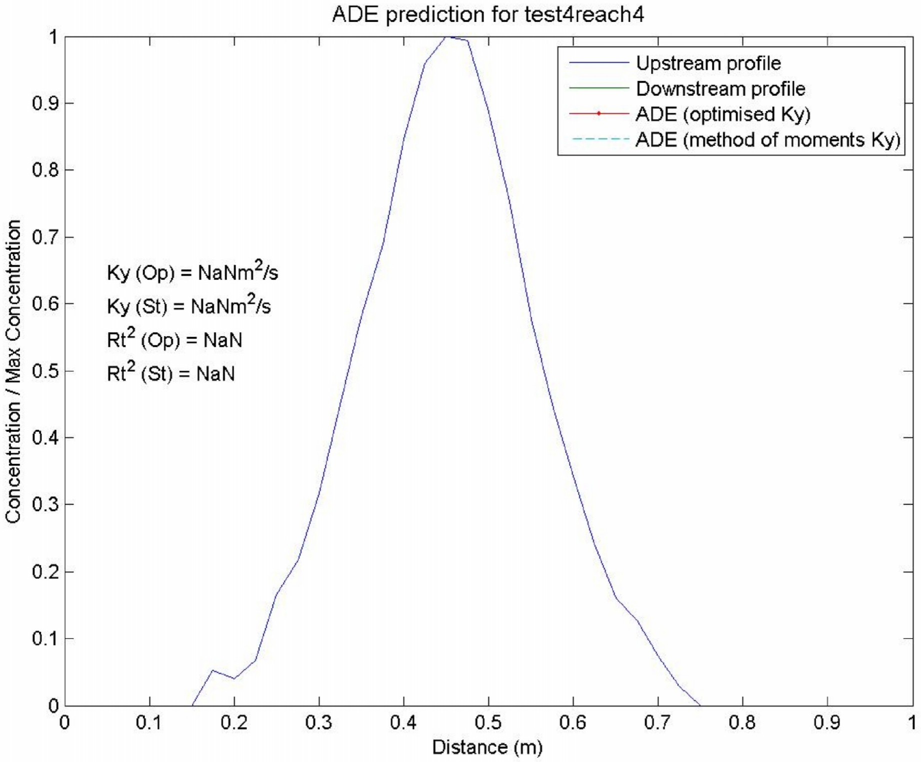
ADE prediction for test4reach4
Upstream profile
Downstream profile
ADE (optimised Ky)
ADE (method of moments Ky)
Ky (Op) = NaNm^2/s
Ky (St) = NaNm^2/s
Rt^2 (Op) = NaN
Rt^2 (St) = NaN
Concentration / Max Concentration
Distance (m)
0
0.1
0.2
0.3
0.4
0.5
0.6
0.7
0.8
0.9
1

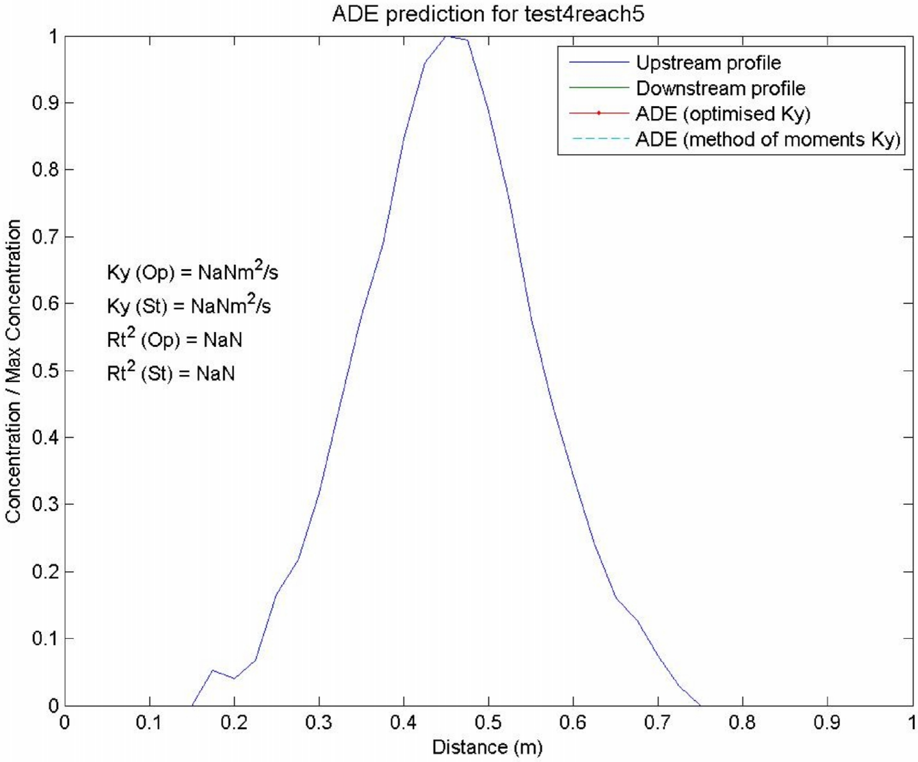
ADE prediction for test4reach5
Upstream profile
Downstream profile
ADE (optimised Ky)
ADE (method of moments Ky)
Ky (Op) = NaNm²/s
Ky (St) = NaNm²/s
Rt² (Op) = NaN
Rt² (St) = NaN
Concentration / Max Concentration
Distance (m)
0
0.1
0.2
0.3
0.4
0.5
0.6
0.7
0.8
0.9
1

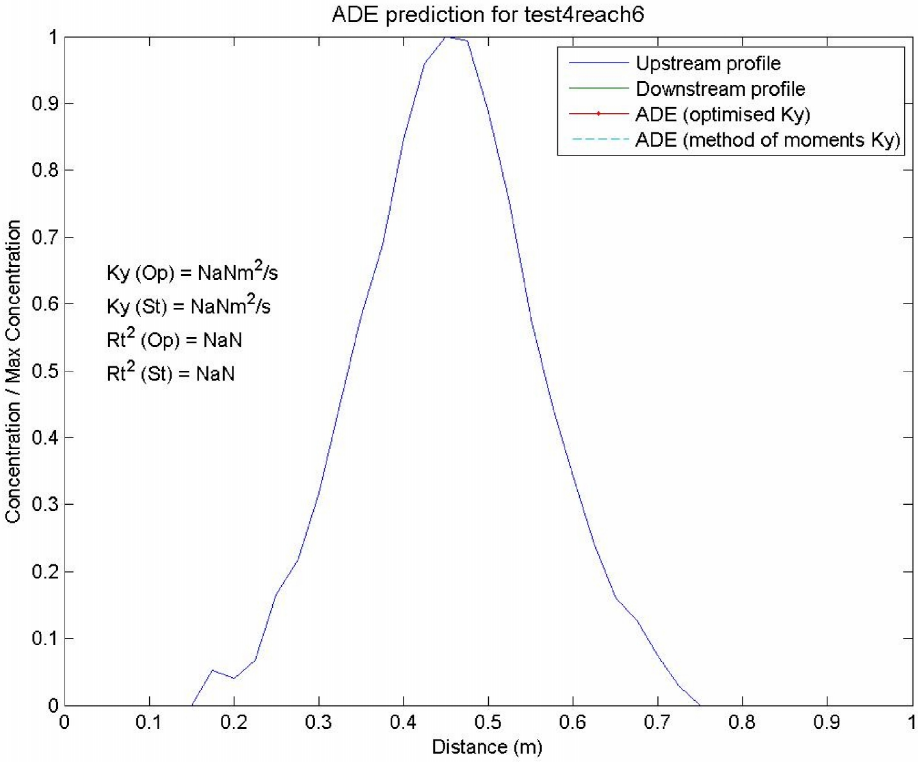
ADE prediction for test4reach6
Upstream profile
Downstream profile
ADE (optimised Ky)
ADE (method of moments Ky)
Ky (Op) = NaNm²/s
Ky (St) = NaNm²/s
Rt² (Op) = NaN
Rt² (St) = NaN
Concentration / Max Concentration
Distance (m)
0
0.1
0.2
0.3
0.4
0.5
0.6
0.7
0.8
0.9
1

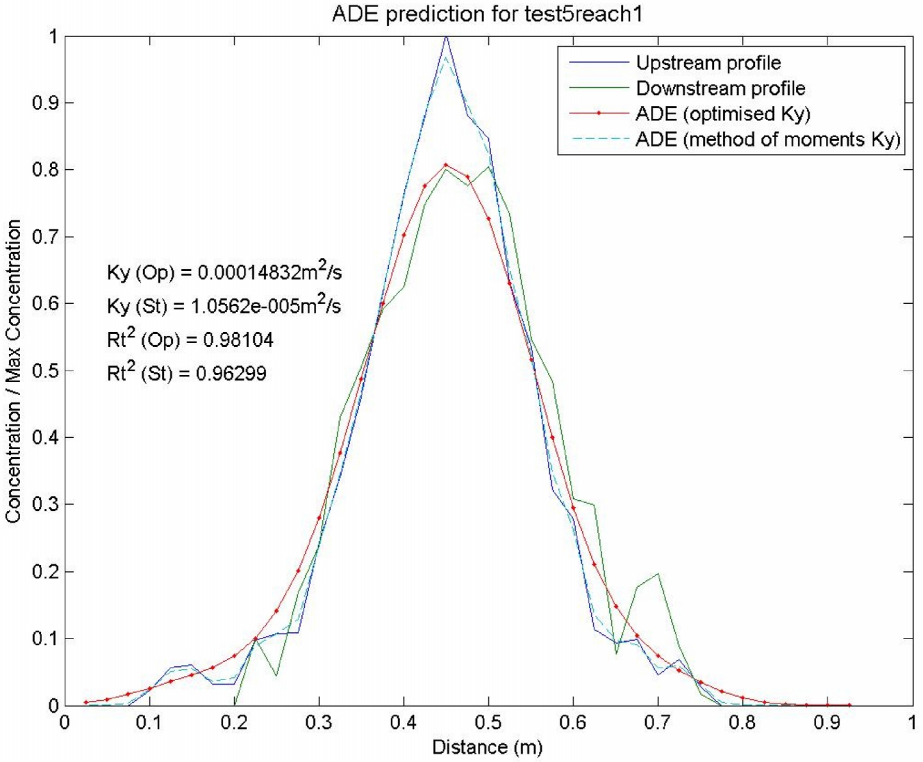
ADE prediction for test5reach1
Upstream profile
Downstream profile
ADE (optimised Ky)
ADE (method of moments Ky)
Ky (Op) = 0.00014832m^2/s
Ky (St) = 1.0562e-005m^2/s
Rt^2 (Op) = 0.98104
Rt^2 (St) = 0.96299
Concentration / Max Concentration
Distance (m)
0
0.1
0.2
0.3
0.4
0.5
0.6
0.7
0.8
0.9
1

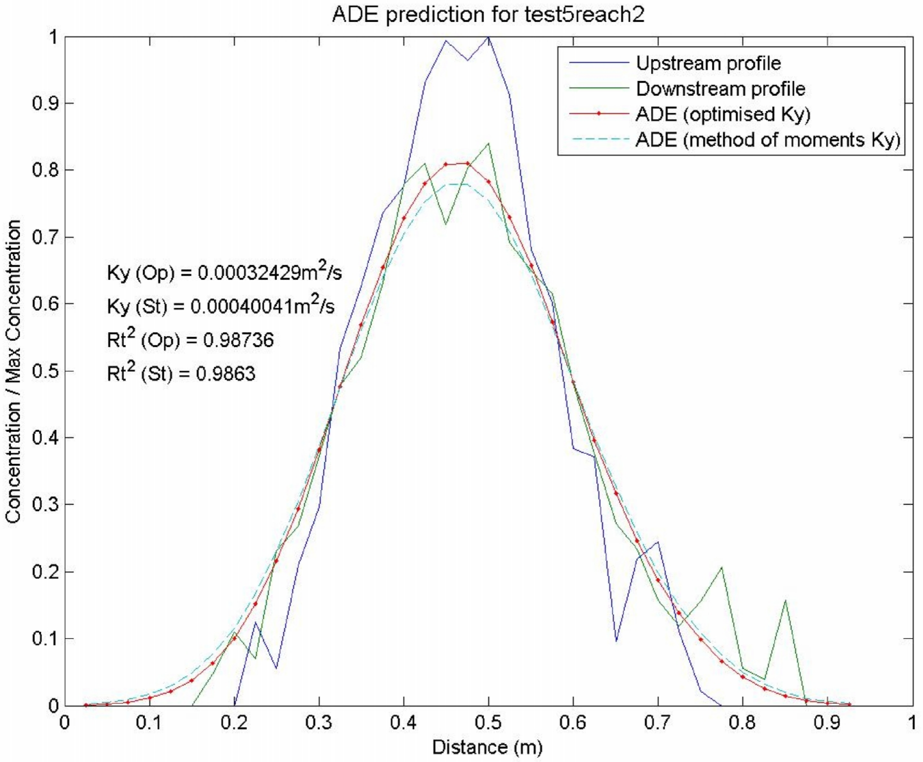
ADE prediction for test5reach2
Upstream profile
Downstream profile
ADE (optimised Ky)
ADE (method of moments Ky)
Ky (Op) = 0.00032429m^2/s
Ky (St) = 0.00040041m^2/s
Rt^2 (Op) = 0.98736
Rt^2 (St) = 0.9863
Concentration / Max Concentration
Distance (m)
0
0.1
0.2
0.3
0.4
0.5
0.6
0.7
0.8
0.9
1

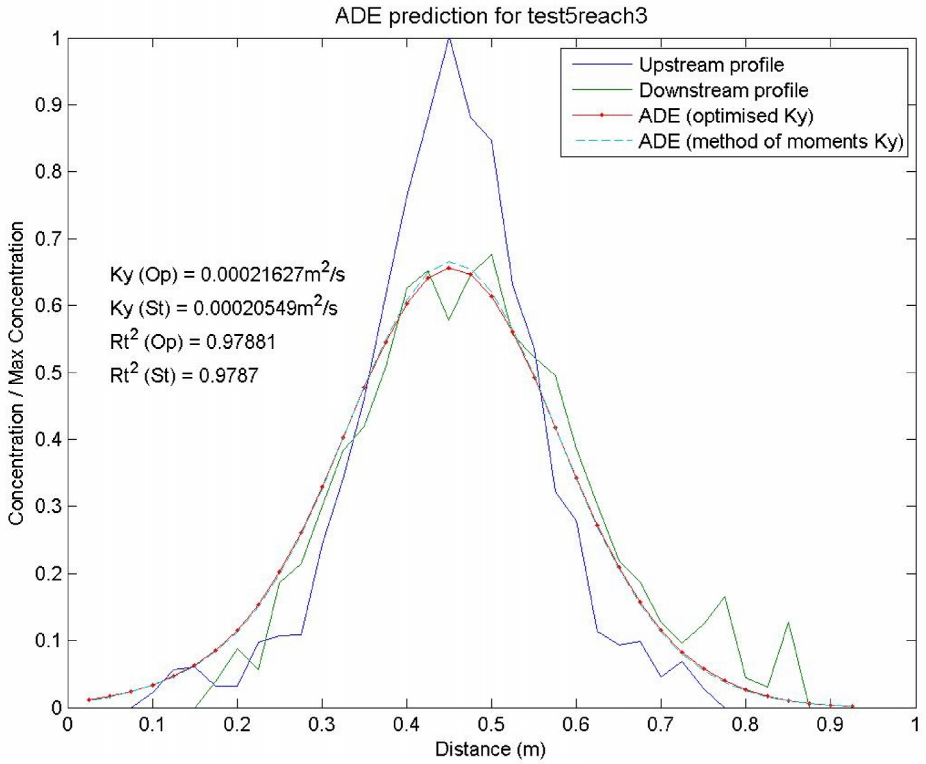
ADE prediction for test5reach3
Upstream profile
Downstream profile
ADE (optimised Ky)
ADE (method of moments Ky)
Ky (Op) = 0.00021627m^2/s
Ky (St) = 0.00020549m^2/s
Rt^2 (Op) = 0.97881
Rt^2 (St) = 0.9787
Concentration / Max Concentration
Distance (m)
0
0.1
0.2
0.3
0.4
0.5
0.6
0.7
0.8
0.9
1

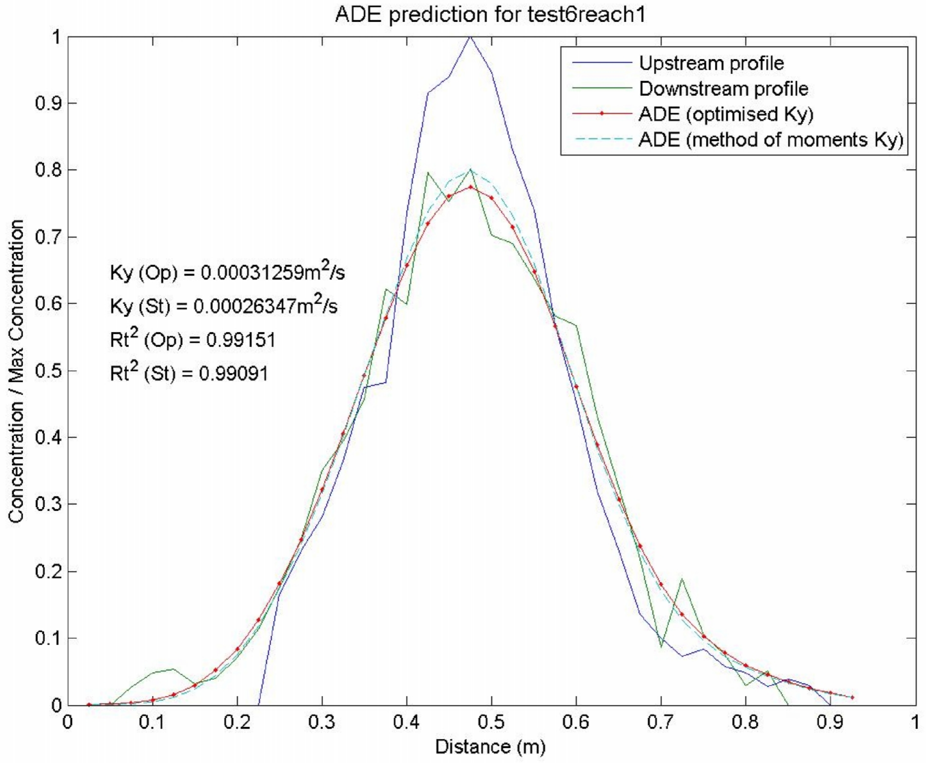
ADE prediction for test6reach1
Upstream profile
Downstream profile
ADE (optimised Ky)
ADE (method of moments Ky)
Ky (Op) = 0.00031259m^2/s
Ky (St) = 0.00026347m^2/s
Rt^2 (Op) = 0.99151
Rt^2 (St) = 0.99091
Concentration / Max Concentration
Distance (m)
0
0.1
0.2
0.3
0.4
0.5
0.6
0.7
0.8
0.9
1

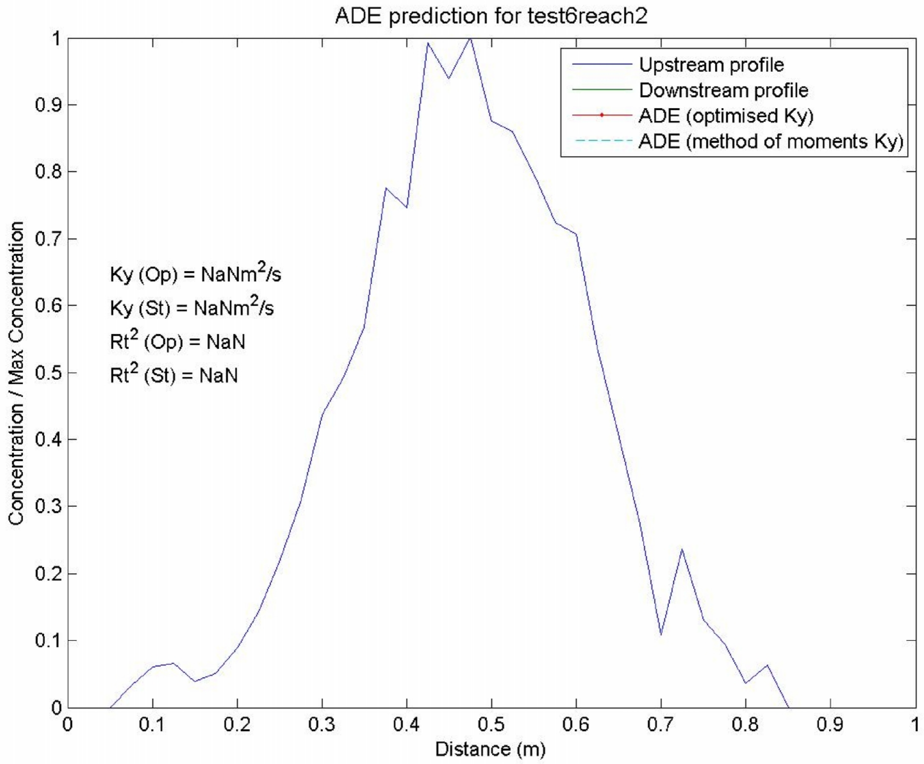
ADE prediction for test6reach2
Upstream profile
Downstream profile
ADE (optimised Ky)
ADE (method of moments Ky)
Ky (Op) = NaNm^2/s
Ky (St) = NaNm^2/s
Rt^2 (Op) = NaN
Rt^2 (St) = NaN
Concentration / Max Concentration
Distance (m)
0
0.1
0.2
0.3
0.4
0.5
0.6
0.7
0.8
0.9
1

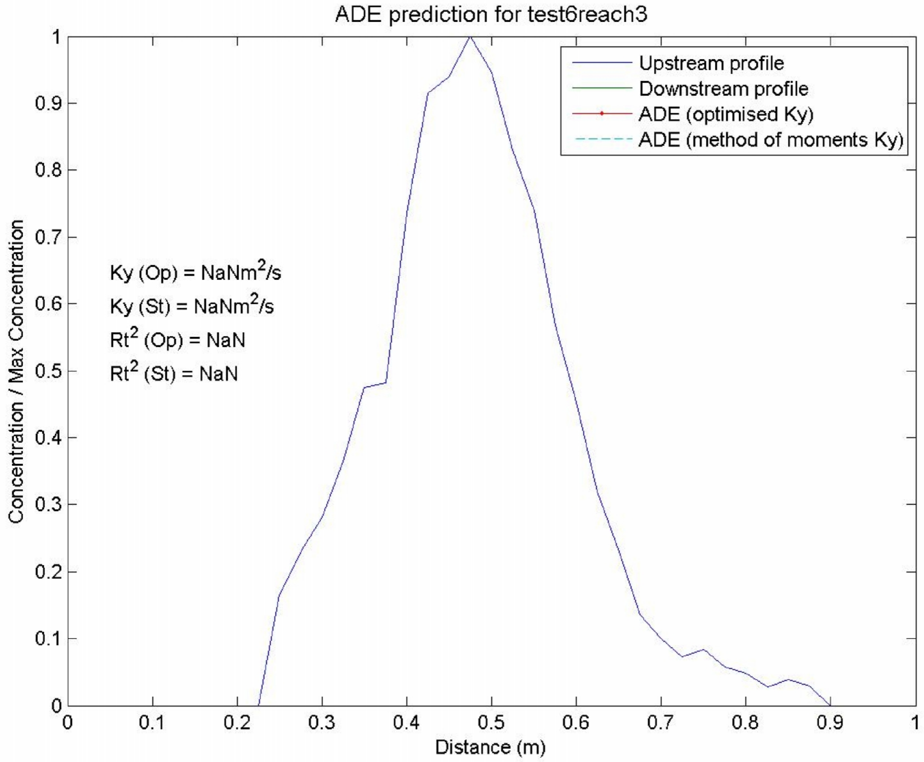
ADE prediction for test6reach3
Upstream profile
Downstream profile
ADE (optimised Ky)
ADE (method of moments Ky)
Ky (Op) = NaNm^2/s
Ky (St) = NaNm^2/s
Rt^2 (Op) = NaN
Rt^2 (St) = NaN
Concentration / Max Concentration
Distance (m)
0
0.1
0.2
0.3
0.4
0.5
0.6
0.7
0.8
0.9
1

Test 7.79A

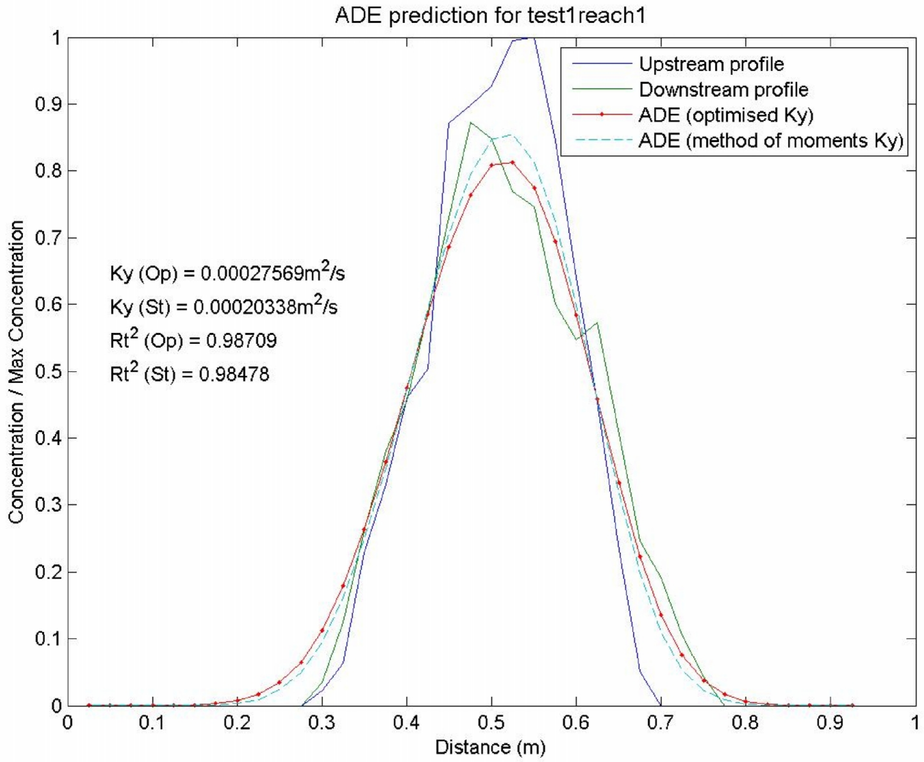
ADE prediction for test1reach1
Upstream profile
Downstream profile
ADE (optimised Ky)
ADE (method of moments Ky)
Ky (Op) = 0.00027569m^2/s
Ky (St) = 0.00020338m^2/s
Rt^2 (Op) = 0.98709
Rt^2 (St) = 0.98478
Concentration / Max Concentration
Distance (m)
0
0.1
0.2
0.3
0.4
0.5
0.6
0.7
0.8
0.9
1

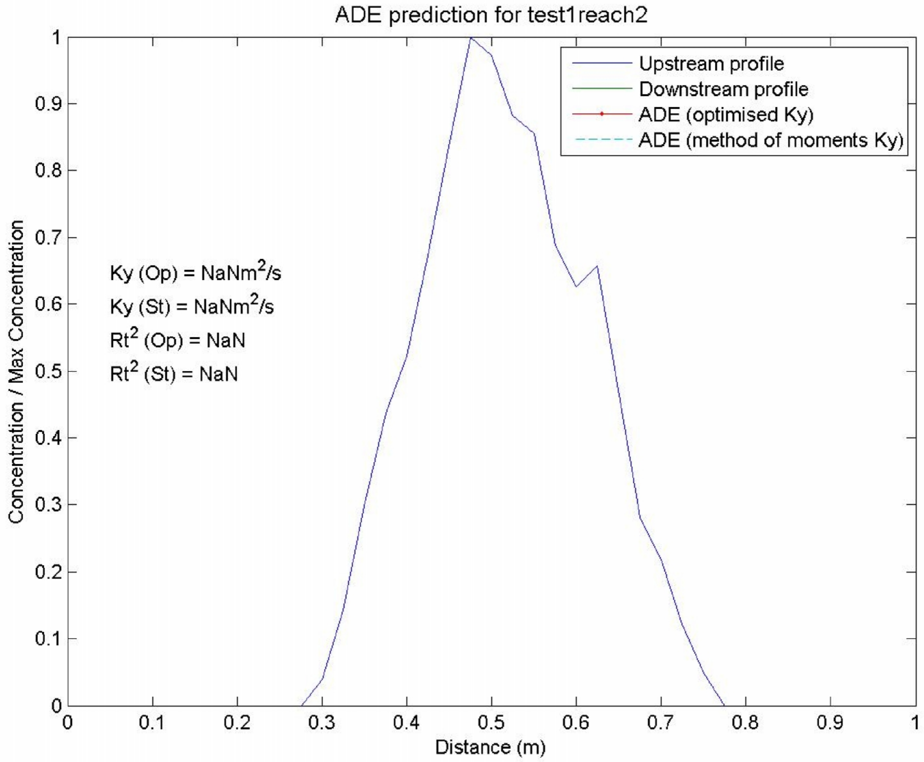
ADE prediction for test1reach2
Upstream profile
Downstream profile
ADE (optimised Ky)
ADE (method of moments Ky)
Ky (Op) = NaNm^2/s
Ky (St) = NaNm^2/s
Rt^2 (Op) = NaN
Rt^2 (St) = NaN
Concentration / Max Concentration
Distance (m)
0
0.1
0.2
0.3
0.4
0.5
0.6
0.7
0.8
0.9
1

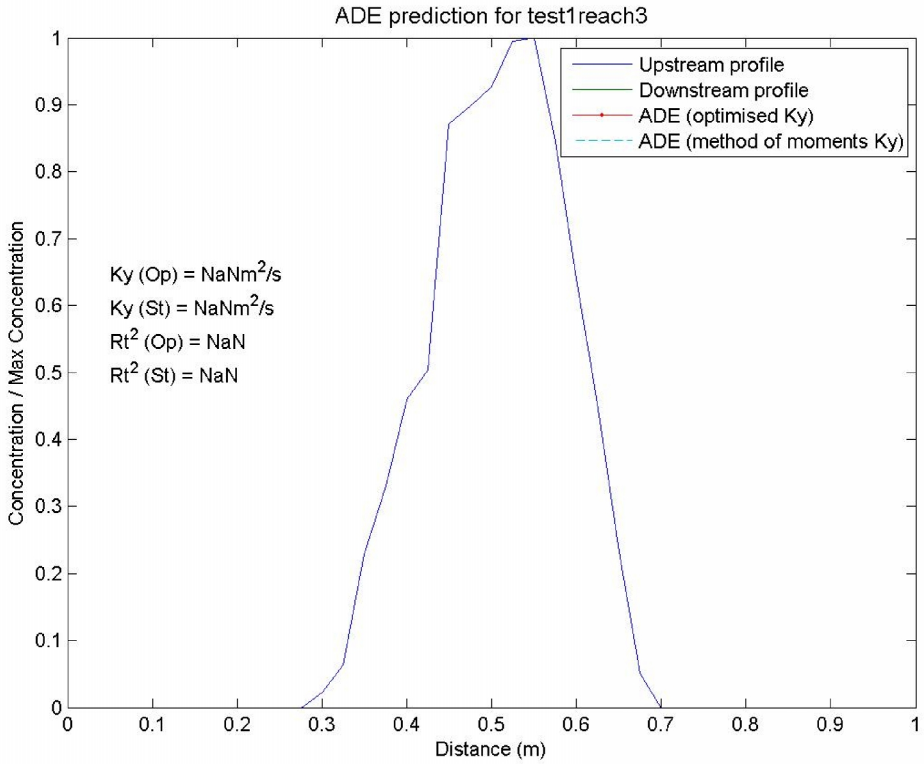
ADE prediction for test1reach3
Upstream profile
Downstream profile
ADE (optimised Ky)
ADE (method of moments Ky)
Ky (Op) = NaNm^2/s
Ky (St) = NaNm^2/s
Rt^2 (Op) = NaN
Rt^2 (St) = NaN
Concentration / Max Concentration
Distance (m)
0
0.1
0.2
0.3
0.4
0.5
0.6
0.7
0.8
0.9
1

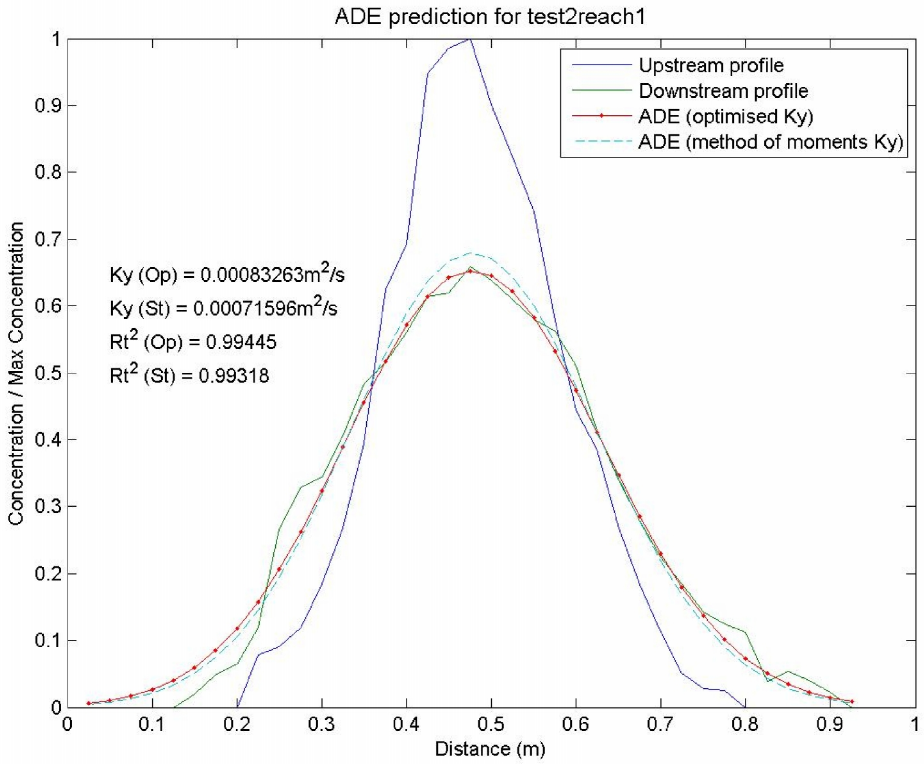
ADE prediction for test2reach1
Upstream profile
Downstream profile
ADE (optimised Ky)
ADE (method of moments Ky)
Ky (Op) = 0.00083263m^2/s
Ky (St) = 0.00071596m^2/s
Rt^2 (Op) = 0.99445
Rt^2 (St) = 0.99318
Concentration / Max Concentration
Distance (m)
0
0.1
0.2
0.3
0.4
0.5
0.6
0.7
0.8
0.9
1

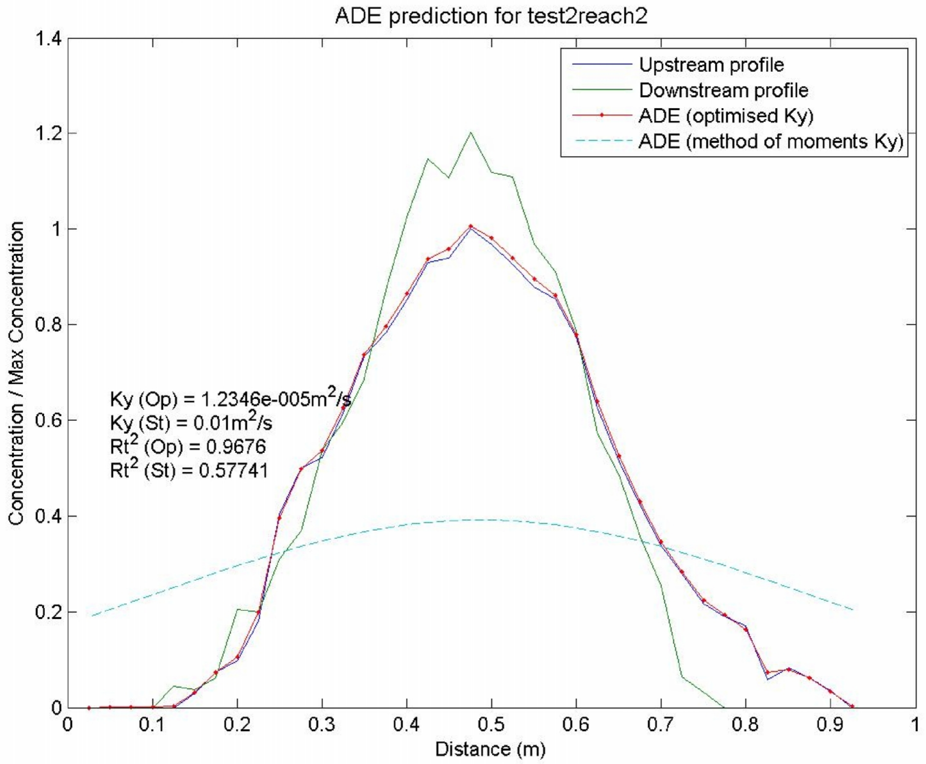
ADE prediction for test2reach2
Upstream profile
Downstream profile
ADE (optimised Ky)
ADE (method of moments Ky)
Ky (Op) = 1.2346e-005m^2/s
Ky (St) = 0.01m^2/s
Rt^2 (Op) = 0.9676
Rt^2 (St) = 0.57741
Concentration / Max Concentration
Distance (m)
0
0.2
0.4
0.6
0.8
1
1.2
1.4
0
0.1
0.2
0.3
0.4
0.5
0.6
0.7
0.8
0.9
1

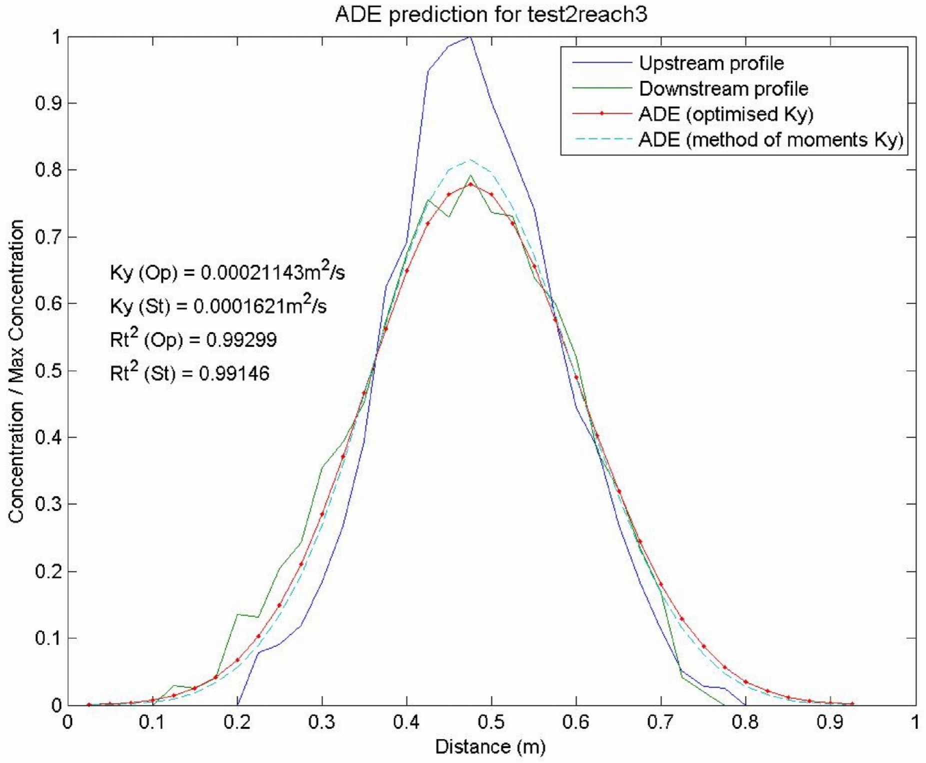
ADE prediction for test2reach3
Upstream profile
Downstream profile
ADE (optimised Ky)
ADE (method of moments Ky)
Ky (Op) = 0.00021143m^2/s
Ky (St) = 0.0001621m^2/s
Rt^2 (Op) = 0.99299
Rt^2 (St) = 0.99146
Concentration / Max Concentration
Distance (m)
0
0.1
0.2
0.3
0.4
0.5
0.6
0.7
0.8
0.9
1
0
0.1
0.2
0.3
0.4
0.5
0.6
0.7
0.8
0.9
1

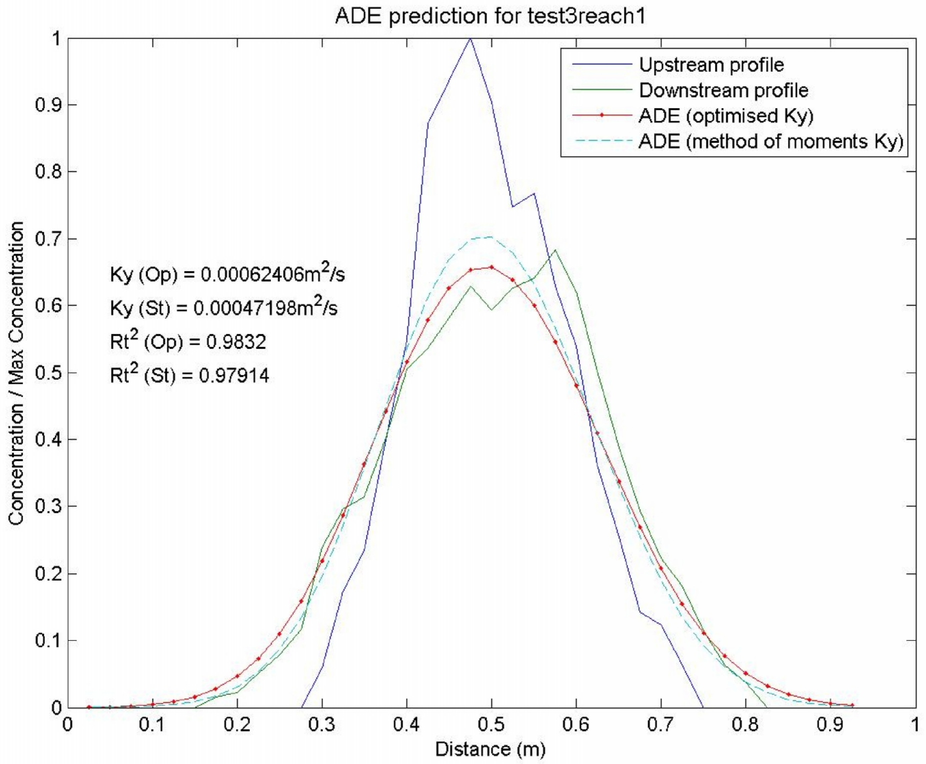
ADE prediction for test3reach1
Upstream profile
Downstream profile
ADE (optimised Ky)
ADE (method of moments Ky)
Ky (Op) = 0.00062406m^2/s
Ky (St) = 0.00047198m^2/s
Rt^2 (Op) = 0.9832
Rt^2 (St) = 0.97914
Concentration / Max Concentration
Distance (m)
0
0.1
0.2
0.3
0.4
0.5
0.6
0.7
0.8
0.9
1

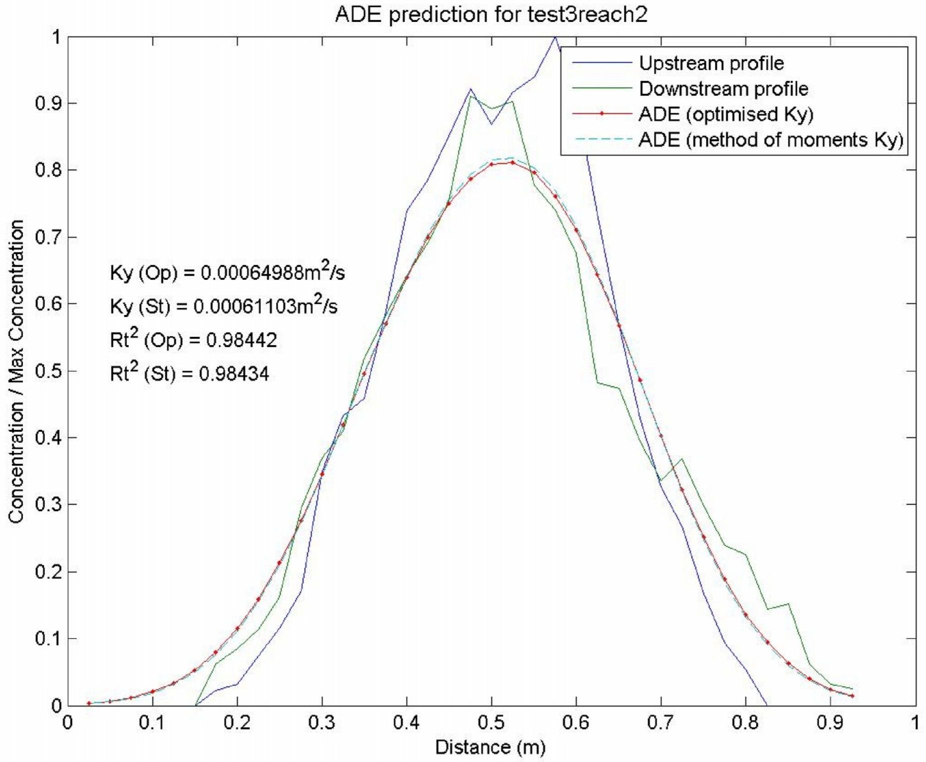
ADE prediction for test3reach2
Upstream profile
Downstream profile
ADE (optimised Ky)
ADE (method of moments Ky)
Ky (Op) = 0.00064988m^2/s
Ky (St) = 0.00061103m^2/s
Rt^2 (Op) = 0.98442
Rt^2 (St) = 0.98434
Concentration / Max Concentration
Distance (m)
0
0.1
0.2
0.3
0.4
0.5
0.6
0.7
0.8
0.9
1

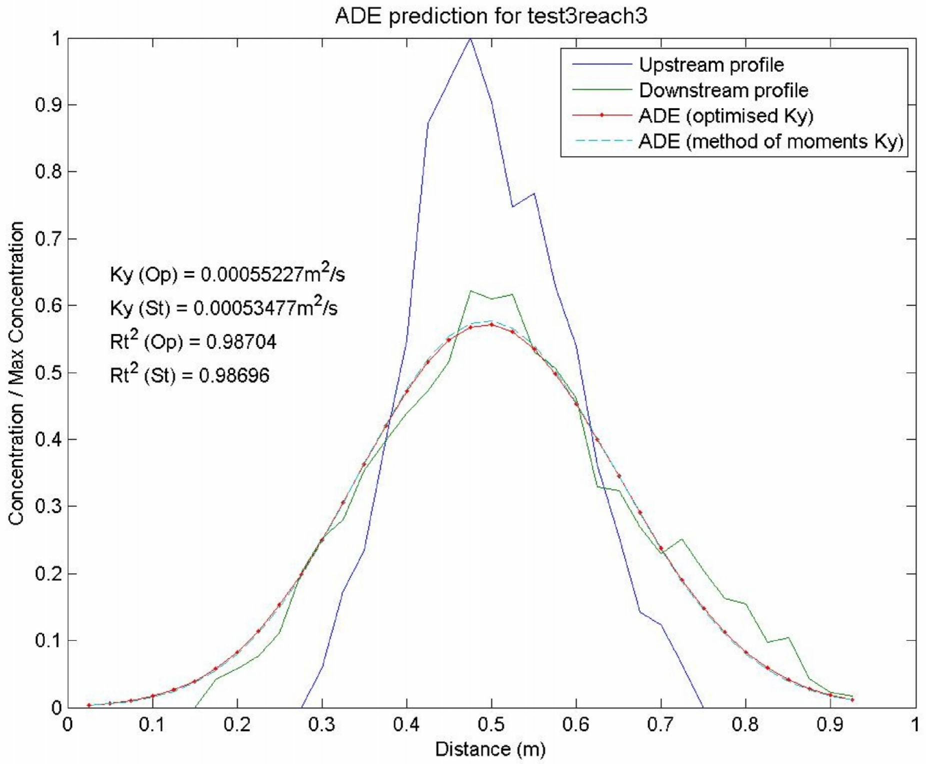
ADE prediction for test3reach3
Upstream profile
Downstream profile
ADE (optimised Ky)
ADE (method of moments Ky)
Ky (Op) = 0.00055227m^2/s
Ky (St) = 0.00053477m^2/s
Rt^2 (Op) = 0.98704
Rt^2 (St) = 0.98696
Concentration / Max Concentration
Distance (m)
0
0.1
0.2
0.3
0.4
0.5
0.6
0.7
0.8
0.9
1

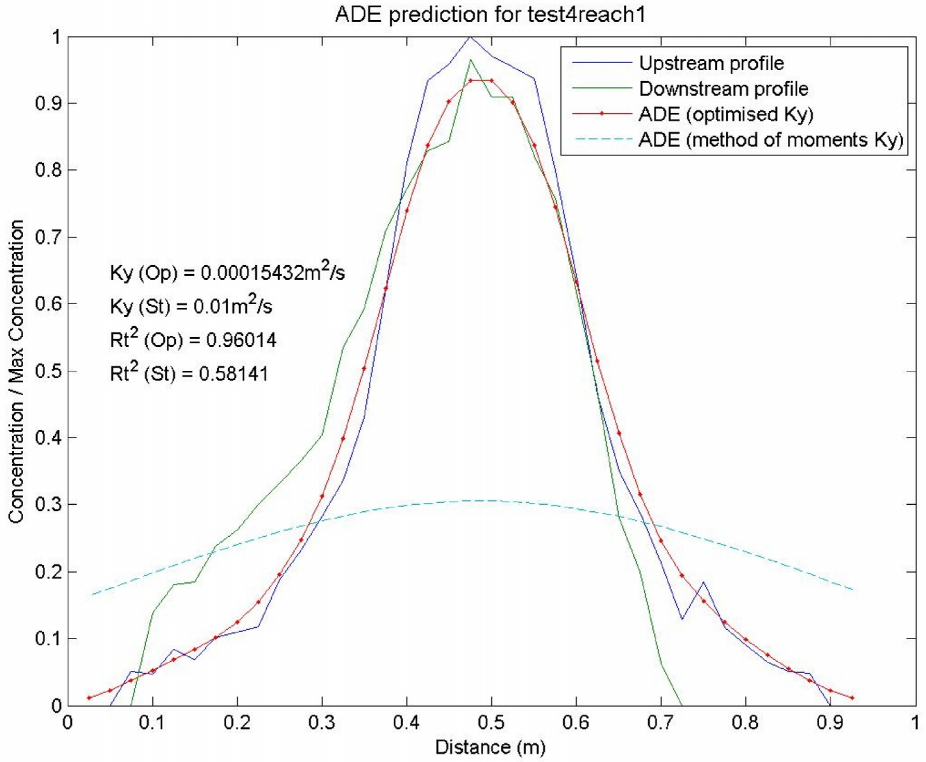
ADE prediction for test4reach1
Upstream profile
Downstream profile
ADE (optimised Ky)
ADE (method of moments Ky)
Ky (Op) = 0.00015432m^2/s
Ky (St) = 0.01m^2/s
Rt^2 (Op) = 0.96014
Rt^2 (St) = 0.58141
Concentration / Max Concentration
Distance (m)
0
0.1
0.2
0.3
0.4
0.5
0.6
0.7
0.8
0.9
1

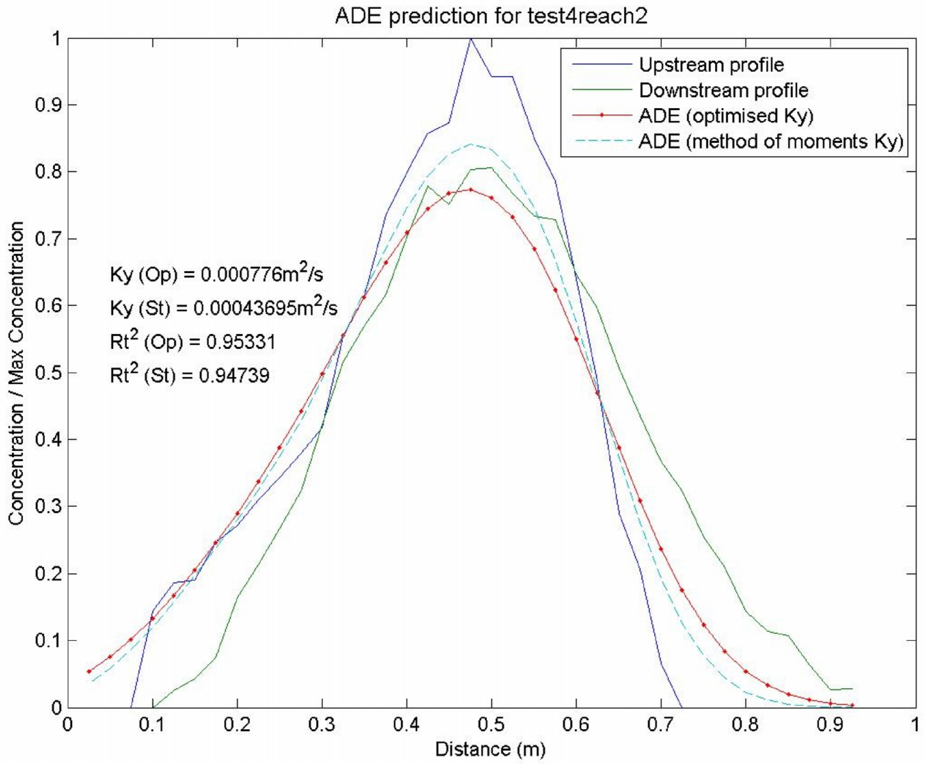
ADE prediction for test4reach2
Upstream profile
Downstream profile
ADE (optimised Ky)
ADE (method of moments Ky)
Ky (Op) = 0.000776m^2/s
Ky (St) = 0.00043695m^2/s
Rt^2 (Op) = 0.95331
Rt^2 (St) = 0.94739
Concentration / Max Concentration
Distance (m)
0
0.1
0.2
0.3
0.4
0.5
0.6
0.7
0.8
0.9
1

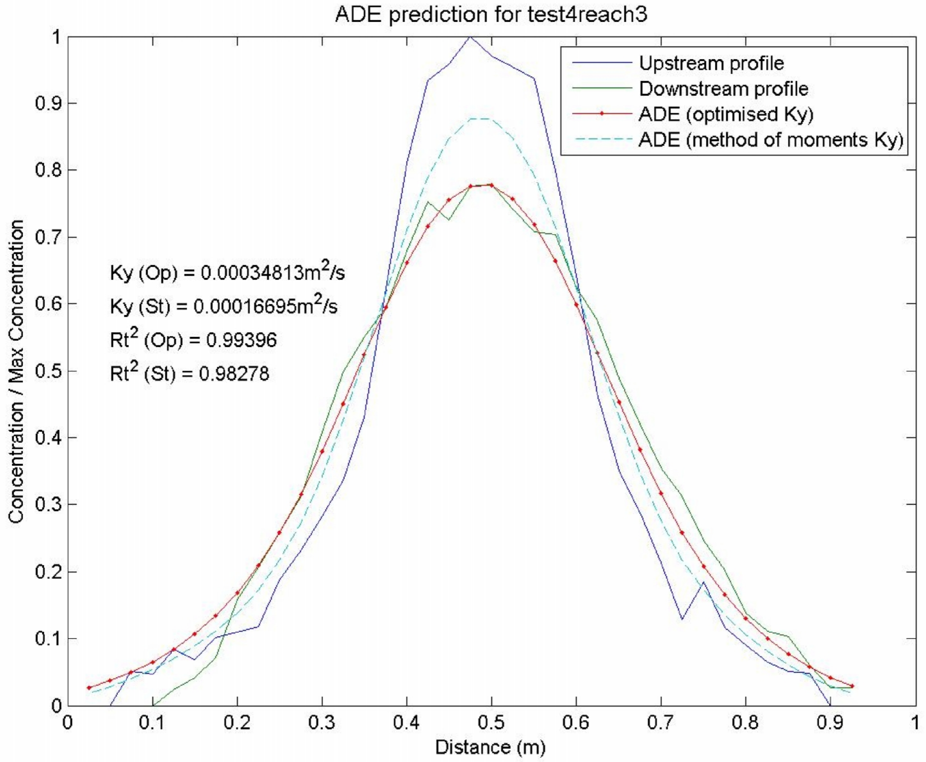
ADE prediction for test4reach3
Upstream profile
Downstream profile
ADE (optimised Ky)
ADE (method of moments Ky)
Ky (Op) = 0.00034813m^2/s
Ky (St) = 0.00016695m^2/s
Rt^2 (Op) = 0.99396
Rt^2 (St) = 0.98278
Concentration / Max Concentration
Distance (m)
0
0.1
0.2
0.3
0.4
0.5
0.6
0.7
0.8
0.9
1

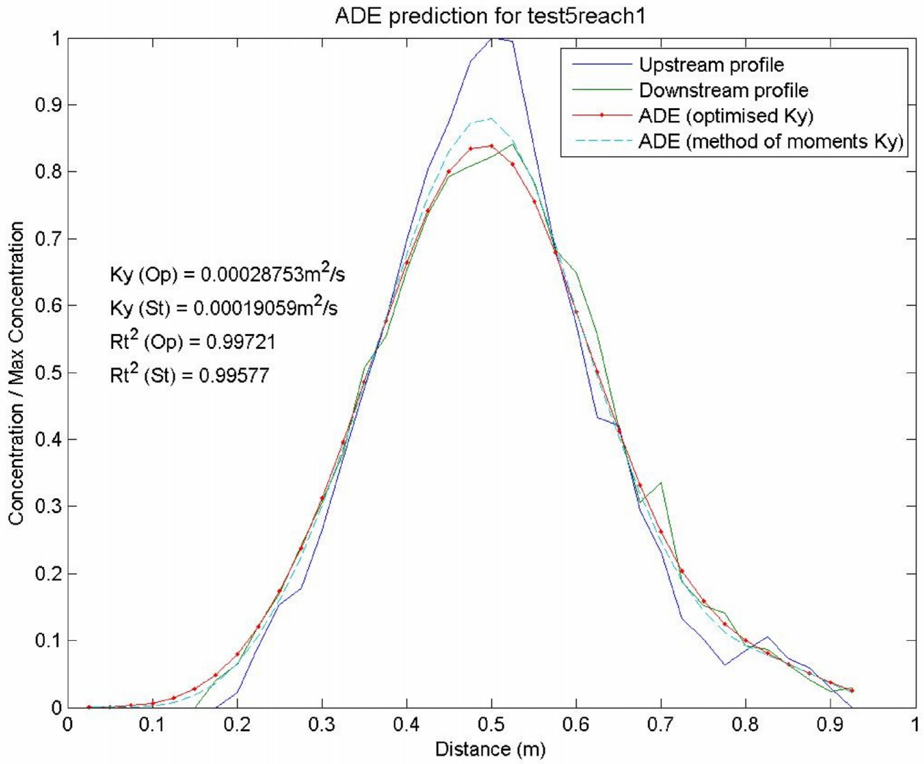
ADE prediction for test5reach1

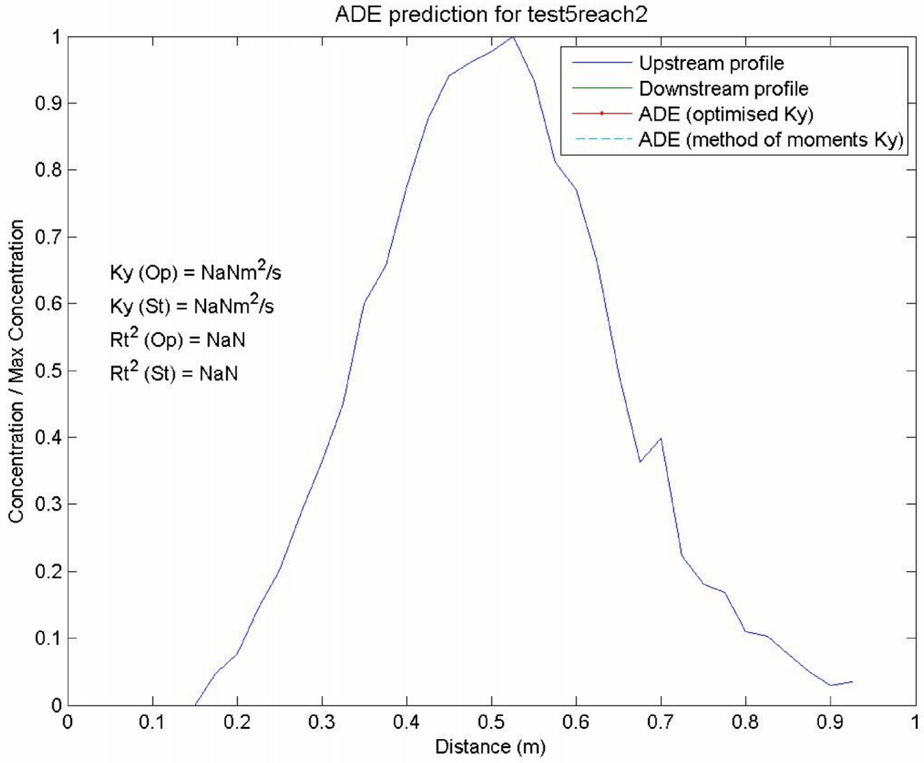
ADE prediction for test5reach2

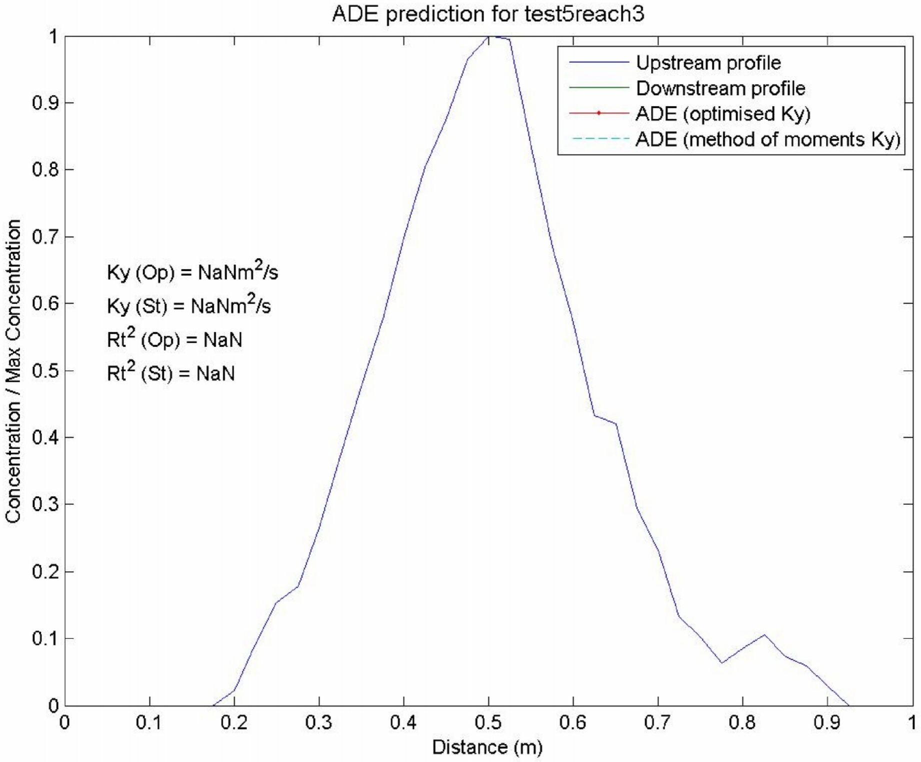
ADE prediction for test5reach3
Upstream profile
Downstream profile
ADE (optimised Ky)
ADE (method of moments Ky)
Ky (Op) = NaNm^2/s
Ky (St) = NaNm^2/s
Rt^2 (Op) = NaN
Rt^2 (St) = NaN
Concentration / Max Concentration
Distance (m)
0
0.1
0.2
0.3
0.4
0.5
0.6
0.7
0.8
0.9
1

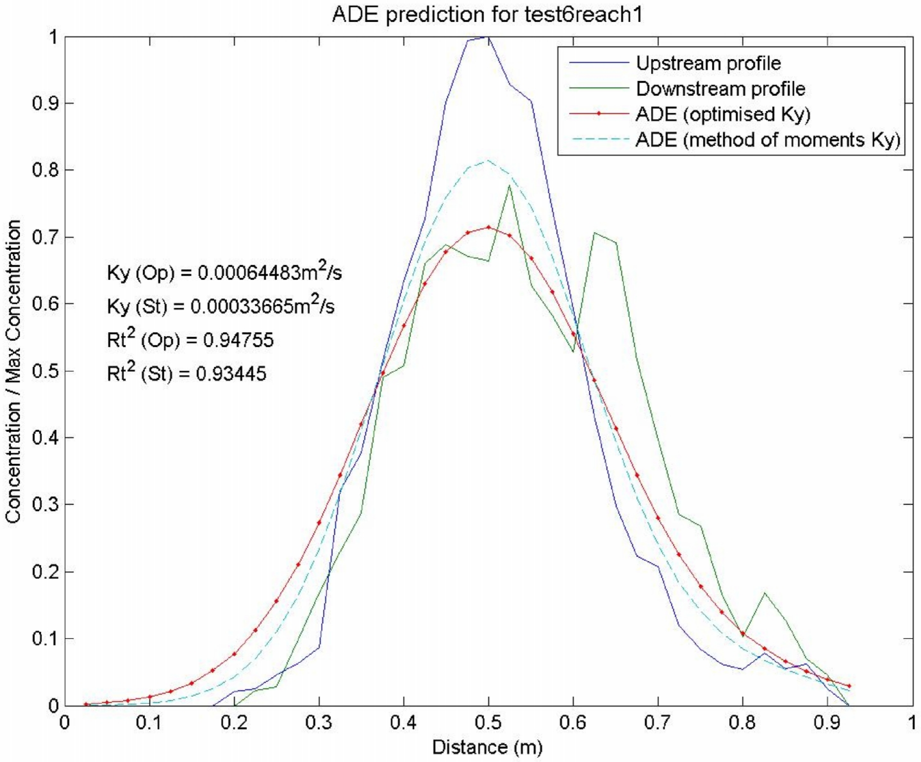
ADE prediction for test6reach1
Upstream profile
Downstream profile
ADE (optimised Ky)
ADE (method of moments Ky)
Ky (Op) = 0.00064483m^2/s
Ky (St) = 0.00033665m^2/s
Rt^2 (Op) = 0.94755
Rt^2 (St) = 0.93445
Concentration / Max Concentration
Distance (m)
0
0.1
0.2
0.3
0.4
0.5
0.6
0.7
0.8
0.9
1

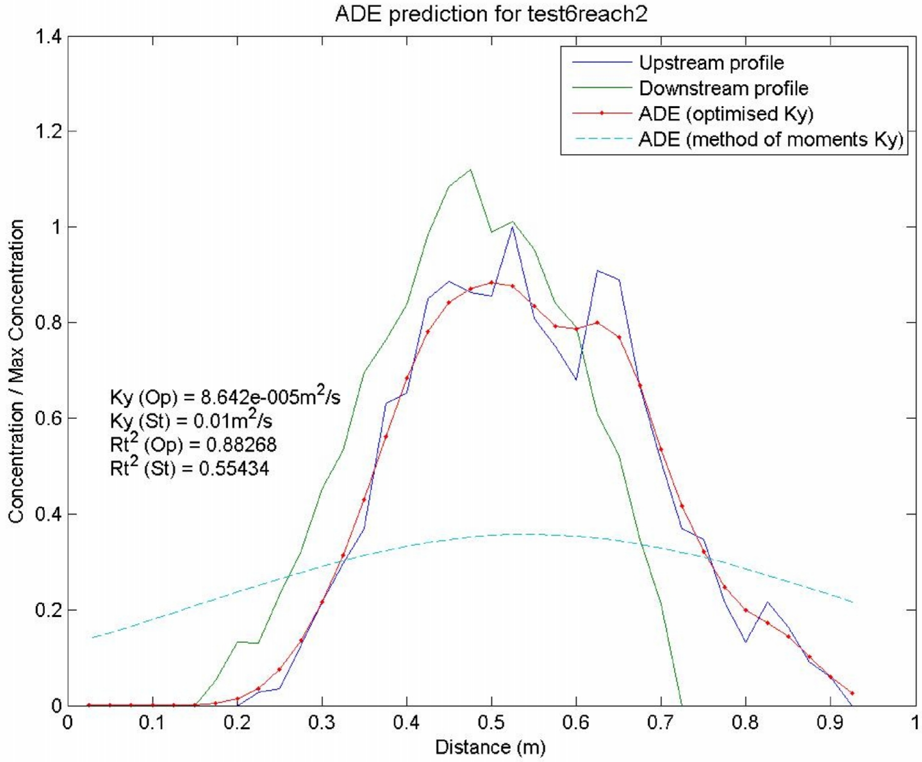
ADE prediction for test6reach2
Upstream profile
Downstream profile
ADE (optimised Ky)
ADE (method of moments Ky)
Ky (Op) = 8.642e-005m^2/s
Ky (St) = 0.01m^2/s
Rt^2 (Op) = 0.88268
Rt^2 (St) = 0.55434
Concentration / Max Concentration
Distance (m)
0
0.2
0.4
0.6
0.8
1
1.2
1.4
0
0.1
0.2
0.3
0.4
0.5
0.6
0.7
0.8
0.9
1

Appendix II

Mass Balance for 0.51S test

	t1	t1	t3	t4	t5	t6
c1	0.97787	1.02332	0.97007	0.97427	1.01996	0.99743
c2	0.49745	1.4201	1.12135	0.63176	0.71264	
c3	0.48644	1.45322	1.08779	0.61551	0.72686	

Transverse Mixing Coefficients K_y for 0.51S

	t1	t1	t3	t4	t5	t6
c1	0.00186008	0.00060083	0.00050540	0.00062040	0.00043740	0.00002469
c2	0.00033951	0.00030852	0.00122788	0.00001235	0.00001852	
c3	0.00052841	0.00046496	0.00086901	0.00009259	0.00009378	

Mass Balance for 0.97S

	t1	t1	t3	t4	t5	t6
c1	1.03795	1.05045	1.00646	1.02736	1.02114	0.99957
c2	0.65874	0.57222	1.61581	1.2813	0.75046	
c3	0.68374	0.6011	1.62625	1.31635	0.76633	

Transverse Mixing Coefficients for 0.97S

	t1	t1	t3	t4	t5	t6
c1	0.00014046	0.00045484	0.00021975	0.00057162	0.00066584	0.00032246
c2	0.00008642	0.00001235	0.00105687	0.00111493	0.00063580	
c3	0.00010494	0.00011690	0.00064564	0.00109317	0.00065512	

Mass Balance for 2.96AM

	t1	t1	t3	t4	t5	t6
c1	0.9888	1.03883	0.96013			
c2	0.96259	1.00661	0.95472			
c3	0.95181	1.0457	0.91665			

Transverse Mixing Coefficients for 2.96AM

	t1	t1	t3	t4	t5	t6
c1	0.00042294	0.00059852	0.00086776			
c2	0.00058446	0.00000038	0.00060283			
c3	0.00049969	0.00051919	0.00082630			

Mass Balance for 3.90A

	t1	t1	t3	t4	t5	t6
c1	0.99681	0.97603	0.96946	0.96361		
c2	2.1124		0.65881			
c3	2.10566		0.63869			

Transverse Mixing Coefficients for 3.90A

	t1	t1	t3	t4	t5	t6
c1	0.00167794	0.00031052	0.00113383	0.00097484		
c2	0.00108044		0.00007407			
c3	0.00069191		0.00031997			

Mass Balance for 5.92AM

	t1	t1	t3	t4	t5	t6
c1	1.00458	0.97863	1.05418	1.0392	0.95486	1.02356
c2	0.94656	1.05278			1.01466	
c3	0.9509	1.03028			0.96886	

Transverse Mixing Coefficients for 5.92AM

	t1	t1	t3	t4	t5	t6
c1	0.0001383	0.0001502	0.0002099	0.0002057	0.0002859	0.0001972
c2	0.0008225	0.0004834			0.0001526	
c3	0.0002724	0.0002958			0.0002199	

Mass Balance for 7.79A

	t1	t1	t3	t4	t5	t6
c1	1.02881	0.98437	0.97093	1.02538	0.95331	0.99619
c2	0.8743	1.74477	0.95069		0.5885	
c3	0.89948	1.71751	0.92305		0.56103	

Transverse Mixing Coefficients for 7.79A

	t1	t1	t3	t4	t5	t6
c1	0.00029645	0.00041673	0.00048504	0.00065871	0.00056943	0.00055397
c2	0.00047818	0.00083107	0.00059220		0.00000617	
c3	0.00036337	0.00056238	0.00048590		0.00023500	

References:

Boxall, J. B. (2000) Dispersion of Solutes in Sinuous Open Channel Flows. Phd Thesis, University Of Sheffield, U.K.

Boxall, J. B. and Guymer, I. (2001) Estimating Transverse Mixing Coefficients. *Proceedings of the Institution of Civil Engineers: Water, Maritime and Energy,* 148(4): 263.

Boxall, J. B. and Guymer, I. (2003) Analysis and Prediction of Transverse Mixing Coefficients in Natural Channels. *Journal of Hydraulic Engineering*. 129: 129 – 139.

Brehm, D. 2008. River plants may play major role in health of ocean coastal waters. *TechTalk,* 52 (16): 4

Chadwick, A. and Morfett, J. (1998) Hydraulics in civil and environmental engineering. E & FN Spon.

Chau, K. W. (2000) Transverse mixing coefficient measurement in an open rectangular channel. *Advances in Environmental Research*. 4 (2000): 287 – 294.

Cheng, N.S. and Nguyen, H. T. (2011) Hydraulic Radius for Evaluating Resistance Induced by Simulated Emergent Vegetation in Open-Channel Flows. Journal of Hydraulic Engineering. 137 (9): 995 – 1004.

Dennis, P. (2000) Longitudinal Dispersion due to Surcharged Manholes. Phd Thesis, University Of Sheffield, U.K.

Duijm, N. J. (1999) Estimates of roughness parameters for arrays of obstacles. *Boundary Layer Meteorology*. 91: 1 – 22.

Dunn, C., López, F., and Garcia, M. (1996). Mean flow and turbulence in a laboratory channel with simulated vegetation. *Hydraulic Engineering Series No. 51, UILU-ENG-96-2009*. Department of Civil Engineering, Univ. of Illinois, Urbana-Champaign.

Douglas, J.F., Gasiorek, J.M., and Swaffield, J.A. (1979). Fluid Mechanics. Longman, UK.

Fischer, H. B., List, E. J., Koh, R. C. Y., Imberger, J. and Brooks, N. H. (1979) Mixing in Inland and Coastal Waters. Academic Press.

Fischer, H.B. (1967) The Mechanics of Dispersion in Natural Streams. *Journal of the Hydraulics Division,* 93(6):187-216

Fischer, H. B. and Hanamura, T. (1975) Effects of Roughness Strips on Transverse Mixing in Hydraulic Models. *Water Resources Research,* 11(2): 362.

Gerrard, J.H. (1978). The wakes of cylindrical bluff bodies at low Reynolds number. Philosophical Transactions of the Royal Society of London A, 288, 351-382.

Goring, D. and Nikora, V. (2002). ”Despiking Acoustic Doppler Velocimeter Data.” *J. Hydraul. Eng.*, 128(1): 117–126

Guymer, I., Wilson, C. A. M. E., Boxall, J. B. (2005) Modelling solutes transport processes in free surface flow CFD schemes. In Bates, P. D., Lane, S. N. and Ferguson R. I. Computational Fluid Dynamics: Applications in Environmental Hydraulics. John Wiley & Sons, Ltd.

Granger, R. A. (1995) Fluid Mechanics. New York: Dover Publications.

Green, J. C. (2005) Modelling flow resistance in vegetated streams: Review and development of new theory. *Hydrological Processes,* 19(6): 1245.

Jeon, T. M., Baek, K. O. and Seo, I. W. (2007) Development of an empirical equation for the transverse dispersion coefficient in natural streams. *Environ Fluid Mech.* 7: 317 – 329.

Jarvela, J. (2002) Flow resistance of flexible and stiff vegetation: A flume study with natural plants. *Journal of Hydrology,* 269(1-2): 44.

Li, R., and Shen, H.W. (1973). Effect of tall vegetation on flow and sediment. *Journal of the Hydraulics Division*, 99(HY5), 793-814.

Liu, D. (2008). Flow through Rigid Vegetation Hydrodynamics. MSc Thesis, Virginia Polytechnic Institute and State University.

Lightbody, A. F., Nepf, H. M. (2006) Prediction of velocity profiles and longitudinal dispersion in emergent salt marsh vegetation. *Limnology and Oceanography* 51 (1): 218 – 228.

Liffen, T. M. R. (2011) Physical ecosystem engineering by emergent aquatic vegetation: the importance of biomechanical traits. PhD Thesis, Queen Mary, University of London.

Malki, R. (2009) The Influence of Saltmarsh Vegetation Canopies on Hydrodynamics in the Iintertidal Zone. PhD Thesis, Cardiff University.

Massey, B. and Smith, J. W. (1998) Mechanics of fluids. Stanley Thornes Ltd.

Nepf, H. M., Sullivan, J. A., Zavistoski, R. A. (1997) A model for diffusion within emergent vegetation. *Limnology and Oceanography* 42 (8): 1735 – 1745.

Nepf, H. M., Mugnier, C. G. and Zavistoski, R.A. (1997) The Effects of Vegetation on Longitudinal Dispersion. *Estuarine, Costal and Shelf Science* 44: 675-684.

Nepf, H. M. (1999) Drag, turbulence and diffusion in flow trough emergent vegetation. *Water Resources Research* 35 (2): 479-489.

Nepf, H. M. (2004) Vegetated Flow Dynamics. p. 137 – 164. In S. Fagherazzi, M. Marani, and L. Blum [eds]. Ecogeomorphology of tidal marshes. Coastal Estuar. Monogr. Ser. 59: doi: 10.1029/59CE09.

Nepf, H. M. (2012) Flow and Transport in Regions with Aquatic Vegetation. *Annual Review of Fluid Mechanic* 44: 123-142

Nortek AS. 2004. Vectrino Velocimeter User Guide.

Paul, S. S., Tachie, M. F. and Ormiston, S. J. (2007) Experimental study of cross-flow in a staggered tube bundle using particle image velocimetry. *International Journal of Heat and Fluid Flow* 28 (2007): 441-453.

Petryk, S. and Bosmajian, G. (1975) "Analysis of Flow though Vegetation." *Journal of the Hydraulics Division,* 101(7): 884.

Righetti, M., and Armanini, A. (2002). "Flow resistance in open channel flows with sparsely distributed bushes." *Journal of Hydrology*, 269, 55-64.

Runkel, R. L. and Bencala, K. E. (1995) Transport of reacting solutes in rivers and streams. p. 137 – 164. In V. P. Singh (ed.). Environmental Hydrology. Kluwer Academic Publishers.

Rutherford, J. C. (1994) River Mixing. J Wiley and Sons Ltd.

Schlichting, H. (1955). "Boundary-layer theory." McGraw Hill, US.

Serra, T. Fernando, H. J. S., Rodriguez, R. V. (2004) Effects of emergent vegetation on lateral diffusion in wetlands. *Water Research* 38 (2004): 139-147.

Shucksmith, J. D. (2008). Impact of Vegetation in Open Channels on Flow Resistance and Solute Mixing. PhD Thesis, University of Sheffield.

Shucksmith, J. D., Boxall J.B. and Guymer, I. (2010) Effects of emergent and submerged natural vegetation on longitudinal mixing in open channel flow. *Water Resour. Res.* 46, W04504, doi:10.1029/2008WR007657.

Streeter, V. L. and Wylie, E. B. (1979) Fluids Mechanics. McGraw-Hill (New York)

Stoesser, T., Kim, S. J. and Diplas, P. (2010) Turbulent Flow through Idealized Emergent Vegetation. *Journal of Hydraulic Engineering*, 136(12), 1003-1017.

Stone, B.M., and Shen, H.T. (2002). "Hydraulic resistance of flow in channels with cylindrical roughness." *Journal of Hydraulic Engineering*, 128(5), 500-506.

Tanino, Y. Nepf, H. M. (2008) Lateral dispersion in random cylinders arrays at high Reynolds number. *J. Fluid Mech.* 600: 339-371.

Tanino, Y. and Nepf, H. M. (2009) Lateral dispersion in vegetated flows: Reynolds number dependence at transitional Reynolds numbers. *33rd IAHR Congress: Water Engineering for a Sustainable Environment*, Vancouver, Canada.

Toth, L. G., Parpala, L., Balogh, C. and Tatrai, I. and Baranyai, E. (2011) Zooplankton community response to enhanced turbulence generated by water level decrease in Lake Balaton, the largest shallow lake in Central Europe. Limnol. Oceanogr., 56(6), 2011, 2211–2222.

Turner Design. (1993) Manual Operating Instructions.

Wahl, T. L. (2000) Analyzing ADV Data Using WinADV. *Joint conference on Water Resource Engineering and Water Resources Planning and Management* 75(3): 1-10.

White, B. L. and Nepf, H. M. (2003) "Scalar transport in random cylinder arrays at moderate Reynolds number." *Journal of Fluid Mechanics,* (487): 43.

Wilson, C.A.M.E., Stoesser, T., Bates, P.D., and Batemann Pinzen, A. (2003) Open channel flow through different forms of submerged flexible vegetation." *Journal of Hydraulic Engineering*, 129(11), 847-853.

WWAP (World Water Assessment Programme). (2003) Water for People, Water for Life. The Executive Summary. Paris, UNESCO.

WWAP (World Water Assessment Programme). (2012). *The United Nations World Water Development Report 4: Managing Water under Uncertainty and Risk*. Paris, UNESCO.

Xavier, P. A. (2009) Floodplain Woodland Hydrodynamics. PhD Thesis, Cardiff University.

Zavistoski, R. A. (1994) Hydrodynamics Effects of Surface Piercing Plants. MSc Thesis, Massachusetts Institute of Technology.

Zong, L. (2011) Interactions among flow, sediments deposition and aquatic vegetation in a channel. MSc Thesis, Massachusetts Institute of Technology.